University of New England

Final Technical Report

A Validated Finite Element Modeling Tool for Hydrodynamic Loading and Structural Analysis of Ocean Deployed Macroalgae Farms

Contract Number: 1726-1519

Award:	DE-AR000917
Sponsoring Agency	USDOE, Advanced Research Project Agency-Energy (ARPA-E)
Lead Recipient	University of New England
Project Team Members	U.S. Naval Academy, Kelson Marine, Callentis
Project Title	A Validated Finite Element Modeling Tool for Hydrodynamic Loading and Structural Analysis of Ocean Deployed Macroalgae Farms
Program Director	Dr. Marc von Keitz / Dr. Simon Freeman
Principal Investigators	Barry A. Costa-Pierce/David W. Fredriksson
Prime RecipientS	University of New England / United States Naval Academy
Contract Administrator	Dr. Dylan Temple
Date of Report	May 31, 2022
Reporting Period	Final

The information, data, or work presented herein was funded in part by the Advanced Research Projects Agency-Energy (ARPA-E), U.S. Department of Energy, under Award Number [DE-AR0000XXX]. The views and opinions of authors expressed herein do not necessarily state or reflect those of the United States Government or any agency thereof.

Please check the appropriate box:

[x] This Report contains no Protected Data.

[ ] This Report contains Protected Data and the award allows data to be marked as protected. Refer to your Attachment 2 for guidance on how to appropriately mark Protected Data. The applicable notice is provided below:

PROTECTED RIGHTS NOTICE

These protected data were produced under agreement no._**N/A**___ with the U.S. Department of Energy and may not be published, disseminated, or disclosed to others outside the Government until 5 years after development of information under this agreement, unless express written authorization is obtained from the recipient. Upon expiration of the period of protection set forth in this Notice, the Government shall have unlimited rights in this data. This Notice shall be marked on any reproduction of this data, in whole or in part.

☐ This Report contains SBIR/STTR Data and the award allows data to be marked as SBIR data. Refer to your Attachment 2 for guidance on how to appropriately mark SBIR Data. The applicable notice is provided below:

These SBIR/STTR data are furnished with SBIR/STTR rights under [Award No. ____**N/A**____ or a subaward under Award No._____**N/A**___].

Table of Contents

Table of Figures

Table of Tables

Public Executive Summary

The objective of this project was to develop and validate a fine-tuned, 3D computational modeling tool for high-fidelity simulations of macroalgae cultivation and harvest systems. To develop this tool, a full understanding of the geometric, material and hydrodynamic properties associated with farming kelp in exposed environments was necessary. Experiments and numerical modeling were done at increasing scales from 1) tank tests with a 1 m model, 2) to field tests with a 61 m culture line at a sheltered site, 3) to field tests with a 122 m culture line at an exposed site and to 4) a 5- line array at the exposed site with 186 m of culture length.

The results of the experimental tank tests yielded a set of hydrodynamic drag-area coefficients for a 1 m aggregate based on densely grown kelp at 16 kg/m with a length up to 3 m as described in Fredriksson et al. (2020). This work provided the basis to model kelp as a 1 m aggregate based on in-situ geometric and material properties to include measurements of kelp blade length and width, number of blades, yield per m, material mass density and cantilever tests to obtain modulus of elasticity.

Initial field work leveraged a National Science Foundation Established Program to Stimulate Competitive Research (EPSCoR) at the University of New England (UNE) to develop a kelp farming capability at a sheltered site near Wood Island in Saco Bay, Maine USA. Work on this project in 2017-2018 initiated the development of a kelp hatchery, kelp farm designs, sampling protocols and engineering instrumentation for mooring load measurements.

As part of this Department of Energy project in 2019, the UNE hatchery was expanded to service not only the Wood Island site, but a new farm at an exposed site just seaward of Ram Island, also in Saco Bay. The kelp farm for the Ram Island site was designed with subsurface corner floats and more robust rope, shackles and anchors for a 122 m culture line. Instrumentation for 2019 include two load cell systems and two Acoustic Wave and Current Sensors (AWACs). The instruments were deployed at both the Wood and Ram Island sites, on separate occasions. The instruments measured waves and currents and corresponding mooring line tension on both the east and west mooring lines, at the two sites. In addition to the engineering datasets, geometric and material properties of the kelp were also obtained from both farms through the spring growing season until harvest in May.

With the hydrodynamic characteristics, a well-defined aggregate representation was developed for model validation purposes using 5 load case datasets from the Ram Island deployment. Initial Hydro-FE model simulations comparing the field datasets, however, yielded overpredicted results. Therefore, a velocity reduction scheme was applied considering a 1-dimensional momentum balance between horizontal advection and the total drag per unit length of kelp growth. With implementation of velocity reduction, field and simulation result comparisons for the 5 load cases were within 15%, thus validating the numerical model.

In the next two years of the project (2020 and 2021), operations expanded to development of a 5-line array kelp aquaculture system at the Ram Island site. The 5-line array system included a 4-point, spread mooring system. Expanded operations included increasing the size of the size of the hatchery, the design and procurement of the new farm and building two new load cell systems to instrument the 4 mooring lines. Engineering datasets were not obtained in 2020 due

to Covid-19 restrictions. In 2021 the entire process was repeated with two successful instrumentation deployments. Seven load cases were identified from the array system datasets for validation purposes to be done as part of follow on work. With these modeling techniques, numerical models were built for multiple Category 1 projects for hectare sized systems. Therefore, the numerical model in now capable of being used as an engineering tool to design macroalgae farms while minimizing uncertainty so systems can be more cost effective.

Acknowledgements

Funding for this research was received from the United States Department of Energy, Macroalgae Research Inspiring Novel Energy Resources (MARINER) program award #DEAR0000917, from the National Science Foundation Established Program to Stimulate Competitive Research (EPSCoR) award #IIA-1355457 to Maine EPSCoR at the University of Maine subaward to the University of New England (UNE), and by the UNE School of Marine and Environmental Programs. The U.S. Naval Academy was funded through the ARPA-E Interagency Agreement No. 89703018SAR000002 associated with the UNE project.

The Principal Investigators (PIs) would like to thank Tollef Olsen for assistance with the project in the field and in the lab. The authors appreciate Tim Arienti and Addie Waters for assistance with vessel operation and project coordination. The PIs also thank Dan Chadbourne for assisting in permitting, connecting with the local marine community, and vessel support. Sincere thanks go also to the professional staff at the U.S. Naval Academy, Hydromechanics Laboratory. Finally, thanks to the former Midshipmen, S. Riedel, K. Robinson, C. Sowerby, K. Mortenson, L. Haller and S. Toski for their macroalgae research at the U.S. Naval Academy that helped to initiate this effort.

Accomplishments and Objectives

1. Milestones and Deliverables

This project was conducted over a 4 year period that included a 1 year, No Cost Extension (NCE). The administrative start date was February 15, 2018, with technical quarterly reporting starting in April, 2018 according to Table 1. In this section, the tasks and milestones are summarized for each quarterly report according to the approved statement of project objectives (SOPO) and shown on Table 2.

Table 1: Reporting was done on a quarterly basis starting in April, 2018.

Year I	Year II	Year III	Year IV (NCE)
Q1: Apr-Jun 2018	**Q5**: Apr-Jun 2019	**Q9**: Apr-Jun 2020	**Q13**: Apr-Jun 2021
Q2: Jul-Sep 2018	**Q6**: Jul-Sep 2019	**Q10**: Jul-Sep 2020	**Q14**: Jul-Sep 2021
Q3: Oct-Dec 2018	**Q7**: Oct-Dec 2019	**Q11**: Oct-Dec 2020	**Q15**: Oct-Dec 2021
Q4: Jan-Mar 2019	**Q8**: Jan-Mar 2020	**Q12**: Jan-Mar 2021	**Q16**: Jan-Mar 2022

Table 2: Gantt diagram of project tasks and milestones

WBS	Task/Milestone Title	G/N	Start	End
1	**Finalize project planning and establish field site**		**1**	**3**
M1.1	Finalize SOPO		1	1
1.2	Determine METOCEAN datasets		2	3
M1.3	Obtain State Aquaculture License	G/N	3	3
2	**Design, Seed & deployment of scalable systems**		1	10
2.1	Design single-line system		1	3
2.2	Grow hatchery seed for single-line system		2	3
2.3	Deploy and monitor seeded single-line system		4	5
M2.4	Recover and harvest single-line system		5	5
2.5	Design a more dense, planar-type system		5	7
2.6	Grow hatchery seed for dense, planar-type system		6	7
2.7	Seed, deploy and monitor planar-type system		8	9
M2.8	Recover and harvest planar-type system		9	9
3	**Morphology, geometry & material prop.**		**3**	**9**
3.1	Develop sampling plan and protocal		1	3
3.2	Collect field samples from 1st deployment		4	6
M3.3	1st Biomass sampling/measurements complete		6	6
3.4	Collect field samples for 2nd deployment		8	10
M3.5	2nd Biomass sampling/measurements complete		10	10
3.6	Develop macroalgae numerical representation		6	11
4	**Instrumenation planning and deployments**		**1**	**9**
4.1	Develop instrumentation sampling and protocals		1	3
M4.2	Finalize dataset load case protocals		3	3
4.3	1st instrumentation deployment		3	5
M4.4	1st instrumentation recovery		5	5
4.5	Load-case development for single-line system		5	7
4.6	2nd instrumentation deployment		7	9
M4.7	2nd instrumentation recovery		9	9
4.8	Load-case development for planar-type system		9	11
5	**Hydro-FE model validation**		**1**	**11**
5.1	Perform Hydro-FE comparisons with experiments		1	2
M5.2	Validate Hydro-FE at experimental model scale		2	2
5.3	Develop scalable model for single-line systems		2	5
5.4	Perform Hydro-FE comparisons with field data		5	7
M5.5	Validate Hydro-FE for single-line system scale	G/N	7	7
5.6	Develop scalable model for planar-type system		6	9
5.7	Perform Hydro-FE comparisons with field data		9	11
M5.8	Validate Hydro-FE for planar-type systems		11	11
M5.9	Develop modeling technique for hectare-sized systems		11	11
6	**Interact with NOAA on permiting (TBD)**		**2**	**10**
7	**Tech to Market and TT&O**		**1**	**12**
7.1	Meet with Cat 1 projects		1	3
M7.2	Identify Cat 1 modeling requirements		3	3
7.3	Plan for Cat 1 phase II		2	4
7.4	Develop Practical Science Master Degree		2	8
7.5	Quarterly Reporting and publication		1	12

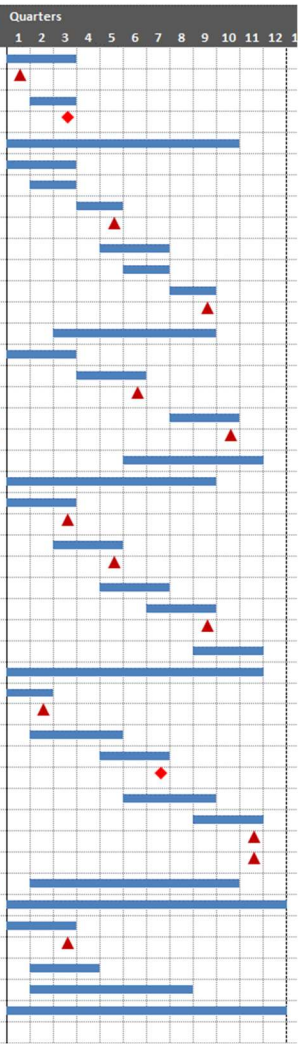

1.1. Task 1: Milestones and Deliverables

The objective of Task 1 was to *Establish an exposed field site in the Gulf of Maine for the validation study*. This included obtaining environmental datasets for engineering and design and obtaining State of Maine permits. Two Limited Purpose Aquaculture (LPAs) and an Experimental Lease permits were obtained. The Experimental Lease was used for this project and then extended for the University of New Hampshire/Trophic project.

Tasks	Milestones, Deliverables and Actual Performance
Task 1	Finalize project planning and establish field site
M1.2	Finalize SOPO
	Q1: SOPO completed and approved.
1.2	Determine METOCEAN datasets
	Q1: METOCEAN data sets were developed for system design and the aquaculture license. These data sets included bottom sediments, waves and currents. **Q2**: Side-scan sonar survey was completed along bottom sediment grab samples and remote operated vehicle video to determine bottom sediment type. **Q3**: The Saco Bay wave dataset adjusted from the Portland Buoy NDBC information was processed to obtain corresponding return period statistics for the 2-, 5-, 10-, 15-, 25-, 50- and 100-year storm conditions.
M1.3	Obtain State Aquaculture License, Go/No Go
	Q2: A State of Maine, Limited Purpose Aquaculture (LPA) Lease was obtained satisfying M1.3. In addition to the LPA, a 4-acre, experimental aquaculture lease application was submitted in September to establish a site for a larger system for gear and instrumentation in 2019-2020. METOCEAN data sets for the experimental lease were obtained. **Q3**: Revisions to the Maine Department of Marine Resources (DMR) 4-acre permit applications were received (October), made and submitted in December. **Q4**: Permit application was submitted, DMR reviewed the application and replied on March 6, 2019 that the materials submitted were complete. According to Maine policy, the application was made public allowing comments to be submitted until April 8, 2019. **Q5**: The Experimental Lease application was accepted and this milestone completed.
	Q10: Even though this Task has been completed, new developments evolved where we now collaborated with the Trophic Team and the University of New Hampshire (UNH). During this quarter, a formal agreement between the University of New England (UNE) and the UNH was initiated. The UNE Wood Island site was used to deploy components of the Trophic macroalgae system for the 2020-2021 growing season from October to May. UNE made the site and lease available to UNH to test their system. Plans were made for the season of 2021-2022 for UNH to utilize the 4-acre site at Ram Island. **Q11**: Permits for experimental sites were renewed, modified, and submitted in this quarter. The Wood Island Site LPA license was used with gear deployed from UNH. UNE completed the mandatory training for renewal and submitted the application and fees. The 2021 license was issued as PIER115. For the Ram Island site, a gear amendment was developed with the UNH and Trophic team for winter season 2021-2022, the research permit amendment was submitted to UNE leadership and approved and submitted to the Maine Department of Marine Resources. **Q12**: Modifications for the 4-acre site approved for UNH/Trophic operations.

1.2. Task 2: Milestones and Deliverables

The objective of Task 2 was to *Design, Seed and Deployment of Scalable Systems* for kelp farming. This comprehensive set of tasks involved developing and growing kelp seed in the hatchery and designing farming systems for kelp aquaculture at increasing scales. With the kelp seed and the farming designs, the farms were deployed at the sites in Saco Bay, Maine.

Tasks	Milestones and Deliverables
Task 2	Design, Seed & deployment of scalable systems
2.1	Design single-line system
	Q1: A preliminary configuration for the 122 m culture line system for deployment in November 2018 for the exposed site LPA was developed. **Q2**: Loading calculations of kelp system was first performed with a version of Morison equation integrated in the horizontal direction. Input to this analytical technique used preliminary hydrodynamic coefficients obtain from tank tests described in Task 5. Hydro-FE model simulations were also performed in the design process with a sugar kelp, Finite Model (FE) representation. A design load of 36kN (8000 lbf) was used to specify system components and the equipment was purchased. **Q3**: A finalized design of the 122 m longline system was completed.
2.2	Grow hatchery seed for single-line system
	Q2: The hatchery at UNE was refurbished and several spools of seeded twine grown for placement on the culture system.
2.3	Deploy and monitor seeded single-line system
	Q3: In late October, the 122 m system was deployed and seeded at the exposed LPA site in Saco Bay, Maine. However, in December, after inspection, it was discovered that while the gear was firmly in place, no kelp was present. On the next available clear weather day, the system was re-seeded. **Q4**: In late February, a field survey of the longline showed that the kelp took hold with lengths up to 30 cm. **Q5**: During late March, kelp was growing on both the exposed Ram Island site with the gear surviving the Gulf of Maine with no damage. During the months of April, May and June, seasonal conditions improved and the frequency of farm activity increased to weekly inspections in addition to planned instrument and biological sampling. Six of the trips focused on the deployment and recovery of instrumentation for three separate sampling events each for about 7 days.
M2.4	Recover and harvest single-line system
	Q5: Harvesting took place at Ram Island on May 22, 2919. To satisfy the leasing agreements through the Department of Marine Resources in Maine, all kelp farming gear including moorings were removed from Saco Bay by May 31, 2019 thus satisfying milestone M2.4.
2.5	Design a more dense, planar-type system
	Q3: A new preliminary design for the planar-system was also done to reflect the capabilities of the deployment vessel and to correspond with a potential Category 1 configurations. **Q6**: The majority of this quarter focused on designing and building the array-type system and growing the kelp to seed it. The team iterated through numerous array designs. The final design required balancing the need to increase the scale of the system, fitting it

	within the size of the 4-acre lease site, and operational manageability. A four-point, mooring leg anchor array system was examined with the Hydro-FE model with the design conditions. The results indicated that gear purchased for the 122 m kelp system could be utilized for parts of the array system to be deployed in 2019-2020. Therefore, only three new anchor legs were purchased for the 2019-2020 deployment. The gear was procured during September, 2019. **Q7**: The design of the array system was completed and therefore Task 2.5 was 100% completed. The array system consisted 5 kelp-lines spaced at 2.3 m connected along the width dimension with a straight-line, funicular polygon. The funicular polygon points and the kelp-line lengths were sized using catenary equations such that the width was set at 30 ft. and anchor-line spread angle 78.69 degrees. All of the components were purchased as off-the-shelf items from Hamilton Marine. The components above the anchor chain included only rope and painted lobster buoys fastened with knots and splices. Prior to deploying the array system, all of the components were labeled and organized in totes. **Q10 (NCE)**: With the No Cost Extension (NCE), the plan was readjusted to redeploy the planar system at the Ram Island site for the 2020-2021 season. The same system geometry was also deployed. One of the issues of the previous array system was related to the use of 1 inch, 3-strand twisted nylon as grow-lines. The three strand nylon rope has deep grooves within the lay of the line that could potentially "trap" the grow twine. Even if the grow twine is wrapped in the opposite direction, it was found that parts of the grow twine still found its way into the grooves. To improve the situation, a new single braided culture line was purchased without deep grooves within the lay. It was also decided to purchase the line to be orange and therefore more visible from the surface. The culture line was also specified with a material that does not absorb water like nylon, making it less heavy and easier to handle.
2.6	Grow hatchery seed for dense, planar-type system
	Q3: Hatchery expansion was completed in preparation for growing seed for the planar-system during the winter of 2019-2020. **Q6**: Sorus tissue was collected from sources in Casco Bay and seed developed in the updated hatchery and seed grown. **Q7**: Task 2.6 to grow hatchery seed for the planar system is also 100% complete. Two seed types were developed. The first seed cohort originated from Casco Bay while the second seed cohort came from Saco Bay. **Q10 (NCE)**: With the No Cost Extension (NCE), the plan was readjusted to redeploy the planar system at the Ram Island site for the 2020-2021 season using hatchery seed from Atlantic Seafarms.
2.7	Seed, deploy and monitor planar-type system
	Q7: The five-line array system was successfully seeded over two field attempts. The first was done on November 26 with three of the five lines were seeded. On December 23, 2019, the remaining two culture lines were seeded with source from Biddeford, ME. While examining the previously seeded lines, the outer most culture line in the array system had very little growth in some areas. To ensure productive kelp growth on every culture line, it was re-seeded while leaving the original, sparsely covered culture line in place to maximize settlement. **Q8**: Harsh conditions existed during the winter months of January through March in the Gulf of Maine so monitoring of the kelp only occurred on February 24, 2020 and March 9, 2020, just prior to Covid-19. Kelp growth was compared from examining the farm on

	each of these days. In general, the kelp had taken to the line in February with some bare locations and evidence of "slime" biofouling. In March, however, the kelp started to dominate, overtaking the biofouling with increase growth through most of the farm. With "stay at home orders," contingencies were made to plan for a year extension to repeat the deployment next year. **Q11 (NCE)**: A major component of the NCE was the redeployment of the array system on November 9, 2020. The deployment procedures applied the "farm-in-the-box" model developed for the previous array deployment in 2019. As described in Task 2.7, the new single braided grow lines were each placed in one of five storage totes on the front deck of the R/V Sakohki. One of the first steps was to slide the seeded spools onto on the culture lines. The culture lines were then attached to the headlines. The entire array was slowly deployed with the R/V Sakohki. The ends with the spools were the last to be placed in the water. With the entire array and mooring system deployed, the smaller R/V Llyr was then used to run the spools along each of the grow lines seeding the system. The entire deployment took approximately 4 hours. **Q12 (NCE**): After field deployment and seeding of the array system in November 2020, the kelp system was left to establish itself during the winter months of January and February. During this time, UNH deployed an ADCP at the Ram Island site to measure both waves and currents. On February 2, 2021, the instrument measured significant and maximum waves of 3.89 and 6.57 m, respectively, with a dominant period of 11.75 seconds with currents at about 0.5 m/s. The 5-line array was examined on March 3, 2021 with the kelp growing on all lines with a nominal length of 0.3 m. The system survived the storm from February 2, 2021, though fishing ghost gear was found wrapped around one of the anchor legs. **Q13 (NCE)**: The field program for the project was successful as Task 2.7 to "Seed, deploy and monitor planar-type system" was 100% complete during this quarter.
M2.8	Recover and harvest planar-type system
	Q9: Even during covid-19, milestone 2.8 to Recover and harvest the planar-type system was achieved during this reporting period following safe pandemic protocols required by UNE administration. While the entire array was deployed, seeded and harvested, instrumentation was not deployed since it was decided that safe distancing could not be done while handling the load cells (see Task 4). The project team did, however, request and received a No Cost Extension (NCE) so that the process could be repeated during for the 2020-2021 season. Regardless of the operational issues created by covid-19, the five-line array system was harvested on June 8, 2020. The harvesting team included UNE project personnel (Adam St. Gelais, Liz Johndrow) and the Saco Bay harbormaster (Dan Chadborne). Having the harbormaster work with the team was critically important because DoE funds were used to contract this local expert and to show him our kelp farming operational details. With the local maritime community engaged, expansion of kelp farming is more likely. The harvesting of the array was accomplished in just a few hours by maintaining the headline structure keeping the five lines together. The harvesting technique first involved releasing the east side of the system. Culture line #5 was attached to the hauler of the lobster boat, which pulled on the system. The other four lines were then guided by hand onto the back deck. Individual lines were placed in bait barrels then lifted by crane onto the local commercial fishing pier. On the following day (une 9, 2020), a local mooring system contractor was hired to remove the moorings.

	Q13 (NCE): The field program for the project was successful and M2.8 to "Recover and harvest planar-type system" was 100% complete during this quarter.

1.3. Task 3: Milestones and Deliverables

The objective of Task 3 was to obtain the *Morphology, Geometry and Material properties* of the kelp for each of the deployments described in Task 2. Biomass sampling was critical for the development of the kelp aggregate model. To represent the kelp in the finite element model, a distinct set of properties were established to include yield (kg/m), mass density (kg/m3), number of blades per m, individual blade length, blade width and if possible, the modulus of elasticity.

Tasks	Milestones and Deliverables
Task 3	Morphology, geometry & material properties
3.1	Develop sampling plan and protocol
	Q1: By leveraging the a NFS-EPSCoR project, work was done at the protected site in Saco Bay at Wood Island, taking samples from the deployed kelp farm in an effort to develop the protocols and to have data for Hydro-FE simulations. **Q2**: Wood Island kelp samples were processed to obtain basic morphology (e.g. length, width) but also the mass density and modulus of elasticity need to develop a finite element model. **Q3**: With the protocol developed, the mass density (1058 kg/m^3) and modulus of elasticity (7.47 MPa) were obtained from the May 2018 field sampling efforts at the Wood Island site. These characteristics were included in the Hydro-FE validation of with the Wood Island culture line system. This was done as part of Task 3.6 to develop modeling macroalgae representations. It was also decided during this reporting period that field sampling for 2019 would be conducted during the months of March, April and May due to logistics of farm access in harsh winter months and the small size of the crop at these times.
3.2	Collect field samples from first deployment
	Q4: Morphological sampling of the exposed site was initiated in March 2019. The sampling protocol (Task 3.1) was changed from 5 locations on the culture line to 3 locations (east – middle – west) to reduce the time required for processing samples before degradation. Successful deployment in December of the sheltered site near Wood Island of the same kelp yielded opportunities for additional sampling and instrumentation deployments. The results from the initial sampling on March 25, 2019 showed an average total length of stipe and blade of 0.936, 0.712 and 0.833 m for the east, middle and west sampling locations, respectively. Mass density values ranged from 1011 kg/m^3 for the intercalary meristem, 1150 kg/m^3 for the blade tip and 1828 kg/m^3 for the stipe. Elasticity values ranged from 0.891 MPa for the intercalary meristem, 1.748 MPa for the blade tip and 4.761 MPa for the stipe. **Q5**: Biological samples were collected during these months processed for geometric and material properties. Sampling sets were obtained on 12 separate days during this reporting period including on March 25 (Ram), April 2 (Ram), April 5 (Wood), April 11 (Ram, Wood), April 17 (Wood), April 24 (Ram), April 25 (Wood), May 3 (Ram), May 9 (Ram), May 16 (Ram, Wood), May 22 (Ram) and May 28 (Wood). In general, early April showed that both the 122 m (Ram) and the 61 m (Wood) culture lines in Saco Bay

	supported developing sporophytes averaging 1.02 m in length. By the middle of May, the sporophytes grew to a new average total length of 2.00 m. Information from these sample datasets were used in the development kelp numerical model representations
M3.3	First biomass sampling complete
	Q5: Tasks 3.1 to M3.3 were completed
3.4	Collect field samples from second deployment
	Q9: Even during convid-19, the five-line array was deployed, seeded and recovered as described in Task 2. During this reporting period, an effort was made to quantify the amount of biomass on the system, with limited personnel adhering to strict pandemic guidelines. The results of the individual blade samples produced an average length of 148 cm with a standard deviation of 29 cm. The average width was 6.97 cm with a standard deviation of 1.65 cm. The mass density of the kelp grown on the array system was determined with wet/dry mass measurements yielding a value of 1043 kg/m^3. Tasks 3.4, M3.5 and 3.6 were repeated as part of the NCE. **Q13**: Extensive sampling was done of the biomass during the April and May field operations. The datasets were processed to develop the geometric and material modeling approach for the 5-line array system validation. **Q14 (NCE)**: The datasets from the sampling of the array system during the grow out period between April and May of 2021 were processed from multiple locations. Sampling was conducted on each of the five lines from locations designated as E (east), ME (middle east), MW (middle west) and W (west). Samples were taken during the deployment and recovery days to bracket the level of growth associated with the instrumentation datasets. Average yield increased from about 3 to 10 kg/m between 15-Apr-21 and 21-May-21.
M3.5	Second biomass sampling complete
	Q12 (NCE): Milestone completed
3.6	Develop macroalgae representation
	Q6: A numerical model representation of macroalgae was done as an aggregate based on the physical model tank tests conducted at the U.S. Naval Academy. The same aggregate approach was completed using the geometric and material properties from the field tests. **Q7**: During this reporting period, the geometric and material properties of the kelp sampling from 2019 were further evaluated. The protocol was to take rectangular swatch samples from the centerline portion of the kelp blade. This was chosen because it seemed to be the stiffest portion of each specimen need to determine flexural rigidity. The flexural rigidity tests needed the weight/length of the swatch sample. With the weight, the mass of the swatch sample was determined. Since the dimensions of the swatch sample could be measured, the volume was determined. With the mass and volume, the mass density of the sample was calculated. The mass density values of the swatch samples seemed to be higher than expected using this technique. To derive a more comprehensive estimate of the net wet weight and effective (average) material density of the kelp along the grow-out line, a hydrostatic numerical model was used to estimate the average effective material density of the kelp based on the volume of kelp and the observed submergence levels of the surface flotation. In this hydrostatic model of the kelp longline, the material density (in kg/m^3) was iterated until the net wet weight

	of the kelp caused the waterlines of the surface floats to match that observed in the field at the time of interest. **Q8**: During this reporting period, the model validation efforts (see Task 5) focused on using a kelp numerical model representative of growth on the Ram Island site during the 2018-2019 growing season. **Q15 (NCE)**: During this reporting period, the approach associated with Task 3.6 (Develop macroalgae representation) was finalized. To complete this task, we identified the macroalgae field measurements required to build an accurate numerical model of the kelp aggregate. With completion of the field work from April 15, 2021 to May 21, 2021 and the sampling of the macroalgae during that time period, the kelp datasets were processed to obtain a representation of biomass for the numerical modeling effort. During this sampling period, the AWAC and load cell instruments were deployed from April 16 to April 28, 2021 and again from May 8 to May 16, 2021. Processing the kelp datasets provided yields between 3.0-4.8 kg/m (ave = 3.9 kg/m) and 6.2-8.1 kg/m (ave = 7.4 kg/m) for each instrumentation deployment, respectively. The length of the kelp was 1.22-1.26 m (ave = 1.24 m) and 1.37-1.40 m (ave = 1.39 m). Kelp mass density measurements were made, but were verified using static model simulations and visual buoy waterline information. An initial numerical model kelp representation was provided for Task 3.6 assuming a mass density of 1050 kg/m^3.

1.4. Task 4: Milestones and Deliverables

The objective of Task 4 was to perform *Instrumentation Planning and Deployment* of engineering instrumentation on each of the kelp farms deployed as part of Task 2 at the sites described in Task 1. The engineering instrumentation included load cell systems and instruments that measure both waves and current profiles. Two robust datasets were acquired for model validation.

Tasks	Milestones and Deliverables
Task 4	Instrumentation planning and deployments
	Q1: Three different types of instrumentation were used for this project. The instruments included (1) Acoustic Wave and Current (AWAC) sensors configured to measure currents, (2) the same AWACs configured to measure waves, (3) load-cells to measure equipment tensions and (4) accelerometers to measure motions. It was found, however, that the accelerometers did not prove very useful. **Q3**: UNE purchased a Nortek Signature 1000 instrument (Sig1000), an instrument frame and three data acquisition and battery pack units for the load cells. The equipment inventory at this point included: 1. Two Nortek AWAC instruments each with a frame, capable of measuring wave and current profiles (but not simultaneously). These were obtained from previous efforts at the US Naval Academy. 2. One Nortek Signature1000 with a new folding frame, capable of measuring turbulence, waves and currents. This instrument has the capability of measuring waves and currents at nearly the same time. It can also measure more detailed, small-scale turbulence.

	3. Three load cell battery packs and data acquisition systems. The data acquisition system has two analog ports for load cells and three digital ports for other instruments. One of the systems was acquired from the NSF project. 4. Three load cells. One of the loads cells has a capacity of 2000 lbf, while the other two have capacities of 10,000 lbf. A fourth load cell was being designed with a capacity of 5000 lbf. 5. Three load cell strong-backs. The strongback are made of stainless steel and are used to mount the submersible load cells, battery packs and data acquisition systems. 6. Three accelerometer packages.
4.1	Develop instrumentation sampling and protocols
	Q2: The sample protocols were completed for each instrument and a deployment schedule initialized with the first deployment in October 2018. Significant progress was made to build two more load-cell strong-backs, refurbish two 10,000 lbf capacity load cells and purchase three battery/data acquisition components
M4.2	Finalize data set load case protocols
	Q4: Instrumentation dataset protocols were completed, though modified during **Q5**.
4.3	First instrumentation deployment
	Q4: Two new load cell systems were completed and calibrated at the U.S. Naval Academy. The load cells are each rated to 10,000 lbf. Large load-cell capacities were chosen in preparation for potential Phase 2, Cat 1 projects. Even though these instruments have a large capacity, they can still measure within 5-8 lbf. A fourth load-cell with a capacity of 5000 lbf was also purchased for intermediate range measurements with expected delivery in May. Also, in preparation for the spring field season, the two AWAC instruments were cleaned and battery pack replaced. Another substantial improvement was the acquisition of a field-instrumentation laboratory space at the UNE-North facility in Portland, Maine. **Q5:** Three instrumentation deployments took place during this reporting period with exceptional data recovery. The first instrumentation deployment was conducted from April 11-17 at the Wood Island site. The effort included the installation of two load-cell systems, two AWACS, two accelerometers and an inverted tilt current meter. The instruments where then recovered, cleaned and the data downloaded. They were then reconfigured and deployed at the exposed, Ram Island site on April 24 and recovered again May 1. After instrumentation turnaround, the suite was redeployed at the Wood Island site from May 16-26.
M4.4	First instrument recovery
	Q5: Tasks 4.1 through Milestone 4.4 complete.
4.5	Load-case development for single-line system
	Q6: Three valuable sets from the AWACs and load-cells were obtained from the Ram and Wood Island sites. The information was downloaded and the raw datasets processed for each of the blue (east) and yellow (west) deployed instruments at each site. During this reporting period, the datasets were further processed to identify potential load cases. Results from the two AWACs for each deployment were averaged to best estimate the velocities acting on the farm. The values were then vector-averaged over the portion of the water column that “nominally” occupied by the biomass. The vertical-average current velocity samples were sorted into 36 directional bins and 9 speed bins and plotted as a current rose. To preserve the integrity of the blind validation experiment, load-cell datasets were normalized by the maximum value measured to prevent bias. To

	enable the comparison of data across multiple instruments, meta-statistics (e.g. time-average velocity, variance in tension) from each burst for each instrument were linearly interpolated onto a common time vector. This time vector spanned the time range during which all instruments were sampling and had a time step of 1 hour. All of the datasets are being evaluated to establish load cases for currents, waves and wave/current combinations validation simulations with Hydro-FE. Progress was also made during this reporting period to complete the fourth load cell system for the project. **Q8:** Work during this period focused on using the load cases from mostly the Ram Island site in the Hydro-FE validation of the 122 m long system (see Task 5). **Q11**: Validation load cases were updated and finalized during this reporting period as shown on Figure 130 and Table 19. The new set of load cases were chosen considering a range of tidal elevations, currents speeds and directions and significant wave height values. Variability is inherent in the oceanic environment, however, so load case criteria were established to assess steady-state conditions. Current speed values from 15-18 and 30-33 minutes past each hour from the east and west AWACS were examined to have a less than 10% relative difference. A similar approach was applied with significant wave height values obtained during the second burst past the hour.
4.6	Second instrumentation deployment
	Q7: During this reporting period, the fourth load-cell system was completed. The load-cell was specified at 5000 lbf with an integrated amplifier. The load-cell, battery pack and data logger were assembled and the calibration verified at the U.S. Naval Academy. The full suite of instruments for the project at this point included four load-cells and two AWACs and a Sig1000. **Q8:** Preparations for instrument deployment have been halted due to shutdown activities. Contingency plans were being made to deploy through a project extension into next year. **Q9**: A request was made and granted to extend the project 1-year due to Covid-19 implications. Arrangements were made to deploy an array system during the 2020-2021 winter season. **Q11**: Validation load cases were updated and finalized during this reporting period. The new set of load cases were chosen considering a range of tidal elevations, currents speeds and directions and significant wave height values. Variability is inherent in the oceanic environment, however, so load case criteria were established to assess steady-state conditions. Current speed values from 15-18 and 30-33 minutes past each hour from the east and west AWACS were examined to have a less than 10% relative difference. A similar approach was applied with significant wave height values obtained during the second burst past the hour. **Q12**: Since covid protocols were still in place and DoD employees not permitted to travel, local personnel were trained to configure the AWACs and the four load cells. One of the initial steps was to learn how the data acquisition software for the load cells worked by taking “zero” measurements. The AWACs were also configured for the same deployment scheme that proved suitable during the spring 2019 measurement effort.
M4.7	Second instrument recovery
	Q13 (NCE): The second instrumentation deployment and therefore this Milestone 4.7 was 100% completed. The two AWACS (blue-east and yellow-west) along with the four load cells (blue-northeast, red-southeast, yellow-southwest and green-northwest) were

	deployed from April 16 to 28, 2021 and from May 8 to 15, 2021. The field datasets are were used to develop load cases to validate the 5-line array kelp farm system.
4.8	Load-case development for planar-type system
	Q14 (NCE): Load-case development for the planar-type system was started by plotting all of the datasets. The most extreme tension time series was identified on April 16, 2021 from 23:00 – 23:30. The loadcell, wave and current velocity profile datasets were further processed for load case development **Q15 (NCE)**: Seven load cases were identified for the array validation effort and were selected to captured near peak wave height and current speed events at a range of tidal elevations and wave and current directions. Samples were selected such that the change in wave and current magnitude between adjacent samples were within 10%. The load cases included five storm events and one near-still-water sample before and one after the April 17, 2021 storm. **Q16 (NCE)**: Load cases have been finalized.

1.5. Task 5: Milestones and Deliverables

The objective of Task 5 was to perform in-depth verification and validation of the Hydro-FE modeling tool. This effort was done first with the results from the tank tests. The second validation effort was performed with 5 load cases for the single-line system. The third validation effort was initiated for the array system with 7 load cases.

Tasks	Milestones and Deliverables
Task 5	Hydro-FE model validation
5.1	Perform Hydro-FE comparisons with tank experiments
	Q1: Model comparisons were performed with the 1 m tank tests and collected load cell and tidal velocity field data from field measurements in May 2018 from the Wood Island site. **Q2**: The normal drag characteristics were replicated with the model with comparison to tow tank results. The tangential drag characteristics showed an offset of about 15 N for the 1-m x 3-m model. The offset value appears to be independent of velocity. The issue is being further investigated but is most likely related to reconfiguration. Comparison of the Hydro-FE model with the forced-oscillation test (with the planar motion mechanism) also provided insight. It was found that performing discrete Fourier analysis might not be appropriate to extract oscillating drag and added coefficients because the kelp model is not a rigid body. Therefore, the hydrodynamic coefficients for the forced oscillation tests are being determined from a multi-variate sensitivity analysis, rather than an analytical solution. **Q3:** Major progress was made to validate the Hydro-FE approach with the experimental results performed at the U.S. Naval Academy with the full-scale model. The experimental results were processed for the Hydro-FE validation efforts using mean angle deflections. Mean angle deflections were considered since they reflect the balance between drag forces and weight and buoyancy forces. Simulations were performed with the perpendicular case with structural properties to represent the 1 m kelp model. Simulation results matched the tank tests and a set of normal and

	tangential drag coefficients have been established. Work was also done to simulate the oscillating tank test with the same drag coefficient to obtain a suitable mass coefficient. **Q4**: Validation efforts focused on refining the force balance model for the Hydro-FE kelp representation. To model the streamlining effect of kelp, it was found necessary to resolve the angles of the material at each speed. This is important because it a dynamic environment with waves, the angle the kelp makes at each instant in time determines the relative velocity (and acceleration) that interacts with the kelp. It was found that drag needs to be decomposed into both normal and tangential components, which is a function of the dynamic angle. Understanding the drag components at each dynamic time step is necessary since kelp reconfigures itself into a streamline orientation where tangential drag is the dominating process over normal drag. This is important because normal drag can be two orders of magnitude larger than tangential drag.
M5.2	Validate Hydro-FE at experimental model scale
	Q6: This Milestone M5.2 was 95% level of completed (Fredriksson et al., 2020). The scalable model associated with Task 5.3 is based on a 1 m aggregate of kelp blades. Results of the field deployments from 2018 and 2019 indicate there could be up to 40 individual blades per 10 cm. Representing each individual blade in the Hydro-FE model is computationally inefficient, while the 1 m aggregate model satisfies the fidelity scale originally proposed. With multiple datasets obtained during the 2019 field deployment efforts, from both the Ram and Wood Island sites, the 1 m aggregate Hydro-FE model is was examined at both the 61 and 122 m culture line scales. **Q7**: This task was completed as the the kelp-aggregate beam model was built by matching geometric, material and hydrodynamic properties of actual kelp and the physical model. **Q8-Q9**: With Fredriksson et al. (2020) published, work focused validating the model with the field datasets.
5.3	Develop scalable model for single-line systems
	Q5: With the instrumentation datasets acquired during the field season of 2019, single kelp-line validation studies were developed at increasing length scales to 122 m. **Q9**: Work was also performed to describe, in more detail, the techniques to represent kelp aggregates in the Hydro-FE model. The techniques relate to field measurement properties including the wet and dry weights of aggregates to obtain volume needed to match the hydrostatics in the model. With the volume and the measured length, a characteristic cross-section can be obtained to normalize projected and surface areas. The normalized projected and surface areas are needed to adjust the normal and tangential drag-area values for implementation in the Hydro-FE software.
5.4	Perform Hydro-FE comparisons with field data
	Q3: The Hydro-FE model was also used in a set of validation simulations for the Wood Island configuration with the datasets obtained in May 2018. With the geometric and material properties of the kelp and AWAC profiles information as input, Hydro-FE was run to calculated mooring line tension response and compared to the load-cell dataset. Calculated tension was estimated to be 40 lbf compared to the measured value of 34 lbf. **Q7**: A Hydro-FE model of the single-line system deployed in 2018-2019 was constructed incorporating the kelp finite element model. **Q9**: Preliminary Hydro-FE comparisons were made with both the tank test results (Fredriksson et al., 2020) and load case data sets from the 2018-2019 field season

	yielding general results within 6.5 and 36%, respectively. More work is needed to refine the velocity reduction technique so that the Hydro-FE model can become more accurate.
M5.5	Validate Hydro-FE for single-line system scale
	Q10: Validation efforts for the single-line system continued with the load-cases developed. However, representation of a wide range of conditions was challenging to replicate equally. One of the efforts to address this issue was to develop a 1-dimensional velocity reduction scheme. To expand from 1-dimension, the Hydro-FE model was updated to accommodate 4-D velocity input from the x-, y- and z-directions along with time. A paper has been initiated with colleagues from the University of New Hampshire to show these results. **Q11**: Model validation during this reporting period was performed with the five new Ram Island validation load cases chosen for being stationary and ergodic processes. The Hydro-FE model was implemented with the kelp aggregate approach empirically determined from the tank tests. It was also implemented with a 1-D velocity reduction schemed to accommodate momentum reduction. Validation results were within the 15% RMSE. This task was completed and a manuscript was prepared for publication.
5.6	Develop scalable model for planar-type system
	Q9: Task 5.6 with milestones 5.8 and 5.9 are postponed for a year as part of the no cost extension.
5.7	Perform Hydro-FE comparisons with field data
	Q14 (NCE): During this reporting period worked commenced to develop the numerical model of the 5-line array to match the as-installed, in-situ conditions. The updated numerical model was used for validation efforts with the measured field data.
M5.8	Validate Hydro-FE for planar-type systems
	To be completed as part of follow on work.
M5.9	Develop modeling technique for hectare-sized systems
	Several hectare sized systems were modeled as part of Category 1 projects.

1.6. Task 6: Milestones and Deliverables

The objective of Task 6 was to leverage existing efforts with National Oceanic and Atmospheric Administration (NOAA) to develop aquaculture engineering guidelines specific to macroalgae production.

Tasks	Milestones and Deliverables
Task 6	Interact with NOAA on permitting
	Q1: This task was included as an opportunity to communicate efforts being conducted with NOAA, Office of Aquaculture to develop technical guidance for culture systems in Federal waters. A draft document, in support of Gulf of Mexico Aquaculture Fishery Management Plan, was submitted after engineering review to the Southwest Regional Aquaculture Coordinator in July 2018. While this initial technical document has a focus on the Gulf of Mexico, it is expected that similar plans will be developed for other regions within federal waters. **Q2**: The draft technical guidelines document, in support of Gulf of Mexico Aquaculture Fishery Management Plan, is presently in legal review. However, in September 2018, a court in Louisiana ruled that NOAA did not have authority to regulate aquaculture the

	under the Magnuson-Stevens Fishery Conservation and Management Act. Therefore, publishing the draft technical guidelines have been put on hold. **Q3**: During this reporting period, a group of Mariner project engineers convened to discuss applicant safety factor and risk levels to be used in the design process for macroalgae systems. A report was submitted to the ARPA-E program titled: Design Criteria for Offshore Macroalgae Growing Systems by David W. Fredriksson (USNA), Tobias Dewhurst (MMC), Zach Moscicki (UNH) and Corey Sullivan (UNH). Our intent was to build upon the draft technical guidelines for the Gulf Plan to have addition information for macroalgae type systems. **Q4**: The technical guidelines for the Gulf of Mexico was completed and published as a NOAA Technical Memorandum. This document is available at https://repository.library.noaa.gov/view/noaa/19836. **Q5**: Collaborative work with the NOAA Office of Aquaculture leveraged datasets acquired through this Cat 3 project. Members of this team worked with NOAA to examine potential whale impacts with kelp farming gear. Datasets obtained during the May 2019 field effort (Task 4) was presented at an Entanglement Workshop at the NOAA Southwest Fisheries Science Center. The MARINER dataset shows how the mooring line tension time-series can be resolved showing the influence of tides, tidal currents, waves and the attachment of the 36 ft research vessel. The research vessel could be analogous to a large marine mammal. By understanding how the source of the forcing mechanisms, the team is pursuing developing an instrument that could perhaps detect a whale impact. **Q8**: A primary focus is to develop engineering techniques to optimize ocean aquaculture systems. Work done with the Category 1 Trophic teams shows how the numerical modeling approach developed and validated by our Category 3 team was used to help design the Trophic Phase II prototype. Besides evaluating design alternatives to find suitable mooring line lengths, anchor leg configurations, and longline and structural line geometries, the numerical model was applied within a design-of-experiments approach. Whereas the initial design resulted in the anchor capacity being exceeded during a worst-case 25-year storm (safety factor of 0.8) this design approach resulted in a system with a predicted anchor safety factor of 2.0 for the same anchors, while keeping eight of the twelve desired culture lines. These techniques were considered to further the development of engineering guidelines. **Q9**: Work with NOAA Entanglement Prevention group expanded with a focus on developing the Whale Simulator model. Part of this work is to examine the response of rope aquaculture systems to the impact of large marine mammals. The interaction is being investigated by examining the kinetic energy of the whale to the potential energy response of the mooring system. Static tank tests were conducted at the USNA to understand the horizontal stiffness of the mooring system using a range of submersible flotation elements. **Q10**: Model tests were done at the USNA Hydromechanics laboratory to investigate the impact of a large mass (such as a whale) on a horizontal aquaculture system.

1.7. Task 7: Milestones and Deliverables

The objective of Task 7 was to develop industry-centric technical transfer and outreach efforts. Tasks 7.1-7.1 were completed first year of the project, while Task 7.5 was ongoing until the final report was completed.

Tasks	Milestones and Deliverables
Task 7	General Outreach and Tech to Market and TT&O
7.0	General Outreach Activities
	Q2: In August 2018, subtask 7.1 was expanded to include modeling work for the Ocean Rainforest team. It was also expanded in September 2018 to collaborate with Pacific Northwest National Laboratory (PNNL) to develop a Multi-Resolution, Multi-Scale Modeling for Scalable Macroalgae Production. **Q3:** General TT&O was performed in support of youth programs in Southern Maine. **Q5:** TT&O efforts during this reporting period focused on interacting with the following entities, 1) Saco City Board/Planning and Parks and Recreation (4/17/19), (2) Maine Public Broadcasting (4/25/19), 3) Seaweed week in Maine (5/1/19), 4) Woods Hole Oceanographic Institution (5/16/19) and 3) Bangs Mussels (5/23/19).
7.1	Meet with Cat 1 projects
	Q3: Modeling work with the Category 1 projected focused on performing simulations for the Adjustadepth system in support of the University of New Hampshire (UNH) and the University of Southern Mississippi (USM). Additional modeling informed design decisions for the Trophic system aimed at reducing CapEx and increasing biomass yields. A version of the University of Alaska (UAF)/Woods Hole Oceanographic Institution (WHOI) was also completed and simulations started.
M7.2	Identify Cat 1 modeling requirements
	Q4: Design material was completed for all of the Category 1 projects including the UAF/WHOI, “Adjustadepth”, “Seaweed Paddock”, “Trophic”, and the Ocean Rainforest efforts.
7.3	Plan for Category 1 Phase II Projects
	Q4: Material was developed for 5 of the Category 1 Projects for the Phase 2 proposals
7.4	Develop Professional Science Master Degree
	Q1-Q8: This project was leveraged to develop a Practical Science Master (PSM) Degree in Ocean Food Systems at the University of New England.
7.5	Quarterly Reporting and publication
	Q1 – Q16: Final reporting is completed with this report.

2. Actual Performance

2.1. Task 1.0: Finalize project planning and establish field site

2.1.1. Milestone 1.1: Finalize the Statement of Project Objectives (2/15/2018)

The Statement of Project Objectives (SOPO) was completed as the project was started.

2.1.2. Task 1.2: Determine METOCEAN datasets: (9/1/2018).

This project was developed to utilized three sites as shown on Figure 1. The three sites were all in the waters of the State of Maine. The dates for which the leases have been obtained are listed below.

1. **Wood Island Site**: This site was first established as part of an NSF project and is being leveraged as part of this project.
2. **Exposed Site Limited Purpose Application (LPA)**: This lease was obtained on January 8, 2018 and therefore this component of the project is 100% complete.
3. **Exposed Site (4-Acre Experimental)**: The environmental site parameters for the exposed site lease was completed during reporting period of July-Sept, 2018. The application to the State of Maine was also completed and submitted during the week of September 17, 2018. The lease application was finalized during the April-June, 2019 reporting period.

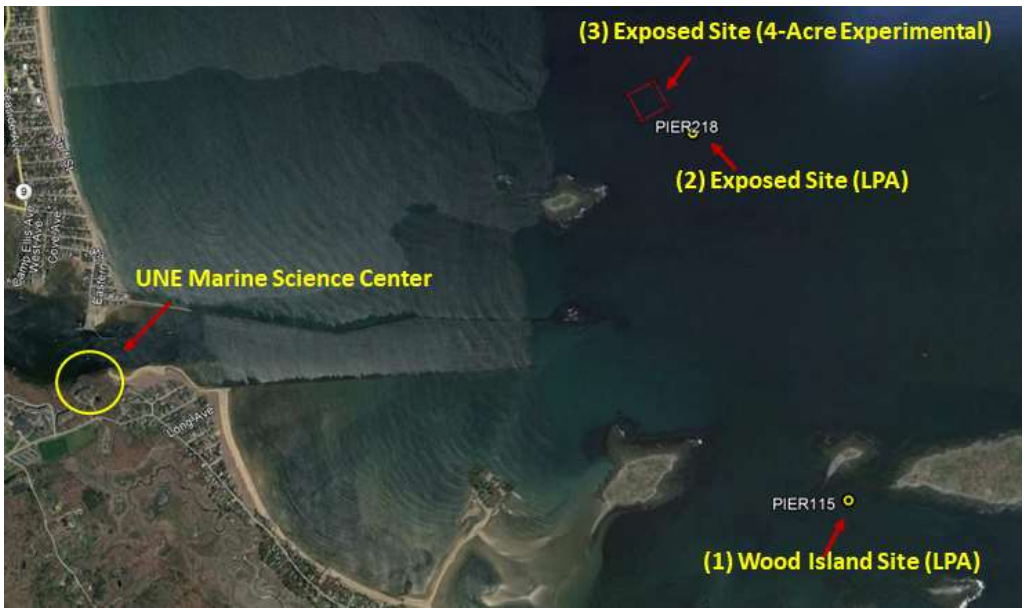

Figure 1: Three permitted sites will be used for the ARPA-E project. Note that the 4-acre site position was modified after a side-scan survey showed rock outcroppings in the northeast corner of the original site. The rock outcroppings are shown on Figure 13 and the new location of the site is shown in Figure 21. Also, during the 2018-2019 field season, the Wood Island site shifted to the east as shown on Figure 23.

The Wood Island site is designated as an LPA with the dimensions of 0.61 x 61 m in a depth of about 6 m. It has been established for 4 years producing consistent sugar kelp growth on a culture system and is being leveraged for comparison purposes as a protected site. The second

site was also an LPA, but is exposed to the Gulf of Maine. It had the dimension of 0.3 x 122 m and is in approximately 12 m of water. It was utilized during the winter 2018-2019 of this project. Both the first and second sites each have established permits. The third site on the list was also exposed and will be utilized in the third year of the project. It had the dimensions of 127 x 127 m with an area of four-acres (1.62 hectares). This lease was submitted to the State of Maine in September 2018 and approved in April 2019 for the winter of 2020 grow out season.

In the July – September 2018 quarter of the project, METOCEAN parameters were obtained completing Task 1.2. The work included the processing of the AWAC data sets, collecting sediment grab samples and completing a side-scan sonar survey of the site.

The Acoustic Wave and Current (AWAC) sensor was deployed on June 27, 2018 at a location right between sites (2) and (3) shown on Figure 2. The intent of deploying the AWAC was to measure the east- and north-going components of the tidal velocities. When these components were plotted with respect to each other, an ellipse is formed with major and minor axes. It was planned to deploy the kelp-line system at site along the major axes of the tidal ellipse. The AWAC was configured to measure 0.5 m bins obtaining 3-min averaged velocity 3-minute components every 10-minutes. Since the region was dominated by the M_2 semi-diurnal tide, only a week was necessary to resolve the orientation of the tidal ellipse. Normally, the instrument would be deployed for two months to resolve the top tidal constituents, however, due to the amount of lobster fishing gear currently that takes place at this location, the decision was made to minimize deployment time and therefore potential interaction with lobster pot gear.

Figure 2: AWAC and sediment sample locations from field survey conducted on 27-Jun-18. Note that the 4-acre site position was modified after a side-scan survey showed rock outcroppings in the northeast corner of the original site. The rock outcroppings are shown on Figure 13 and the new location of the site is shown in Figure 21.

During the reporting period from July – September 2018, the AWAC was recovered (on July 11, 2018) and the datasets were downloaded and processed. Recall that the AWAC was set to collect current profile vectors at 0.5 m depth bins from 0.9 to a maximum of 8.4 m above the acoustic transducers. The datasets were processed to examine the tidal velocity components of the north- to the east-going components (degrees true). When these components are plotted with respect to each other, the orientation of the tidal velocity ellipse can be obtained. This

orientation was needed to develop a strategy of the mooring system orientation for deployment. Tidal velocity component results (North- vs. East-going) are shown on Figure 3. On the Figure, the black squares represent the data for all profile depths, the red circles represent the depth-averaged components and the blue dots represent the calculated tidal components from harmonic analysis, which consists primarily of the M2 tide due to short time series.

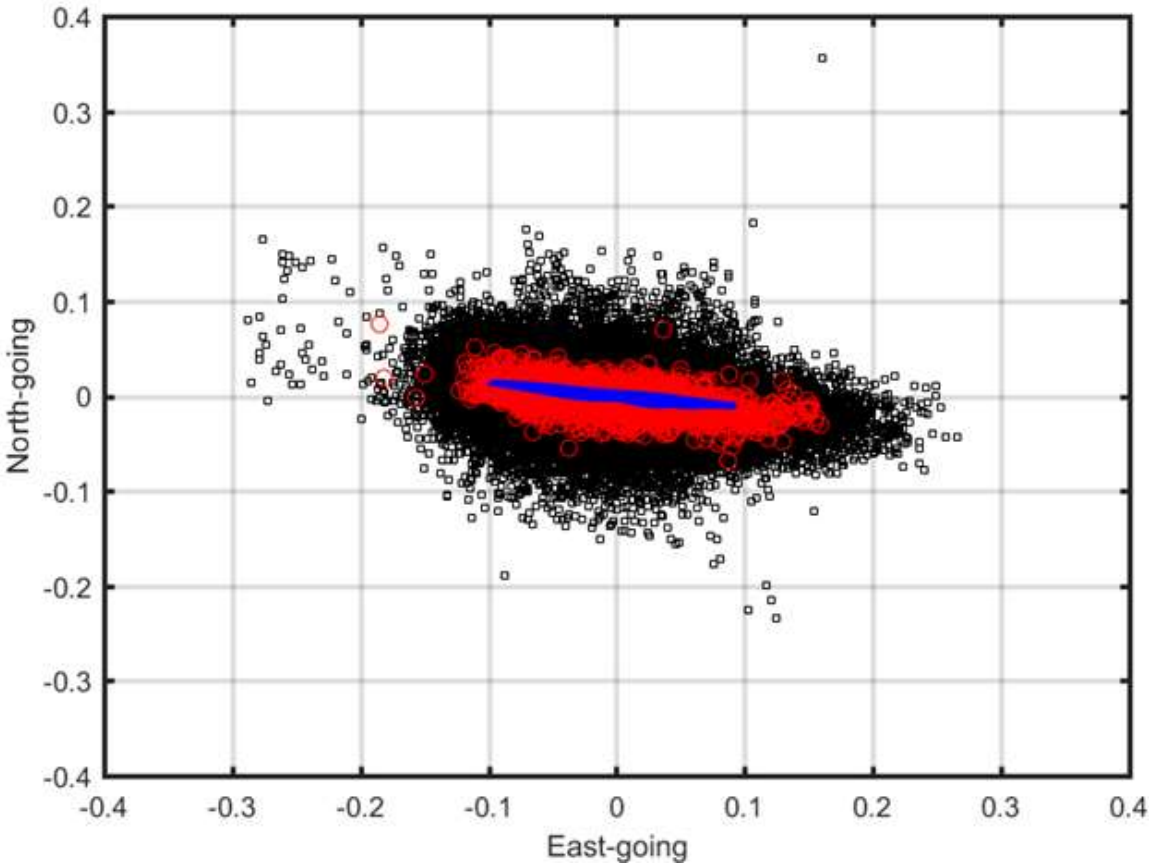

Figure 3: Tidal velocity component results (North- vs. East-going). The black squares represent the data for all profile depths. The red circles represent the depth-averaged components. The blue dots represent the calculated tidal components from harmonic analysis which incomplete due to short time series.

The profile dataset was further processed to examine the surface velocities. The surface velocities were examined since these values would have the highest impact of drag forces on the kelp farming system. The surface component currents and speed results are shown on Figure 4. The data set shown represent an average of bin locations from the MSL of 2.2 to 3.7 m. Typical speeds measured were below 0.2 m/s with the maximum at 0.27 m/s. This value was considerably lower than the design current at 1 m/s that has been used for the design of open ocean aquaculture systems in the region (Fredriksson et al., 2004). However, this data set only represented a period of 2 weeks during the summer months. Additional AWAC deployments were conducted as a part of Task 4.3 with the datasets being assessed to refine the design current condition. Recall that the objective of this summer deployment was to obtain the tidal ellipse so

the orientation of the system to be deployment could be communicated in the Experimental Lease Application.

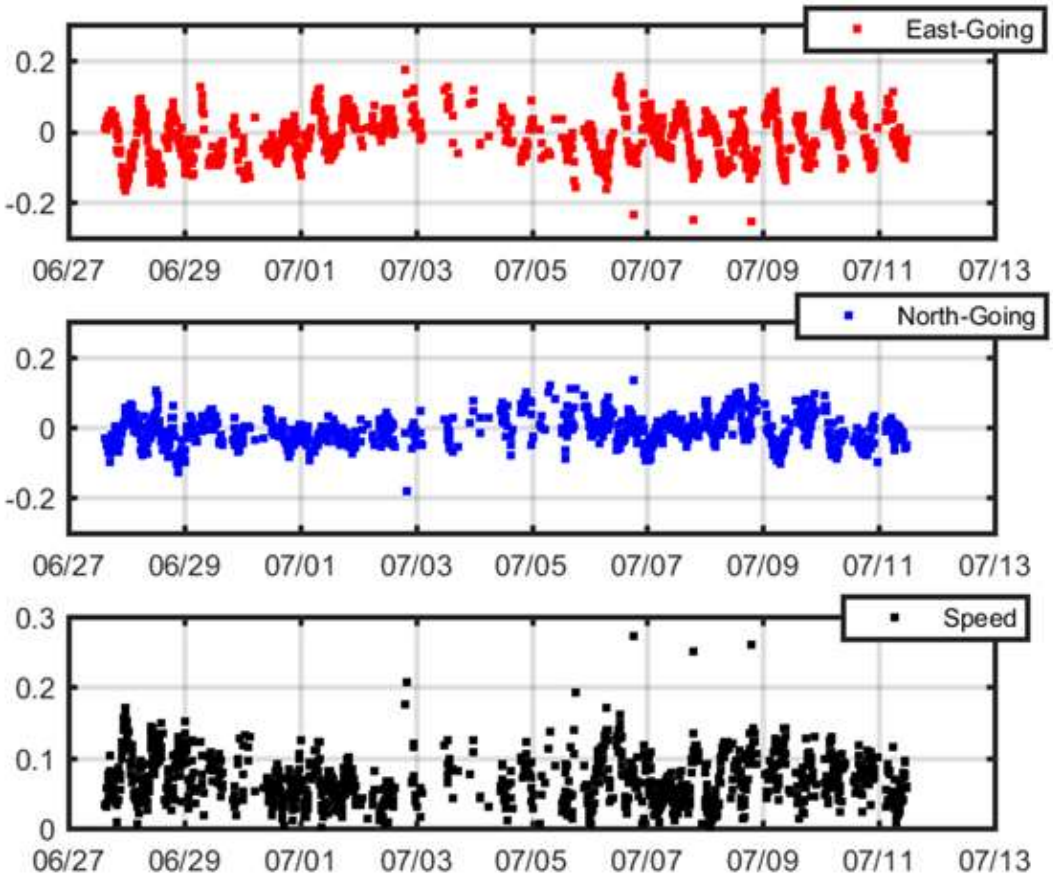

Figure 4: Surface component currents and speed. The dataset shown represent an average of bin locations that represent the depths from MSL of 2.2 to 3.7 m.

Return period analysis was also done to develop a design wave condition for the Saco Bay aquaculture sites. The technique involves utilizing existing long-term datasets complemented with measurements and modeling results if possible. The design wave condition was developed by utilizing datasets from the National Data Buoy Center (NDBC) Portland buoy, the U.S. Army Corps of Engineers, Wave Information Study (WIS) model hindcast and from an Acoustic Wave and Current (AWAC) sensor deployment in Saco Bay near the site. These dataset locations are also shown Figure 5. In addition to these datasets, information was also obtained from model simulations described in Xie et al., (2016) and used for comparison purposes.

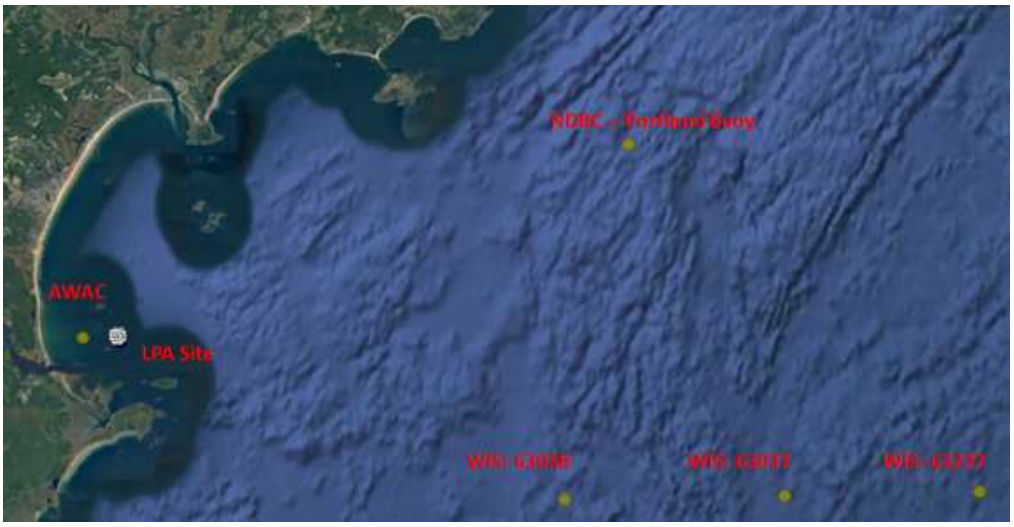

Figure 5: The local wave data sources that were used to develop a design condition for the longline system design for the exposed LPA site in Saco Bay.

One of the primary sources of wave information was obtained from the National Data Buoy Center (NDBC), Portland buoy (https://www.ndbc.noaa.gov/) 44007. During the April-June 2018 reporting period, 35 years of maximum wave condition information was downloaded from the website (Table 3) for return period analysis.

The return period analysis follows the approach described in Goda (2010) for extreme data points applying Wiebull distribution functions. The Weibull distribution functions were applied with the significant wave height data sets (i.e. energy-based H_{m0}) consisting of yearly values (Table 3) as to estimate return period statistics. The conditional form of the Weibull Distribution is given as

$$F\left(H_{max} \le \widehat{H}_{max}\right) = 1 - e^{-\left(\frac{\widehat{H}_{max}-B}{A}\right)^{k}} \quad (1)$$

where $F\left(H \le \widehat{H}_{max}\right)$ is the probability of $\widehat{H}_{max}$ not being exceeded. Also, in equation (1), B is a location parameter, A is a scale parameter and k is a shape parameter. The plotting-position formula can be obtained from equation (2) as shown by Goda, (2010),

$$F\left(H_{max} \le \widehat{H}_{sm}\right) = 1 - \frac{m-0.20-\frac{0.27}{\sqrt{k}}}{N+0.20+\frac{0.23}{\sqrt{k}}} \quad (2)$$

where $F\left(H_{max} \le \widehat{H}_{sm}\right)$ is the probability of m^{th} maximum wave not being exceeded, H_{sm} is the m^{th} value in the ranked maximum wave height, m is the ranked yearly maximum wave height value = 1, 2, …., N, and N is the total number of events during the length of the record. The scale and location parameters, A and B, are obtained using linear regression analysis described by the following relation,

$$H_{sm} = Ay_{sm} + B, \text{ m = 1, 2,…,N,} \quad (3)$$

where y_m is the reduced variate defined as,

$$y_m = \left\{-ln\left(1 - F(H_s \le H_{sm})\right)\right\}^{1/k} \quad (4)$$

The location and scale parameters are then used to find the return periods (years), T_r for each of the ordered maximum wind speeds (H_{sr}),

$$H_{sr} = Ay_r + B \quad (5)$$

where $y_r = \left[\ln\left(\lambda T_r\right)\right]^{1/k}$, and λ is the average number of events per year. Using a shape parameter value of k = 2, the maximum wave height distribution, as a function of the return period is plotted on Figure 6. Shown on the Figure are the estimated 25-, 50- and 100-year storm wave conditions. Note that the Patriots Day Storm (H_{m0} = 9.64 m) is estimated to have a return period of about 60 years based on this technique.

Table 3: The largest yearly storm events from the NDBC Portland Buoy (44007). The Patriots Day Storm occurred on April 16, 2007.

Date	Wind Spd (m/s)	Wind Dir (degT)	H_{m0} (m)	T_p (s)	T_{ave} (s)	Wave Dir. (degT)
4/4/1982	-	-	4.8	8.3	7.2	-
2/8/1983	13.4	10	6.8	12.5	9	-
2/29/1984	11.1	77	6.7	11.1	8.6	-
2/13/1985	6.2	160	6.3	11.1	8.6	-
12/3/1986	99	999	6	10	8.2	-
1/23/1987	13	160	6.1	11.1	8.3	-
2/13/1988	16	80	7.3	11.1	9	-
11/17/1989	16	160	4.1	9.1	7.2	-
1/30/1990	15.8	28	5.2	11.1	8.2	-
10/31/1991	15.1	28	6.9	14.3	10.7	-
12/13/1992	16	32	6.8	14.3	9.7	-
3/14/1993	16.9	21	7	11.1	8.7	-
1/4/1994	14.1	3	5.6	11.1	8.7	-
11/15/1995	13.9	33	7.3	12.5	9.6	-
10/21/1996	15	81	7	11.11	8.59	-
1/28/1997	16	180	6.14	9.09	7.59	-
2/19/1998	12.4	39	5.59	10	7.9	-
3/22/1999	15.9	127	5.58	10	7.54	-
3/22/2001	15.1	55	6.69	11.11	8.66	-
11/17/2002	13.8	12	5.87	11.11	8.87	-
12/7/2003	18	17	7.09	12.9	9.02	-
11/29/2004	13.9	130	5.06	10	7.13	-
5/24/2005	17.8	65	5.95	11.43	7.85	-
10/28/2006	17.7	142	6.28	10	7.84	-
4/16/2007	-	-	9.64	11.43	9.28	-
11/26/2008	9.9	127	6.23	10.81	8.51	106
12/9/2009	16	91	6.21	10	7.81	113
2/26/2010	18.9	77	11.7	12.12	10.25	125
4/17/2011	16.2	148	5.87	10	7.88	-
12/27/2012	0	180	8.12	12.12	9.85	-
3/8/2013	-	-	6.4	12.12	9.52	-
12/10/2014	14.7	31	5.37	12.12	8.67	78
1/27/2015	17.2	6	5.05	12.9	8.23	39
2/17/2016	12.1	177	4.77	10	7.52	156
1/24/2017	12.9	20	6.05	12.9	9.2	88

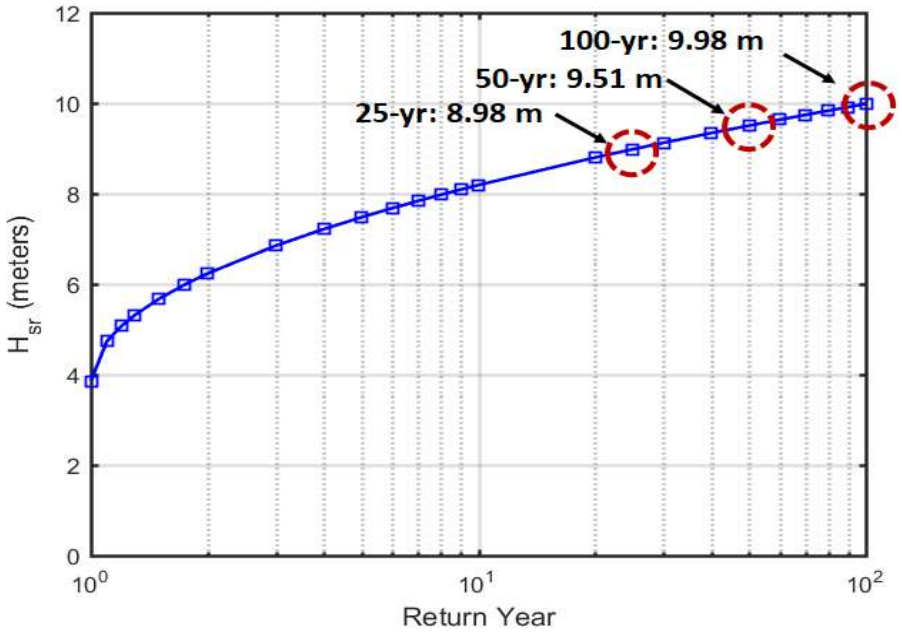

Figure 6: Return period significant wave height statistics for the NDBC 44007 buoy near Portland Maine. Statistics will have to be adjusted for the Saco Bay sites.

Information from the U.S. Army Corps of Engineers was also used in the analysis in which publish wave hindcast datasets as a part of the Wave Information study (WIS) available at http://wis.usace.army.mil/. Wave hindcast information was obtained from the three offshore station shown on Figure 5. The WIS website provides the results of wave return period analysis. The results from the station 63038 are shown on Figure 7.

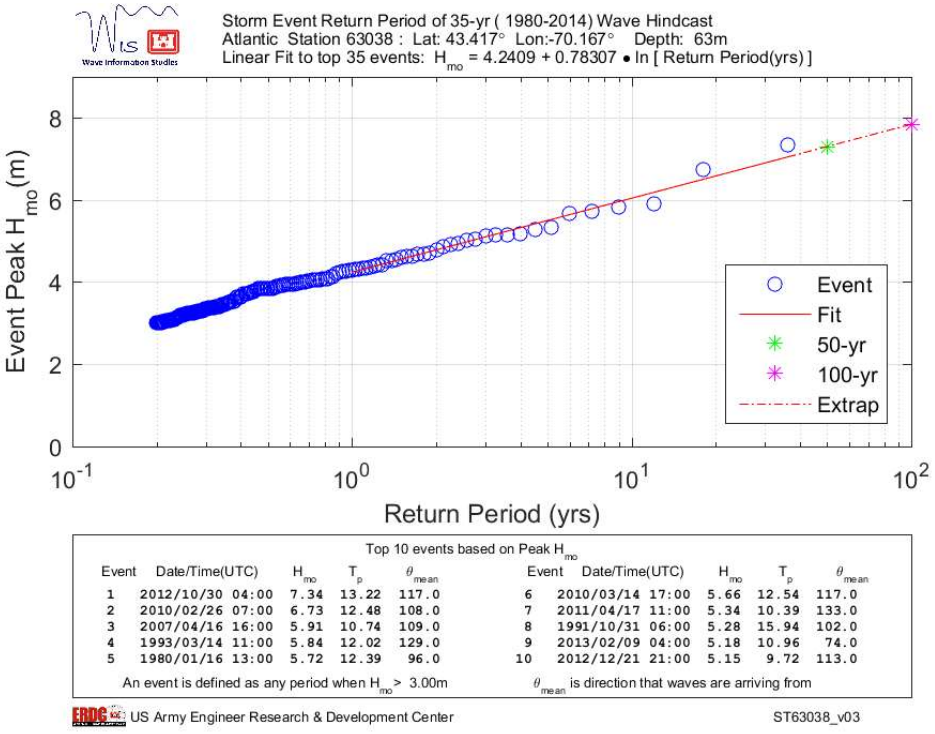

Figure 7: Return period analysis from the WIS station 63038 website at http://wis.usace.army.mil/.

The Figure shows that the Patriot's Day Storm was the third highest event in a period of 35 years with an H_{m0} = 5.91 m, Tp = 10.74 coming from a direction of 109 degrees. These results show that that the Patriot's Day event was about a 10-year storm. While this result does not seem consistent to those obtained with the measured NDBC data sets, the information is still considered since it provides order of magnitude value H_{m0}, T_p and wave direction (θ_{mean}) information closer to the LPA site which can be used for comparison purposes. The Patriot's Day storm results from the other WIS stations (63037 and 63237) are provided in Table 4.

Table 4: WIS hindcast information from the Patriot's Day storm.

WIS Station	Depth (m)	H_{m0} (m)	T_p (s)	Wave Direction (deg)
63038	63	5.91	10.74	109
63037	100	6.07	10.75	108
63237	118	6.19	10.75	108

To establish the conditions of the Patriot's Day storm in Saco Bay, a data set obtained during winter of 2015-2016 was also considered. During this winter, an AWAC was deployed in a bottom-mounted frame at 43.47047°N and 70.36642°W in Saco Bay. The instrument was deployed on November 12, 2015 and recovered on April 14, 2016, though only enough memory was available on the instrument to collect data until March 25, 2016.

During the deployment, the AWAC was operated in wave-measuring-mode where velocities, pressures and surface tracking datasets were acquired in bursts at the beginning of each hour. Each burst collected wave data at a rate of 1 Hz for 1024 samples (17.47 minutes) using the techniques described in Siegel et al. (2006), Siegel (2007) and Pedersen and Siegel (2008). The dataset was processed with instrument software that incorporates the Maximum Likelihood Method (Krogstad, 1988) modified for use with surface tracking (Pedersen et al., 2002) to obtain the wave spectral parameters including the energy-based significant wave height (H_{m0}) and peak periods (T_p). The processing software also determined the average height of the top 1/3 waves (H_s) from each surface-track time series. Both the H_{m0} and the H_s are forms of the significant wave height with the former being obtained from the 0th moment about the spectral energy density curve and latter a statistical peak counting entity. The values for both the H_{m0} and H_s are shown on Figure 8 for each burst of measurements.

The spectral curves (not shown) obtained from the measurements represent the distribution of energy density as a function of wave frequency (f) in units of cycles/s. The frequency for which the highest value of energy density occurs from each burst of measurements is the peak frequency (f_p). The dominant wave period (T_p) is then calculated as $1/f_p$ and is shown on Figure 8 for each burst. The data sets from Figure 8 show that the maximum values of H_{m0} and $H_{1/3}$ were 2.08 and 2.02 m, respectively. A maximum wave height was also measured to be 3.1 m. From Figure 8, the dominant periods were between 2 and 13 seconds. Throughout the deployment period, the average wave direction was from 83 degrees (magnetic) or 98 degrees (true).

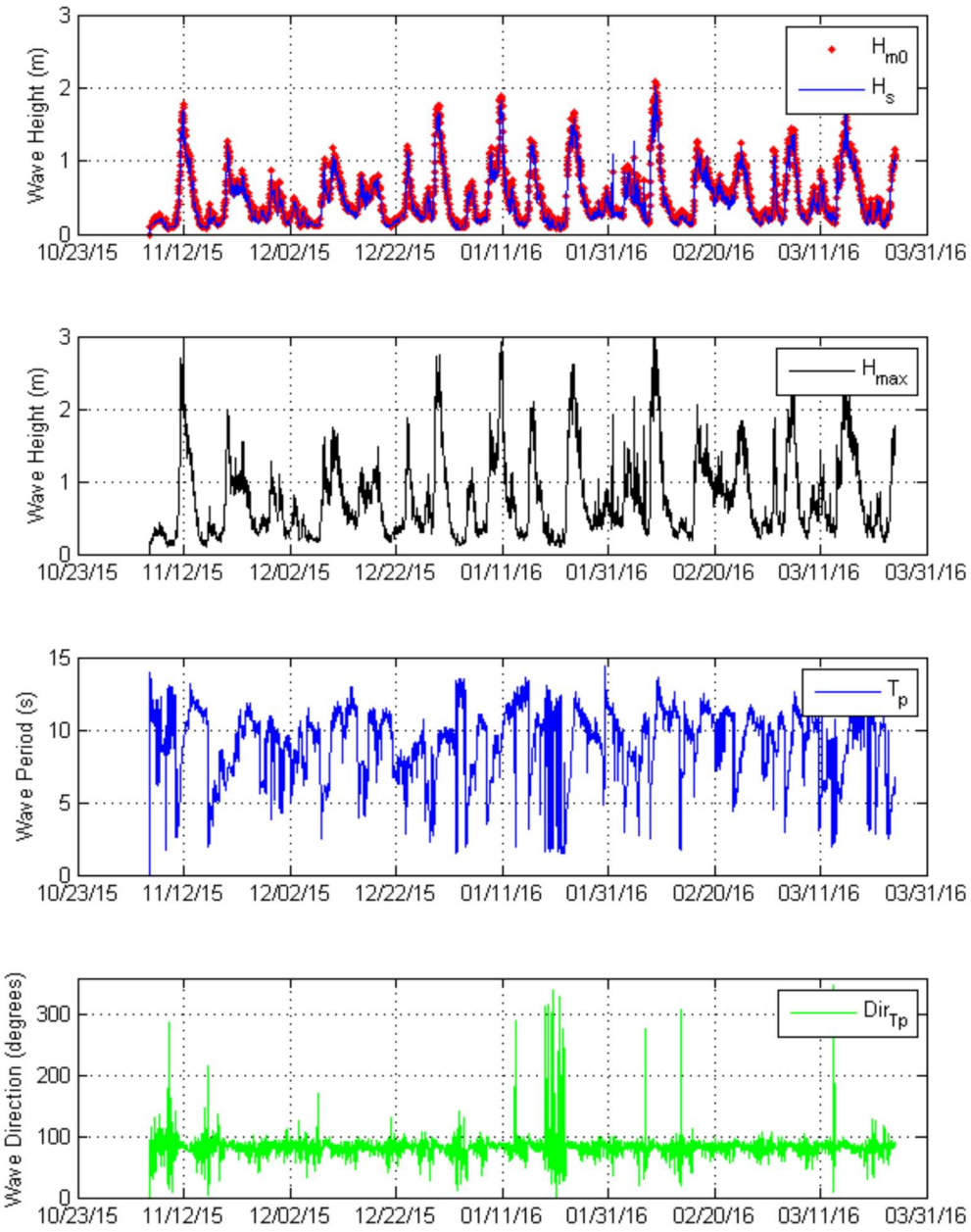

Figure 8: Wave data obtained from an AWAC deployed in Saco Bay during the winter of 2015-16.

The AWAC deployed in Saco Bay was placed approximately 1 km inland, due east from the LPA site. The H_{m0} and H_s data shown on Figure 8 was replotted with the H_{m0} data from the NDBC for the same time (Figure 9). Examining the datasets shown on Figure 9 indicate a strong correlation with mostly a magnitude difference. This shows that the events that influence the conditions at the NDBC Portland site also influence Saco Bay. With wave transformation processes such as refraction and bottom-friction energy dissipation, the wave heights measured in Saco Bay are less than measured at the Portland buoy. To examine this difference, a ratio of the mean NDBC H_{m0} (1.18 m) to the mean AWAC H_{m0} (0.51 m) was calculated with a resulting value of 2.32 defined here as the mean-ratio-factor.

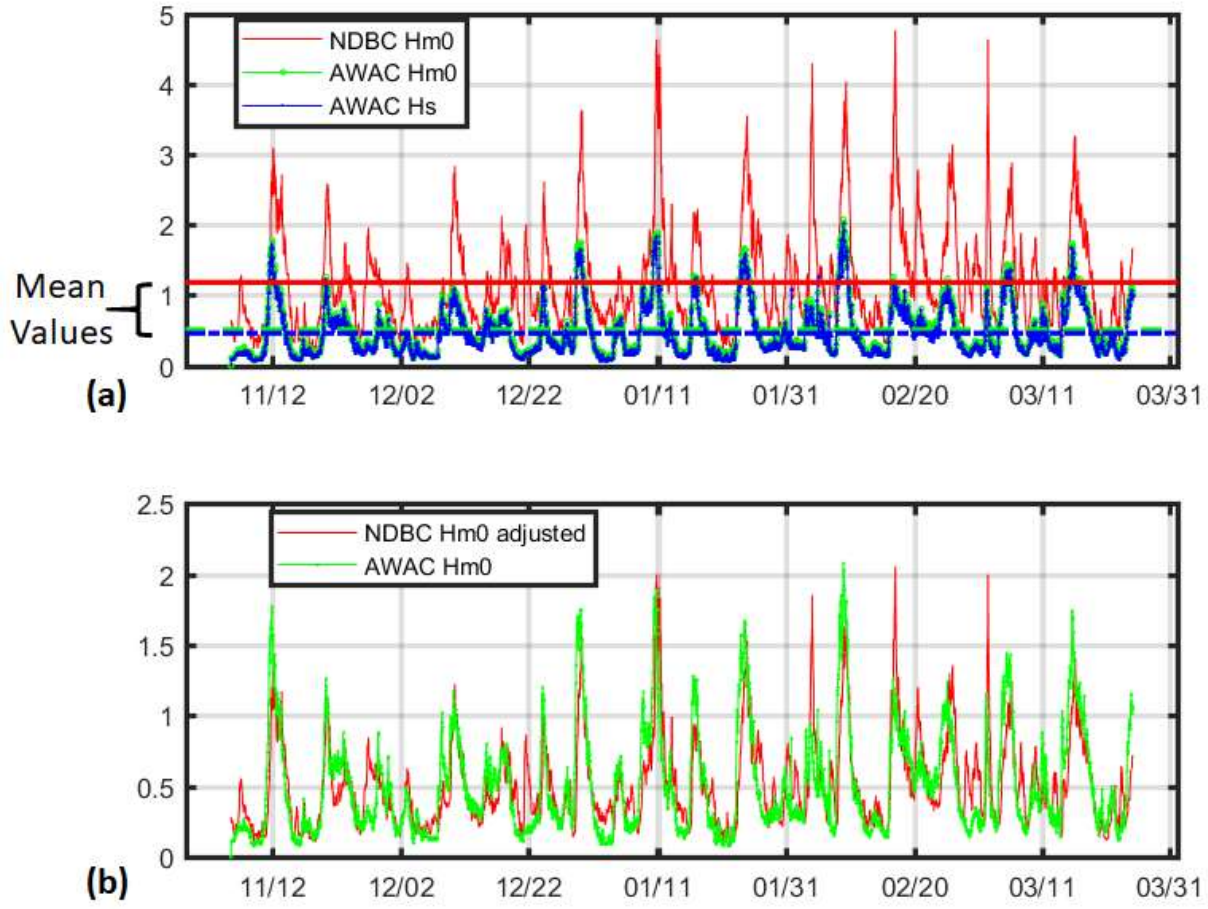

Figure 9: (a) Comparison of the NDBC data with measured AWAC in Saco Bay. (b) Adjusting the NDBC data with the mean-ratio-factor.

The NDBC H_{m0} dataset was reduced with the mean-ratio-factor as shown on Figure 9(b). While not all peaks match exactly, the resulting time series does look representative of the measured AWAC H_{m0} since the mean values are the same. The mean-ratio-factor was then applied to the Patriot's Day storm value of 9.64 m providing a possible Saco Bay H_{m0} value of 4.2 m. It was then assumed that the dominant period for this storm was 11 seconds with a direction coming due east after considering the WIS information.

Wave model simulations were also done by Xie et al., (2016) to describe the Saco Bay wave field for the same Patriots Day storm of 2007. The wave model results were compared with NDBC buoy data and shown to have reasonable results as described in Xie et al., (2016). From the model results, it was estimated that during the Patriots day storm, the significant wave height at the LPA site was 4-5 m with a direction coming from due east without and with storm surge Figure 10a and b, respectively). These results seem to match with the approach used with the mean-ratio-factor.

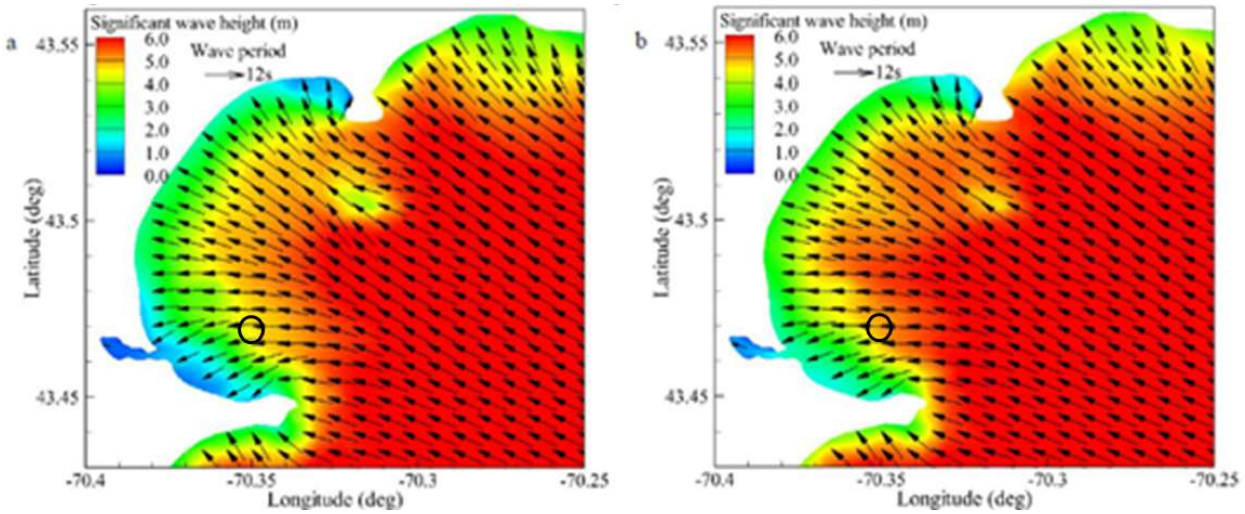

Figure 10: Patriot's Day storm wave simulations for Saco Bay as described in Zou and Xie (2016) without (a) and with (b) estimate storm surge. Note that this figure is taken directly from the paper and should not be published without permission. It is included here for internal descriptive purposes.

To examine the relationship between H_{m0} and the maximum wave height (H_{max}), the wave time series, obtained with the surface track capability of the AWAC, was examined for the largest condition. The largest condition occurred on February 8, 2016 at 2148 UTC. The surface elevation time-series is shown on Figure 11.

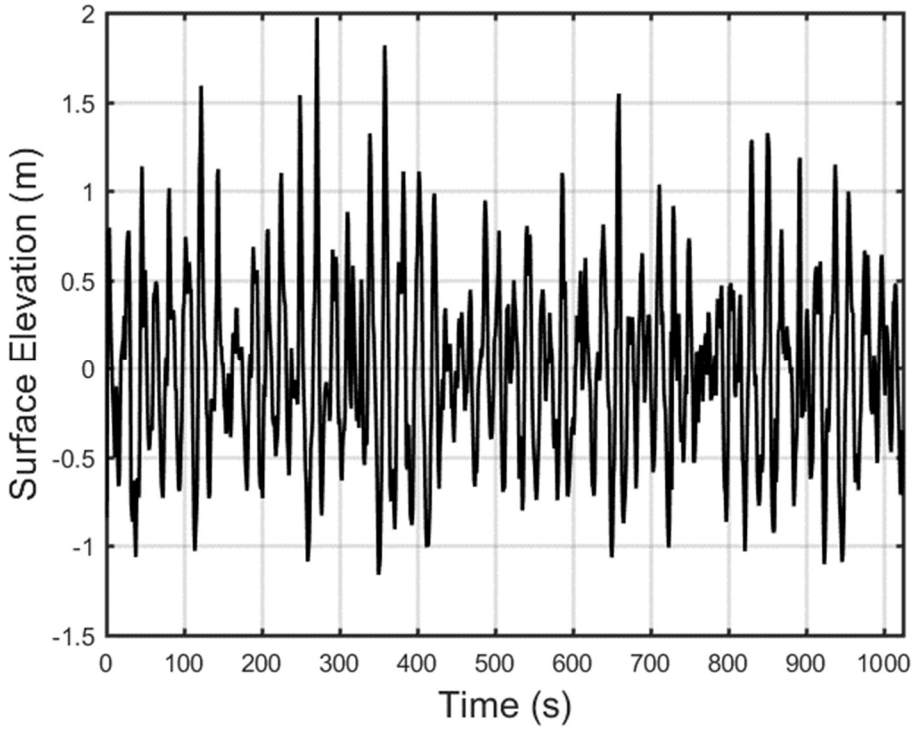

Figure 11: Measured surface elevation time series from the surface track function of the AWAC obtained on February 18, 2016 at 2148 UTC.

During this particular storm, the measured maximum wave (H_{max}) was 3.1 m. The corresponding H_{m0} and H_s values were 2.08 m and 2.02 m, respectively. With the dataset, the H_{max}/H_{m0} ratio was calculated to be 1.5. Applying this factor to the design wave condition with an H_{m0} = 4.2 m (associated with the Patriot's Day storm), the maximum wave (H_{max}) was determined to be 6.3 m. These wave height characteristics are associated with a dominant period of 11 seconds. This became the design wave condition for the exposed Saco Bay site.

Next, the NDBC that was adjusted for the Saco Bay site was processed to obtain corresponding return period statistics. The same approach as described in equations (1) through (5) were applied to the Saco Bay dataset as shown on Figure 12. This dataset shows that the Patriot's Day storm has return period near 60-years.

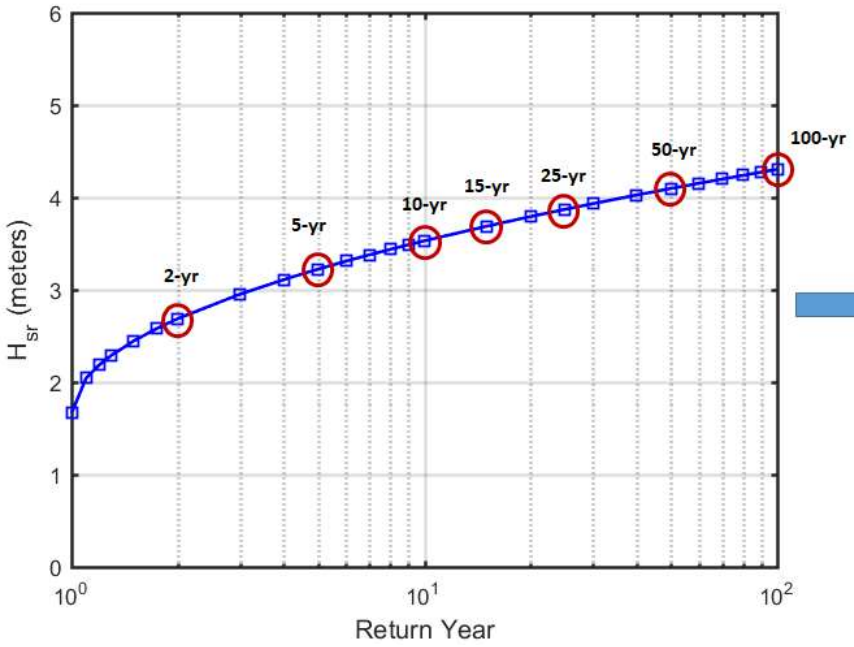

Significant Wave Heights (m)	
Return Year	Saco Bay
2	2.69
5	3.22
10	3.53
15	3.69
25	3.87
50	4.10
100	4.30

Figure 12: Saco Bay significant wave height return period analysis.

On June 27, 2018, bottom sediment samples were obtained from the proposed experimental lease sites. Each sample was collected with a 1728-G30/ 1728-G40 Petite Ponar Grab. Sample 1 (43°28.1881, 070°21.05833) and Sample 2 (43°28.24005, 070°21.15086) were both comprised primarily of very fine sand. Both samples were processed using a 32910 Fieldmaster Screen Sieves Kit, which incorporates a series of seven sieves ranging from 5 to 250 microns. 84% of Sample 1 and 83% of the Sample 2 total mass collected in the 230-micron sieve. Other than hand, there were very small traces of living organisms. Only 3% of Sample 1 and 9% of the Sample 2 mass contained invertebrate remains like, soft shell clam, mahogany clam, green urchin spine and slipper shells. The seafloor under the proposed experimental lease site revealed no living organisms or plant material that would be disturbed. The grainsize analysis results from the two samples are provided on Table 5.

Table 5: Grainsize sediment sample results obtained during the Apr-June 2018 reporting period.

Sample 1					
Mesh Size	Grain Size (mm)	Phi Size	Raw Weight (g)	Individual Weight Percent	Cumulative Weight Percent
5	4.00000	-2.0	2.79	0.49	0.49
10	2.00000	-1.0	7.36	1.30	1.80
35	0.50000	1.0	17.3	3.07	4.87
60	0.25000	2.0	6.32	1.12	5.99
120	0.12500	3.0	30.38	5.38	11.37
230	0.06300	4.0	476.27	84.41	95.78
250	0.05800	4.1	19.78	3.51	99.29
325	0.03125	5.0	4.01	0.71	100.00
		Total	564.21	100	

Sample 2					
Mesh Size	Grain Size (mm)	Phi Size	Raw Weigth (g)	Individual Weight Percent	Cumulative Weight Percent
5	4.00000	-2.0	0	0.00	0.00
10	2.00000	-1.0	0.15	0.06	0.06
35	0.50000	1.0	2.19	0.92	0.98
60	0.25000	2.0	2.01	0.84	1.83
120	0.12500	3.0	10.99	4.62	6.44
230	0.06300	4.0	197.35	82.87	89.32
250	0.05800	4.1	8.24	3.46	92.78
325	0.03125	5.0	17.2	7.22	100.00
		Total	238.13	100.00	

During April-June 2018, inconsistent weather and strong winds made obtaining clear footage through side-scan sonar difficult. Since the experimental site is not protected, there was strong wave action in an area currently with a high density of lobster gear. Plans were therefore made to organize another field survey before the end of July to obtain side-scan sonar and ROV video footage of the seafloor at the experimental lease site are ongoing.

A successful side-scan and ROV video footage at the site was obtain in July 2018. The side-scan survey encompassed the entire 4-acre site of the Experimental Lease location. The side-scan survey results shown on Figure 13 indicate that there are no features of significance within the area (e.g. rock outcroppings). Therefore, there are no spatial restrictions to the placement of ground tackle.

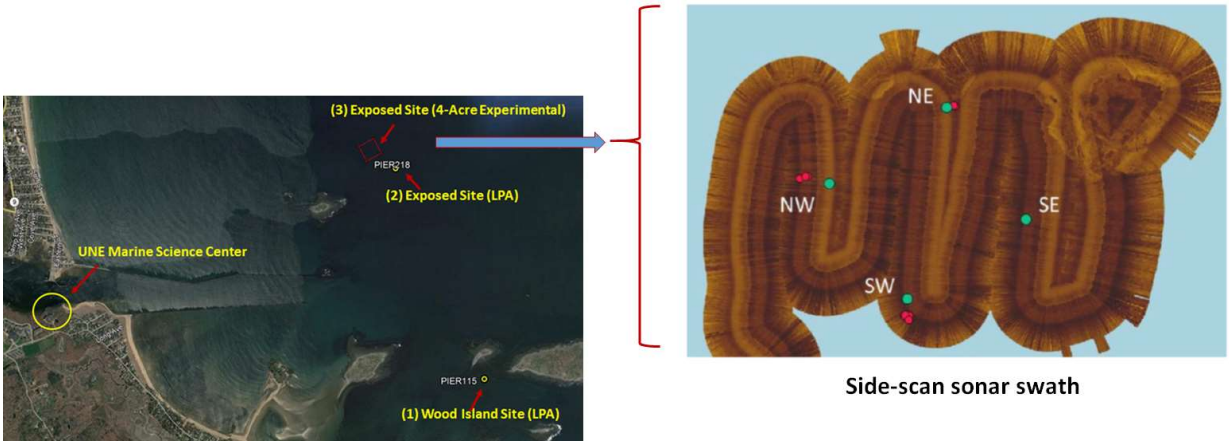

Figure 13: A side-scan sonar survey was conducted covering the entire 4-acres of the experimental lease location as defined by the NE, SE, SW, and NW corners.

In addition to the sediment samples and the side-scan survey, an ROV was used to investigate three of the four corners of the Experimental Lease site. The position of the ROV was determined by triangulation with acoustic transducers. To triangulate the position of the ROV, four surface transducers were mounted off the gunnel of the research vessel with the target transducer mounted on the GoPro attached the ROV. Still photographs of the three locations are shown in Figure 14.

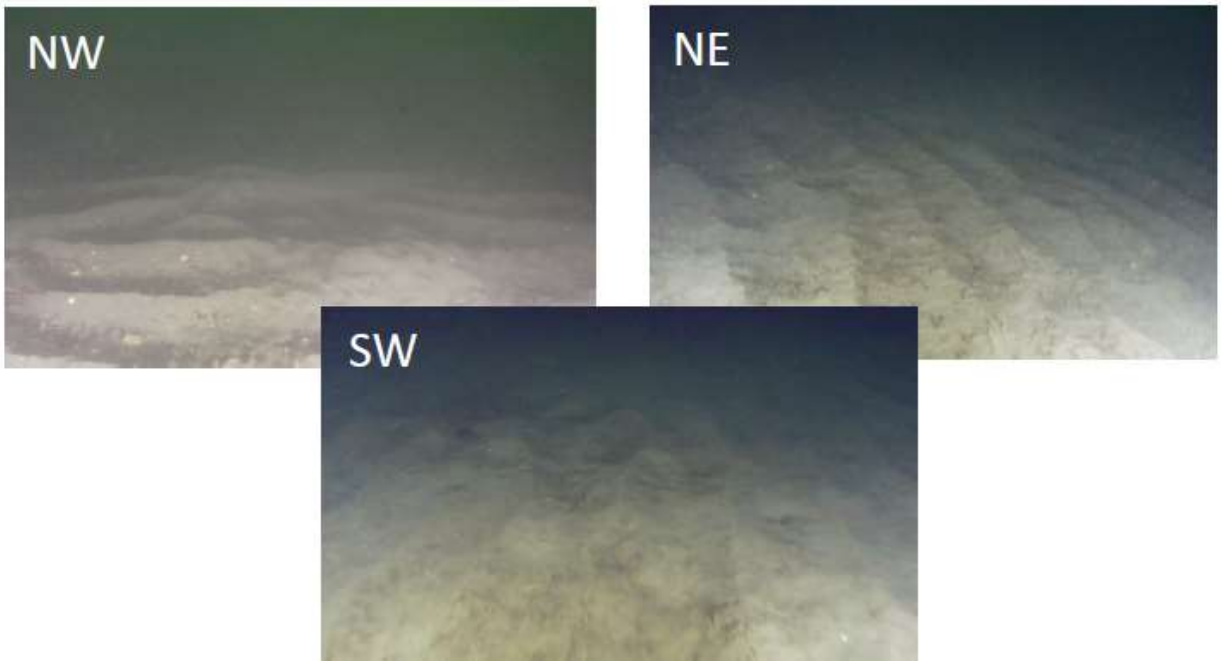

Figure 14: GoPro videos from an ROV was obtained from three of the four corners of the Experimental site. The survey indicated a mostly sand bottom ideal for drag embedment anchors.

With the sediment samples, the side-scan survey and the ROV footage, it was clear the bottom at the Experimental site consists mostly of sand with no detectable rock outcroppings. Therefore, the design strategy was confirmed to use drag embedment anchors at the site. Typically, drag embedment anchors perform best in seafloor bottom types consisting of sand. It is expected that during the winter months, however, that sand movement from the beach area will migrate in the offshore location. This could potentially cover the ground tackle and bottom instruments deployed. From the results of this survey, the position of the 4-acre site was modified to avoid the rock-outcroppings. The new location is shown on Figure 21.

2.1.3. Milestone 1.3: Obtaining State of Maine Permits (2/15/2018)

The first LPA was obtained from the Department of Marine Resources (DMR) for the State of Maine (license # PIER218) on February 15, 2018. At this time, an application for a State of Maine Experimental Aquaculture Lease in Saco Bay was submitted. In October 2018, UNE received from DMR a request for revision which was submitted in December 2018. Once the permit application was submitted, the Maine Department of Marine Resources reviewed the application and replied on March 6, 2019 that the materials submitted were complete. According to State of Maine policy, the application was made public allowing comments to be submitted until April 8, 2019. Since fewer than three comments were submitted, a public hearing was not necessary and the

experimental lease application was accepted. With the experimental lease approved for the exposed site seaward of Ram Island, preparations for the array system effort were initiated for the 2019-2020 season.

With the Wood Island site available after 2018-2019 season, the LPA was modified to accommodate the portion UNH/Trophic system design for 2020-2021. Components of the UNH/Trophic system that was deployed at the LPA site are shown in Figure 15.

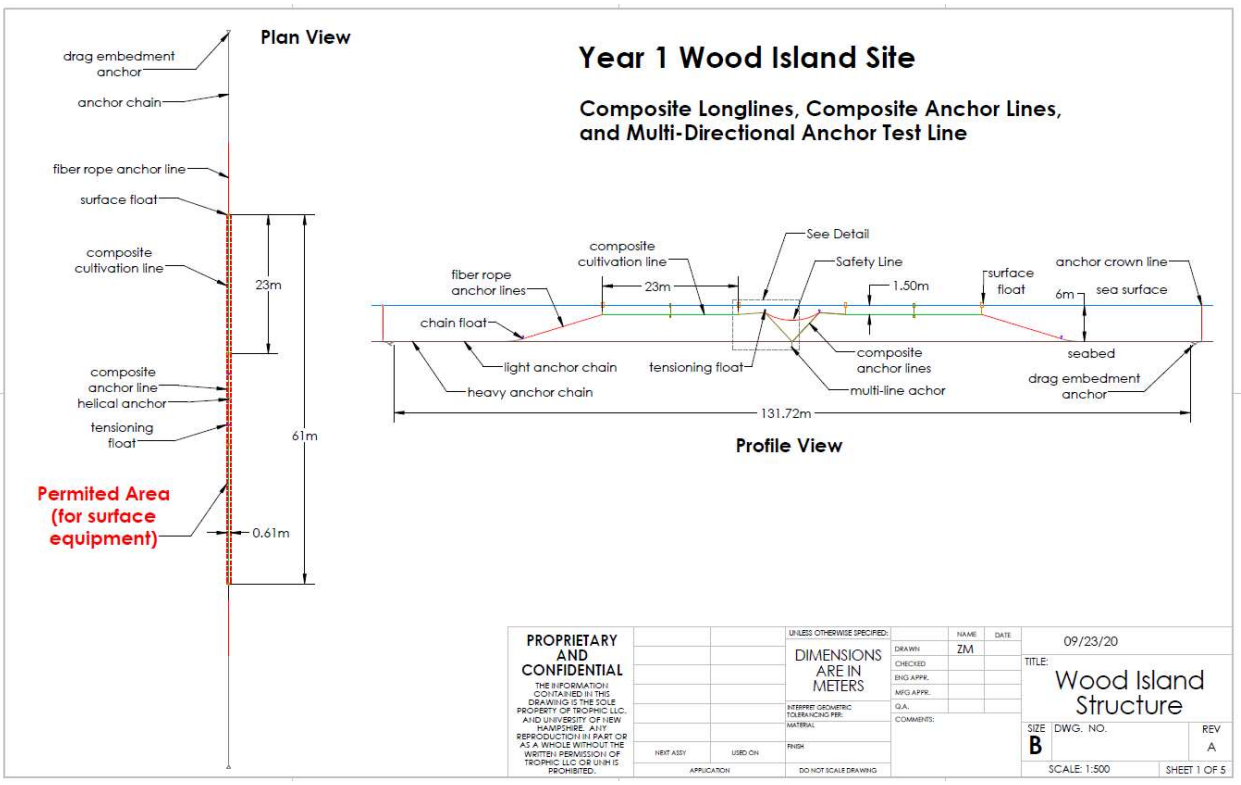

Figure 15: A schematic of the UNH/Trophic system deployed at the UNE LPA site in Saco Bay, Maine.

After two successful UNE deployments at the Ram Island site (2019-2020) and (2020-2021) a gear amendment was developed with the UNH and Trophic team for the winter season 2021-2022. The new lease with the gear modifications was approved for the Ram Island site on June 3, 2021.

2.2. Task 2.0: Design, Seed & Deployment of scalable systems

2.2.1. Task 2.1: Design single-line system (10/1/2018)

As described in Task 1, a preliminary design for the system to be deployed at the exposed site LPA was needed for the permit application. In this process, environmental conditions were developed to estimate loading from waves and currents prior to performing Hydro-FE simulations and for first-iteration validation of the model. Wave-current loading on a potential culture system for the LPA site on Figure 16 was performed using Morison equation integrated along the longline direction defined as the x-direction such that,

$$\frac{df}{dx} = \frac{1}{2} C_d\left(L_{kelp}\right)\rho[|u(x,z) + U|(u(x) + U)] + C_m\rho\left(\frac{V_{kelp}}{L_{model}}\right) a_x(x,z). \quad (6)$$

In equation (6), L_{kelp} is the nominal value of 3 m used to obtain the drag coefficient of C_d=0.35 from the axial tow tests described in Task 5. The volume of the kelp (V_{kelp}) per axial distance (x) was obtained by finding the mass of the 1 m model (L_{model}) divided by the composite mass density. The inertia coefficient (C_m) was found from the planar motion mechanism tank tests described in Task 5 equal to (C_a + 1) = 1.2, where C_a is the empirical added mass coefficient. Equation (6) was integrated in the x-direction over the length of the longline assumed 120 m. The integrated quantity also assumed that the crest of the wave was located at leading edge of the longline where the origin was set at x=0 m. The horizontal wave velocity (u) and acceleration (a_x) components are a function of both x and z according to

$$u(x,z) = \frac{\pi H}{T} K_x(z) cos(kx) \quad (7)$$

and

$$a(x,z) = \frac{2\pi^2 H}{T^2} K_x(z) sin(kx) \quad (8)$$

where

$$K_x(z) = \frac{cos\ (kz+\ \ )}{sin\ (kd)}. \quad (9)$$

In equations (7) – (9), z = -2.5 m and is the depth of the longline, k=(2π/L) is the wave number defined by the dispersion relation,

$$\omega^2 = (gk)\tanh(kd)\,, \quad (10)$$

where L is the wavelength, d is the depth, ω=2π/T, g is the acceleration constant and T is the wave period. Equations (7) – (10) are based on linear wave theory (Dean and Darlymple, 1984). A calculation was performed with the integrated version of equation (6) assuming the H=6 m, T = 12 seconds and U = 1 m/s. The horizontal integrated force was calculated to be 35.7 kN (8022 lbf). This design value was used to size the upper limit of the load cell capacity and to specify components for a preliminary design for cost estimates and Hydro-FE simulation modeling.

The preliminary configuration and component list for the longline system was based on initial design load calculations described in Task 2, with an estimated combined wave/current loading of 25.7 kN (8022 lbf). The initial design approach was to use a submerged longline at 2.5 m and spread mooring making a 45° angle with the bottom at a depth of 12 m (Figure 16). To reduce

potential snap loads, it was decided to pretension the longline to a value no more than 450 N (100 lbf).

The numbered details on Figure 16 show the components that were first considered for the longline system and include (1) drag embedment anchor, (2) ground chain, (3) pyramid anchor, (4) anchor line, (5) submerged flotation and (6) seeded longline. The components are being specified based on the estimated design load of 36.12 kN (8621 lbf). Model simulations for LPA design were completed after the models for the Category 1 systems were completed for the "Halftime" meeting at the end of July.

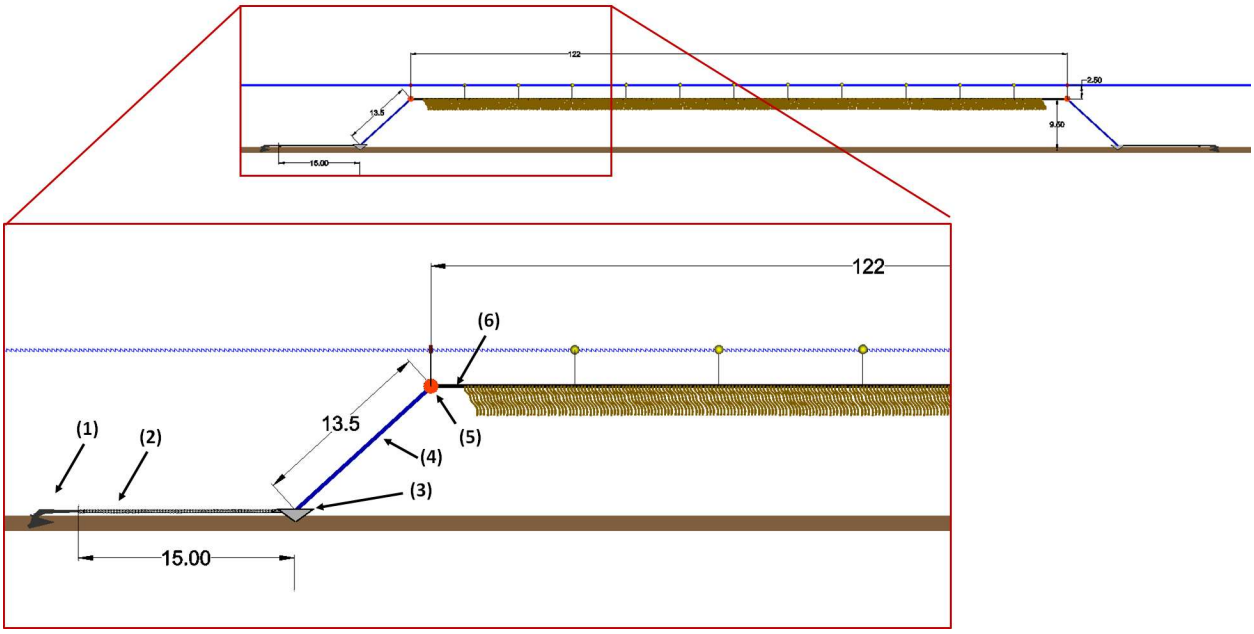

Figure 16: Preliminary configuration for the longline system to be deployed at the exposed LPA site.

Additional design work was conducted for the LPA site during the July-September 2018 reporting period. After a team design review, it was determined that the configuration shown in Figure 16 would be difficult to deploy and service with the available research vessels. The system was modified so that the pyramid anchor (#3 in Figure 16) was not necessary to force horizontal loads on the drag-embedment anchor. The modified system shown on Figure 17 replaced the pyramid anchor with a chain catenary. The weight of the chain in the catenary was designed to offset the flotation at the corner of the longline. The pretension of the anchor leg and the longline are determined by the weight of the chain, the buoyancy of the corner floats and the geometry of the system. The pretension value was determined with catenary equations by first considering the amount of flotation at the corner buoys to be equal to 50 lbf (F_{buoy}). The mooring leg was designed to incorporate 5/8" long-link chain weighing 3.4 lbf/ft (P_{chain}). With these two values, the length of chain that is pulled up into the water column to form the catenary (S_{chain}) is calculated with

$$S_{cha} = \frac{F_{buoy}}{P_{chain}} = 14.7\ feet. \quad (11)$$

Since approximately 52 feet of rope was incorporated into the mooring leg with the longline at a depth of 8 feet and making an angle to the bottom of 32 degrees, the horizontal pretension in the longline (T_H) and the anchor-leg (T_{anchor}) was calculated at 80 and 94 lbf, respectively. With these parameters, the horizontal (x_{cat}) and vertical (y_{cat}) components of the catenary was calculated as

$$x_{cat} = \frac{T_H}{P_{chain}} sinh^{-1}\left(\frac{P_{chai}\ S_{chain}}{T_H}\right) = 13.89 \text{ ft} \quad (12)$$

and

$$y_{cat} = \frac{T_H}{P_{chain}}\left(cosh\left(\frac{P_{chain}S_{chain}}{T_H}\right) - 1\right) = 4.22 \text{ ft}, \quad (13)$$

which defines the shape of the catenary shown in Figure 17. The chain catenary (with the corner floats) pretensions the entire system to reduce snap loads. The catenary also incorporates a restoring force and compliance in the system.

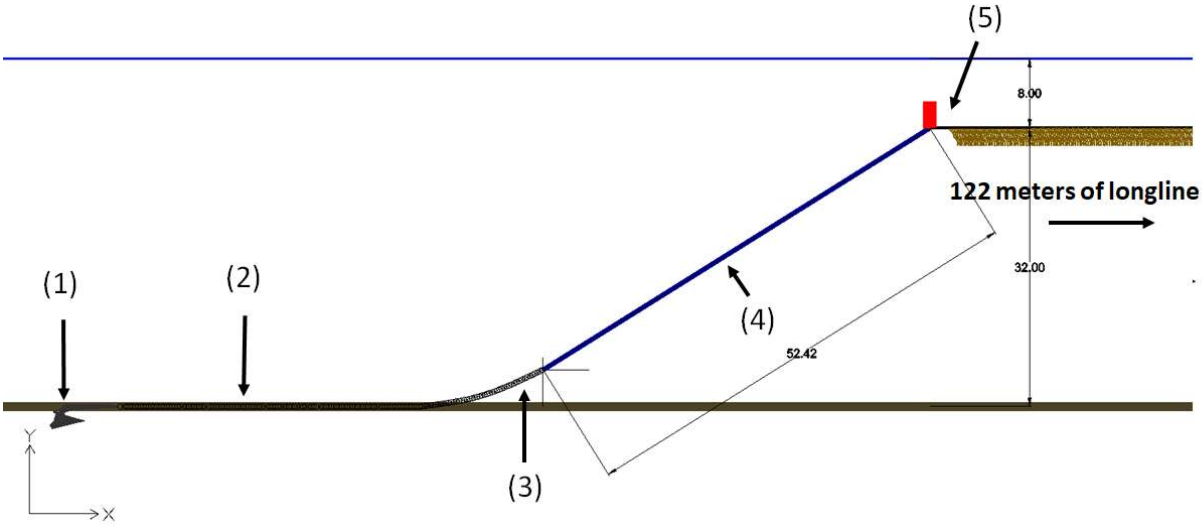

Figure 17: The second design iteration of the longline mooring leg incorporating a chain catenary.

The design loads were calculated assuming a tidal current of 1 m/s and a maximum wave height of (H_{max}) of 6.3 m (see Task 1). This extreme storm condition was estimated as the maximum wave in Saco Bay from the Patriot's Day Storm. For the single culture line case, random wave simulations were conducted using the Hydro-FE model and compared with calculation from an integrated horizontal Morison equation approach. The structural properties of the kelp were taken from prior measurements of fresh samples of *Saccharina latissima*. Hydrodynamic properties were derived from prior tank tests of a physical model of a 1 m section of a kelp culture line with 3 m long kelp fronds. Normal and axial drag coefficients, as well as added mass coefficients, estimated from tow tank and forced oscillation testing of the physical model (Task 5). These physical and hydrodynamic properties were incorporated into Hydro-FE. Simulation time-steps are shown on Figure 17(a) and (b) with tension results and enhanced visualization, respectively.

Simulations were done with the Hydro-FE model for both nylon and polyester mooring line resulting in tension values between 40 and 35 kN (9000 and 8000 lbf), respectively. This value was compared with the integrated horizontal Morison equation approach, drag and inertia force on just the longline were a value of 31 kN (7000 lbf) was calculated. By considering both of these approaches, a design load of 35 kN (about 8000 lbf) was estimated for the single line system for the extreme storm event.

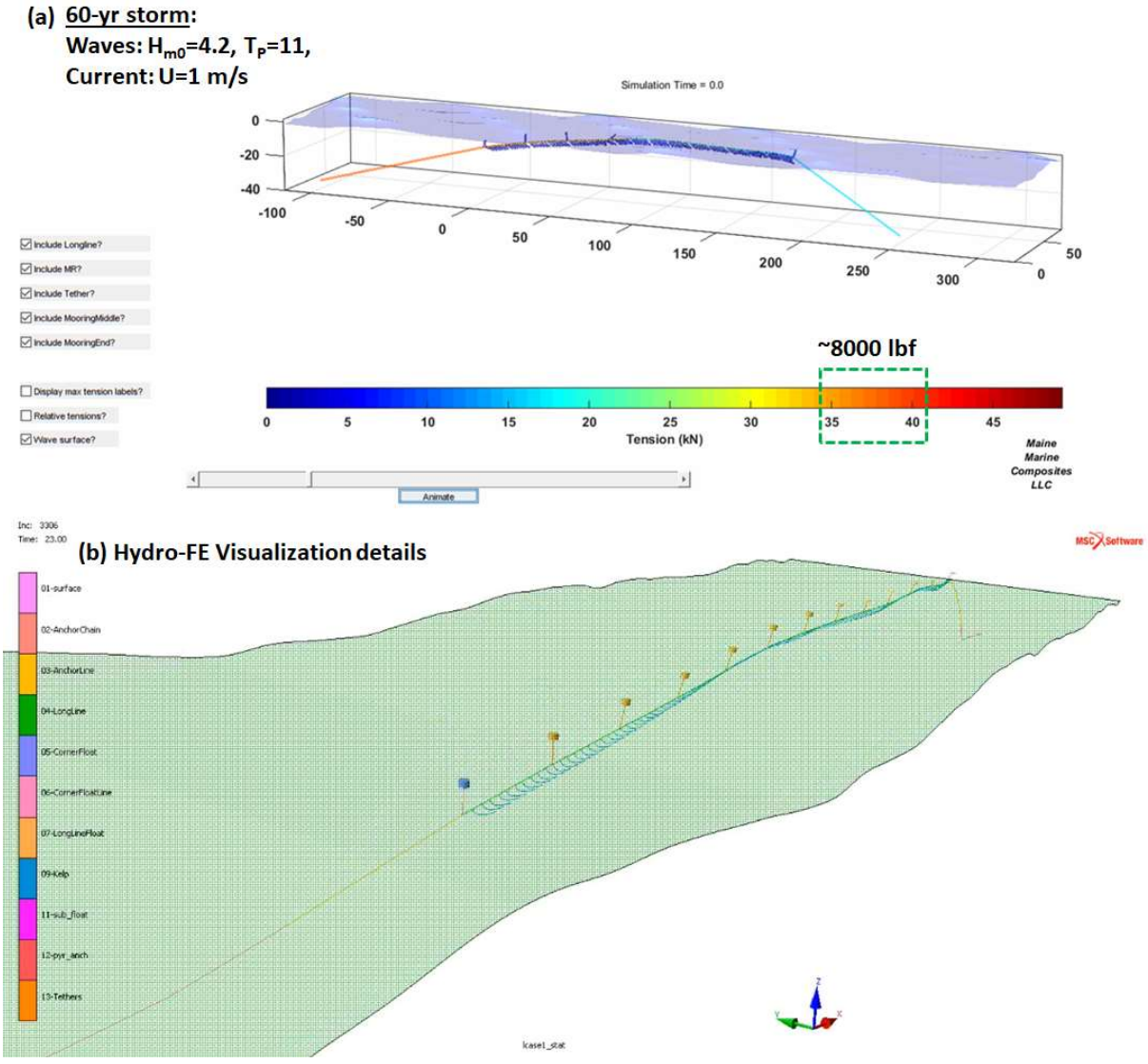

Figure 18: (a) Hydro-FE model of single kelp longline designed for the exposed LPA site for 60-year storm conditions. (b) Hydro-FE visualization details.

With the design load, the following component specifications were obtained.

1. 110 lbf Claw anchor: Holding Power is estimated between 6000 and 7000 lbf.
2. 25 ft of 5/8 longlink chain (3.4 lb/ft): Working Load Limit: 6900 - 9750 lbf
3. 15 ft of 5/8 chain: Using catenary equations the angle going up to the buoy is 32 deg. This is 51 lbs in the water column, offset by the corner floats.

4. 52 ft of nylon rope (1”): Working load is 1850 lbf with a factor of safety of 12. The rope was reuse for the 2019-2020 deployment.
5. A stack of lobster floats with about 50 lbf buoyancy.

In this process, the model was also used to evaluate design alternatives for the system configuration. The model was applied to understand the effects of varying design parameters including mooring line scope, mooring pretension, mooring line stiffness (e.g. nylon versus high modulus rope), and the inclusion of clump weights on the anchor chain. The system response was also quantified for variations in environmental forcing factors including relative current and wave direction and tidal elevation. For example, Figure 19 shows the sensitivity of current angle with the resulting mooring line tension at each end of the longline.

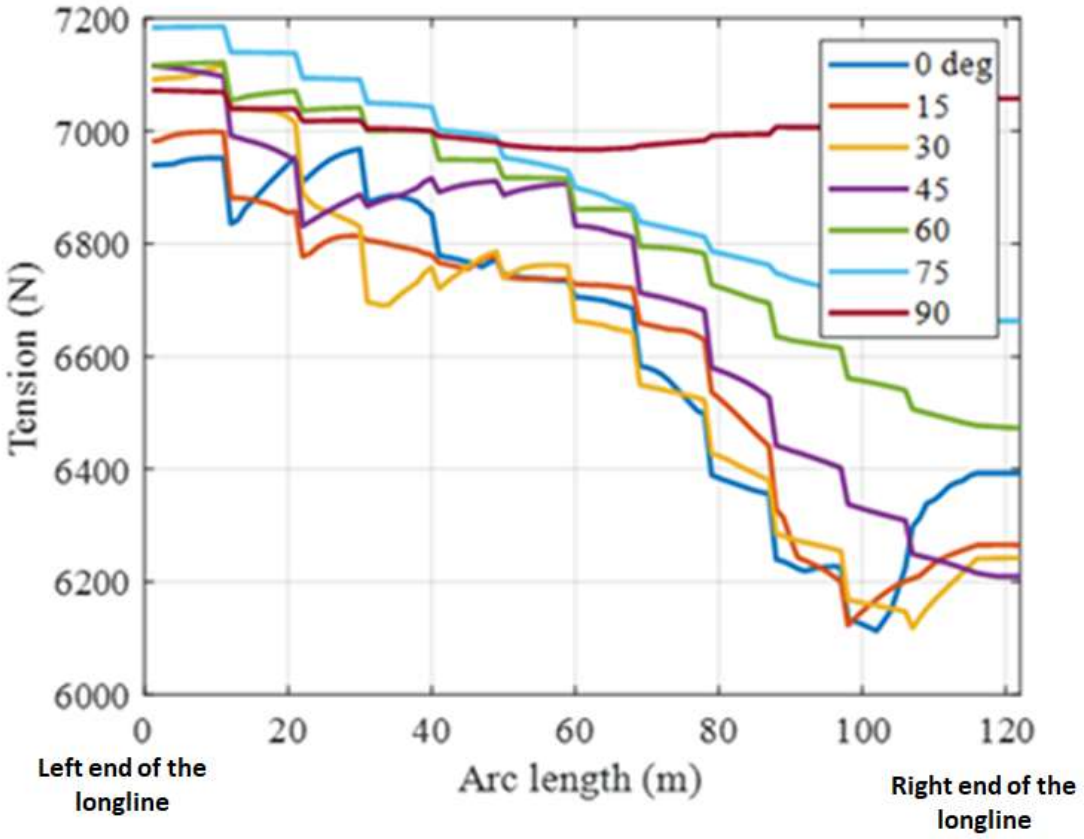

Figure 19: Example of longline tension as a function of arc length (distance along longline) and incoming current direction.

Final design work was conducted for the LPA site during the July 2018 period. Prior to deployment, review of the design shown in Figure 17 yielded an inaccurate mean depth at the LPA site. Readings from the actual site showed that the mean depth was actually 50 feet (not 40 feet) so therefore the length of the anchor leg needed to be increased to 75 feet. The geometry of the chain catenary, however, did not change. The final farm system geometry with the increase in the mooring line in each anchor leg is shown in Figure 20 (a). Not shown on the Figure

are details regarding the longline support floats and splices to accommodate the load-cells. Figure 20 (b) shows the actual system components.

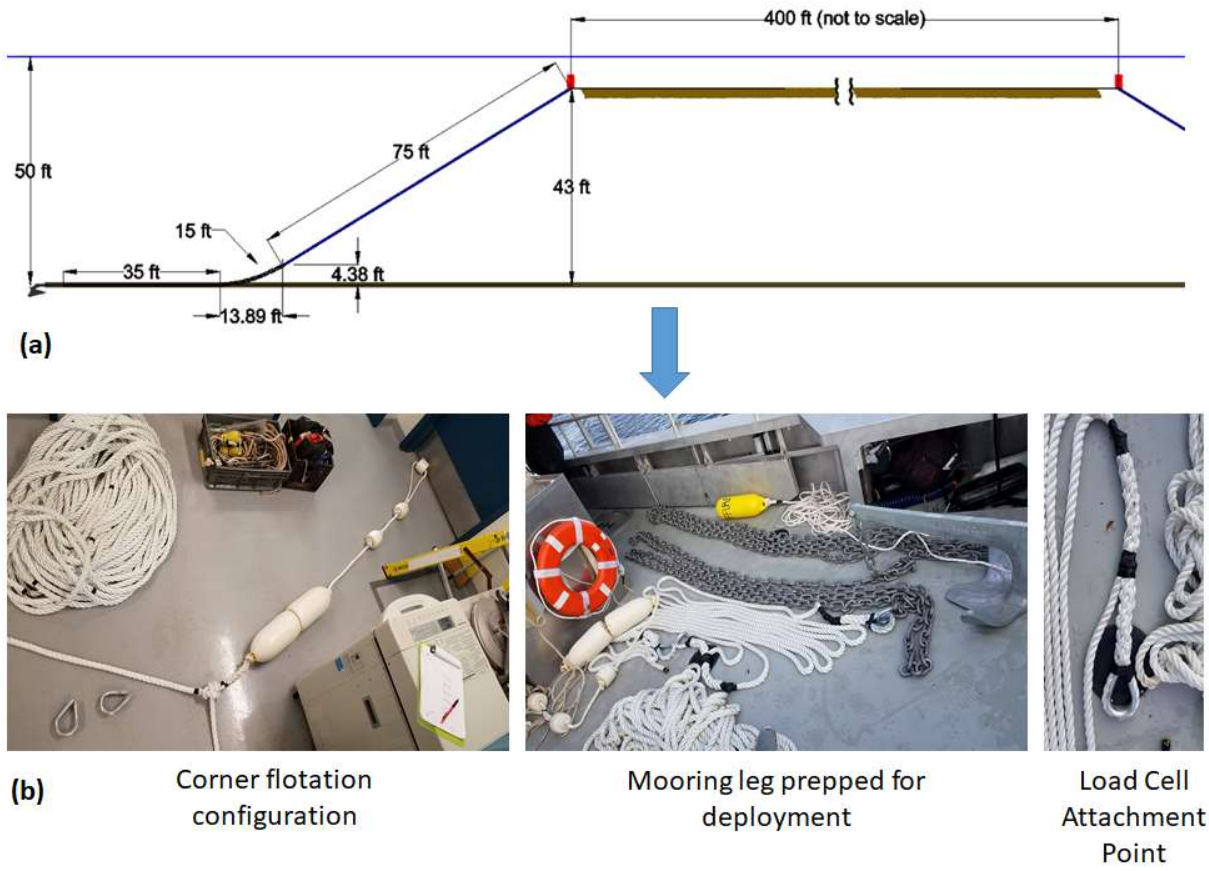

Figure 20: (a) The final LPA longline system with increased mooring line length. (b) Fabrication of system prior to deployment.

2.2.2. Task 2.2: Grow hatchery seed for single-line system (12/15/2018).

The hatchery was expanded at UNE in June 2018 moving into a larger kelp nursery space. In the improved nursery, LED light bars were installed on the walls and on a custom-made PVC frame. In addition to the 20 gallon culture tanks previously used for growing seed, a 100 gallon tank was procured as part of the expansion. A list of essential materials that were required to complete the nursery set up and allow for operation for the fall of 2018. A new batch of seeding twine was purchased that had already been spooled and treated, which happens prior to releasing kelp spores from the reproductive sorus tissue. The new hatchery set up was finalized with custom plumbing, new water pumps, the addition of Ultraviolet filters and custom-made Plexiglas lids for each aquarium. The choice to eliminate all clear tubing and switch to grade 40 PVC for the tank plumbing was installed to prevent unwanted bacteria and algae growth and thus decrease the chance of contamination within the system. Introducing Ultraviolet filters and lids for each aquarium also helped to reduce the presence of other contaminants in the nursery.

By August 2018, the nursery and seed spools were assembled and ready for full-scale kelp production. At this time, UNE was able to work closely with industry partner Tollef Olson, President and Co-Founder of Ocean's Balance LLC. Collaborating with Mr. Olson was paramount in the initial search for viable reproductive sorus tissue needed to start the kelp hatchery. After multiple trips, plenty of productive sorus tissue was collected from Casco Bay, Maine and brought back to UNE for processing.

At the UNE Marine Science Center, the wild collected sorus tissue was prepped for spore release. After selecting the desired reproductive tissue and sterilizing it, the kelp was stressed overnight in the refrigerator. The following day, the reproductive tissue was reintroduced to fresh seawater to induce the release of kelp spores. After the approximate hour-long process, a successful amount of kelp spores was released and seen under the microscope. Using a hemocytometer, active, mobile spores were counted to calculate the desired stocking density.

The UNE kelp nursery supported 10 spools of seed. The first five spools were seeded on September 10, 2018 and introduced to the hatchery on September 11, 2018. Spools 6 through 10 were seeded on September 18, 2018 and introduced to the hatchery on September 19, 2018. During September, daily management of the hatchery included recording daily salinity, temperature, and pH values while maintaining water quality in each aquarium. At minimum, weekly water changes for each tank were performed while monitoring other parameters like room temperature, light intensity and duration, aeration, and providing the essential growth nutrients.

To obtain the greatest biomass for the Ram Island LPA in the first year, UNE also purchased seed from Tollef Olsen to out-plant during the farm deployment, scheduled for the last week of October (29-31). The most viable spools were maintained in the hatchery and used on UNE's past farm location protected by Wood Island. The remaining nursery spools were donated to the Kelp4Kids program that teaches children from Peaks Island, ME how to grow and operate a seaweed farm. UNE helped the Kelp4Kids deploy their 50 ft kelp farm during the first week of November. Current hatchery protocol continued until the seed spools were deployed for farm grow-out.

Also, during the Fall 2018, UNE hosted educational and partnership visits to share our current work in the kelp nursery with others in the seaweed industry. These parties included:

- James Crimp the Hatchery Manager from Ocean Approved,
- Jaclyn Robidoux a Marine Extension Associate focusing on seaweed for Maine Sea Grant,
- Charlotte Quigley a PHD candidate working with Alaria at the University of Maine, Orono,
- Jennifer Zimmerman a representative for Sea-Bird Scientific,
- Members of the Swedish seaweed community from the University of Gothenburg and KTH Royal Institute of Technology, and
- Numerous students, parents, staff, and faculty at the University.

2.2.3. Task 2.3: Deploy and monitor seeded single-line system: (5/28/2019)

One of the major accomplishments during this reporting period was the deployment of the 122 m longline at the exposed LPA, Saco Bay site. On the first deployment day (October 30), the gear was placed at the site with the load installed on the eastern anchor leg. Two AWACs were also deployed on the eastern (exposed) side of the farm, one to measure currents and the other measuring waves and currents (but not simultaneously). The location of the AWAC instruments relative to the site are shown on Figure 21. The kelp line was also seeded and gear was placed at the site in a slack configuration at the coordinates shown on Figure 21.

The intent of deploying the instruments at this time was to obtain a load case dataset with no macroalgae. After putting all of the gear in the water and seeding the long line, it was planned to stretch out the mooring system into the design configuration. A small craft warning, however, was initiated for which all at-sea operations had to be terminated according to UNE policy. Therefore, the gear was left overnight in the slack configuration with the load cell and AWACs collecting data.

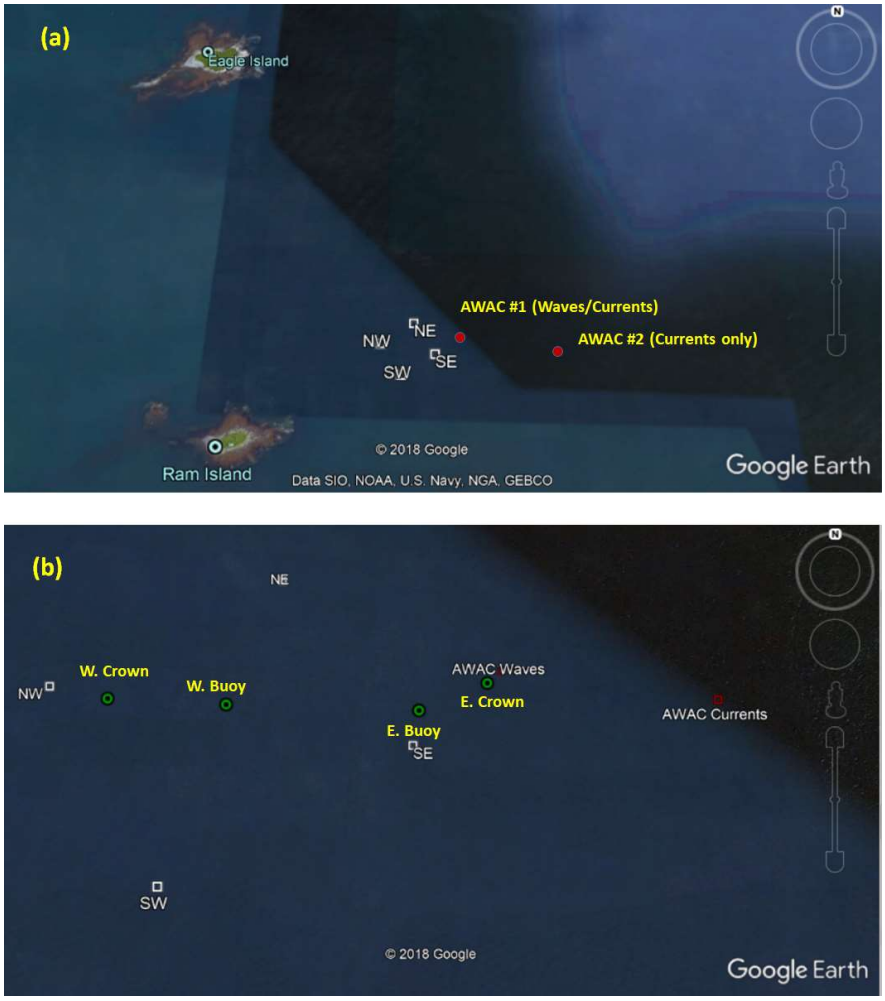

Figure 21 (a): The LPA site is within the four points of the exposed 4-acre coordinates. (b) The coordinates of the non-tensioned longline system during the instrumentation deployment.

On October 31, 2018, the small craft warning subsided and so the team went back out to the site and recovered the load-cell and the two AWACs. The datasets are described in Task 4. Once the instruments were on the vessel, the culture system was stretched out to its design configuration. After this operation was completed, a side-scan survey of the deployed mooring configuration was performed with the results shown on Figure 22 compared with a scaled drawing of the system.

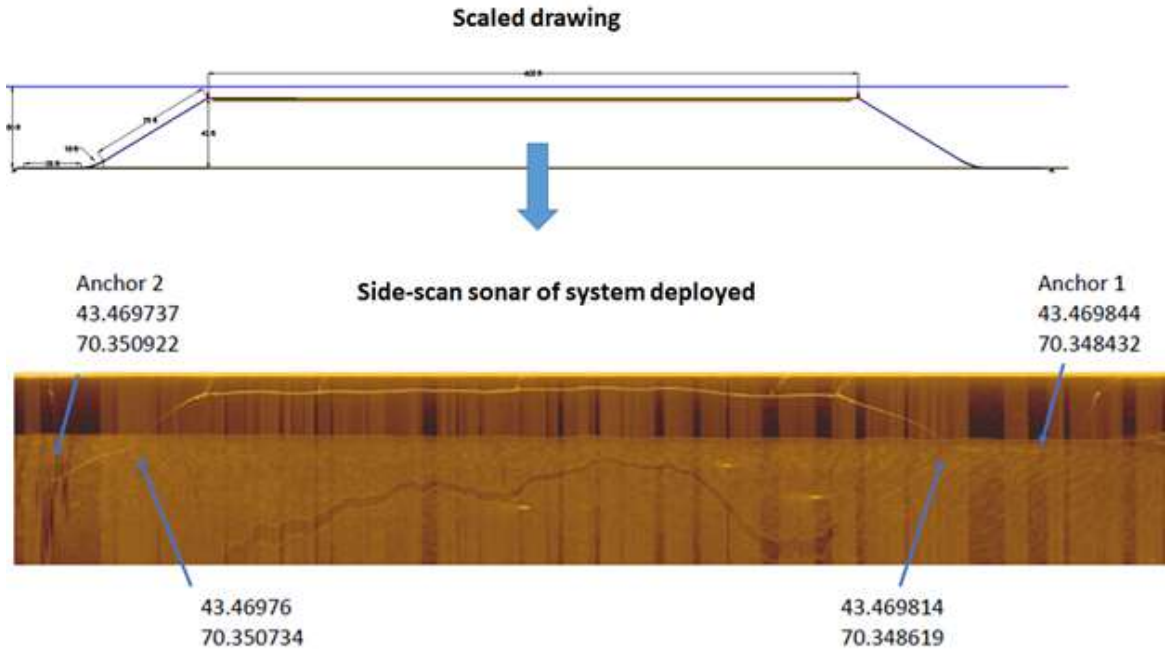

Figure 22: A scaled drawing with the side-scan sonar image of the deployed longline system at the exposed Saco Bay site in Maine.

In addition to the exposed Ram Island Kelp farm, UNE continued to support the Wood Island Kelp farm for the fourth consecutive season. On December 5, 2018, the 61 m system was deployed at the site with the coordinates of 43°27'17.64" N, 70 °20'16.404" W (Western crown line) and 43°27'17.208" N, 70 °20'11 W (Eastern crown line) as shown on Figure 23. The Wood Island system was also seeded with the same material as the Ram Island system.

Figure 23: The Wood Island, 61 m longline was deployed in December 2018 and seeded with the same material as the Ram Island longline

On December 5, 2018, the UNE team deployed the 61 m kelp farm at the Wood Island Site in Saco Bay. After this system was deployed, it was discovered during the survey of the 122 m system at the exposed site that no kelp was present, despite the farm gear being in the correct location. The original seed line was still wrapped to the culture line and correctly tensioned to minimize relative movement between the seeded twine and the rope. A consistent coating of fouling slime, however, covered the top surface of the entire culture line length, leaving a clear distinction when the culture line was shifted by hand off the long line (Figure 24). After discussion, it is hypothesized that that the kelp seed was too small to survive in this high energy, exposed location. Perhaps to grow macroalgae in stronger wave and current environments it is likely that the kelp seed needs to be larger and therefore more mature than what is already being successfully grown in protected environments.

With this new information, the field team decided that it was vital to reseed the total 122 m grow line at the exposed site. The UNE Hatchery provided two new spools that were part of the original seed batch started in the hatchery in September. After the seed outgrew the hatchery, it was moved to an above ground pool as a holding tank at the Marine Science Center. This seed had more time in the hatchery than what is normally required. Therefore, the individual sporophytes were double the size of what is ordinarily able to survive in protected environments. Since we had an early initial deployment in November, it was still early enough in the season to get a complete grow out season while reseeding in December.

Figure 24: The culture twine is being moved by hand from its original position under tension to reveal a clean section of the long line that was not fowled. This showed that the culture line is secured in place so chafing from excess movement is most likely not the cause of kelp loss.

In early February 2019, the 122 m kelp system had maintained its position at the exposed site in the configuration shown on Figure 22. The UNE field team examined the kelp on the site and verified growth. Figure 25 (a) shows the exposure of the longline system to the east and the open water of the Gulf of Maine. Figure 25 (b) shows that the kelp had grown to lengths of 10 – 30 cm.

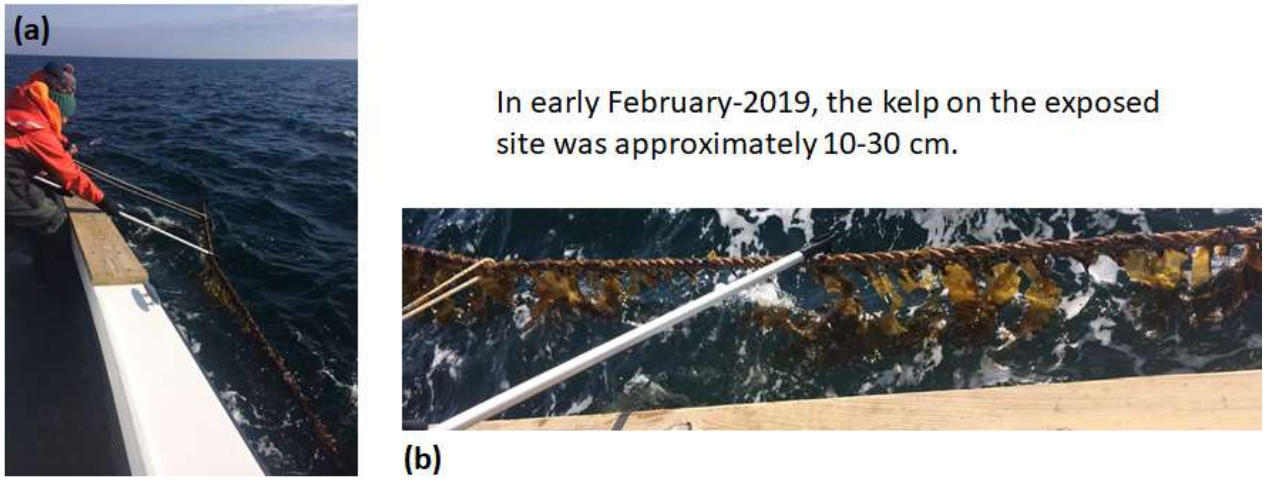

Figure 25: (a) The 122-m kelp longline was still in place at the exposed site in early February 2019. (b) The kelp on the longline had grown to lengths of 10 – 30 cm.

March 2019 in Maine began with hazardous weather conditions so the first opportunity to inspect the gear at each site was on March 20, 2019. At the site it was found that all components had survived the winter and kelp was growing along the entire line lengths on both the Ram and Wood Island sites. Starting on March 25, 2019, at least one team member visited the farm each week for routine inspections. During each visit, biological samples were collected for laboratory processing to understand overall biomass of the farm and the material properties of the kelp sporophytes. Samples were collected in 10 cm segments at east, middle and west locations along each kelp line. Within each 10 cm segments, the individual sporophytes growing on were removed and brought back to the laboratory where mass and size values were obtained. Results are provided in Task 3. In addition to collecting biological samples, instrument deployments were successfully executed through the following dates:

1. April 4-11, 2019: Wood Island site,
2. April 25-30, 2019: Ram Island site and
3. May 15-28, 2019: Wood Island site.

For every instrument deployment in 2019, a minimum of two AWACs and two Load-cell instruments were installed at the sites. Dataset results are provided in Task 4.

During each instrumentation deployment, passes were made with the R/V Sahkoki using the vessel mounted side-scan sonar. Passes were made along the north and south sides of the each of the culture lines during the three deployment days (April, 11, 25 and May 28). Clear imaging was obtained from both attempts at the protected, Wood Island site (April 11 and May 28). Clear images were not obtained, however, at the exposed Ram Island site (April 25) because of rougher surface conditions due to ocean exposure. The two sets of Wood Island site side-scan sonar images were reconstructed by L. Hayden (MS student in Oceanography at UNE) with results shown on Figure 26 and Figure 27. The reconstructed images show the kelp growing along the line, the flotations elements and the load cells deployed on both mooring legs.

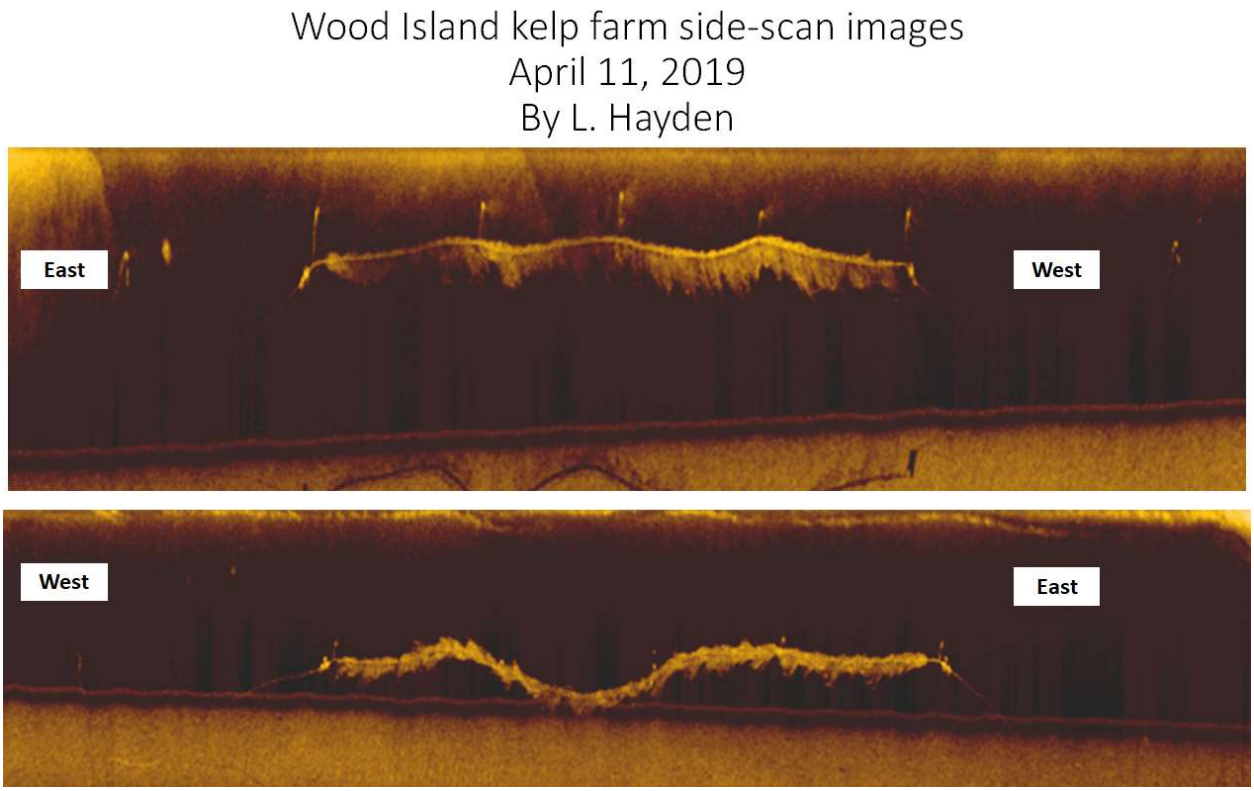

Figure 26: Wood Island side-scan images taken by L. Hayden on April 11, 2019.

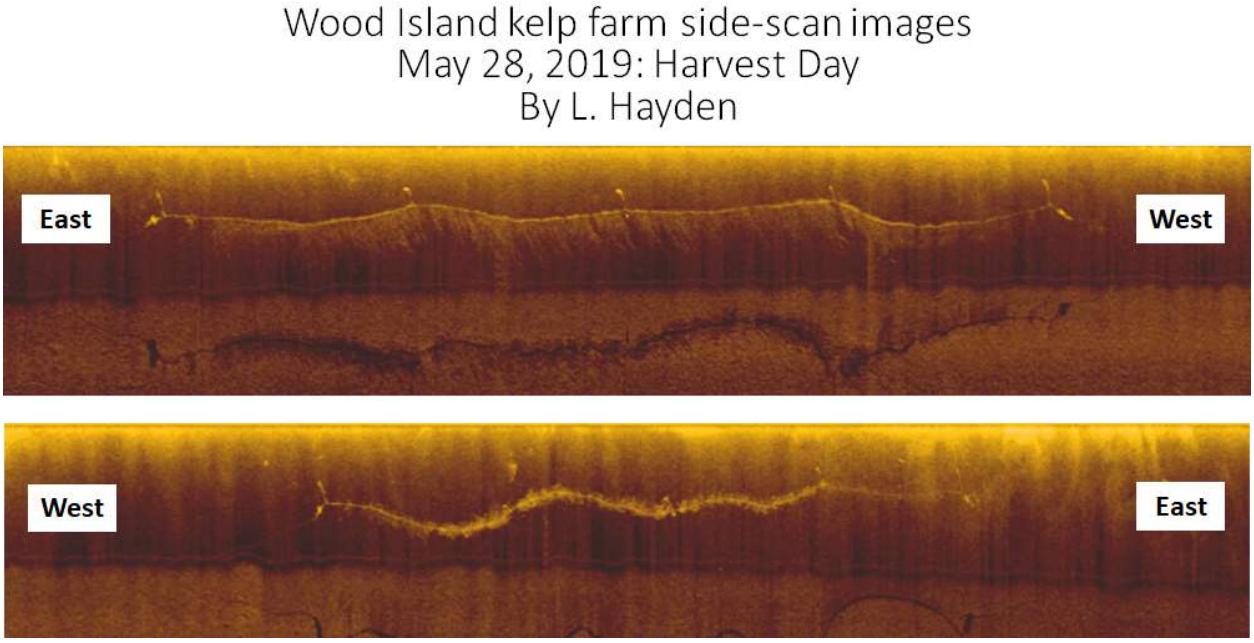

Figure 27: Wood Island side-scan images taken by L. Hayden on May 28, 2019.

2.2.4. Milestone 2.4: Recover and harvest single-line systems (05/14/19)

On May 22, 2019, the MARINER team, members from the UNE School of Marine Programs staff and students, industry partner Tollef Olson of Ocean Balance, LLC and local media outlets boarded UNE, R/V Sahkoki to harvest the Ram Island kelp farm. Over the course of 5 hours, the 1545 kg of kelp was harvested over the 122 m farm and all of the non-mooring equipment was recovered from the site. The harvested kelp was stored onboard the vessel in large coolers, then transported back to shore.

The following week, the 61 m Wood Island kelp farm was harvested. An estimated harvest of 909 kg was cut and collected, stored in coolers onboard and transported back to shore. Tollef was able to take the cut crop to his land-based greenhouse drying facility in South Portland, ME where the bulk of the kelp was hung. Photos of the harvest are shown in Figure 28 (a)-(c).

Kelp products from Ocean Balance vary from fresh frozen, purees, to dried flakes. See drying process on Figure 29. It is expected that the donated UNE kelp will go towards their current best-seller Shitake Seaweed Sprinkle along with future innovative products. Fresh, kelp was also donated to Sodexo dinning services for the Experience UNE dinner where many members of the University community were able to enjoy as an appetizer ingredient and pickled garnish.

Media Outlets/Coverage from Ram Harvest:

- UNE Article Website: https://www.une.edu/news/2019/une-advances-kelp-research-successful-ocean-farm-harvest.
- Portland Press Harold, Front Page Sunday Paper 5/26/19 full article: https://www.pressherald.com/2019/05/28/une-researchers-harvest-kelp-from-farm-in-saco-bay/ .
- WMTW News Channel 8 TV story: https://www.wmtw.com/article/une-students-find-new-ways-to-grow-harvest-seaweed/27564053.
- New Center Maine TV Story: https://www.newscentermaine.com/article/news/local/now/seaweed-revolution-for-maine-the-planet/97-3ed7d982-f760-4de8-bd52-16ae1a8885fa.

Figure 28: (a) Barry & Team working to harvest kelp from the Ram Island farm on 5/22/19 in Saco Bay. (b) Grad Student Lauren Hayden and Tollef Olsen of Ocean's Balance harvesting Sugar Kelp at Wood Island farm on March 28, 2019 in Saco Bay. (c) Kelp Harvest Crew: L to R Tim Arienti (UNE Vessel Captain), Barry, Toby, Liz, Adam (MARINER Team members), Gretchen Grebe (UMaine Phd student at UNE) Emma Jones (UNE undergrad).

Figure 29: Kelp harvested from Saco Bay hung up to dry in South Portland, ME.

2.2.5. Task 2.5: Design a more dense planar type system (9/1/19)

First Design Iteration of Planar Type System for Experimental Lease: A preliminary configuration of the planar array system (array) was developed for the experimental lease application and submitted in August 2018 (Figure 30). The preliminary configuration consisted of an array of nine longlines each with a length of approximately 60 m. Equipment component for the multiple array were designed to be similar to those described for extended longline (Figure 17) but adjusted to accommodate the larger environmental loads. The array system shown on Figure 30 incorporates a curved member designed such that when pulled at the anchor ends and opposing the opposite side, maintains a constant tension in all of the seeded longlines.

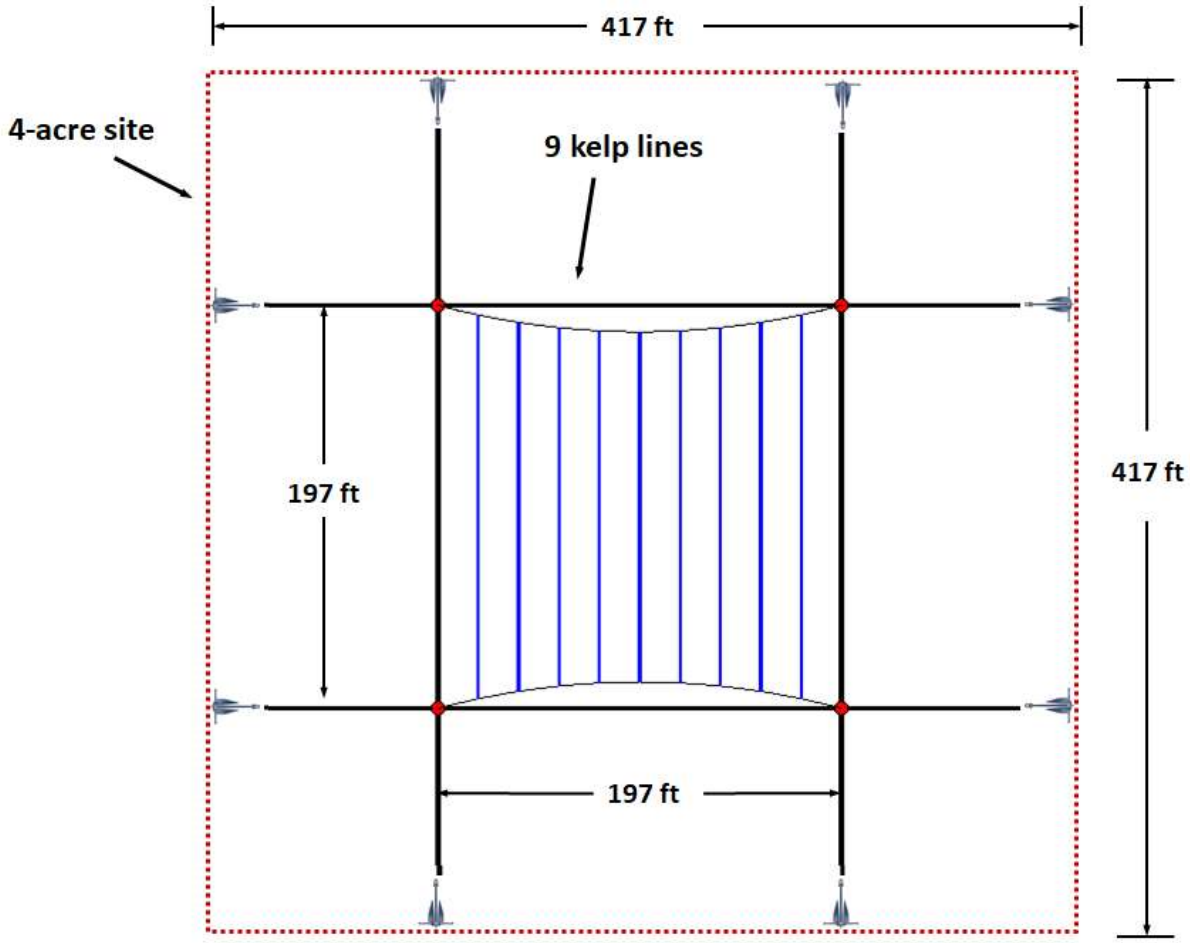

Figure 30: First design iteration for the experiment lease for deployment during the winter of 2020.

A second design iteration for the experimental lease was also considered using the experience of deploying the 122 m long-line system in October 2018. It was discussed to reconsider the experimental lease design shown in Figure 30 to be simpler like a header-bar type array first proposed in the full application as shown on Figure 31 (a) and (b). A simpler system was needed

to maintain safe operations with the UNE vessels. It was also decided to take advantage of experience being obtained working with the WHOI/Alaska Category 1 team and the modeling efforts presently being performed (See Task 7).

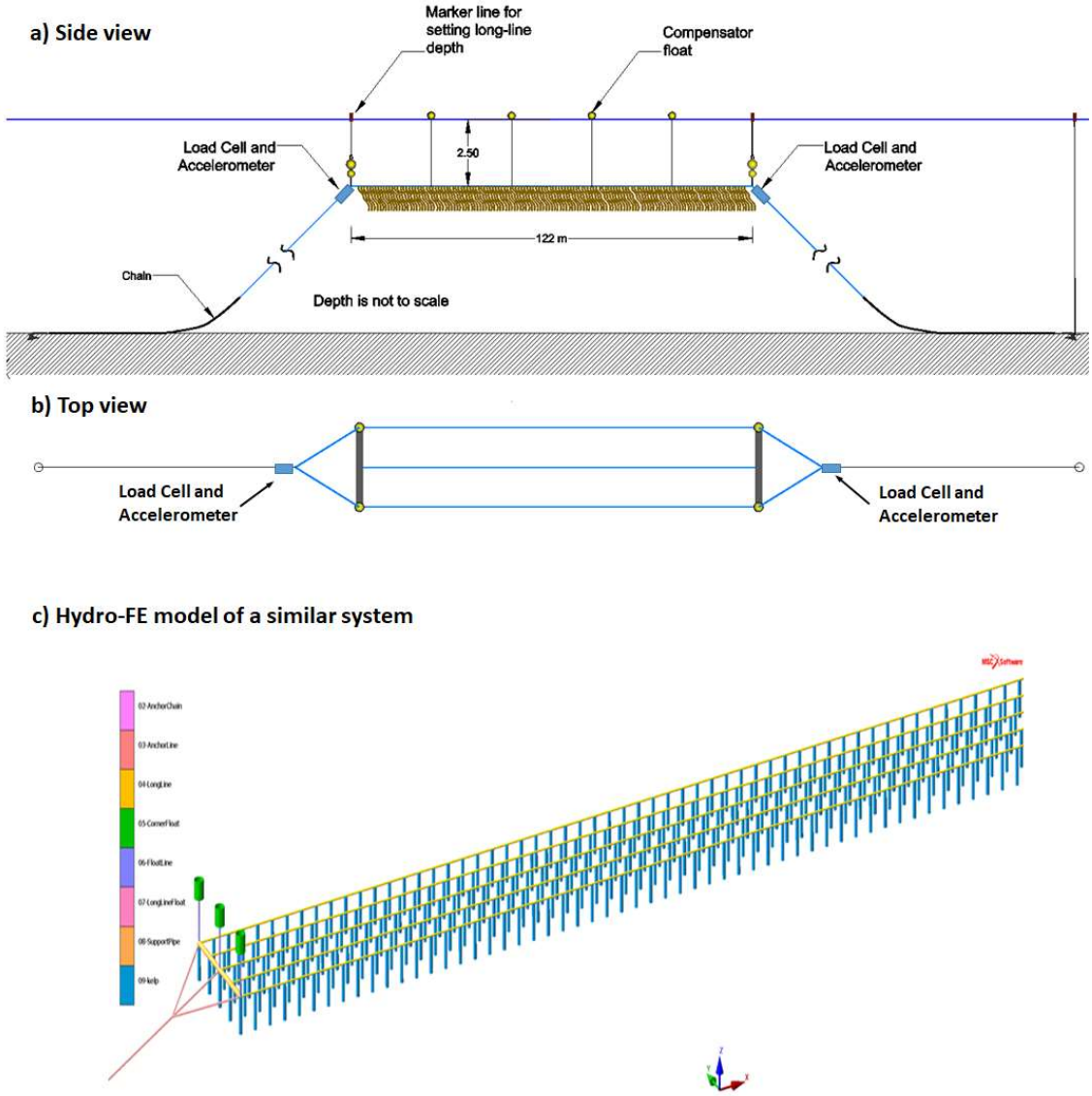

Figure 31: (a) A side view of the header-bar array proposed in the full application. (b) A top view of the header-bar array. (c) A Hydro-FE model of the array type system being used for the WHOI-Alaska Cat 1 project.

As part of the work conducted for the WHOI-Alaska team from January to March 2019, CCG performed simulations to examine the static pre-tension and flotation requirements for the array system shown in Figure 31 (c). Static simulations were conducted for a 18 -m culture line with 0 and 50% pre-tension and corner floats of 12 and 24 kN. The results showed that with the corner floats of 24 kN at 50% submerged (over 2500 lbf each) would keep the longline taut with full growth (Figure 32). However, utilizing intermediate flotation would reduce the need to larger corner buoys.

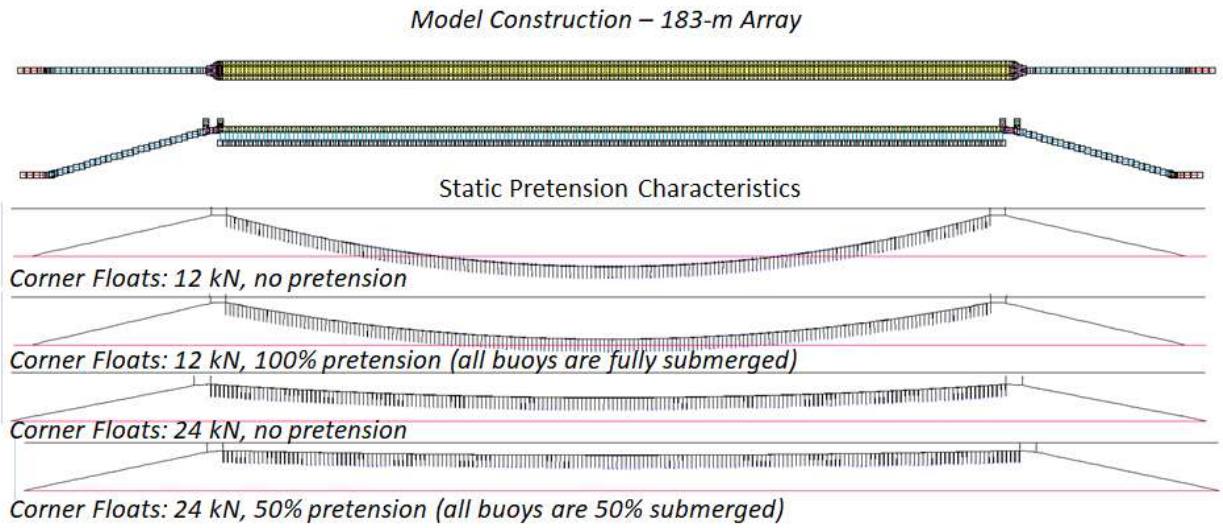

Figure 32: The sensitivity of pre-tensioning and corner floats on the static geometry of a 183-m array.

One of the major advantageous working with the Category 1, Phase 1 projects was the opportunity to analyze several types of systems to gain insight of design implications. From this modeling and especially our field experience, it became evident that large amounts of flotation would be required if intermediate flotation was not used along a kelp-line or array of kelp-lines to prevent sag. It was also clear from our field experience that large culture line pretension would make it difficult to sample and install and recover the load cell systems.

From July to September 2019, a strong focus was given to the next design iteration of the planar-type system to be deployed in November 2019. The design iterations are shown on Figure 33(a), (b), (c) and (d) to fit the 4 acre site. The design iteration process first considered small length-wise arrays with either 2- or 4-anchor systems as shown on Figure 33(a) and (b). These designs were similar to the system originally proposed, however, the team decided that this configuration had too small of an aspect ratio to distinguish it “hydrodynamically” from a single line system. The team also revisited the large system shown in Figure 30, but decided that it would be too difficult to manage. An offset array was also considered to have a better aspect ratio and to maximize the growth area within the central grid (Figure 33d). It was called an offset array because the anchor legs did not form continuous diagonals. It was decided this system would be too difficult to deploy with “offset” anchors.

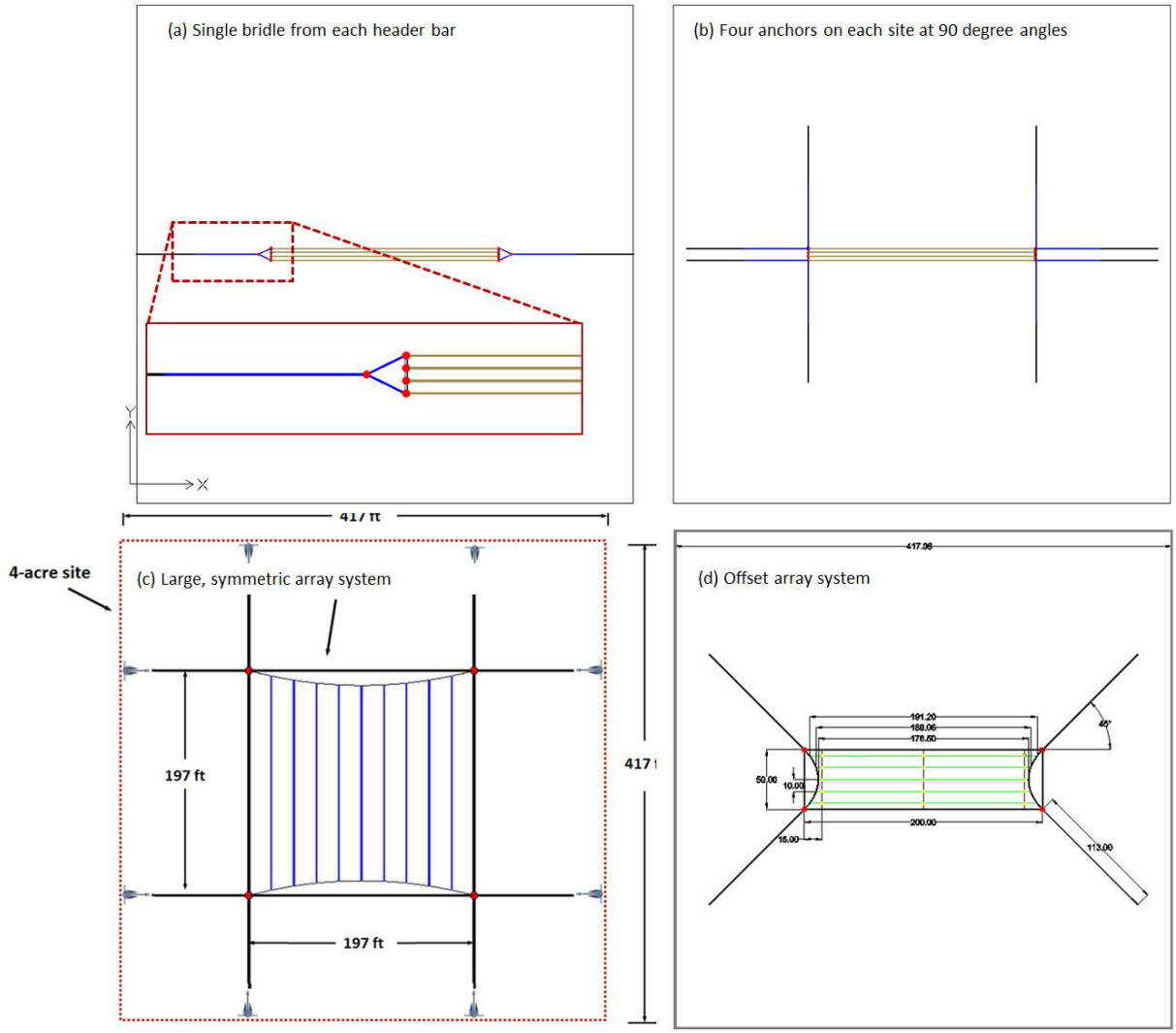

Figure 33: Four of the design iterations considered for deployment at the 4 acre lease site in Saco Bay. (a) Single bridle with header bar. (b) Header bar with four anchors on each side. (c) A non-symmetric array system to maximize planar area. (d) A large symmetric array to fill the entire lease site.

The final system design was a compromise of those shown in Figure 33. It was decided that a system with an aspect ratio of at least 5:1 (length to width) would likely show hydrodynamic characteristics more of a "plate" than a "line." To design this the planar-type system, a constraint was set so that the grow-out area was contained in a 30 ft. x 150 ft. grid. With a width of 30 ft., five parallel kelp-lines could be spaced 7.5 ft. apart. The 150 ft. dimension was chosen such that the anchor lines would fit into the 4 acre permitted site (≈ 417 ft. x 417 ft.) having a mooring spread-angle of 78.69 degrees. This spread-angle was calculated as the diagonal of the 30 ft. x 150 ft. box. If necessary, a temporary rope could be connected across the diagonal during the deployment process to set opposing anchors.

The array system was designed to have the header rope spread by the mooring legs on the east and west side of the system to keep the plane in tension. In this configuration, the header rope

on each side of the system can be defined as a funicular shape. Both structural catenaries and parabolas are funicular shapes, though mathematically distinct. The structural catenary equations are derived based on the assumption the forces are evenly distributed across the curved segment length, like a hanging wire supported at each end, hydrodynamic drag on an oil boom (Swift et al., 1992) or chain mooring (Faltisen 1991). The structural parabolic equations are derived assuming the forces are evenly distributed along the horizontal axis, like the weight of the deck supported from hangers in a suspension bridge. While both catenaries and parabolas are continuous, in essence they become funicular tension polygons when discrete point loads are applied with the endpoints fixed. In the application of an array of culture lines in a spread mooring configuration, the point loads on each header line are variable and the anchor attachments line are never truly fixed in the ocean environment with waves and currents. As long at the anchor lines are deployed with pretension in an opposed configuration, the funicular shape will adjust to a state of equilibrium in the dynamic load environment. The design strategy here was to have the endpoints of the header rope be close to the 78.7 degree angle of the diagonal, while having at least 600 ft of culture line.

Two funicular shapes were investigated based on the continuous catenary and parabolic shapes. The goal was to fit the header rope shape across the 30 ft space with a depth within 30 ft to obtain 5 culture lines with a total length of at least 600 ft. The equation for the catenary is described as

$$y = B\left[cosh\left(\frac{x}{B}\right) - 1\right] \quad (14)$$

and that for the parabola a

$$y = Cx^2 \quad (15)$$

Values for B and C as shown on Figure 34 were determined to be 6.5 ft and 0.125/ft respectfully. Straight lines were then used to connect the points between the 7.5 ft widths required for the spacing of the culture lines. The resulting funicular polygons are also shown on Figure 34. With the outside culture line edge of 150 ft., the interior culture line lengths were calculated as provided in Table 7.

Table 6: Load-cases, static and extreme loading.

Line Location	Catenary (ft)	Parabola (ft)
Outer (2)	150	150
Interior (2)	106	108
Center (1)	97	94
Total	609	610

With the points of the funicular tension polygon, the lengths of the culture lines were calculated with the longest length (on the outside of the grid) equal to 150 ft. The planar array system also included a 20 ft section to facilitate the connection of load-cells on each of the mooring legs as shown on Figure 35(a). The anchor legs were specified to be identical to the 122 m culture line deployed during the winter of 2018-2019. The anchor leg details are shown on Figure 35 (b).

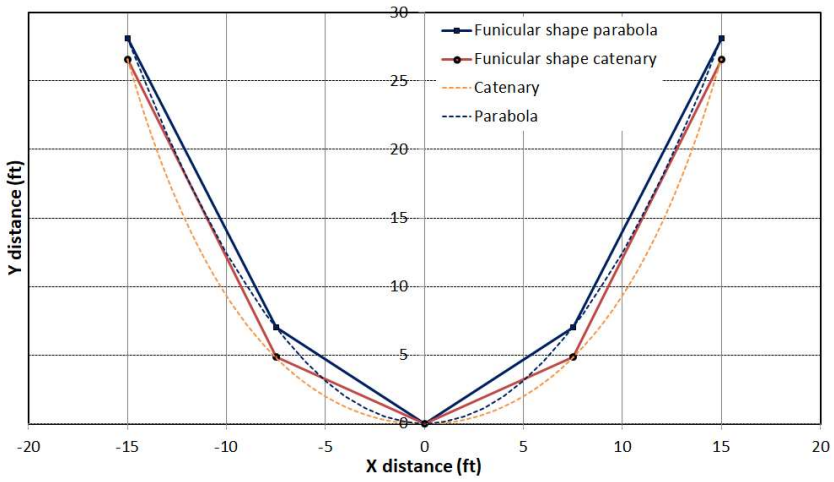

Figure 34: The header line rope shape was investigated using both catenary and parabolic shapes and corresponding funicular polygons.

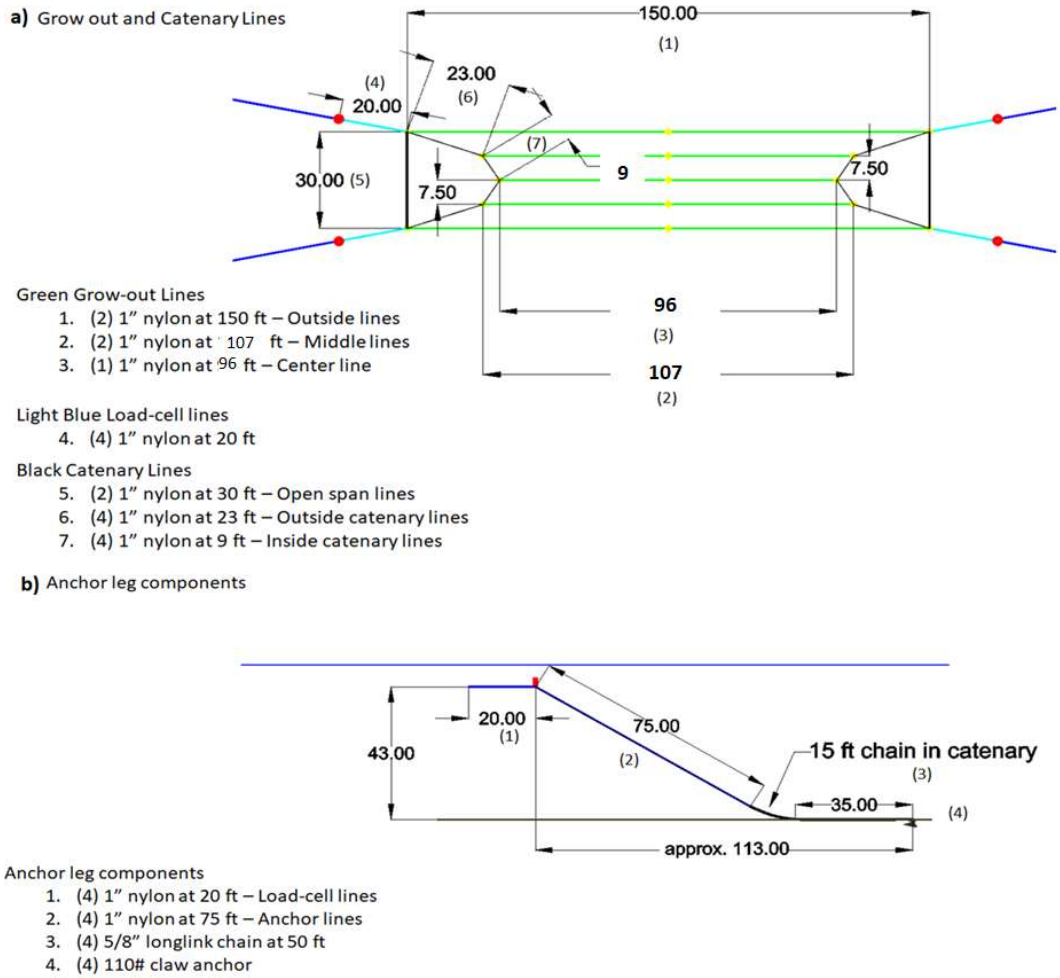

Figure 35: Final design iteration of the array-type system for deployment at the experimental lease site. Dimension are in feet.

A set of simulations was performed to estimate the response of the proposed system design. The first simulation examined the system in a static configuration to examine initial stability. The next two examined environmental loading scenarios as two different load cases with wave and currents as describe in the next paragraph. A Hydro-FE model was constructed of the array-type system as shown on Figure 36 (a) and (b). Simulations were done under the conditions of zero and maximum (all buoys submerged) pretensions. The Hydro-FE model was discretized into finite elements with equivalent geometric/hydrodynamic and inertial properties. The drag characteristics were calculated using the empirical formulae based on the results of the tanks tests.

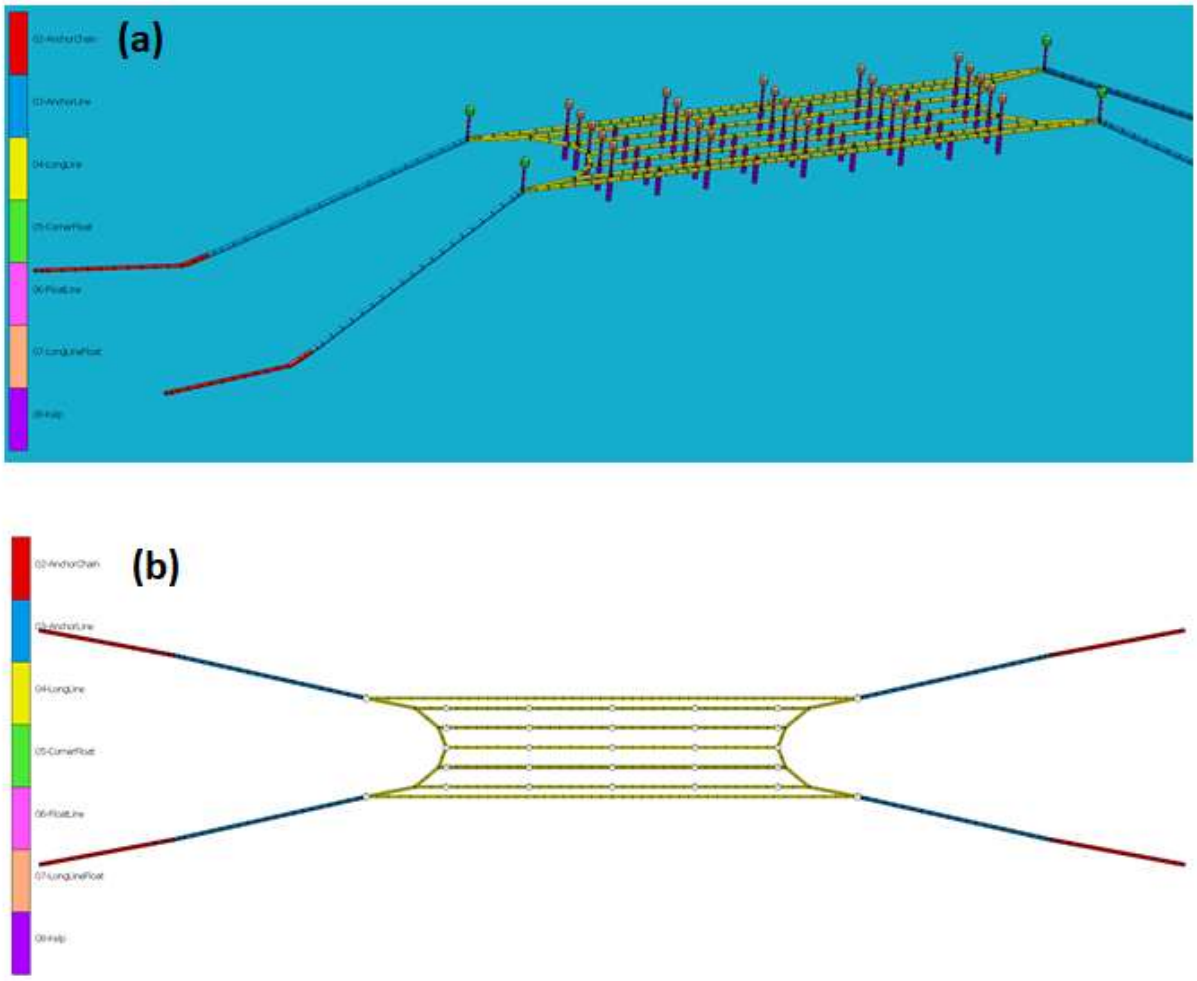

Figure 36: (a) Setup of the Hydro-FE model of the array. (b) Plan view of the system.

In the Hydro-FE program, ocean waves were modeled using a JONSWAP spectrum such that irregular waves with significant wave height of 4.2m and period of 11s were created and with currents at 1m/s based on the extreme 50-year storm condition (Figure 37). Two load case conditions were examined. Simulations with load case #1 were conducted with the waves and currents propagating in a co-linear orientation. Simulations with load case #2 were done with the waves and currents propagating at 90 degrees.

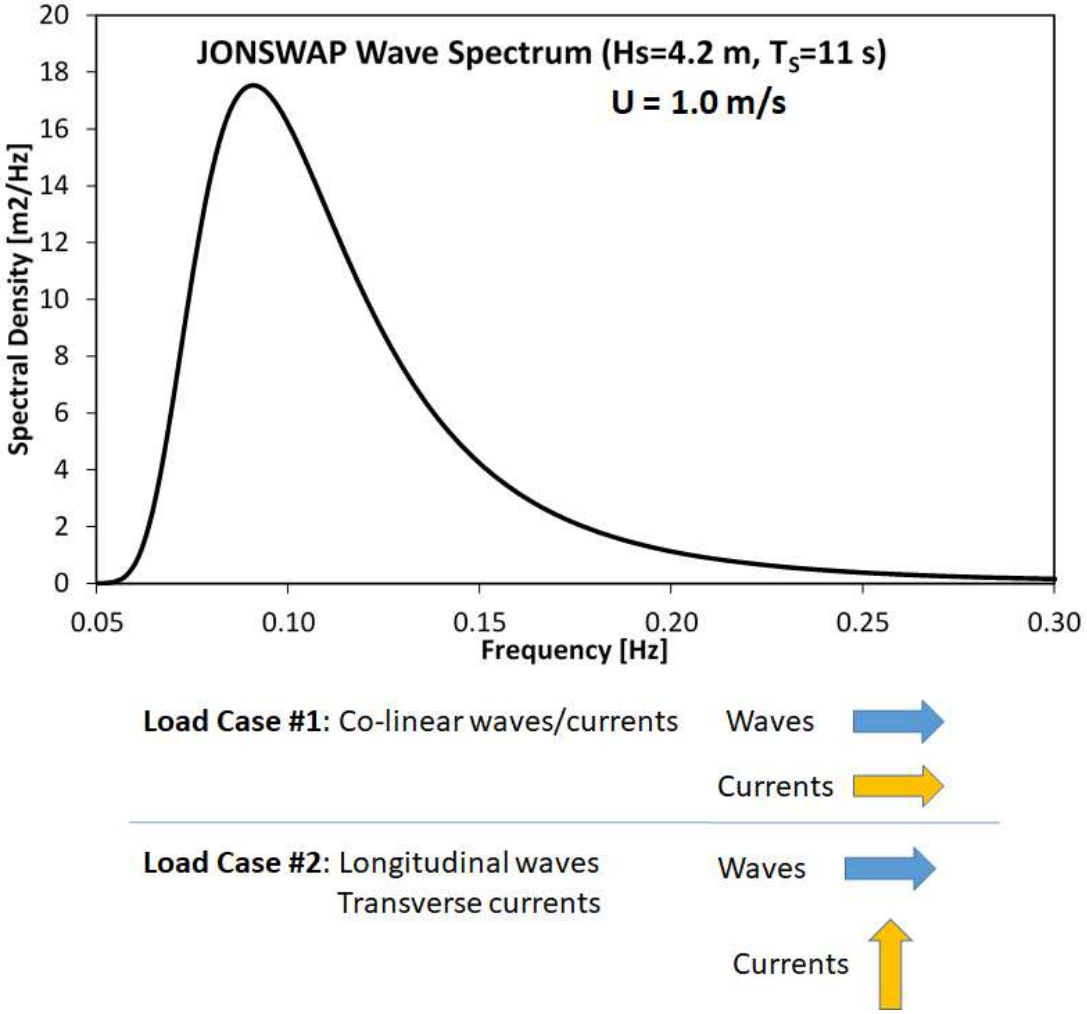

Figure 37: Input to the Hydro-FE model included a JONSWAP wave spectrum of the 60-year storm condition with a 1.0 m/s current. Two load case simulations were conducted with waves and currents propagating in a co-linear direction and at 90 degrees.

The dynamic responses of the system with the Hydro-FE model are shown on Figure 38 (a), (b) and (c). In Figure 38 (a), the system shows the quasi-static response due to the wet weight of the kelp aggregates. In Figure 38 (b), deflection of the system is shown with load case #1. Figure 38 (c) shows the deflection of the system with load case #2.

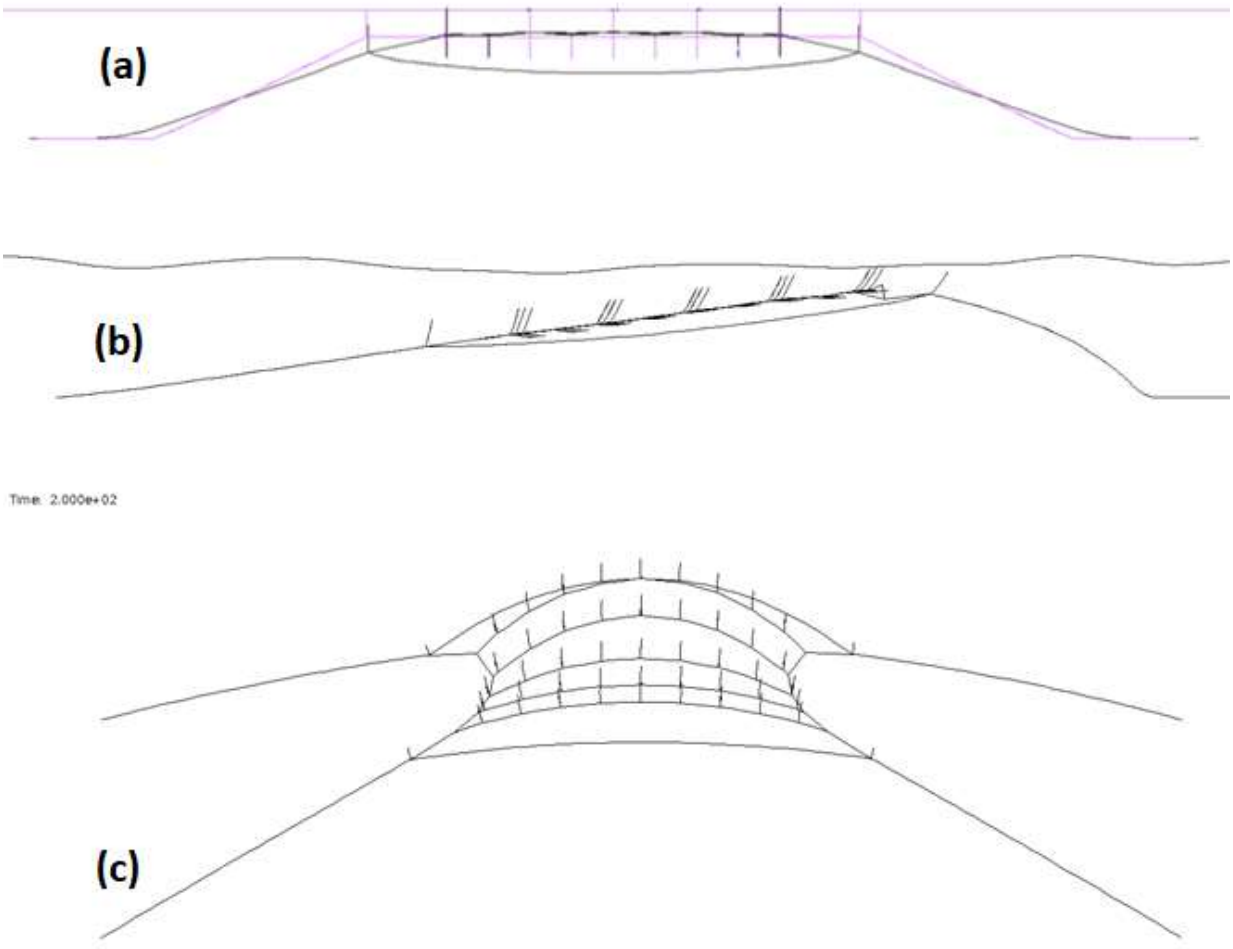

Figure 38: (a) View of the system with pretension under quasi-static conditions. (b) View of the system with pretension subjected to co-linear waves and currents. (c) View of the system with pretension subjected to longitudinal waves and transverse currents.

With the load case simulations, tension values in the anchor chain, anchor lines, kelp long lines and the float lines were obtained. The results are shown on Figure 39 (a) and (b). The results of load case #1 provide a nominal maximum value of 7000 lbf, though the oscillations were substantial. The results of load case #2 provide a nominal maximum value of 8000 lbf. With these design loads, the components specified for 2018-2019 deployment would be appropriate.

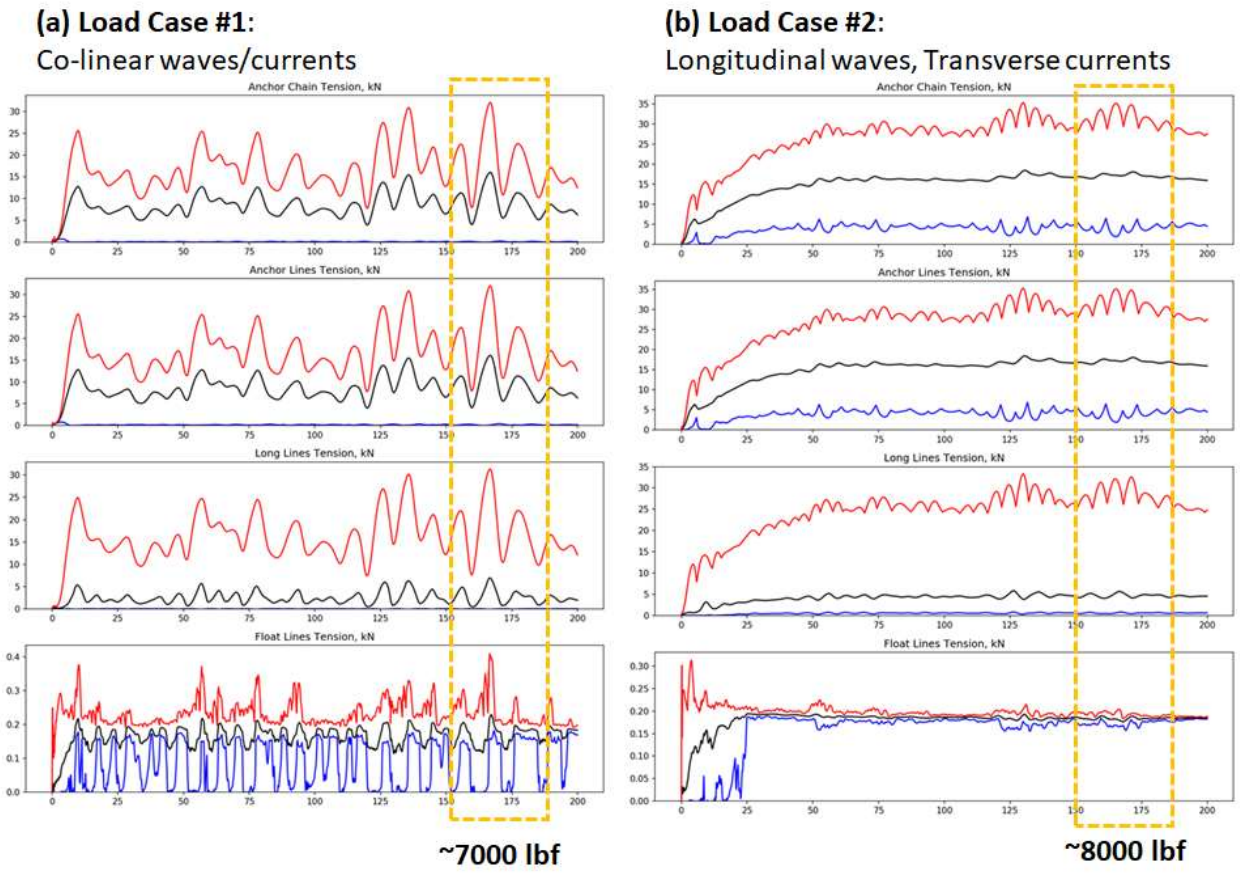

Figure 39: (a) Results of load case #1 yielded maximum tensions on the order of 7000 lbf. (b) The results of load case #2 yielded maximum tensions on the order of 8000 lbf.

A dataset was also acquired from the Hydro-FE simulations to examine the connections between the longline and the catenary lines. The location of the attachment point in the model are shown on Figure 40 (a) and the time series result on Figure 40 (b).

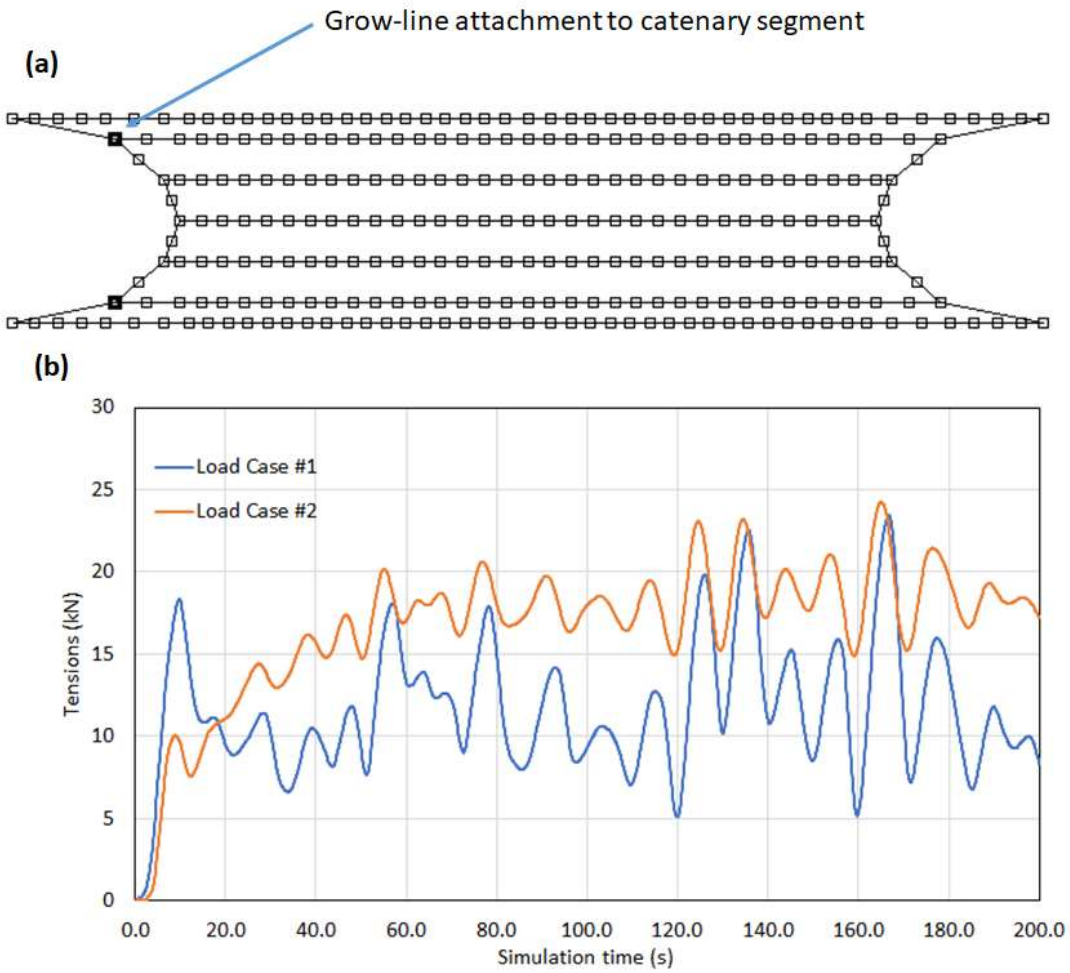

Figure 40: (a) Connection nodes between the long line and the catenary lines. (b) The tension results from load case #1 and #2.

As discussed in the previous section, by August 2019 the UNE, USNA, CCG and MMC partners came to a final design decision for the 2019-2020 experimental Ram Island kelp farm. At this point, purchases for farm materials began and by the end of September 2019, all essential items were ordered, purchased and delivered from Hamilton Marine to UNE-North. Items ordered included two 110 lbs. claw anchors, an additional 100ft of 5/8 in, long-link mooring chain, and a coil of ½ "and 1 in nylon rope to create the deployment grid, culture lines, and catenary lines. An assortment of deployment tools, buoys for submerged and intermediate flotation, and instrumentation hardware were also purchased to complete the farm assembly. Infrastructure hardware was utilized from the previous farm season. Both mooring legs, composed of two 110 lbs. claw anchors, 100 ft total of 5/8 in long-link mooring chain, and the 400 ft of 1 in nylon culture line was used in the 2019-2020 experimental farm design along with previous hardware and flotation. Table 7 shows a material list and construction plan for the 2019-2020 design. The components are shown on Figure 35, with details on Table 7 showing parts utilized from the 122 m culture line system deployed for the 2018-2019 season.

Table 7: Array system component details utilizing parts from the 2018-2019 deployment.

Whole Parts We Have:	Cut Pieces (ft):	Purpose of Cut Piece:
New 1 in Line 600 ft reel	160 160 117 117 46 600	Outside Culture Line 1 Outside Culture Line 5 Inside Culture Line 2 Inside Culture Line 4 Catenary Open Span (1of 2)
New 1 in Line 400 ft	149 149 298 (102 Remaining)	East Catenary (5 Culture Line attachments) West Catenary (5 Culture Line attachments)
New 1 in Line 220 ft	107 40 147 (73 Remaining)	Inside Culture Line 3 Catenary Open Span (2of 2)
Old Culture 1 in Line 1 in 400 ft	100 100 100 100 400	75 ft Mooring Leg 1 (2 splices) 75 ft Mooring Leg 2 (2 splices) 75 ft Mooring Leg 3 (2 splices) 75 ft Mooring Leg 4 (2 splices)
New ½ in Line 600 ft coil	163 163 274 (326 Remaining)	Deployment Diagonal (153+10=163 ft) Deployment Diagonal (153+10=163 ft)

Learning from past kelp farm experiments, areas that required improvement were addressed to benefit field logistics, instrumentation, data collection and safety. In the 2018-2019 field season, it was found difficult to compensate for the tension on the farm when attaching the load cells to the single kelp line design. Therefore, for 2019-2020 experimental kelp farm design, a 20 ft load-cell line extension was included on each corner of the array (see Figure 35). This provided additional space for the instruments, making the deployment easier by allowing access to corner connections regardless of the tides. In addition to accessing the load cell attachment points, securing the instrument onto the farm was difficult when opposing wind and currents were not favorable. For this season, a smaller, removable attachable rope was inserted into the 20 ft section, so while the load cell is not deployed, a secure line was in place to take the tensions and forces affecting the farm components. The previous Ram Island kelp farm also experienced an excess of biofouling on all surface flotation used to visually identify the farm. Therefore, all surface flotation was painted fluorescent orange with marine paint to prevent fouling and aid in visibility for the team and all other vessels in the area. Construction details are shown on Figure 41 (a), (b), (c) and (d).

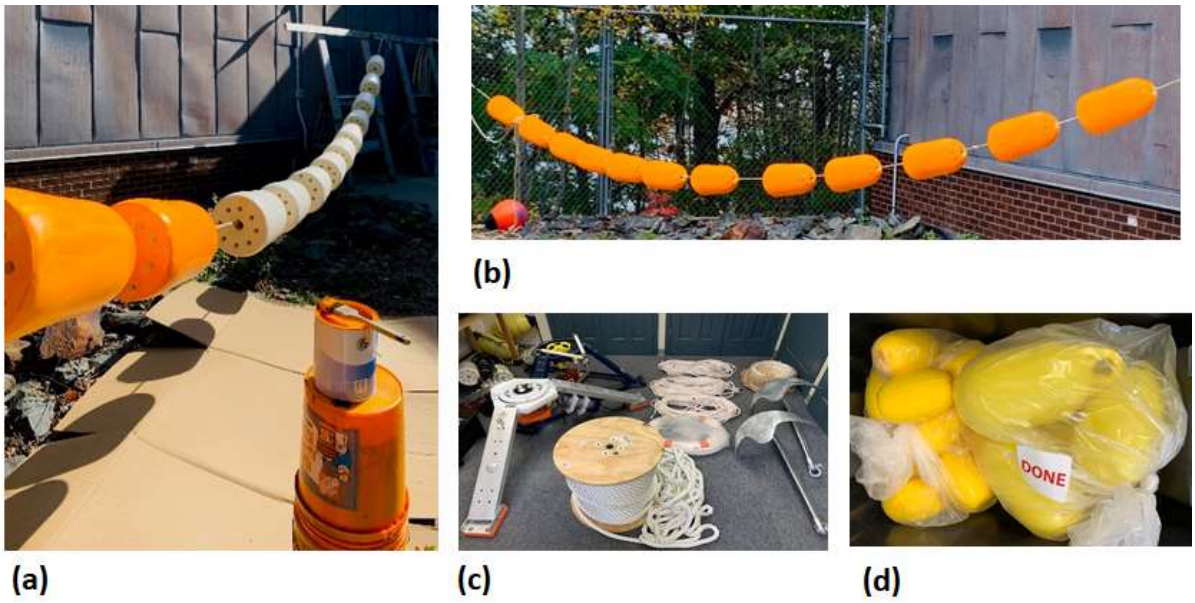

Figure 41: (a) and (b) The contrast between the original white and the new orange paint on the surface flotation. Each picture represents 1 case of 24 floats. (c) The system also includes new anchors, ½ and 1 in nylon rope and (d) buoys used to mark lease boundaries on the crown lines, and toggle depth markers. All are bright orange and yellow to help increase visibility.

2.2.6. Task 2.6: Grow hatchery seed for dense, planar-type system (11/15/19)

The equipment necessary to produce seed for the planar-type has was purchased between July and September 2018. The equipment included two 20 gallon tanks (used for previous hatchery efforts) and a 50 gallon tank to support the necessary amount of seed for the dense, planar-type system. From April to June 2019, the hatchery was updated with new filtration and sterilization units. The new UV filter was purchased was installed with the new plumbing features to decrease possible contamination in the nursery. The completion of the 50 gallon nursery tank system provided more space for water changes and seed grow out. With spools, twine, culture nutrients, lights, water chillers, and filtered fresh salt water, the hatchery expansion was complete at UNE.

Following hatchery completion, wild kelp sorus collection was done in September 2019 and brought to the hatchery at UNE. After a successful spore release, 5 spools were initiated and moved into the nursery by the middle of September 2019. With two additional sorus tissue collection efforts on September 14 and 17, active spores were produced active spores for spool settlement resulting in a total of eighteen spools in the UNE nursery. The sorus material collected on September 9 and 14 was obtained in South Portland Maine. While looking primarily for sorus tissue on mature *S. latissima* blades, viable sorus material was also found on *S. latissima forma angustissima* and *Laminaria digitata* in South Portland, ME. Sorus material from *S. latissima forma angustissima* was successfully spored in the UNE lab, but no productive spore settlement occurred on the seed twine. Sorus material collected on September 17 was possible through collaboration with industry partner Tollef Olson, of Ocean's Balance, in Casco Bay, ME. Successful collection of sorus material from *S. latissima* occurred in three different locations of the bay. Example of sorus material are shown on Figure 42 (a) and (b).

Figure 42: (a) An example of *Saccharina latissima* sorus tissue collected in South Portland, ME. (b) *Laminaria digitata* with sorus material in South Portland, ME found washed onto rocky shoreline.

Once the sorus tissue was collected from the field, it was brought back to the laboratory for release preparation, refer to Figure 43 (a) through (c). In Figure 43 (a), the sticky outside of multiple blades of active sorus tissue on *S. latissima forma angustissima* is shown prior to sorus tissue preparation. In Figure 43 (b), the beaker on the left shows active spores in the UNE laboratory after 15 minutes of release. The beaker on the right contains the sorus tissue prior to spore release after 2 minutes of submersion in clean salt water. It can take anywhere from 15 minutes to 1 hour for spores to be released from the tissue. In Figure 43 (c), the initial 18 spools are shown with spores added in the UNE nursery.

Additional sporing details are exhibited on Figure 44 (a) and (b). Figure 44 (a) shows a sample string under 10x magnification from an 8 day spool. Visible spore settlement can be seen along with foggy areas of contaminant species growth. Figure 44 (b) shows another image of 8 day old settled spores under 20xmagnification. Spores and contaminants can be seen on the culture twine.

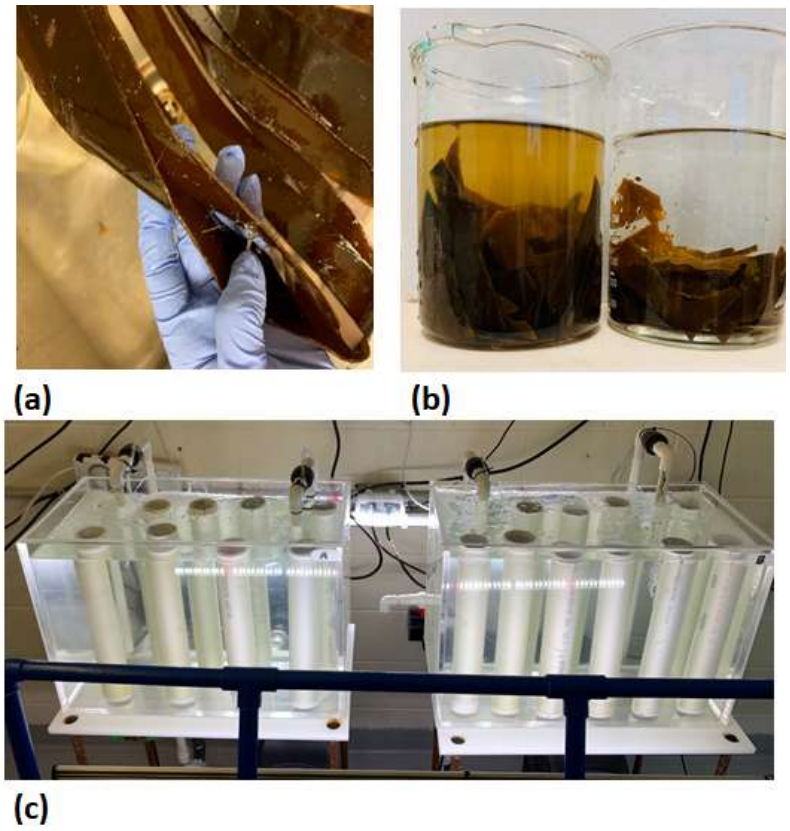

Figure 43: (a) The sticky outside of multiple blades of active sorus tissue on *S. latissima forma angustissima* can be seen prior to sorus tissue preparation. (b) Beaker on the left shows active spore release in the UNE laboratory after 15 minutes of release. The beaker on the right, shows the sorus tissue prior to spore release after 2 minutes of submersion in fresh salt water. (c) The initial 18 spools with spores added in the UNE nursery in September 2019.

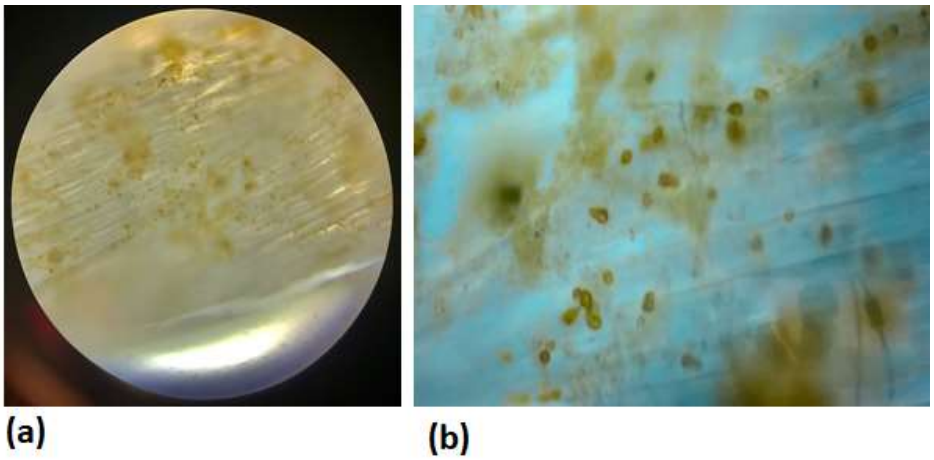

Figure 44: (a) A sample string under 10x magnification from an 8 day spool. Visible spore settlement can be seen along with foggy areas of contaminant species growth. (b) Another image of 8 day old settled spores under 20xmagnification. Spores and contaminants can be seen on the culture twine.

By day 14 in the UNE macroalgae nursery (October 2019), no advancements in seed growth were visible at 1X or under the microscope. It was found that the culture tanks were contaminated with filamentous green algae (Figure 45 a). Numerous attempts to address the contamination with fresh water baths and spot treatments were unsuccessful.

To prevent postponing the kelp farm deployment due to lack of seed, another effort to collect sorus tissue on October 15, 2019 was successful. With the sorus tissue, spores were release on October 16. The spores were introduced to seven new spools in a sterile tank in the nursery on October 17, 2019. All seven of the new spools produced sufficient *S. latissima* sporophytes for farm out-planting. Another successful collection of sorus material occurred on October 22, with the sorus material prepared in the UNE laboratory on October 23. This sorus material produced spores on October 24 and new nine seed spools introduced to the nursery on October 25, 2019 (Figure 45 b) with growth shown on Figure 45 (c). This second effort produced in nine additional spools *S. latissimi* seed. In total, the UNE nursery was able to cultivate all 16 spools to viable sporophytes for farm out-planting Figure 46 through Figure 50.

(a)

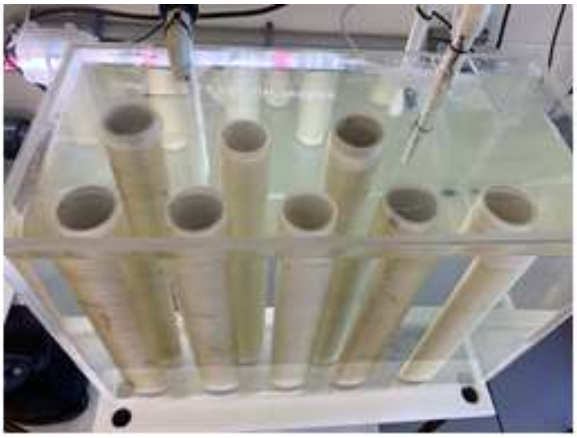

(c)

(b)

(a): *Shows the spools with contamination that were removed from the nursery to create new, viable seed spools.*

(b): *On October 25th, 2019 nine new Sugar Kelp seed spools were introduced to the UNE nursery*

(c): *Seed Spools on Nov. 6th 2019 in the UNE Nursery*

Figure 45: (a) Shows the spools with contamination that were removed from the nursery to create new, viable seed spools. (b) On October 25, 2019 nine new Sugar Kelp seed spools were introduced to the UNE nursery. (c) Seed Spools on November 6, 2019 in the UNE Nursery.

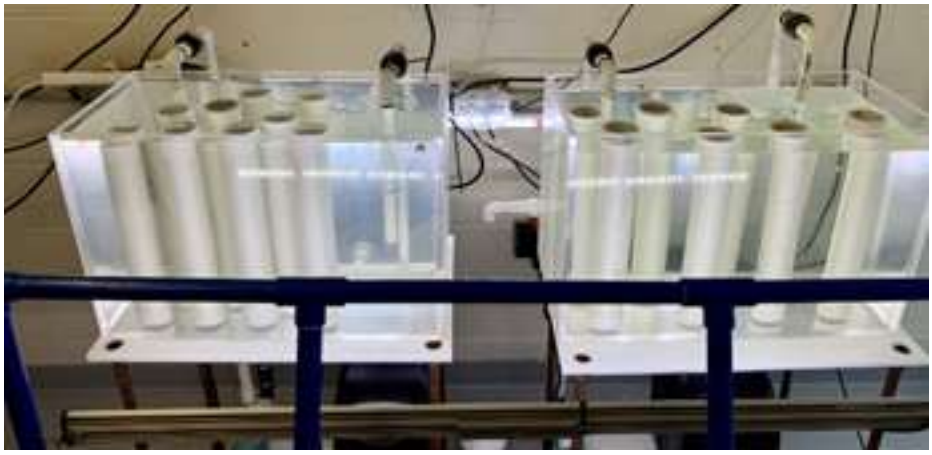

Figure 46: All 16 productive seed spools in the UNE Nursery for 2019 season on October 28.

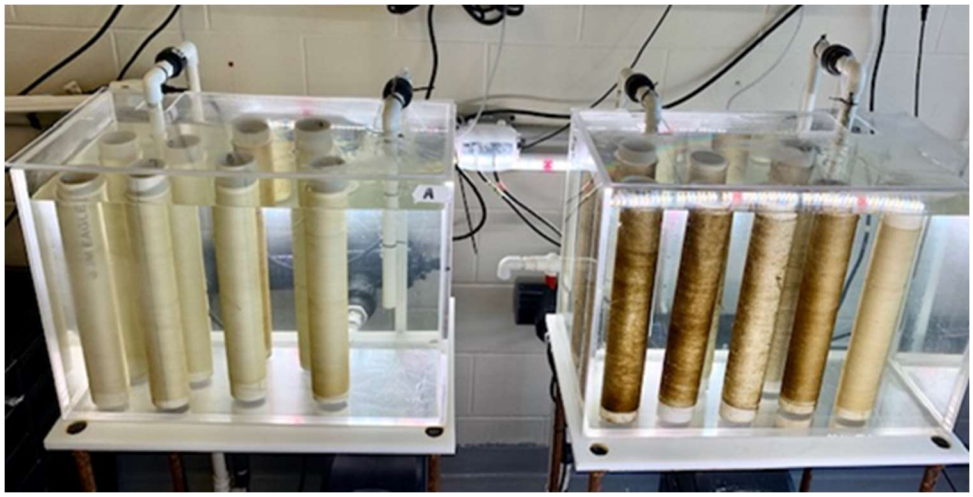

Figure 47: All 16 productive seed spools in the UNE Nursery for 2019 season on November 13.

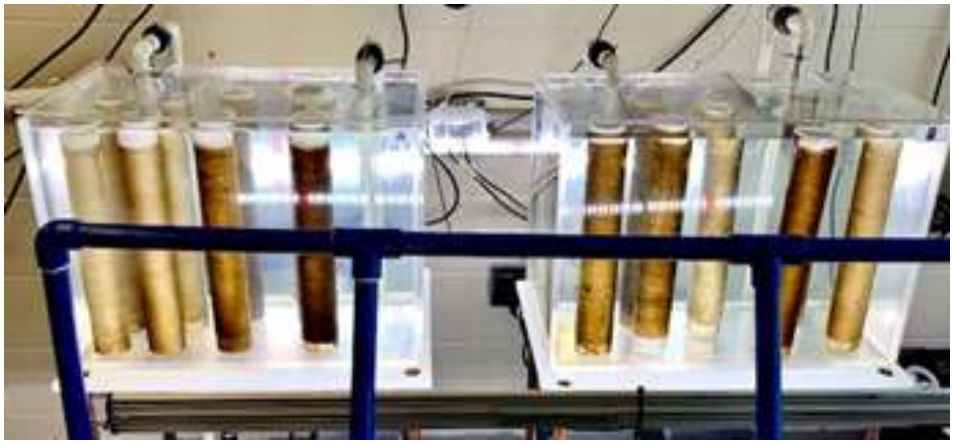

Figure 48: All 16 productive seed spools in the UNE Nursery for 2019 season on November 26.

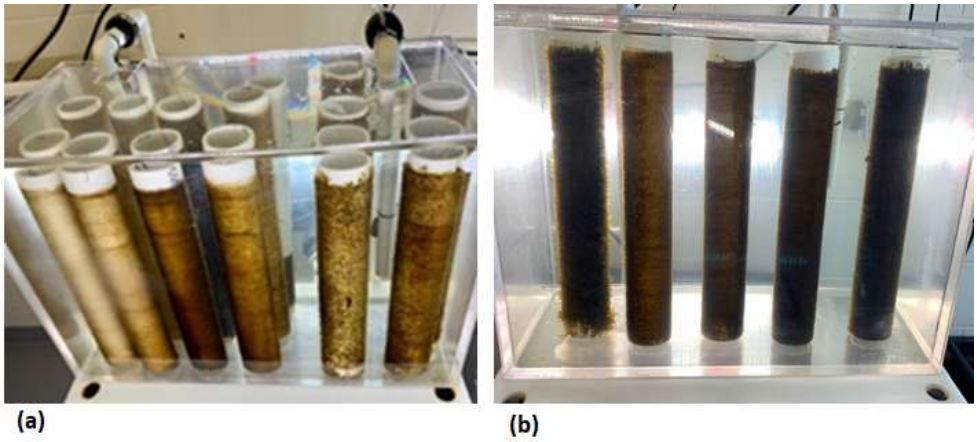

Figure 49: (a) December 4, 2019, 12 remaining seed spools in UNE nursery after farm out-planting. (b) December 19, 2019, 5 remaining seed spools in the UNE nursery after additional farm out-planting.

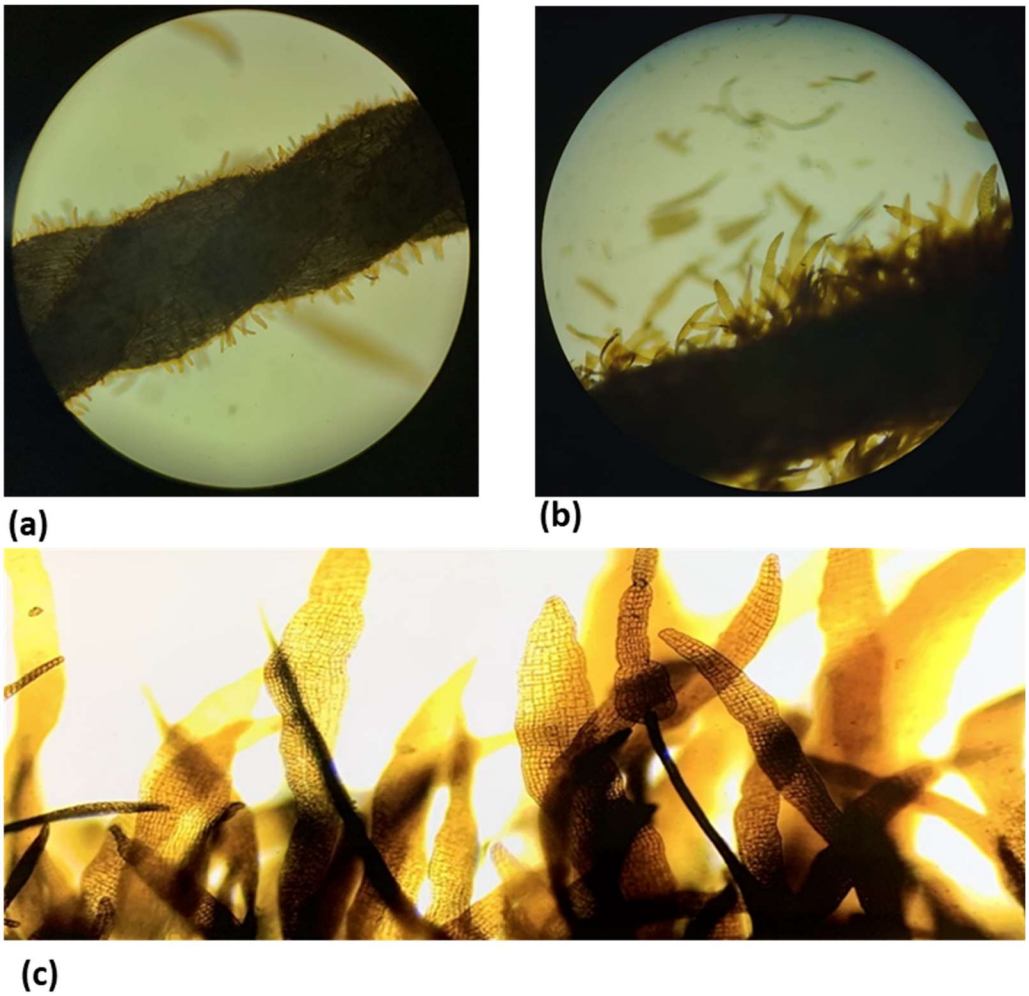

Figure 50: (a) Standing *S. latissima* sporophytes on day 19 in the nursery, under 5x magnification. (b) Mature standing *S. latissima* sporophytes on day 26 in the nursery, under 10x magnification. (c) High density settlement of *S. latissima* sporophytes, on day 26 in the nursery, under 20x magnification.

2.2.7. Task 2.7: Seed, deploy and monitor planar-type system (5/21/20 and 6/9/21)

Prior to deploying the kelp farm in early November, 2019, the field team organized and staged all farm pieces on the UNE dock and vessels. The field team was able to consolidate the bulk of all farm materials inside ten labeled fish totes and then easily assemble them in the field during the deployment of the farm as shown Figure 51.

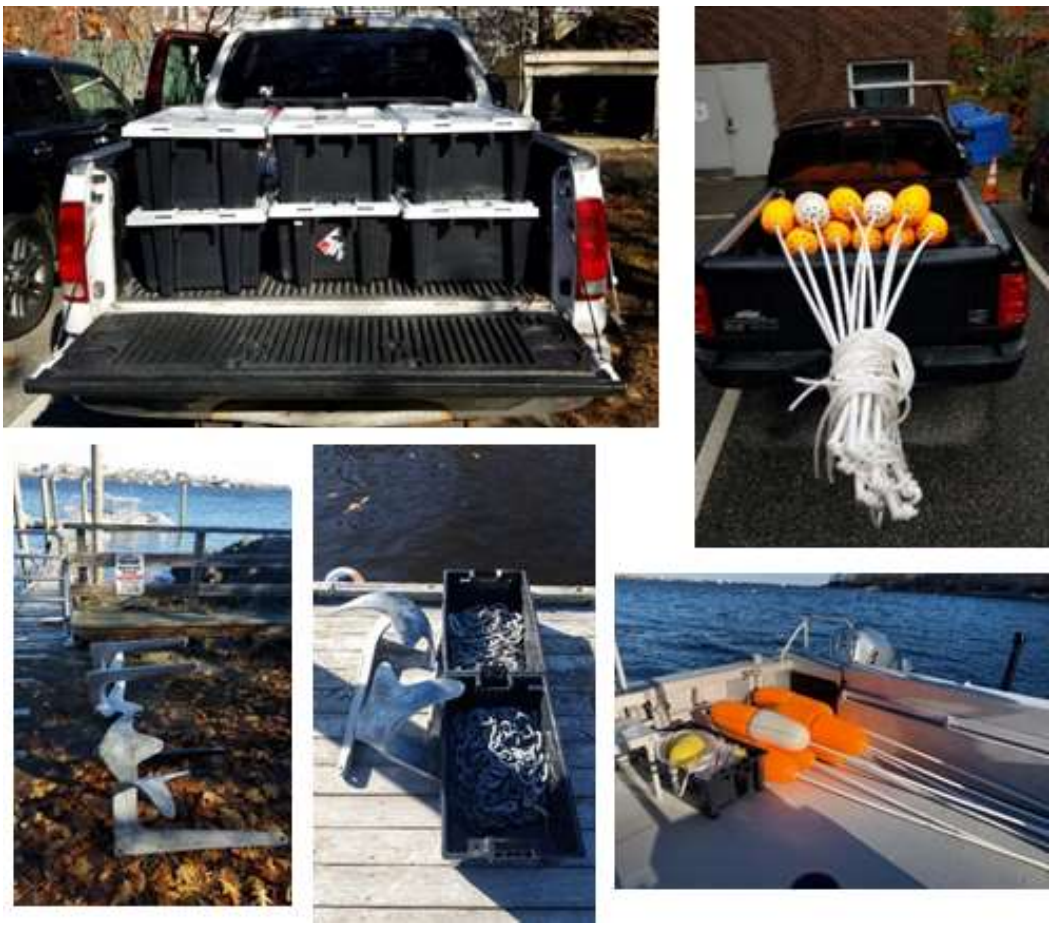

Figure 51: This collection of pictures shows how the entire array system was organized into totes that fit into two pickup trucks.

On November 7, 2019, the 5-line array system was successfully deployed at the Ram Island site in Saco Bay, ME. To deploy the farm, the MARINER team partnered with UNE Vessel Captain Tim Arienti, UNE MSC assistant director Addie Waters, Maine SeaGrant agent Jaclyn Robidoux, UNH field personnel Arron Jones, and UNH MARINER team member Zach Moscicki. The field team first deployed each of the four mooring legs separately. The mooring legs each consist of a 110 lb claw anchor, attached with a shackle to 15.24 m (50 ft) of 5/8 in long link mooring chain. The mooring chain is measured to have 10.67 m (35 ft) of chain situated on the seafloor with the remaining 4.57 m (15 ft) of chain suspended off the seafloor. The elevated chain is connected with a shackle and spliced thimble to the 1 in three strand nylon rope having a length of 22.86 m (75 ft) long. The free end of the mooring leg 1 in line was tied to the submerged corner flotation with an additional 6.09 m (20 ft) of line for instrumentation. Once the two complete mooring legs (from anchor to corner floats) were deployed on the west end of the farm they were attached to

the first half of the headrope with funicular tension polygon shape. The headrope was tied to the free end of the 6.09 m instrumentation line. The headrope incorporates five attachment points for each culture line and a corresponding surface float. Since the east end of the farm was designed with same components, it was deployed in the same manner. Once all four mooring legs were deployed and then connected to the corresponding headrope, they were connected with the five culture lines. Surface floats were added to give intermediate flotation along the farm. Once all of the farm materials were in place, the structure was spread under tension to maintain its size, shape and overall structural components. Parts of the deployment procedure are shown on Figure 52 (a) through (d). The mooring equipment was staged and deployed from the 32 ft UNE landing craft Sakohki. The culture lines and surface floats were deployed from the 23ft UNE center console Maritime Skiff the Llyr. The crew is shown deploying the system from the Llyr on Figure 52 (a). Orange buoys marking the attachment locations on the array system are shown on Figure 52 (b). Figure 52(c) shows a view looking SSE toward Ram Island with the array system set within the 4-acre tests site. Figure 52(d) shows the orange buoys of the farm appearing to be magnified from a distance.

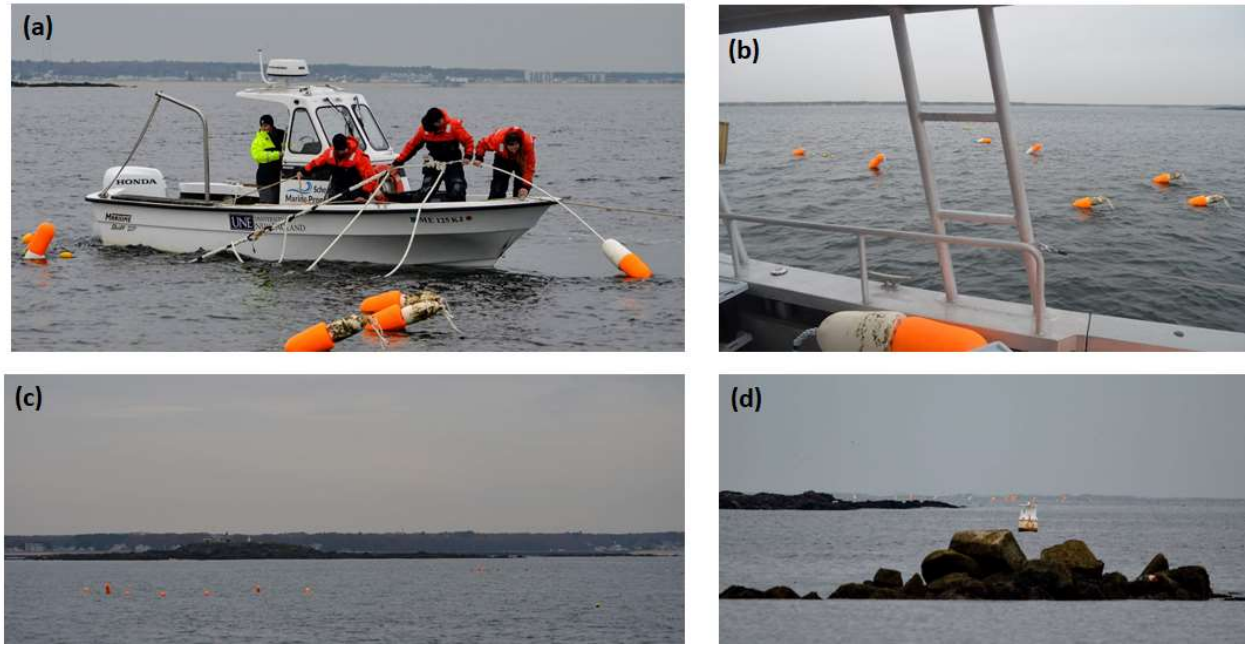

Figure 52: (a) Most of the system deployment was conducted from the 23 ft Lyr. (b) Orange buoys mark the attachment locations on the array system. (c) A view looking SSE toward Ram Island showing the array system set within the 4-acre tests site. (d) The orange buoys of the farm appearing to be magnified from a distance.

A few days after the system was deployed, a side-scan survey of the array was performed at the exposed site as shown on Figure 53. Even with the surface chop, a clear view of the rope and buoys is evident.

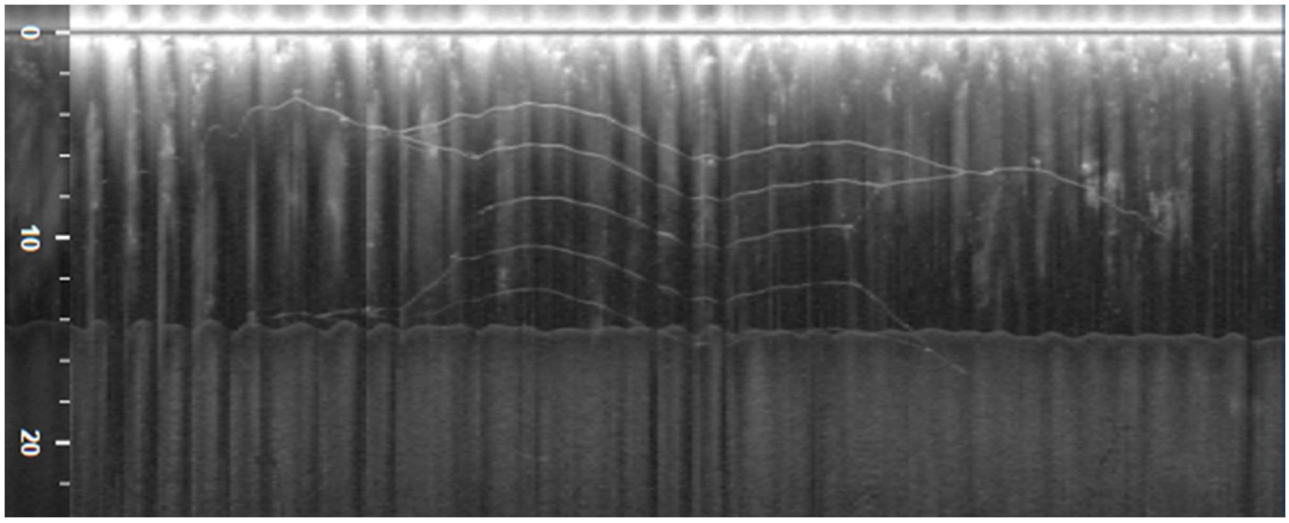

Figure 53: A side-scan sonar image of the planar-array system deployed in November-2019.

The 5-line array system was successfully seeded over two field attempts. The first was conducted on November 26, 2019 and then completed on December 23, 2019. In November, three of the five lines were seeded. Due to hazardous weather conditions, the remaining culture lines were not seeded until the next safe operational day. Seed sourced from South Portland, ME was used on all the culture lines during the first attempt. On December 23, 2019, the remaining two culture lines were seeded with source from Biddeford, ME. While examining the previously seeded lines, the outer most culture line in the array system had very little, to no growth in some areas on the culture line. To ensure productive kelp growth on every culture line, it was re-seeded while leaving the original, sparsely covered culture line in place to maximize settlement. Farm visits confirmed seed settlement on each of the five culture lines (Figure 54).

Figure 54: Seed growth one month after initial out-planting. Seed was deployed November 26, 2019 and photographed on December 23, 2019.

With the five culture lines seeded as identified on Figure 55, a qualitative assessment of growth progression of each was made on February 24, 2020 and on March 9, 2020.

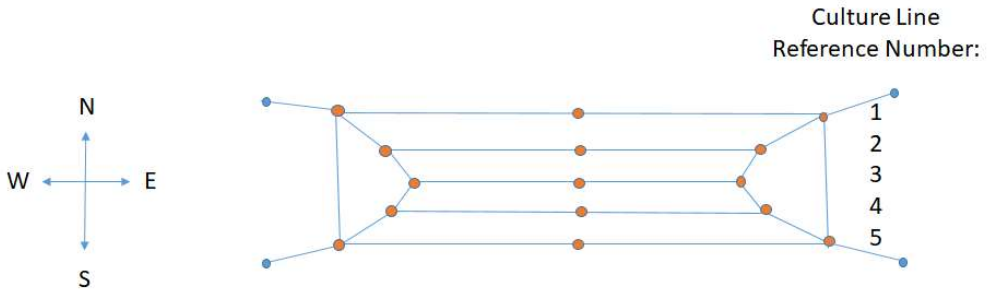

Figure 55: Reference schematic showing the numbered culture lines.

The assessment of culture line #1 is shown on Figure 56. Overall culture line #1 had some of the best growth, most likely because it contained two seed twines. Line #1 was first seeded on November 26, 2019, but did not take very well so it was reseeded on December 23, 2019. Growth progression is shown on Figure 56 (a) through (d). From these photographs, it appeared as if both sets of seed were attached to the grow line, though some size variation in the blades existed. These photos were taken to the east of the middle surface float. Figure 56 (b) is provided as a size reference showing a good section of the seed beside the floats/boat on February 20, 2020. It was estimated individual blade lengths were about 1-8 cm at this time. This photo was taken to the east of the middle float. Figure 56 (c) shows that visible growth on line #1 apparent on March, 2020. The line has more consistent coverage and blade length has increased by at least 5 cm. On Figure 56 (d), however, a noticeable issue became apparent as the seed twine was sagging on the culture line. Therefore, zip ties were used to tighten the two twines to make it more secure.

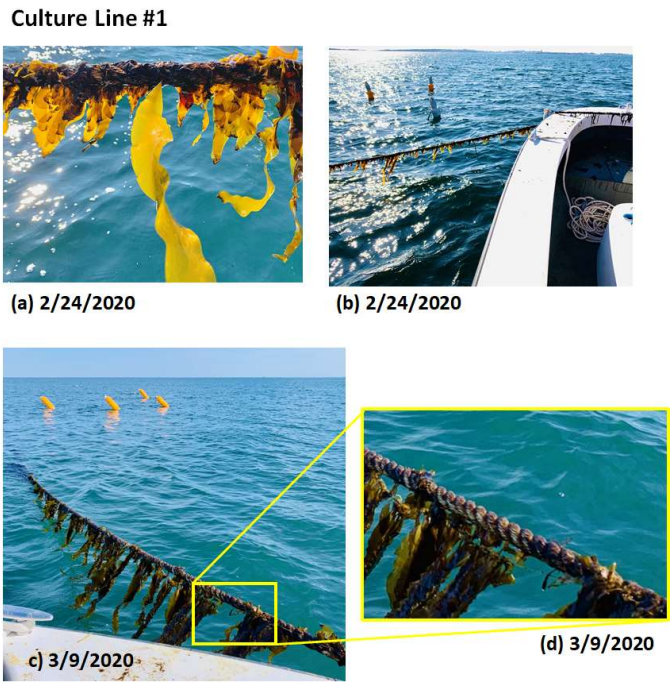

Figure 56: Growth progression of culture line #1 from February 24 to March 9, 2020.

The growth assessment of culture line #2 is shown on Figure 57 (a) – (c). Photos taking to the east of the middle float from February 24, 2020 are shown on Figure 57 (a). The Figure shows some kelp was growing beneath the center float, slightly more than was seen on culture lines 3-5. Substantial growth was evident as shown on Figure 57 (b) and (c) from March 9, 2020, also looking to the east.

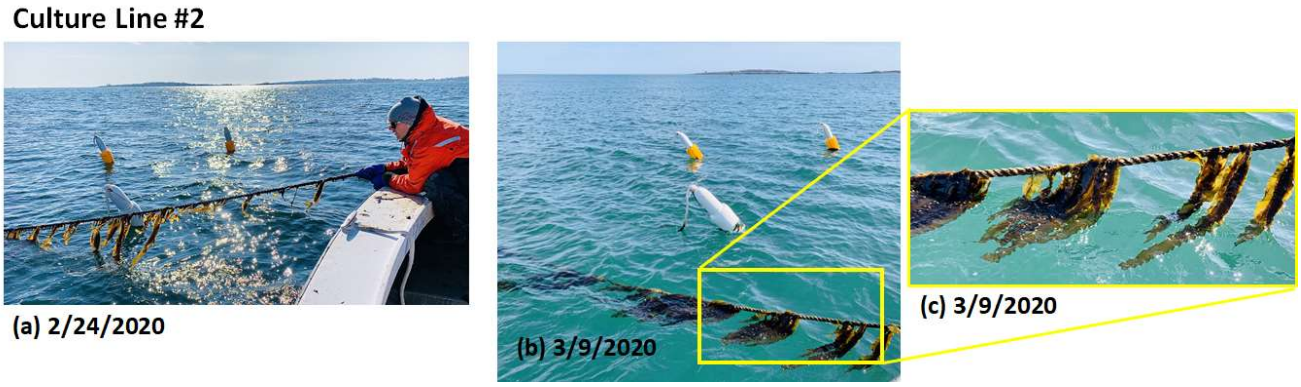

Figure 57: Growth progression of culture line #2 from February 24 to March 9, 2020.

The assessment of culture line #3 is shown on Figure 58 (a) through (f). The photo shown on Figure 58 (a) was taken at the middle surface float on February 24, 2020. It was observed that little growth existed beneath this marker buoy. More growth on line #3 was observed on the west side than the east side. Figure 58 (b) shows the growth on March 9, 2020 directly to the east of the center surface float, with less biofouling and more kelp coverage. Figure 58 (c) shows the growth on March 9, 2020 looking to the east of the center surface float. Kelp density seems to be greater further from the center of the culture line in both directions, with higher coverage to the west. A substantial gap in kelp coverage was observed west of the center surface float on March 9, 2020 as shown on Figure 58 (d) in the yellow box. A closer view of the gap is shown Figure 58 (e) and (f) where the seed line broke. Fortunately, the seed line only unraveled about 5 ft. Outside of the small affected area, the rest of the growth on the line looked healthy.

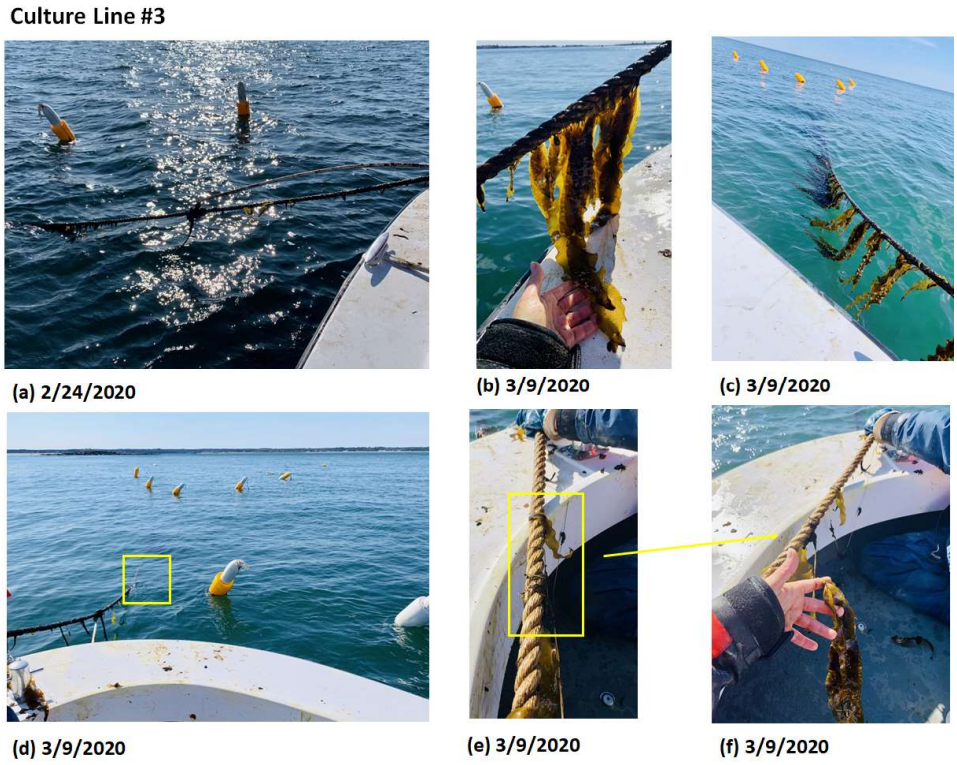

Figure 58: Growth progression of culture line #3 from February 24 to March 9, 2020.

The assessment of culture line #4 is shown on Figure 59. Figure 59 (a) was taken on February 24, 2020 directly beneath middle surface float. Once again, there seemed to be an area with minimal growth at this location compared to the rest of the line in both directions. More biofouling was found on Figure 59 (b) in the form of brown filamentous algae. It was generally hypothesized that fresh water, ice melt and general high precipitation from the Saco River in the previous two months made conditions difficult for young kelp to adhere to the 1 in nylon line. If the seed was older or set earlier, it might have withstood the fresh water stress better. However, the kelp eventually outcompeted the filamentous algae. Figure 59 (c) was taken on March, 2020 looking east from the center float. This section of culture line #4 appeared to be the least productive with sparse growth even towards the outer edges of the culture line. Looking to the west of the center float, shown Figure 59 (d), slightly more growth is evident though some gaps between the seed and culture line was evident. The gaps were fixed by reattaching sagging areas with zip ties.

Culture Line #4

(a) 2/24/2020

(b) 2/24/2020

(c) 3/9/2020

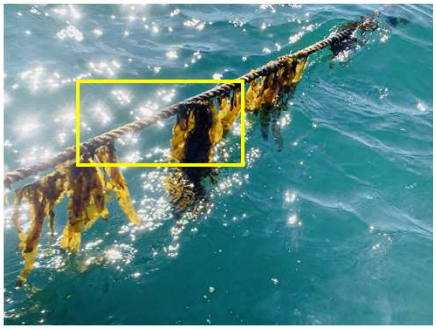

(d) 3/9/2020

Figure 59: Growth progression of culture line #4 from February 24 to March 9, 2020.

The assessment of culture line #5 is shown on Figure 60 (a) through (e). Figure 60 (a) shows a photo taken on February 24, 2020 to the west of the middle surface float. On this photo, fouling (slime) is evident adjacent to some good growth. Figure 60 (b) was taken to the east of the center float on March 9, 2020 where fouling had decreased with more consistent coverage throughout the entire culture line. The photo on Figure 60 (c) was also taken on March 9, 2020 directly east of the center float showing good growth. The section of line #5 to the west of the center surface float is shown on Figure 60 (d) where better growth and coverage was evident. It was also found that a portion of the seed twine was sagging on line #5, shown on Figure 60 (e), though it was fixed with zip ties.

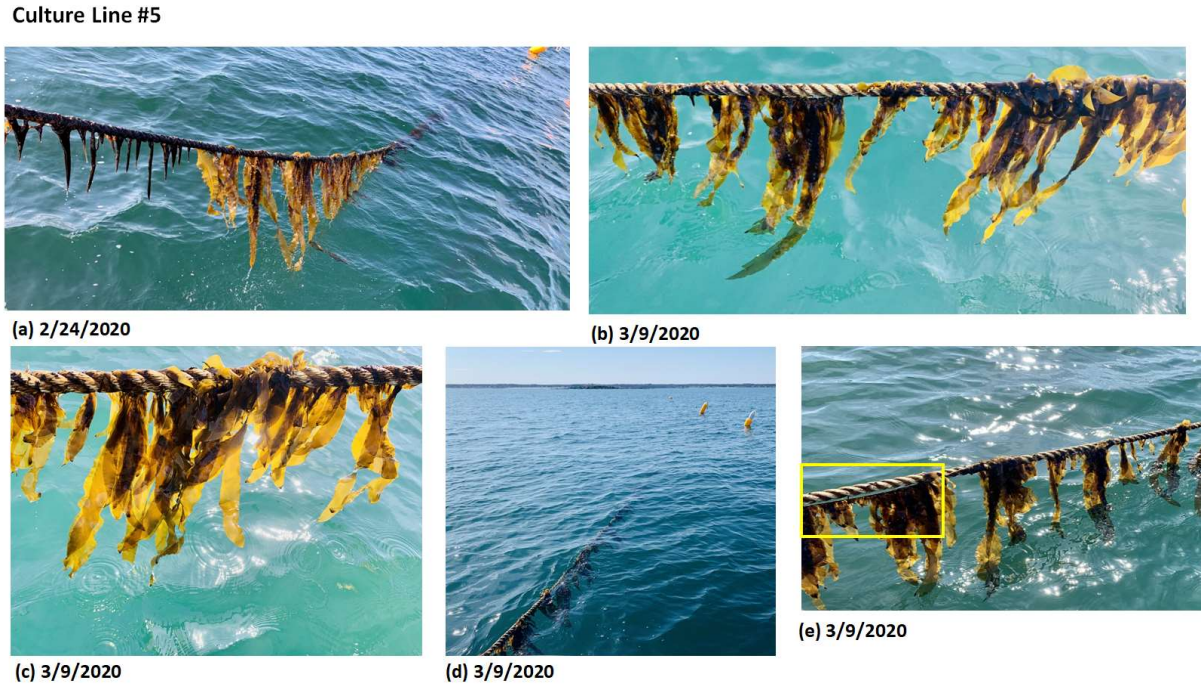

Figure 60: Growth progression of culture line #5 from February 24 to March 9, 2020.

2.2.8. Milestone 2.8: Recover and harvest planar-type system

Harvesting operations for the array system (during COVID) began on June 8, 2020 with the UNE field team and the Saco Bay Harbor Master on a 30 ft lobster boat located at Camp Ellis Pier. Once at the Ram Island site, it was clear that the kelp was weighing down the surface floats (Figure 61) with the majority of the 15 double stacked orange lobster floats partially submerged. Closer inspection showed that for each double stack, ¾ of the bottom float was submerged, leaving ¼ of the bottom float and the entire top float visible above the water line. Since the farm was approached at low tide (between 8-8:15am), all three toggles were visible on the four corner surface markers. This simple, yet informative built-in monitoring tool allowed the field team to assess the depth of the corner buoys due to growth and the vertical position of the farm without having to access any of the submerged structure. Note that this technique was first utilized on the 122m longline during the 2018-2019 growing season and implemented successfully again on the 5-line array system during the 2019-2020 season.

Figure 61: The surface flotation of the Ram Island kelp farm at low tide, before harvest on June 8, 2020. Flotation includes four corner floats comprised of two lobster buoys and three toggles with 222 N buoyancy and fifteen culture line floats comprised of two lobster buoys stacked on 3 ft of schedule 40 PVC.

The harvesting goal was to maintain the array structure of the farm and keep all of the culture lines connected. The crew was able to untie three out of the four mooring legs to detach the culture line array. The SE corner of the system was untied first, and then the NE corner was cut to release the eastern end of the system. The cut was made in a sacrificial area that could be replaced with a 1 m line splice if needed in the future. With both the Eastern corners were released, all of the five culture lines were simultaneously hauled into the boat. This was done by connecting culture line 5 to the lobster pot hauler to pull the entire system (Figure 62). This kept the boat in line with the array while four lines were hauled into the boat by hand.

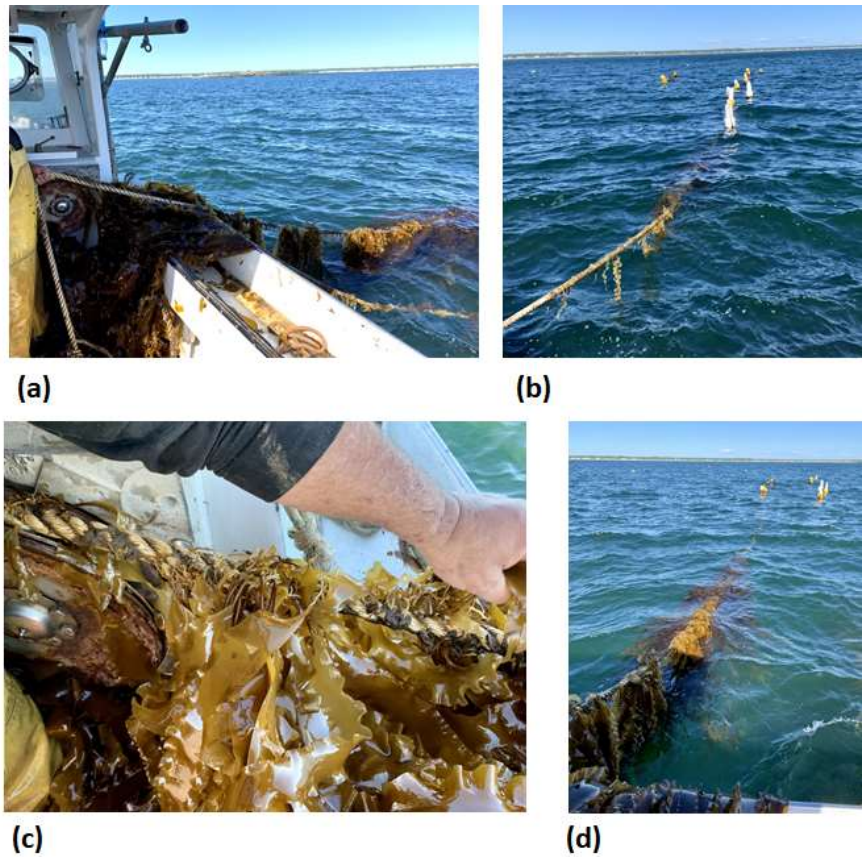

Figure 62: The system was harvested and recovered using the Saco Bay harbormaster vessel. (a) Culture line 5 was recovered with the lobster pot hauler. While the pot hauler was pulling on line 5, the other 4 lines were brought on the boat by hand. (b) Looking west, culture line 4 showed the least amount of growth along the array system. (c) Shows the dense kelp holdfast community seen on areas of the farm where the seed line was properly secured to culture line on the farm. This holdfast grouping was observed on culture line 5. (d) Looking west, culture line 5 shows substantial kelp coverage. Surface flotation from the array is shown in the background.

During the recovery, the surface lollipop floats were removed from the culture lines as they were hauled into the boat to help maintain workable space aboard the vessel. The surface flotation was intact and remained untangled during the farm season, just as they were set and deployed in November 2019. Photos of each culture line were taken to document the kelp growth. Random 1m aggregate samples from each culture line for further examine the morphological characteristics.

As the culture lines were brought onto the vessel, kelp samples were taken for morphological and biomass analysis by taking random 1 m samples as shown on Figure 63 (a). The harvest of the 5 culture lines are shown on Figure 63 (b) on the stern of the boat.

Figure 63: (a) As the culture lines were brought onto the vessel, kelp samples were taken for morphological and biomass analysis by taking random 1 m samples. (b) The harvest of the 5 culture lines are shown on the stern of the harbor master vessel.

Once the culture lines were completely on the vessel, the west end of the array was detached, leaving the four mooring leg and the lease corner floats in the water. After a 10 min transit, the vessel arrived back at Camp Ellis pier at 10:15am (Figure 64 a). The culture lines were unloaded using the pier hoist (Figure 64 b) with the kelp being removed from the culture lines. The kelp was placed in lobster bait barrels separated from the culture lines (Figure 64 c). The full harvest filled a total of eight bait barrels (six shown on Figure 64 d), one large commercial fishing tote and seven large sample coolers. The crew unloaded the remaining equipment and kelp, which was donated to the contracted fisherman, who used the kelp as compost for his personal garden in Waterboro, ME. The operation was completed by 1245.

Figure 64: (a) The 30 ft work vessel loaded with kelp at the Camp Ellis Pier. (b) After a successful harvest, the kelp was hoisted off the lobster boat in bait barrels. (c) Shows the completely harvested array system rope culture lines and catenary along with filled barrels of kelp. (d) The full harvest filled a total of eight bait barrels (six shown), one large commercial fishing tote and seven large sample coolers.

On June 9, 2020, the anchor legs were retrieved with a local contracted mooring specialist (Todd Stewart), and offloaded them on the Camp Ellis Pier. The gear was then brought it back to the UNE Biddeford campus to be stored for the 2020-2021 season as shown on Figure 65 (a) and (b).

(a) (b)

Figure 65: (a) Mooring equipment retrieved from the Ram Island kelp farm. (b) All mooring equipment was transported and stored back at the UNE Biddeford campus using the "Farm in a Box" technique for organized deployment next season.

After a visual inspection aboard the vessel, it was clear that growth rates varied among the five culture lines. Culture lines 1, 2, 3, and 5 all were approximately 75% covered with mature kelp growth, with some patchiness. Culture lines 1 and 2 showed the most robust kelp growth. Recall that culture line 1 was seeded with two twines and was located on the outside of the array on the northern part of the system. It was also the furthest line away from the mouth of the Saco River. These were all factors that influenced kelp growth on line 1. Culture line 5 was also heavily covered with mature kelp blades and tight holdfast communities. Culture line 3 was more productive than line 4, but less than lines 1, 2, and 5. Culture line 4 was the lease productive in the system, showing very low kelp density. Other than the 1 m samples, the majority of the kelp was left on the line while it was hauled into the boat to better understand the growth distribution.

The morphological characteristics of the kelp showed it was much longer and skinnier than grown on the 122 m long-line system during the 2018-2019 season. In general, the stipes were long and solid, not hollow like in past Saco Bay deployments. It is also worthwhile to note that we did not add any additional counter weights beneath the surface flotation during the 2019-2020 season. Large aggregate holdfast sections were observed on the culture lines that were denser and (structurally) than observed at this site in the past. This could be related to the fact that seed deployed on the farm was sourced from Biddeford Pool in late September to early October of 2019. There was also very little fouling on the kelp, with almost no presence of bryozoans and hydroid settlement on the blades. There was, however, an increase in fouling in the holdfast community on the culture lines. Wild set *Mytilus edulis* (blue mussels)*, Mya arenaria* (soft shell clam) and *Semibalanus balanoides* (acorn barnacle) along with predatory *Littorina obtusata* (flat periwinkle), *Littorina saxatilis* (rough periwinkle), and *Littorina littorea* (common periwinkle) along with their egg casings and other wild set seaweeds like *Palmaria palmata* (dulse)*, Alaria*

esculenta (winged kelp)*, Chondrus crispus* (irish moss), and *Porphyra umbilicalis* (purple laver) beside the cultivated *Saccharina latissima*. Sorus tissue was also present on mature blades attached to the farm. Examples of the kelp during sampling are shown on Figure 66 (a) and (b) on the vessel and back at the laboratory, respectively.

(a) (b)

Figure 66: (a) Harvested sample kelp just after being removed from the culture line. (b) Liz and Barry examine freshly harvested kelp back at the UNE laboratory.

2.2.9. No Cost Extension: Reperforming Activities for Task 2.5, 2.6, 2.7 and 2.8

Because of the covid-19 situation that occurred during the 2019-2020 season, instruments were not deployed on the array system even though it was installed, seeded and recovered. Therefore Tasks 2.5, 2.6, 2.7 and 2.8 were repeated for the 2020-2021 season.

Task 2.5 - Modification of the UNE array for the 2020-2021 season: Since the array system had to be redeployed for the 2020-2021 season, it was decided to modify the culture line components based on the experience of the previous deployments. In both the single and array line systems, the seed twine was installed on 1 in, 3-strand nylon rope. This rope had a new breaking strength of approximately 22,230 lbf and a working load of up to 4446 lbf. With 1 in, 3 strand rope, the seeded twine would find its way into the grooves of the lay regardless of the twist direction. The nylon rope also absorbed water making it heavy to handle. It was therefore decided to modify the culture line specification with ¾" polyester with a single braid construction (PE12). Out of water, this line is approximately ½ the weight, but still comparable to the 1 in nylon having a

breaking strength of 20925 lbf and a working load of 4650 lbf. In addition, with the single braid construction, the deep grooves within the lay did not exist. A visual comparison of the two rope types are shown in Figure 67. Also, note the orange color of the new grow-line for better visibility purposes.

Figure 67: A visual comparison of the nylon grow-line with the polyester (PE12) grow-line to be deployed during the 2020-2021 season.

To improve upon the 2019-2020 design and to apply the kelp modeling validation approaches described in Task 5, a new set of modeling simulations were performed for the array type system. A screen-shot of a time step is shown in Figure 69. Input to the model simulation includes the validation techniques described in Task 5. The system was identical to the 2019–2020 system, except that the grow lines were ¾" single braid PE-12 (polyester) rope as shown on Figure 67. The geometric and material properties of the entire system are provided in Table 8.

Table 8: Geometric and material properties used as input for the numerical modeling effort.

Component	Material	Qty	Length	Net Buoyancy	Density	Diameter	Volume	Mass/length
				Total			Each	
			m each	kg	kg/m3	m	m^3	kg/m
Anchor Chain	5/8" Long-link	2	4.6	-44	7880	29.9E-3	3.22E-03	5.55
Mooring Line	1" Nylon	2	29.0	-1	1140	15.9E-3	5.73E-03	0.23
Mooring Line	1" Nylon	2	6.10	0	1140	15.9E-3	1.21E-03	0.23
Mooring Line Float	2X Spongex 9X16	4	0.81	98	6.67E+01	200.3E-3	2.56E-02	2.10
Corner Surface Floats	2X Spongex 9X16	4	0.81	98	66.67	0.20	2.56E-02	2.10
Tether	PVC-shielded P-E	4.0	2.13	0	1025	2.10E-02	7.39E-04	0
Header	1" Nylon	2	19.5	-1	1140	15.9E-3	3.86E-03	0.23
Longline	3/4" P-E 12	3	31.5	-10	1380	19.1E-3	8.97E-03	0.39
Longitudinal	3/4" P-E 12	2	45.7	-9	1.4E+3	19.1E-3	1.30E-02	0.39
Transverse	1" Nylon	2	9.1	0	1.1E+3	15.9E-3	1.81E-03	0.23
Kelp	Kelp	94.39351	2.0	-24	1.06E+03	68.0E-3	7.26E-03	3.848
Growline Floats	Polyform A0	11	0.813	63	66.667	0.200	6.00E-03	0.49
Tether	pvc	11.0	2.134	0	1025.000	0.021	7.39E-04	0.355
				192				

To perform the assessment, extreme loading simulations were performed with the new planar system by using the modeling techniques developed in this project. Extreme storm conditions specified for a 60-year storm were a 1 m/s current collinear with a 4.2 m significant wave height, 11 s peak period sea-state, combined with a maximum tidal elevation of 3 m. The model incorporates 2 m long kelp blades. Four load cases were examined:

1. Static conditions; no waves and no currents.
2. Waves and current aligned with the grow lines.
3. Waves and current aligned with a single anchor line.
4. Waves and current normal to the grow lines.

The load-cases are summarized in Table 9.

Table 9: Load cases, static and extreme loading.

Load case	Surface Elevation	Current Speed	Current direction (toward)	Wave Height (significant)	Wave Period (Peak)	Wave direction	Notes
	m	m/s	degrees	m	s	degrees to	
1	1.5	0	0	0	5	0	Static, mid-tide
2	3	1	180	4.2	11	180	Parallel, 60yr
3	3	1	210	4.2	11	210	Diagonal, 60yr
4	3	1	270	4.2	11	270	Perpendicular, 60yr
5	1.5	0.1	150	0.5	5	150	Typical

For each load-case, the maximum expected loading under a one-hour long storm was calculated from the mean and variance of the tensions observed in the simulation. The resulting design loads are given in Table 10 provided in N. The maximum tensions were calculated were 24,312 N equivalent to 5466 lbf. The array response to typical forcing conditions is shown in Figure 68: Array response to typical environmental conditions.. The response to an extreme (60-year) storm in illustrated in Figure 69.

Table 10. Maximum expected loads in system during a 1-hour storm (load cases 1-4).

Moorings	Headers	Longlines	Anchors		Load case
Tension, N			Horizontal, N	Vertical, N	
1,421	528	404	729	2,710	Statics
21,426	13,022	9,634	20,006	4,355	Parallel
24,312	16,588	8,871	22,549	4,656	Diagonal
18,174	11,702	5,257	16,685	3,821	Perpendicular

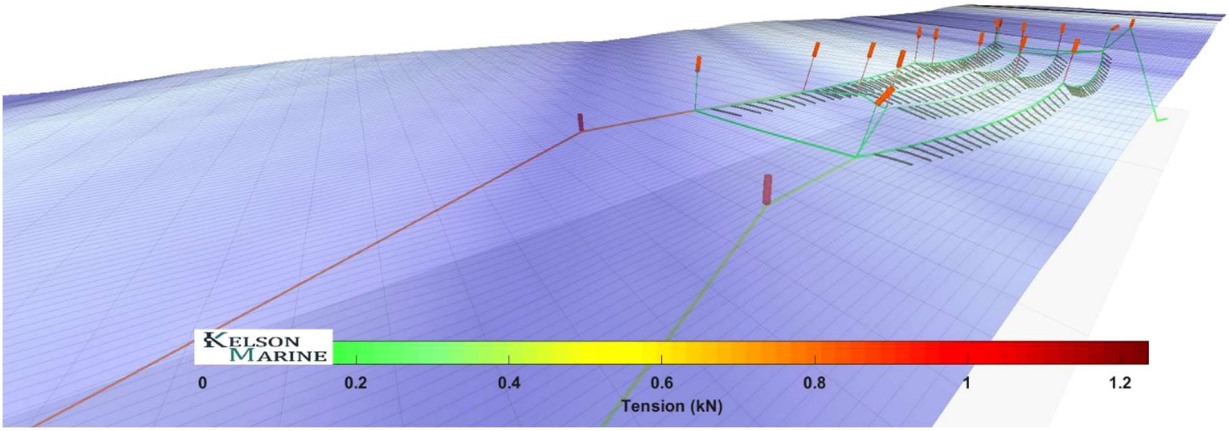

Figure 68: Array response to typical environmental conditions.

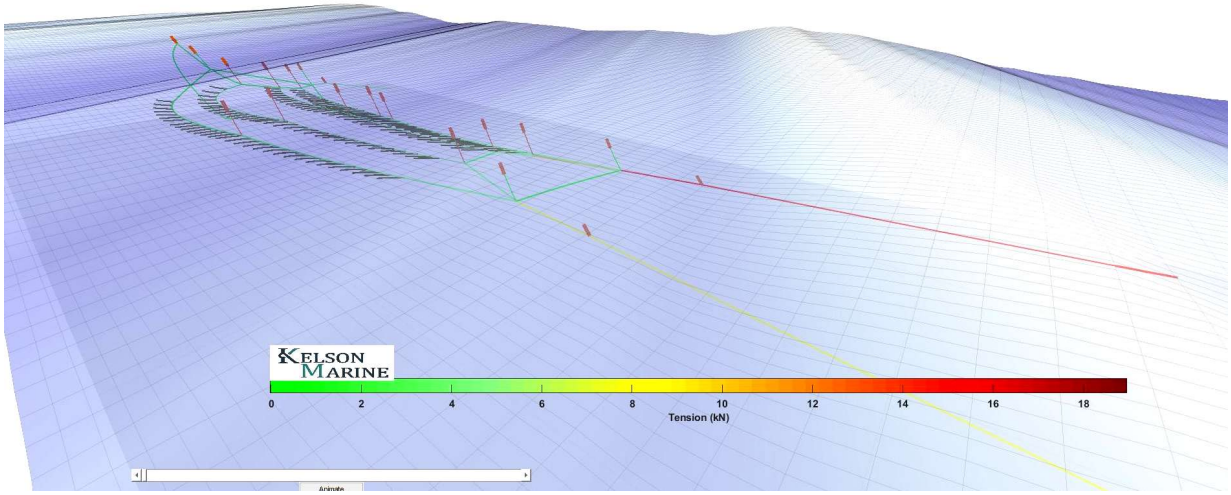

Figure 69: Planar array system in 60 year storm conditions at high tide, with waves and currents parallel to a single anchor line. Input to the model simulation includes validation techniques described in Task 5.

During the summer and fall of 2020, it was decided not to obtain sorus tissue nor grow the kelp seed in the UNH hatchery. Instead, it was found to be more efficient to purchase 10 spools of hatchery seed from Atlantic Sea Farms (https://atlanticseafarms.com/).

During the fall of 2020 as part of the NCE, farm components were prepared for deployment. As part of these preparations, all farm components were pre-measured and cut on shore and flaked into labelled totes. On November 9, 2020, the R/V Sakohki was loaded with the Ram Island, 'farm-in-the-box" array system and headed out to the site. Once at the site, the five bins of orange culture lines were arranged on the forward deck of the vessel (Figure 70a). As shown on the Figure, preparations were done to attach premeasured and cut culture lines to the eastern header line. The culture lines were then attached to the header at pre-determined positions indicated by alpine butterfly knots. The kelp seed spools were housed in settling tubes with seawater as shown on the bottom of Figure 70a.

Prior to deployment, the east and west catenary headers were attached to grow ropes that were flaked in containers (Figure 70b). Depth control flotation (e.g. "lollipop" floats) were also attached to each header rope at the predetermined locations. Header rope terminations were attached to the four mooring lines that were temporarily lashed together and secured along the gunwales (see Figure 70b lower right).

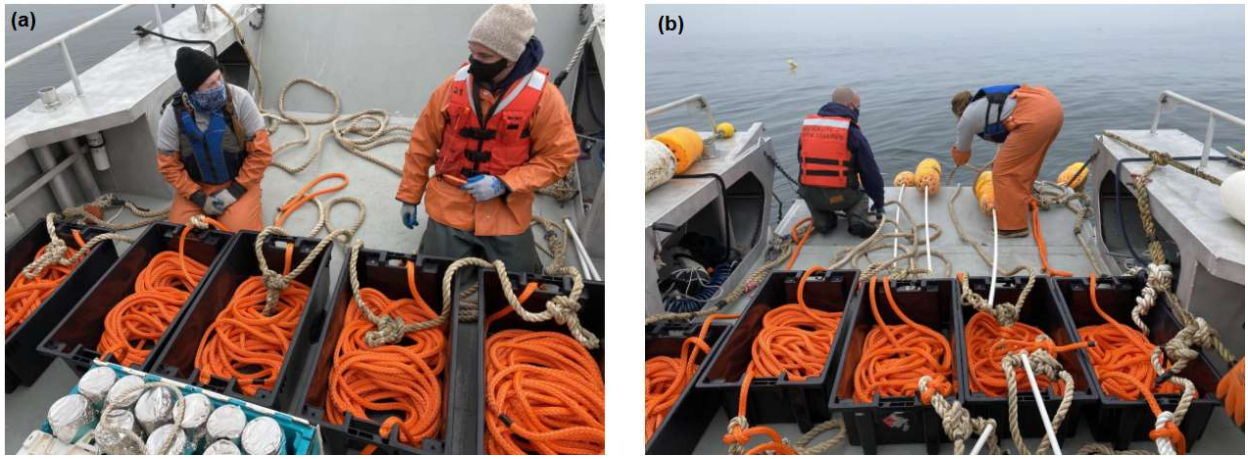

Figure 70: (a) The orange grow lines were pre-staged in storage totes. Note the butterfly hitches on the head line. (b) The culture lines were attached to the head line with a sheet bend. Lollipop floats were attached at the same locations. The system was stage for deployment of the bow of the R/V Sakohki.

Figure 71(a) shows the kelp seedlings being threaded onto culture lines on the western end side of the farm. They were threaded before culture lines were tied into the headers. The excess grow line was then passed back over the top of the spool and temporality tied to prevent movement and allow spool access after the array is deployed. The spools were then placed back in seawater tubes while the farm was deployed. On Figure 71 (b), western header is shown after being deployed with the vessel backing to the east. This deployment procedure allowed for the culture lines to un-flake from the totes. Note kelp spools were still in seawater tubes. On Figure 71 (c), the kelp spools and eastern catenary are shown being deployed as the vessel continued to back to the east between the northeast and southeast moorings.

Figure 71: (a) On the back end of the array, the seed spools were placed on the culture lines. (b) With everything attached, the front end was deployed, laying out the gear as the vessel moved backwards. (c) At the back end of the array, the seed spools were softly placed into the water.

Figure 72 (a) shows the farm immediately after deployment looking west from the eastern header line. The photo was taken prior to mooring placement adjustments and farm was not yet fully tensioned (note corner floats with toggles fully at the surface). As shown on Figure 72 (b), a smaller vessel was then used to untie spools and seed farm from east to west taking about 20 minutes to complete. Once the seed was deployed, depth control buoys were attached and the farm was fully tension. The tensioning procedure was done by attaching the vessel to the northwest and southwest mooring crown lines and backing down until the top toggle on the corner floatation was just below the surface. Small adjustments were then made to the eastern moorings to ensure proper location, tensioning and farm geometry.

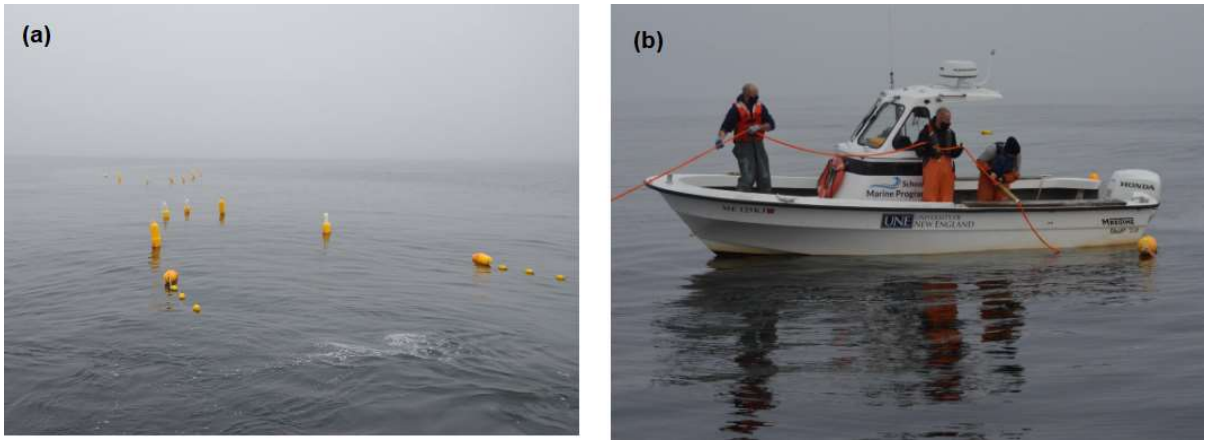

Figure 72: (a) The entire array system is deployed with floats marking the header lines. (b) A smaller vessel was then used to run the spools along the grow lines installing the seeded twine.

From January to February 2021 during the NCE, the kelp system was left to establish itself after field deployment and seeding of the array system in November 2020. During this time, UNH deployed an ADCP at the Ram Island site to measure both waves and currents. On February 2, 2021, the instrument measured significant and maximum waves of 3.89 and 6.57 m, respectively, with a dominant period of 11.75 seconds. Currents with magnitudes of about 0.5 m/s were also measured during the same time. The 5-line array was examined on March 3, 2021 with its configuration still intact as shown on Figure 73 (a), having survived the storm from 2-Feb-21 (though fishing ghost gear was found wrapped around one of the anchor legs). The kelp was found growing on all lines with a nominal length of 0.3 m despite heavy freshwater input from early winter storms as shown on Figure 73 (b) and (c). The kelp appeared healthy.

Figure 73: (a) The five-line array was inspected on March 3, 2021 and was still intact after storm on February 2, 2021. (b) and (c) The kelp was found growing on all lines with a nominal length of 0.3 m despite heavy freshwater input from early winter storms.

Monitoring of the kelp farm continued on April 9, 2021 with an inspection that showed healthy kelp growing well, dominating over the slime that was typical during the early stages of the grow out at this Saco Bay site (Figure 74). With the farm and kelp in good condition, the four load cells, blue-northeast, red-southeast, yellow-southwest and green-northwest with the AWACS (blue-east, yellow-west) were deployed on April 15, 2021. The green load cell is shown in Figure 75. The instruments were deployed just prior to a Northeast storm event that occurred on April 26, 2021. The instruments were recovered on April 28, 2021. During the instrument deployment, biomass measurements were made on both the deployment and recovery days. An example of the kelp monitoring operation is shown in Figure 76 conducted on April 15, 2021. Measurements were made of the length of the kelp at five locations in the farm, with one shown on Figure 76(a). Photographs were also taken showing the waterlines of the support buoys (Figure 76b). The waterline information was used with static numerical model simulations to assess system hydrostatics with mass density estimates. Mass density values were also estimated by making in and out of water measurements of 1 m kelp aggregates in still saltwater tanks (Figure 76c).

Figure 74: Kelp starting to accelerate grow and dominating over the slime that is typical at the Saco Bay site during survey operations on April 9, 2021.

(a) (b)

Figure 75: (a) The green load cell prior to deployment of the NW anchor line and (b) the two AWACS prior to deployment on the East and West sides of the farm on April 15, 2021.

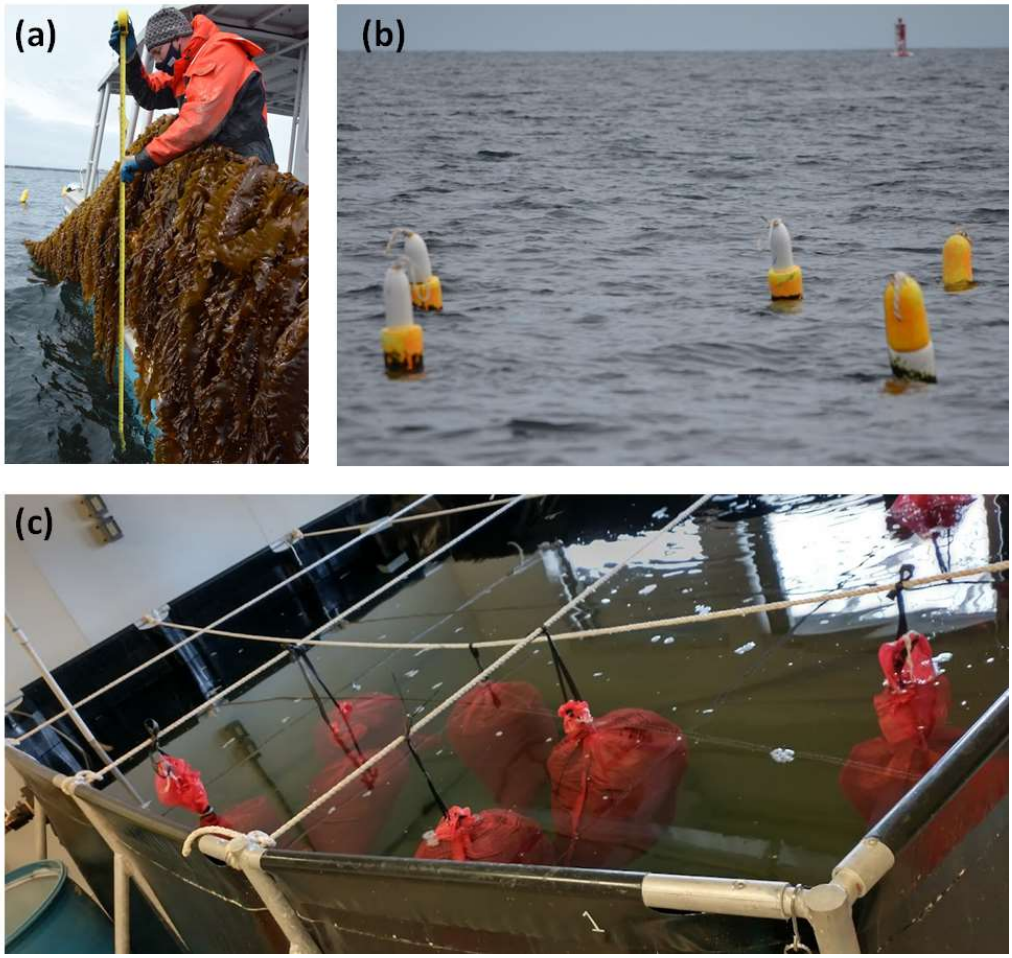

Figure 76: Monitoring of the kelp on 15-April-21 included measuring the length (a), estimating buoy waterline for biomass assessment (b) and performing in/out water weight measurements in still water (c).

The AWAC and load cell instruments were recovered on April 28, 2021. Once again, biomass on the farm was estimated using the same techniques. The instruments were taken back to the shore for data download and then to assess data quality and power consumption. The dataset assessment was necessary to justify a quick turnaround for redeployment that occurred on May 7, 2021. The red load cell is shown being re-installed on Figure 77 (a). Figure 77 (b) shows biomass during the assessment process also on May 7, 2021. The instruments were then recovered on May 20, 2021.

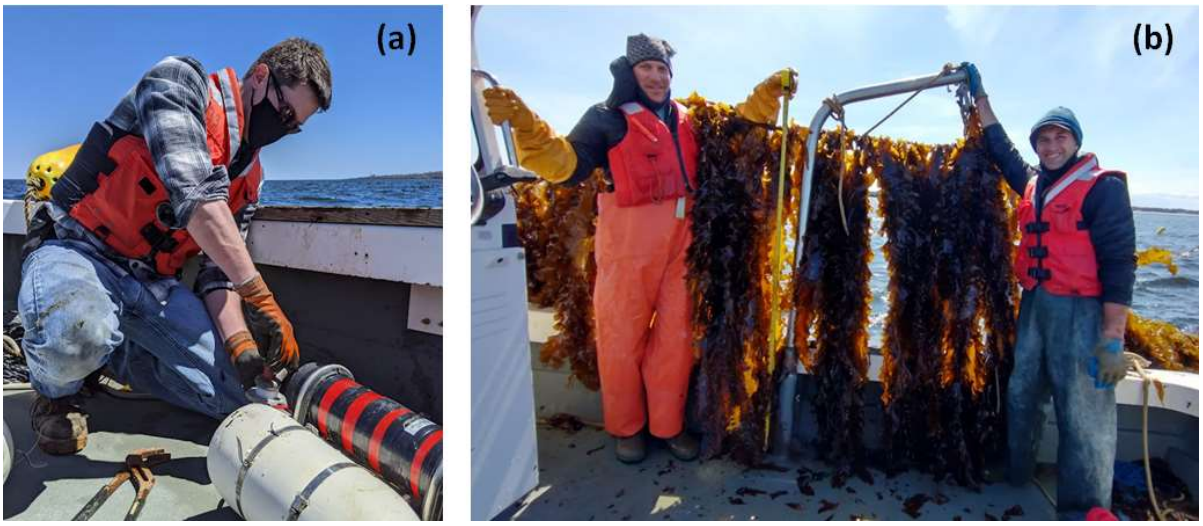

Figure 77: (a) The red load cell being installed on the southeast mooring leg. (b) Biomass assessments being made on the farm on 07-May-21.

Milestone 2.8 Recover and harvest planar-type system: Harvesting of the 5-line array took place on May 21, 2021. Photos on Figure 78 show a 1 m section that was previously sampled (a), final biomass sampling (b), measuring lengths of kelp in an aggregate (c), the harvest of the system (d), removing the 5 grow lines (e) and harvest on the UNE dock (f). A total of 36, 1 m samples were taken during the Spring of the 2021 field season across four separate days. Nine, 1 m samples were taken when oceanographic instruments (AWAC and Load Cells) were either deployed or retrieved. Sampling procedure was to take 1 m sections at the four outside corners on the Ram Island farm on the outer most lines, 1 m sections on the adjacent interior line midway between the outside of the line and the center of the farm, and a 1m section at the center of the middle line. This created an "X" in the farm. Sampling was conducted in this way to ensure an accurate representation/estimation of total biomass as we have experienced highly variable growth throughout the project season and across years.

The field program for the project was successful as Task 2.7 to "Seed, deploy and monitor planar-type system" and M2.8 to "Recover and harvest planar-type system" were both 100% completed by May 21, 2021.

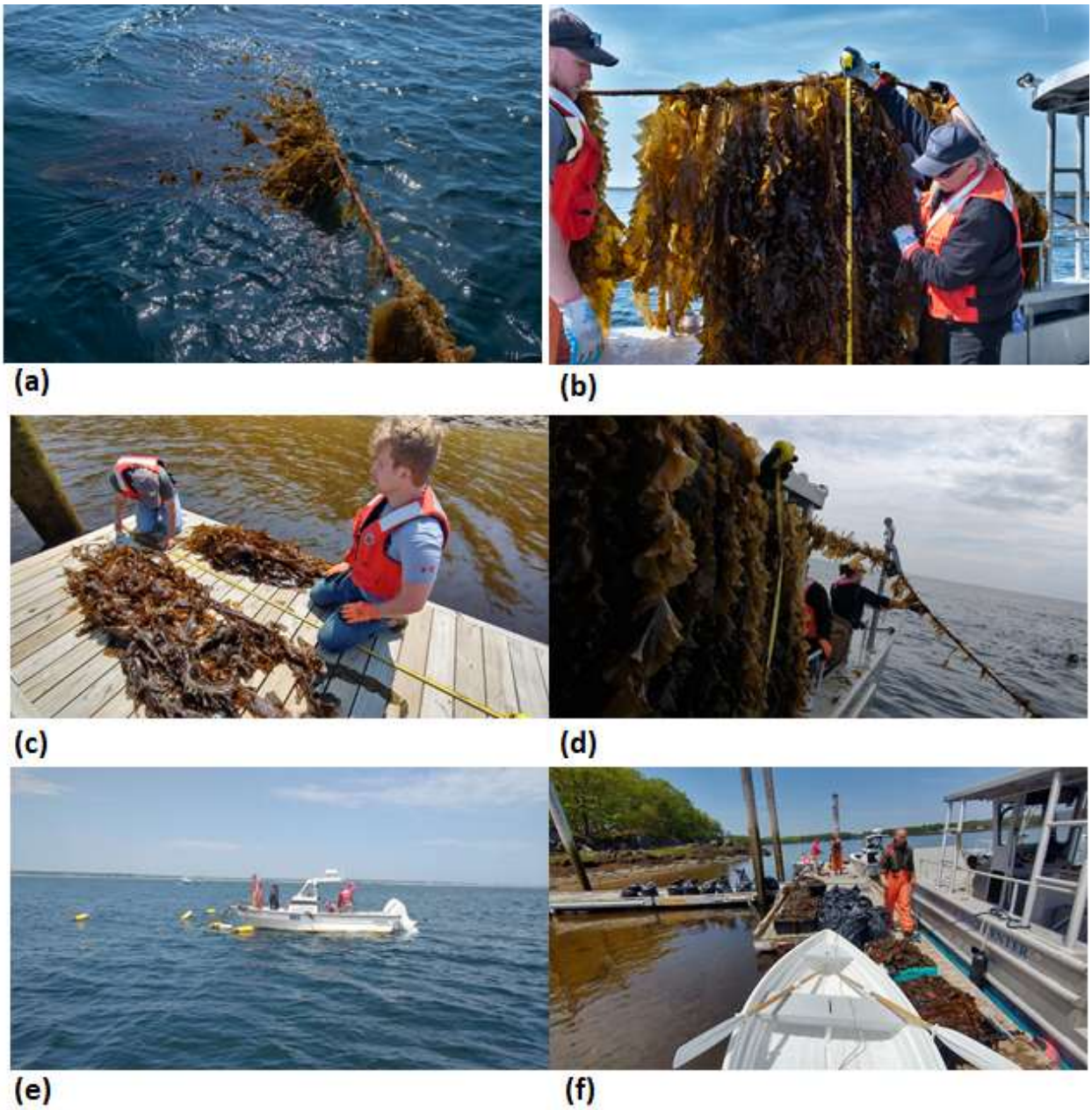

Figure 78: A 1 m section that was previously sampled (a), final biomass sampling (b), measuring lengths of kelp in an aggregate (c), the harvest of the system (d), removing the 5 grow lines (e) and harvest on the UNE dock (f).

2.3. Task 3.0: Morphology, geometric & material properties

The geometric and material properties of kelp is a critical component necessary to resolve the response of these aquaculture structures in waves and currents. Kelp blades will reconfigure into streamline orientations, minimizing drag forces to maintain holdfast integrity. In steady fluid flow, the static orientation of kelp blades is determined from the balance of external, internal and body forces. The external forces consist of a combination of normal and tangential drag forces as a function of the relative velocity vector as described in Fredriksson et al. (2020). Internal forces in this application consist of mostly of kelp bending resistance characterized by the flexural rigidity,

$$Flexural\ Rigidity = EI. \quad (16)$$

In equation (16), E is the modulus of elasticity and I is the second area moment about the cross-section. Dominating body forces are volumetric as weight

$$Weight = \rho_{kelp} g V_{kelp} \quad (17)$$

and buoyancy

$$F_b = \rho_w g V_{kelp}. \quad (18)$$

In equations (17) and (18), ρ_{kelp} is the mass density of the kelp, ρ_w is the mass density of the water and V_{kelp} is the volume of the kelp assuming that it is all submerged.

In this part of the study, multiple opportunities were utilized to examine the geometric and material properties of the kelp grown at both the Wood and Ram Island sites in Saco Bay for the purpose of understanding how to represent kelp in the Hydro-FE model. The approach was based on the 1 m aggregate, full scale model used in the tank tests. The field deployment opportunities are described below.

1. 2018: Wood Island site, 30 m culture line
2. 2019: Wood Island site, 61 m culture line
3. 2019: Ram Island site, 122 m culture line
4. 2020: Ram Island site, 186 m, five culture line array
5. 2021: Ram Island site, 186 m, five culture line array

2.3.1. Task 3.1: Develop sampling plan and protocol: (10/15/2018)

The planned protocol for collection of field samples was based on a field experiment that took place at the Wood Island site in the spring of 2018. During this experiment, approximately 30 m of a 60 m culture line was used for kelp grow out. The sampling approach at the time was chosen that would minimize the impact of measuring tension with the load cells due to the biomass, but still cover the length of the culture line. The first step in the protocol was to perform an overall survey of the entire culture line length to gauge growth distribution noting growth density and length of the kelp. Once the initial survey was completed, it was planned to collect 10 cm kelp segments at two locations along the 30 m section of culture line.

From the two sample locations in this preliminary survey, 43 individual blades were counted in the first 10 cm segment with an average length of 43 cm and a total mass of 0.686 kg. In the

second 10 cm segment, 38 blades were measured with an average length of 0.49 m and a total mass of 0.683 kg. Distributing the mass over the 30 m seeded length, the total mass on the culture line was estimated at 206 kg or 6.87 kg/m.

From this experience, it was therefore decided to sample the single line culture systems for the 2019 season on both the Wood (61 m) and Ram (122 m) site at west, middle and east locations (Figure 79). The intent of the sampling effort was to obtain the geometric and material properties and the growth density of biomass. The protocol also included sampling to be done to coincide with load cell measurements planned for 1-2 week intervals from March-May based on available weather windows.

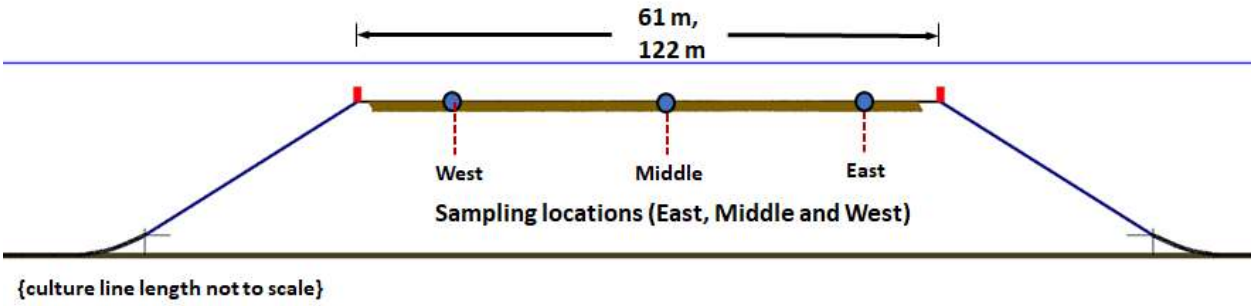

Figure 79: Sampling was conducted on both 61 m and 122 m culture line systems at west, middle and east locations. A 61 m culture line was deployed at the Wood Island site and a 122 m culture was deployed at the Ram Island site.

Samples obtained at the west, middle and east locations were processed for general dimensions of the blade and stipe with corresponding masses. The second set of measurements subsampled the blades from the intercalary meristem (IM) and the blade tip (BT) into swatch samples to determine the kelp mass density (ρ_{kelp}) and the modulus of elasticity (E_{kelp}) in an effort to represent a 1 m aggregate of kelp.

The measurement protocol was to obtain the length (L_{swatch}), width (b_{swatch}) and thickness (t_{swatch}) of swatch blade portions. These geometric properties were first used to obtain the volume of the sample (V_{swatch}). The dimension also provided the second area moment (I) of the swatch sample as a rectangular cross-section described as,

$$I_{swatch} = \frac{1}{12} b_{swatch} t_{swatc}^{3} \ . \quad (19)$$

The mass of the sample was also obtained with it being wet, but not dripping. With the V_{swatch} and the mass, the mass density of the kelp (ρ_{kelp}) was calculated. The modulus of elasticity of the sample was then determined by performing a cantilever beam test to obtain the flexural rigidity (equation 16) and from

$$\text{Flexural Rigidity} = E_{kelp} I_{swatc} \ = \frac{\mathrm{w} L_{swatch}^{4}}{8\, \delta_B}, \quad (20)$$

with δ_B as the deflected distance and w as the distributed weight defined as

$$w = \frac{\rho_{kelp} g V_{swat}}{L_{swatch}}. \quad (21)$$

The May 2018 preliminary experiment at the Wood Island site provided an opportunity to investigate laboratory techniques to determine the mass density and modulus of elasticity of the kelp. The technique is fully described in Zhu et al. (2021) and summarized here. As shown on Figure 80 (a) and (b), calipers were used to measure the length and width of each swatch. A micrometer (or caliper) was used to measure the thickness and a scale to measure the mass of the swatch (Figure 80c). Each of the length, width and thickness measurements were made at each corner and the results averaged. The mass was measured on a scale, then the mass density calculated by knowing the volume of the sample.

The modulus of elasticitiy was then determined by performing a cantilever test as shown in Figure 81 (a) and (b). Figure 81 (a) shows a schematic defining the terms to obtained the flexural rigidity,

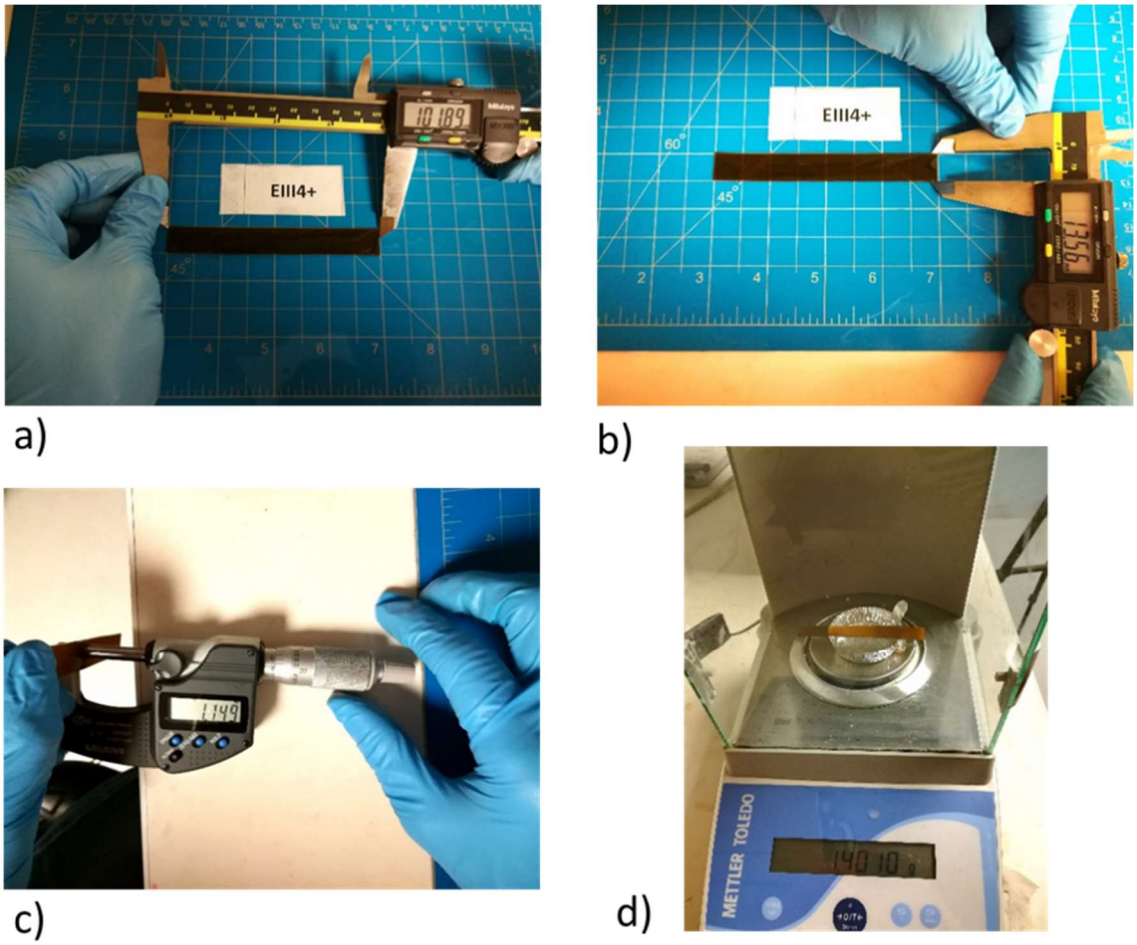

Figure 80: Kelp swatch sample measurement of a) length, b) width, c) thickness and d) mass.

As shown on Figure 81 (b), the deflected value can be obtained by using high resolution, digitized methods and with equation (20), the flexural rigidity was calculated. With the second area moment of the cross-section, the modulus of elasticity was calculated at the different sections.

Previous results show that the material properties change along the length of the blade Figure 81 (c).

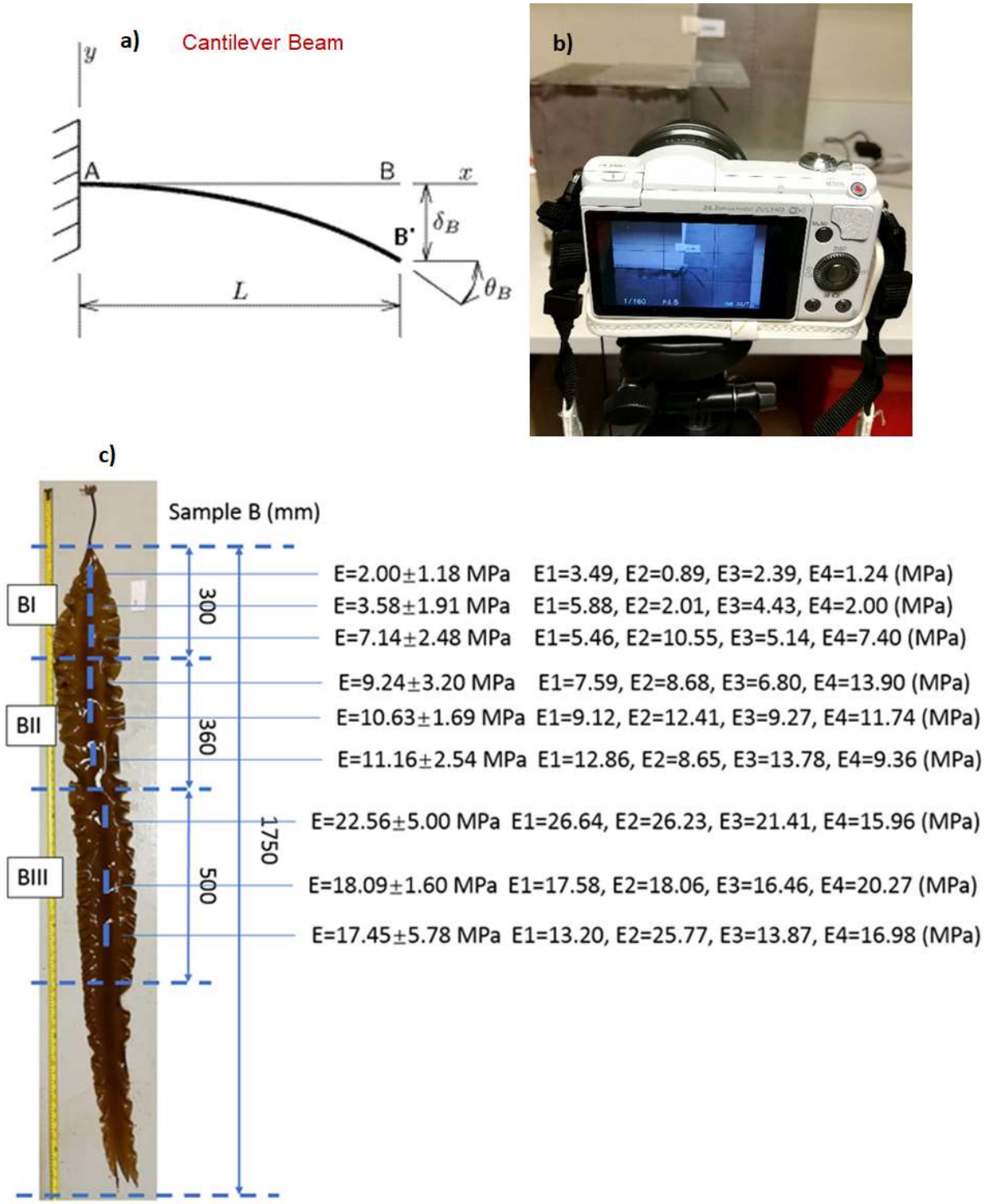

Figure 81: (a) A schematic defining the terms associated with the cantilever beam tests. (b) Digitized or caliper methods will be used to measure deflection. (c) Results show that in this case, the modulus of elasticity changes along the blade.

2.3.2. Task 3.2: Collect field samples from first deployment (5/28/19)

Utilizing the preliminary May 2018 dataset from the Wood Island site, the samples were processed to determine the material properties of kelp grown on the 30 m section of the 60 m culture line. The sampling effort included picking five blades off the culture line and labeling them A, B, C, D and E. For each of the five blades, the total length was subdivided in sections identified as I, II and III. One to three swatch samples were cut from each section at positions along the thicker, more developed main axis of the blade. The geometric characteristics of the swatch samples were measured to include L_{swatch}, b_{swatch} and t_{swatch}. With the geometric properties, the volume and second area moment of the cross-section was calculated and the mass measured. Then the mass density was calculated. The swatch sample was then use in the cantilever beam tests, as shown on Figure 81 to determine the flexural rigidity and using the second area moment (I), E_{kelp} was calculated. Forty-one subsamples were used from the set of five blades. The results are provided in Table 11 with details in Zhu et al. (2020).

With the experience from the 2018 season at the Wood Island site, the sample protocol was applied to the 61 m and 122 m single culture line system at both the Wood and Ram Island sites during spring 2019. During this sampling period, 198 kelp samples were obtained from both sites at the west, middle and locations on each farm. General morphological measurements were made with five replicate blades at each location. The results are provided in Table 12. Samples were also processed to obtain the material properties of mass density and modulus of elasticity based on the cantilever-beam test procedure. At each location, five subsamples were taken from the intercalary meristem (IM), the blade tip (BT) and the stipe (ST). Swatches were cut from each location with the nominal dimensions of 5 cm by 2 cm for the IM and BT samples. Actual dimensions were then obtained for the length, width and thickness of each swatch then weighed to find the mass. With the mass and volume, the density of the sample was calculated. From the cantilever beam test, the flexural rigidity (EI) of the sample was calculated and then the modulus of elasticity obtained by knowing the second area moment (I). The results for the spring 2019 sampling period are provided in Table 13 for the Wood Island site and in Table 14 for the Ram Island site. Averages are also provided on the Tables for each sampling day.

Table 11: Material property raw data results of sampling five kelp blades from the May 2018.

Sample No.	Blade & Location	Length (l) (mm)	Width (b) (mm)	Thickness (t) (mm)	m (g) (g)	V (cm^3)	I (cm^4)	ρ (g/cm^3)	E (MPa)	Stdev (MPa)
1	AI1	76.68	13.12	0.97	1.02	0.97	9.83E-05	1.053	7.09	1.52
2	AI2	75.89	13.35	0.92	0.99	0.93	8.67E-05	1.064	5.94	0.71
3	AI3	75.64	13.30	0.96	1.00	0.97	9.87E-05	1.029	4.52	1.74
4	AII1	77.05	13.13	0.96	1.00	0.97	9.63E-05	1.033	14.55	2.46
5	AII2	76.74	13.09	0.98	1.03	0.99	1.03E-04	1.047	11.69	3.26
6	AIII1	64.16	12.72	0.92	0.78	0.75	8.26E-05	1.040	8.46	1.58
7	AIII2	64.05	12.55	0.84	0.74	0.68	6.22E-05	1.101	5.27	0.64
8	AIII3	64.05	12.55	0.84	0.74	0.68	6.22E-05	1.101	4.45	0.64
9	BI1	63.80	13.11	1.01	0.93	0.84	1.11E-04	1.108	2.36	1.24
10	BI2	76.08	13.03	0.97	1.07	0.96	9.99E-05	1.111	3.91	1.76
11	BI3	76.55	12.92	1.01	1.07	1.00	1.10E-04	1.075	7.14	2.32
12	BII3	76.49	13.04	1.09	1.13	1.09	1.40E-04	1.041	11.51	2.98
13	BII2	76.76	12.80	1.07	1.12	1.05	1.29E-04	1.065	10.52	1.36
14	BII1	76.70	12.81	1.02	1.08	1.00	1.14E-04	1.079	9.37	2.88
15	BIII1	76.70	12.75	1.04	1.07	1.02	1.19E-04	1.058	22.38	5.06
16	BIII2	76.43	12.58	1.05	1.08	1.01	1.21E-04	1.069	17.52	1.85
17	BIII3	76.56	13.06	1.07	1.13	1.07	1.33E-04	1.059	16.70	4.93
18	CI1	50.86	12.66	0.96	0.64	0.62	9.26E-05	1.035	9.02	3.72
19	CI2	51.65	13.10	0.96	0.68	0.65	9.59E-05	1.056	5.20	1.96
20	CI3	50.33	12.23	0.94	0.63	0.58	8.52E-05	1.086	4.09	1.04
21	CII1	51.20	12.43	0.80	0.54	0.51	5.31E-05	1.051	5.25	0.87
22	CII2	63.58	12.69	0.91	0.78	0.74	8.09E-05	1.053	6.48	1.17
23	CII3	50.86	13.06	0.87	0.61	0.58	7.19E-05	1.049	4.57	1.19
24	CIII1	44.32	12.59	0.63	0.37	0.35	2.68E-05	1.037	3.48	0.77
25	CIII2	45.94	12.42	0.69	0.42	0.40	3.46E-05	1.056	4.19	1.68
26	CIII3	50.37	12.62	0.71	0.48	0.45	3.82E-05	1.057	5.83	2.56
27	DI1	50.81	12.85	0.81	0.55	0.53	5.61E-05	1.053	4.72	0.79
28	DI2	50.36	12.83	0.82	0.59	0.53	5.98E-05	1.103	4.26	0.78
29	DI3	50.71	12.72	0.79	0.58	0.51	5.30E-05	1.130	3.23	0.46
30	DII1	50.88	12.59	0.75	0.50	0.48	4.51E-05	1.042	7.67	2.55
31	DII2	38.63	12.75	0.79	0.41	0.39	5.31E-05	1.054	4.45	1.20
32	DII3	51.10	12.72	0.80	0.56	0.52	5.37E-05	1.074	4.53	0.99
33	DIII1	37.99	12.76	0.56	0.28	0.27	1.85E-05	1.040	4.65	1.48
34	DIII2	51.00	12.95	0.59	0.41	0.39	2.25E-05	1.048	10.77	3.12
35	DIII3	50.78	12.88	0.66	0.46	0.43	3.06E-05	1.064	6.05	1.12
36	EI1	51.14	12.51	0.82	0.53	0.52	5.67E-05	1.018	5.87	1.96
37	EI2	50.78	12.98	0.83	0.58	0.55	6.16E-05	1.054	5.14	0.82
38	EI3	50.74	12.71	0.80	0.56	0.52	5.44E-05	1.088	2.98	0.57
39	EII1	38.25	12.75	0.63	0.31	0.30	2.60E-05	1.002	8.55	3.80
40	EII2	50.83	13.02	0.62	0.42	0.41	2.63E-05	1.007	14.22	6.30
41	EII3	50.90	12.85	0.65	0.42	0.43	3.00E-05	0.992	7.77	1.73

Table 12: General morphological results for spring 2019 sampling at the both Ram and Wood Island sites.

Date	Year	Site	Location on Kelp-line	Total Length (mm)	Blade Lendth (mm)	Stipe Length (mm)	Width 1 (mm) near stipe	Width 2 (mm) middle	Width 3 (mm) near blade tip	Stipe Weight (g)	Blade Weight (g)	Total weight (g)
3/25/2019	2019	RAM	E	936.10	879.14	54.36	114.20	109.60	83.40	0.600	34.788	35.386
3/25/2019	2019	RAM	M	712.60	677.04	35.36	105.30	95.78	75.44	0.408	20.858	21.193
3/25/2019	2019	RAM	W	833.26	785.02	48.24	117.00	111.60	84.42	0.452	22.488	22.940
4/2/2019	2019	RAM	W	963.66	903.72	59.94	107.60	111.60	71.40	0.716	37.414	38.130
4/2/2019	2019	RAM	M	1084.04	1026.88	57.16	112.60	142.00	94.80	0.748	49.076	49.824
4/5/2019	2019	WOOD	E	679.00	623.63	55.37	56.53	52.55	38.11	0.486	14.276	14.762
4/5/2019	2019	WOOD	M	1180.80	1111.20	69.60	103.42	119.03	74.41	1.084	50.268	51.352
4/5/2019	2019	WOOD	W	1268.20	1225.35	42.85	114.67	127.61	79.22	0.692	74.274	74.966
4/11/2019	2019	RAM	E	796.20	709.60	86.60	81.74	84.77	57.32	1.106	18.370	19.476
4/11/2019	2019	RAM	M	959.65	895.30	64.34	136.24	128.26	109.16	1.184	54.846	56.030
4/11/2019	2019	RAM	W	833.20	744.40	88.80	107.91	117.48	75.18	1.452	36.178	37.630
4/11/2019	2019	WOOD	M	1255.40	1160.45	94.95	83.77	96.70	56.00	1.610	55.522	57.132
4/11/2019	2019	WOOD	W	1022.40	914.00	108.40	83.48	74.02	56.68	2.064	29.444	31.508
4/17/2019	2019	WOOD	E	1645.87	1557.60	88.27	152.57	143.21	88.57	1.742	105.198	106.940
4/17/2019	2019	WOOD	M	1286.70	1204.79	81.90	113.48	124.79	73.71	1.464	70.376	71.840
4/17/2019	2019	WOOD	W	783.00	717.21	65.78	85.40	84.72	61.76	1.102	27.666	28.768
4/24/2019	2019	RAM	E	1018.04	930.19	87.85	116.96	103.49	77.97	1.610	48.356	49.966
4/24/2019	2019	RAM	M	1021.46	876.42	145.04	119.52	103.06	75.88	3.536	53.446	56.982
4/24/2019	2019	RAM	W	1289.40	1158.93	130.47	98.97	93.00	65.94	2.596	72.818	75.414
4/25/2019	2019	WOOD	E	1227.03	1143.47	83.56	107.67	92.06	50.23	1.792	67.810	69.602
4/25/2019	2019	WOOD	M	1417.16	1226.72	190.44	96.07	79.67	51.59	4.542	57.146	61.688
4/25/2019	2019	WOOD	W	1284.23	1160.84	123.39	89.05	83.24	49.81	2.592	58.140	60.732
5/3/2019	2019	RAM	E	1165.40	1087.77	77.63	147.70	153.32	101.08	1.800	76.472	78.272
5/3/2019	2019	RAM	M	1137.97	1047.15	90.81	150.65	165.72	109.53	2.348	85.324	87.672
5/3/2019	2019	RAM	W	1051.76	983.75	68.00	122.03	124.99	62.89	1.330	53.556	54.886
5/9/2019	2019	RAM	E	846.93	723.04	123.90	104.77	125.06	78.56	3.166	52.598	55.764
5/9/2019	2019	RAM	M	930.60	849.16	81.44	97.88	111.02	84.70	1.562	38.208	39.770
5/16/2019	2019	RAM	E	1309.20	1159.07	150.13	138.65	150.83	128.77	4.850	94.828	99.678
5/16/2019	2019	RAM	M	3151.20	3022.27	128.93	149.67	160.31	101.10	3.076	95.570	98.646
5/16/2019	2019	RAM	W	1544.64	1450.36	94.28	145.51	160.16	123.16	2.506	132.262	134.768
5/16/2019	2019	WOOD	E	1021.43	926.58	94.85	94.34	99.96	76.09	1.980	42.308	44.288
5/16/2019	2019	WOOD	M	1424.96	1336.44	88.52	102.39	126.71	77.62	1.994	91.830	93.824
5/16/2019	2019	WOOD	W	1007.00	918.93	88.07	74.79	82.08	54.21	1.710	40.420	42.130
5/22/2019	2019	RAM	E	1302.73	1092.99	209.74	124.80	139.96	91.40	7.198	73.612	80.810
5/22/2019	2019	RAM	M	1317.87	1228.21	89.67	134.23	132.76	91.04	1.970	92.462	94.432
5/22/2019	2019	RAM	W	1293.60	1052.00	241.60	129.19	134.71	99.72	9.058	90.708	99.766
5/28/2019	2019	WOOD	E	895.40	809.84	85.56	89.88	115.15	131.47	2.042	61.422	63.464
5/28/2019	2019	WOOD	M	1889.38	1801.56	87.82	104.77	126.07	94.90	2.048	137.966	140.014
5/28/2019	2019	WOOD	W	1216.80	1124.30	92.50	102.94	105.08	61.62	1.932	70.418	72.350

Table 13: Material property results of the sample swatches for the protected Wood Island site for the 2019 growing season.

Date	Site	Location	Mass (g)	Thickness (t) (cm)	Width (w) (cm)	Length (l) (cm)	Volume (cm^3)	Mass Density (g/cm^3)	Second Area Moment (I) (m^4)	Modulus of Elasticity (E) (MPa)
4/5/2019	WOOD	IM-East	0.776	0.073	1.909	5.146	0.724	1.119	8.560E-13	5.102
4/5/2019	WOOD	IM-Middle	1.106	0.101	1.988	5.242	1.055	1.053	1.761E-12	2.089
4/5/2019	WOOD	IM-West	1.196	0.104	1.985	5.260	1.080	1.098	2.035E-12	1.850
							Average:	**1.090**		**3.013**
4/5/2019	WOOD	BT-East	0.588	0.057	1.928	5.208	0.575	1.060	3.953E-13	9.325
4/5/2019	WOOD	BT-Middle	1.000	0.090	1.988	5.356	0.911	1.092	1.081E-12	2.906
4/5/2019	WOOD	BT-West	0.994	0.086	1.977	5.255	0.895	1.105	1.202E-12	2.972
							Average:	**1.086**		**5.068**
4/11/2019	WOOD	IM-Middle	1.460	0.104	2.072	5.206	1.125	1.284	2.136E-12	1.866
4/11/2019	WOOD	IM-West	1.326	0.090	2.109	5.127	0.972	1.356	1.387E-12	1.925
							Average:	**1.320**		**1.895**
4/11/2019	WOOD	BT-Middle	1.362	0.089	2.097	5.259	0.979	1.391	1.345E-12	3.892
4/11/2019	WOOD	BT-West	1.092	0.067	1.973	5.141	0.680	1.661	5.608E-13	6.006
							Average:	**1.526**		**4.949**
4/17/2019	WOOD	IM-East	1.712	0.122	2.019	5.323	1.315	1.300	3.246E-12	1.763
4/17/2019	WOOD	IM-Middle	1.372	0.104	2.087	5.434	1.163	1.203	2.211E-12	2.697
4/17/2019	WOOD	IM-West	1.306	0.096	2.113	5.420	1.099	1.203	1.644E-12	3.085
							Average:	**1.235**		**2.515**
4/17/2019	WOOD	BT-East	1.398	0.089	2.045	5.295	0.982	1.464	1.421E-12	3.241
4/17/2019	WOOD	BT-Middle	1.434	0.096	2.066	5.321	1.061	1.357	1.606E-12	2.548
4/17/2019	WOOD	BT-West	1.164	0.068	2.001	5.143	0.700	1.643	5.846E-13	4.976
							Average:	**1.488**		**3.588**
4/25/2019	WOOD	IM-East	1.394	0.090	2.070	5.251	0.969	1.463	1.474E-12	2.418
4/25/2019	WOOD	IM-Middle	1.190	0.084	2.042	5.252	0.896	1.348	6.707E-13	2.323
4/25/2019	WOOD	IM-West	1.376	0.098	2.039	5.195	1.044	1.326	1.765E-12	1.780
							Average:	**1.379**		**2.174**
4/25/2019	WOOD	BT-East	1.078	0.086	2.054	4.986	0.890	1.206	1.156E-12	1.306
4/25/2019	WOOD	BT-Middle	0.888	0.088	2.023	5.288	0.948	0.987	1.310E-12	2.169
4/25/2019	WOOD	BT-West	1.080	0.066	2.124	5.210	0.741	1.508	6.657E-13	2.364
							Average:	**1.234**		**1.946**
5/16/2019	WOOD	IM-East	1.334	0.113	2.031	5.287	1.213	1.105	2.458E-12	2.925
5/16/2019	WOOD	IM-Middle	1.754	0.136	2.219	5.179	1.554	1.129	4.820E-12	4.211
5/16/2019	WOOD	IM-West	1.502	0.120	2.017	5.326	1.295	1.167	3.090E-12	3.508
							Average:	**1.134**		**3.548**
5/16/2019	WOOD	BT-East	1.058	0.079	2.163	5.420	0.929	1.137	9.128E-13	7.196
5/16/2019	WOOD	BT-Middle	1.414	0.100	2.092	5.332	1.124	1.256	2.091E-12	7.076
5/16/2019	WOOD	BT-West	1.112	0.085	2.098	5.401	0.966	1.160	1.116E-12	5.350
							Average:	**1.184**		**6.541**
5/28/2019	WOOD	IM-East	1.666	0.141	1.974	5.116	1.425	1.244	4.675E-12	1.702
5/28/2019	WOOD	IM-Middle	1.932	0.145	1.972	5.278	1.512	1.279	5.143E-12	1.607
5/28/2019	WOOD	IM-West	1.298	0.107	2.121	5.155	1.139	1.130	2.436E-12	3.245
							Average:	**1.218**		**2.185**
5/29/2019	WOOD	BT-East	1.544	0.110	2.086	5.232	1.212	1.255	2.630E-12	2.161
5/28/2019	WOOD	BT-Middle	1.258	0.103	1.969	4.877	0.995	1.264	1.964E-12	2.188
5/28/2019	WOOD	Bt-West	1.020	0.080	2.186	5.352	0.930	1.094	1.059E-12	6.061
							Average:	**1.204**		**3.470**

Table 14: Material property results of the sample swatches for the exposed Ram Island site for the 2019 growing season.

Date	Site	Location	Mass (g)	Thickness (t) (cm)	Width (w) (cm)	Length (l) (cm)	Volume (cm^3)	Mass Density (g/cm^3)	Second Area Moment (I) (m^4)	Modulus of Elasticity (E) (MPa)
3/25/2019	RAM	IM-East	0.936	0.082	2.056	5.237	0.892	1.057	1.128E-12	3.512
3/25/2019	RAM	IM-Middle	0.708	0.068	2.026	5.265	0.726	0.981	6.244E-13	4.561
3/25/2019	RAM	IM-West	0.752	0.070	2.020	5.307	0.752	1.001	5.988E-13	3.459
							Average:	**1.013**		**3.844**
3/25/2019	RAM	BT-East	0.756	0.061	2.149	5.319	0.721	1.060	6.363E-13	8.523
3/25/2019	RAM	BT-Middle	0.543	0.052	2.042	5.321	0.573	0.949	2.837E-13	6.391
3/25/2019	RAM	BT-West	0.586	0.051	1.997	5.292	0.537	1.097	2.251E-13	7.211
							Average:	**1.035**		**7.375**
4/2/2019	RAM	IM-West	0.858	0.081	1.947	5.272	0.835	1.036	9.977E-13	3.259
4/2/2019	RAM	IM-Middle	0.894	0.084	1.907	5.264	0.851	1.086	1.191E-12	5.238
							Average:	**1.061**		**4.249**
4/2/2019	RAM	BT-West	0.828	0.067	1.953	5.339	0.702	1.200	5.685E-13	5.233
4/2/2019	RAM	BT-Middle	0.738	0.069	1.962	5.180	0.710	1.082	6.729E-13	5.142
							Average:	**1.141**		**5.187**
4/11/2019	RAM	IM-East	0.798	0.066	1.924	5.290	0.677	1.161	5.327E-13	3.936
4/11/2019	RAM	IM-Middle	1.016	0.084	2.036	5.494	0.936	1.086	1.043E-12	4.219
4/11/2019	RAM	IM-West	0.994	0.082	2.025	5.349	0.884	1.152	9.924E-13	2.809
							Average:	**1.133**		**3.655**
4/11/2019	RAM	BT-East	0.656	0.051	1.915	5.179	0.502	1.295	2.551E-13	8.533
4/11/2019	RAM	BT-Middle	0.960	0.074	2.104	5.366	0.846	1.159	8.840E-13	7.044
4/11/2019	RAM	BT-West	0.798	0.061	1.953	5.308	0.630	1.299	4.073E-13	5.749
							Average:	**1.251**		**7.109**
4/24/2019	RAM	IM-East	1.420	0.088	2.059	5.356	0.977	1.324	1.356E-12	3.024
4/24/2019	RAM	IM-Middle	1.510	0.096	2.123	5.429	1.104	1.368	1.652E-12	3.182
4/24/2019	RAM	IM-West	1.504	0.088	1.985	5.208	0.905	1.668	1.302E-12	4.216
							Average:	**1.453**		**3.474**
4/24/2019	RAM	BT-East	0.926	0.062	2.092	5.421	0.706	1.326	4.683E-13	6.287
4/24/2019	RAM	BT-Middle	1.028	0.062	2.006	5.172	0.642	1.618	4.430E-13	5.158
4/24/2019	RAM	BT-West	1.140	0.064	1.956	5.137	0.640	1.820	6.035E-13	6.514
							Average:	**1.588**		**5.986**
5/3/2019	RAM	IM-East	1.410	0.106	2.026	4.985	1.078	1.315	2.089E-12	2.309
5/3/2019	RAM	IM-Middle	1.598	0.122	2.095	5.337	1.367	1.169	3.267E-12	2.116
5/3/2019	RAM	IM-West	1.242	0.096	1.952	4.982	0.936	1.320	1.590E-12	1.906
							Average:	**1.268**		**2.110**
5/3/2019	RAM	BT-East	0.990	0.075	2.095	5.327	0.836	1.186	7.734E-13	3.358
5/3/2019	RAM	BT-Middle	1.238	0.092	2.173	5.465	1.089	1.140	1.454E-12	3.629
5/3/2019	RAM	BT-West	0.890	0.066	2.027	5.281	0.698	1.297	6.144E-13	5.693
							Average:	**1.208**		**4.227**
5/9/2019	RAM	IM-East	1.456	0.104	2.211	5.372	1.240	1.175	2.119E-12	4.724
5/9/2019	RAM	IM-Middle	1.263	0.090	2.092	5.295	1.007	1.274	1.395E-12	2.998
5/9/2019	RAM	BT-East	0.998	0.080	2.028	5.366	0.866	1.150	8.848E-13	3.858
							Average:	**1.199**		**3.860**
5/9/2019	RAM	BT-East	0.998	0.080	2.028	5.366	0.866	1.150	8.848E-13	3.858
5/9/2019	RAM	BT-Middle	0.694	0.048	2.156	5.307	0.554	1.284	2.545E-13	19.815
							Average:	**1.217**		**11.836**
5/16/2019	RAM	IM-East	1.580	0.128	2.212	5.196	1.470	1.075	3.909E-12	2.912
5/16/2019	RAM	IM-Middle	1.264	0.104	2.213	5.197	1.201	1.055	2.298E-12	1.961
5/16/2019	RAM	IM West	1.702	0.130	2.246	5.433	1.587	1.075	4.243E-12	1.955
							Average:	**1.069**		**2.276**
5/16/2019	RAM	BT-East	1.378	0.102	2.114	5.396	1.167	1.185	1.934E-12	9.907
5/16/2019	RAM	BT-Middle	1.034	0.079	2.167	5.343	0.920	1.133	9.642E-13	6.202
5/16/2019	RAM	BT-West	1.388	0.098	2.324	5.446	1.248	1.134	1.934E-12	5.141
							Average:	**1.151**		**7.083**

The datasets were also processed as a function of biomass per m versus time. The summaries for the Ram and Wood Island sites are provided in Figure 82 and Figure 83, respectively.

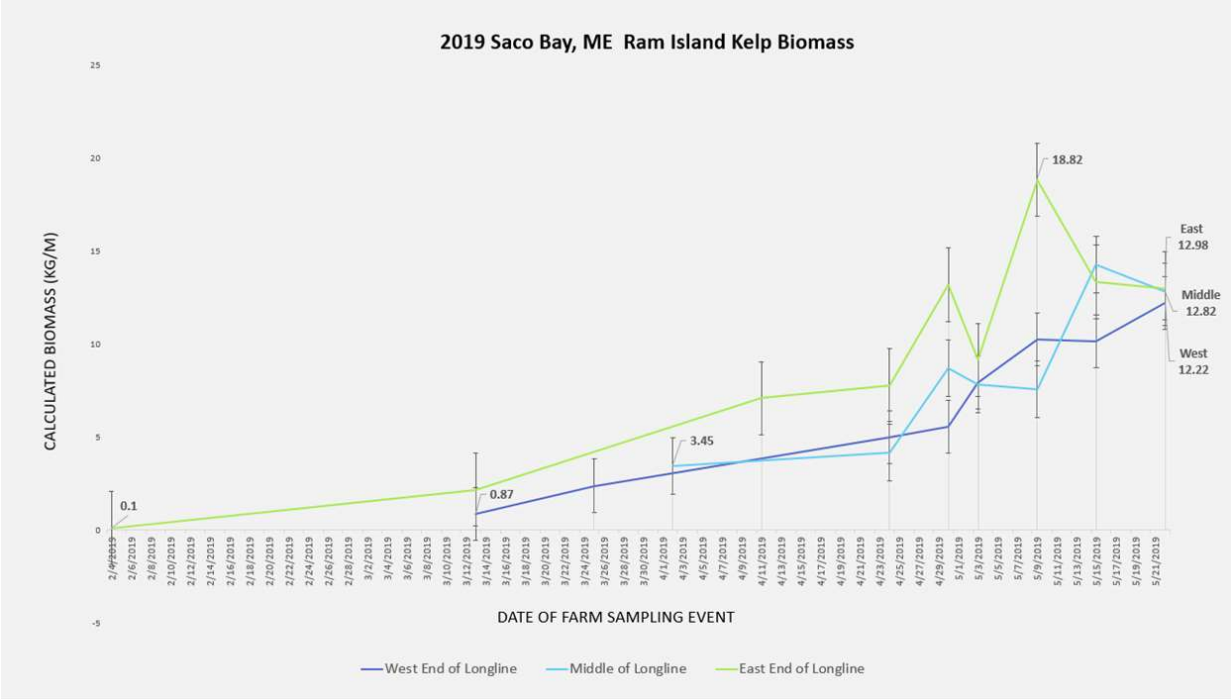

Figure 82: Biomass summary for the exposed Ram Island site for the 2019 season.

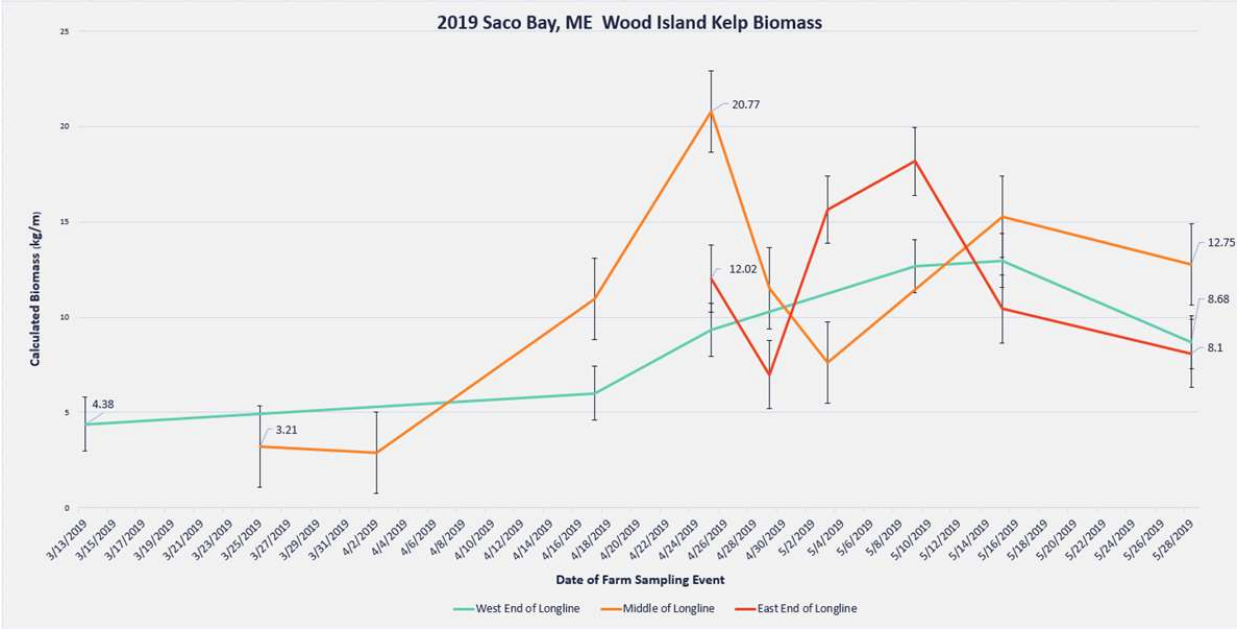

Figure 83: Biomass summary for the protected Wood Island site for the 2019 season.

2.3.3. Milestone 3.3 – First biomass sampling complete (5/28/2019).

Summaries of measured and derived biomass properties for both the Wood and Ram Island datasets are shown on Figure 84 and Figure 85, respectively. The Figures show biomass, blade length, mass density and total wet weight for the east (E), middle (M) and west (W) sample locations as a function of sample data. The Figures also provides average values. The yield (kg/m) of the Ram Island dataset was also processed using a logistic curve fit as described in St. Gelais et al. (2022).

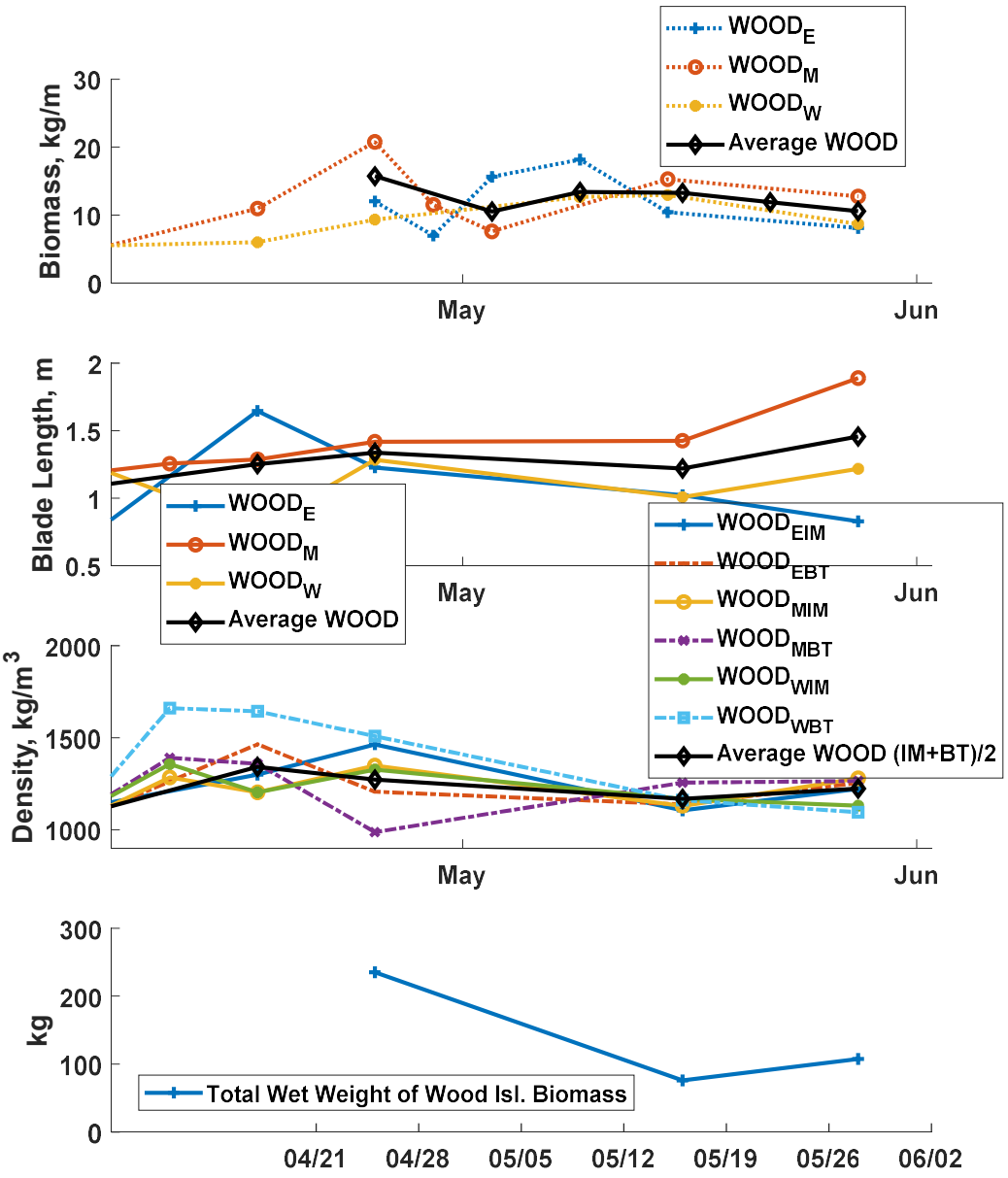

Figure 84: Measured and derived biomass parameters for Wood Island, 2019.

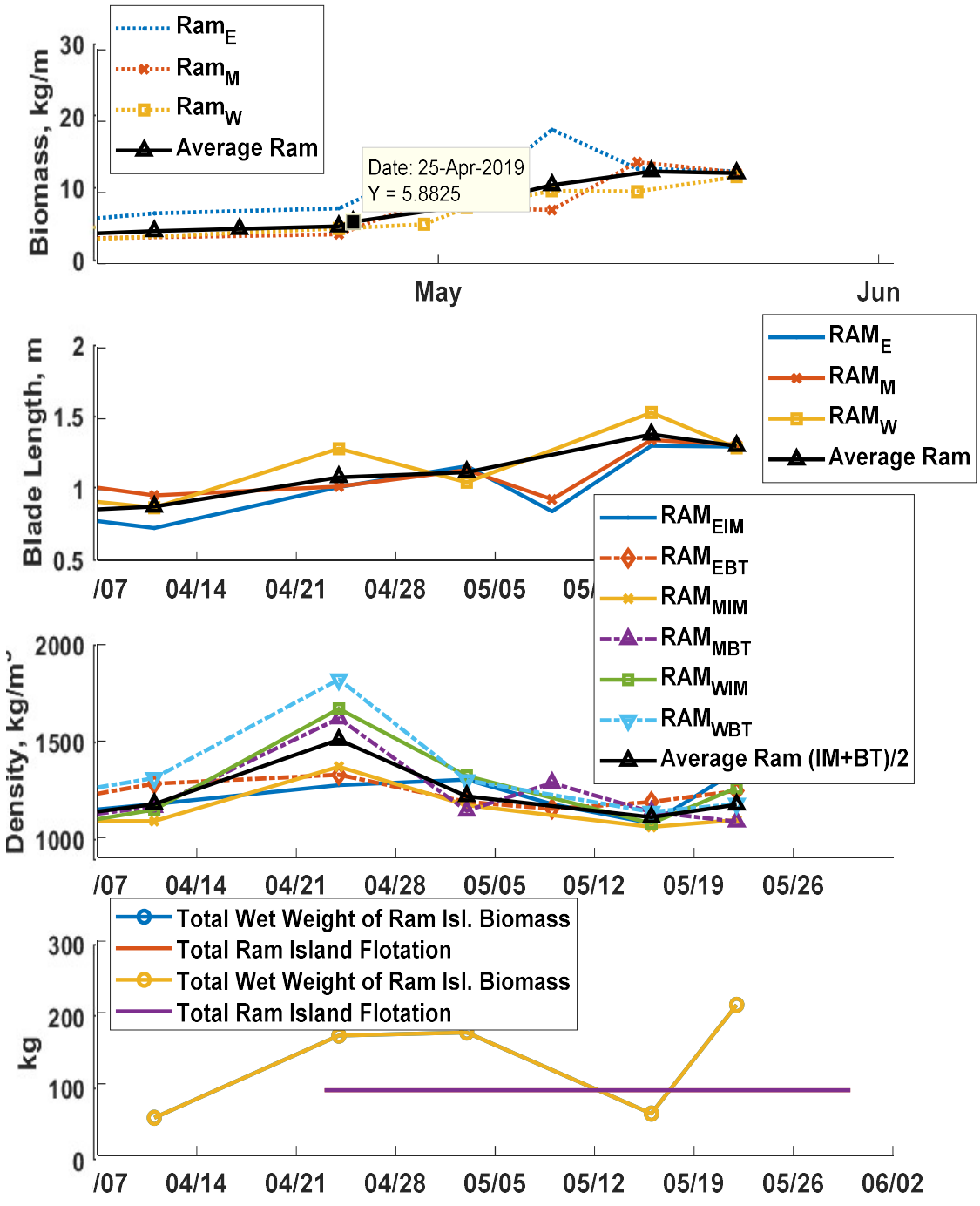

Figure 85: Measured and derived biomass parameters for Ram Island, 2019.

2.3.4. Task 3.4: Collect field samples from second deployment (6/8/2020).

The second deployment at the exposed Ram Island site took place from November 2019 to June 2020 amidst Covid-19. The single culture line system was replaced with an array with 5 culture lines as shown Figure 35. Field activities were limited during this season. Though some kelp monitoring took place, there were no instrument deployments. Kelp monitoring consisted of general morphological characteristics of length and with (geometric) and mass density (material) properties. Information regarding the number blades per m. Subsamples and cantilever beam tests were not done and therefore values for the modulus of elasticity were not obtained.

Sampling of the kelp farm array took place during harvest on June 8, 2020. The sampling protocol was adjusted from the 10 cm detailed sampling efforts to general 1 m random samples collected from each of the five individual culture lines. The 1 m samples were stored in coolers during the kelp harvest and then transported to the UNE laboratory at the Marine Science Center for morphological and biomass measurements. The samples were processed in the laboratory and patio space following all COVID-19 safety protocols applied at the University. In general, samples were processed to obtain the (1) blade length and width of 56 individuals from the canopy cover, (2) aggregate number of individuals per 1 m sample (3) the wet weight (in water), and (3) dry weight (in air).

The 5 sections contained 370 total blades. Of the total amount, 56 were chosen for length and width measurements. In this process, each sample was laid flat and straight on level ground against a measuring tape. A representative sample is shown on Figure 86. The length of the blade was measured from the end of the stipe to the tip. With each of the kelp blades laid out at straight and flat, a width measurement was taken using digital calipers. The width was recorded the widest point of the blade, generally located in the center of the kelp blade. The results of the individual blade samples are shown on Figure 87 with the average length 148 cm with a standard deviation of 29 cm. The average width was 6.97 cm with a standard deviation of 1.65 cm.

Figure 86: A representative kelp sample from harvesting June 8, 2020.

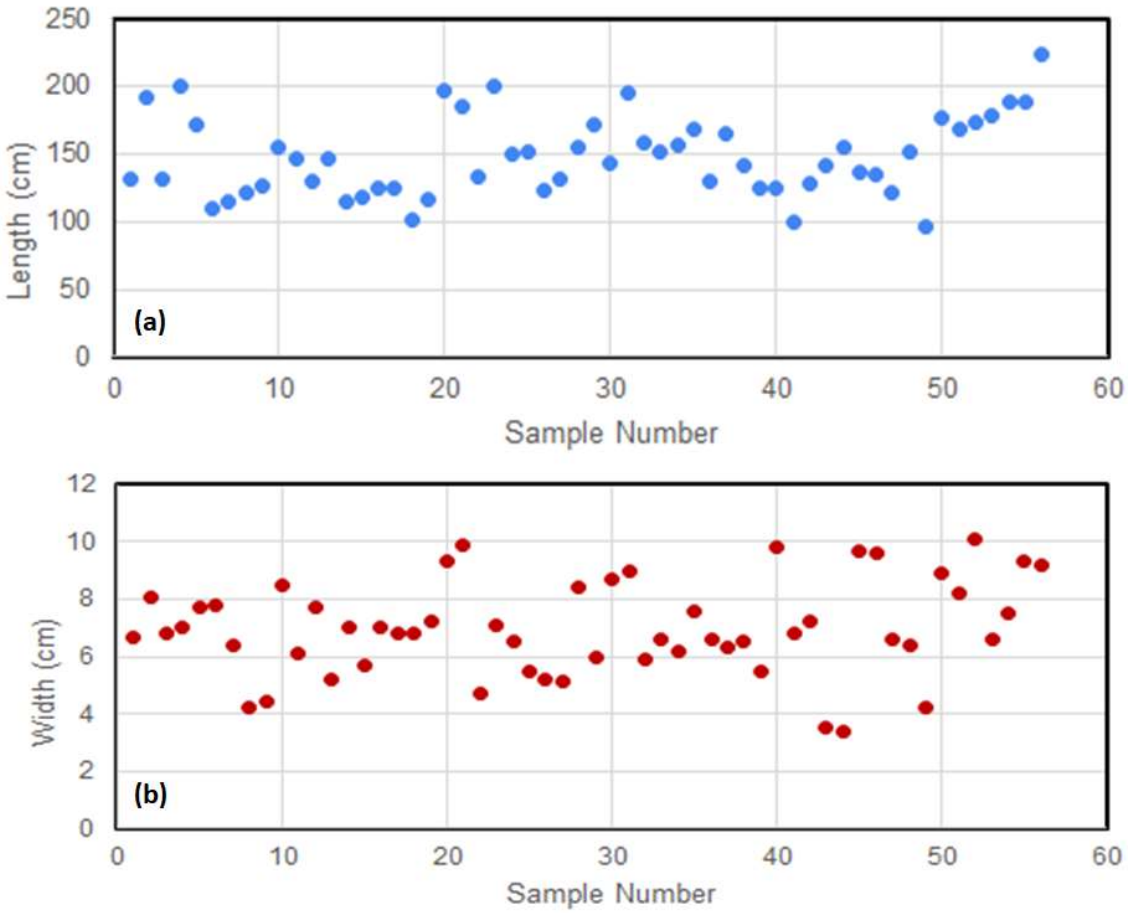

Figure 87: (a) The length dataset from the 56 samples. (b) the width dataset from the 56 samples.

In addition to the geometric properties, the mass density of the kelp aggregate is one of the most important properties of the kelp that influences both the static and dynamic response of the entire farm system. Previous methods to measure kelp mass density were done with samples taken of the meristematic portion of the blade. This technique yielded higher values than published results but was necessary because dimensions (and mass) of the samples were needed for the cantilever beam tests to estimate the modulus of elasticity of the kelp. See average values on Table 14. It was also qualitatively observed that the meristematic portion of the blade was denser than the fringes and the tips. However, when the Hydro-FE model was applied and static simulations were performed, it was found that stability was not achieved and the system was not supported by the floats and that the denser values of the meristematic portion of the blade were representative of the composite mass density. Since Saco Bay kelp is just negatively buoyant, it was decided to calculate the mass density of a 1 m aggregate sample from wet weight measurement in a pool of still ocean water and dry weight measurements hanging in air.

The technique was to take the aggregate sample and bind it together at the holdfast with one zip-tie and attached a hanging digital spring scale. The spring scale was then suspended over a large quiescent above ground pool located on the outside patio at the MSC. The kelp sample was

submerged in chilled, salt water and manipulated by hand to remove any access air pockets trapped between the submerged kelp blades to remove trapped buoyancy. After multiple attempts at measuring each 1 m sample individually, the in-water weight values were too small to register on the scale. Therefore, all five 1 m samples were weighed simultaneously. After the sample was settled and secured to the scale, the weight of the kelp sample was recorded. The combined weight of the zip ties was subtracted from the aggregate weight of the measured kelp.

The wet weight of the 5 samples was measured at 0.225 kgf (2.21 N). The five, 1 m aggregate clumps are shown in the still saltwater pool on Figure 88(a). The aggregate kelp sample was then weighed using the same spring scale, but this time suspended in air. After being submerged in seawater, the kelp sample was secured to the spring scale measuring attachment and shaken slightly to remove the excess water so that the sample was wet but not dripping before recording the sample weight. The weight of the five, 1 m sections of kelp in air was 12.37 kgf (121.35 N) as shown on Figure 88 (b) and (c). Note that wet and dry measurements of the zip-ties were considered negligible.

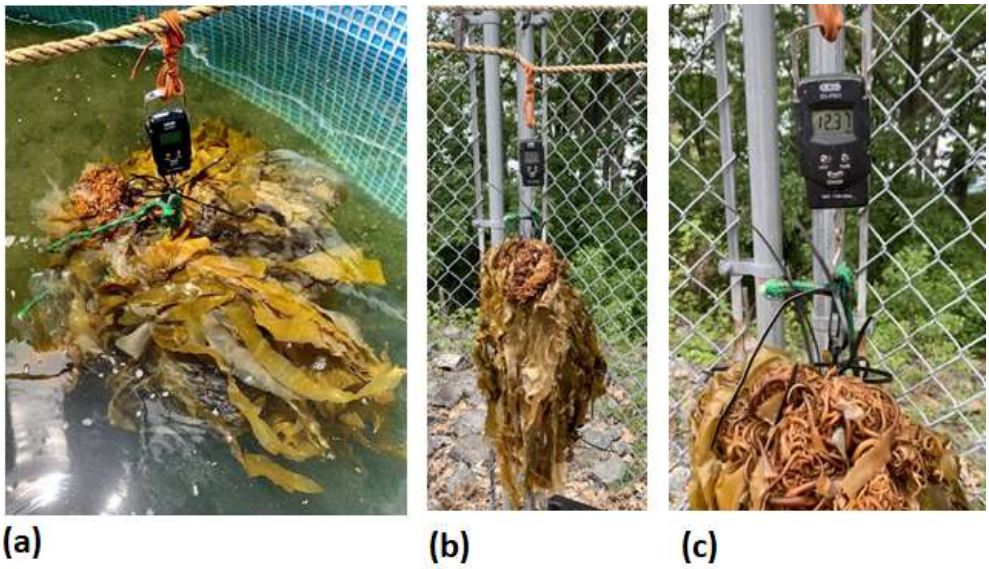

Figure 88: The mass density of a 1 m aggregate of kelp was calculated from the (a) wet and (b), (c) dry weight measurements.

With the dry (wt_{dry}) and wet (wt_{wet}) weight values, the displacement of the aggregates ($\Delta_{aggregates}$) was calculated to be 119.14 N from

$$\Delta_{ag} = wt_{dry} - wt_{wet} = V_{ag}(\rho_{sw})g. \quad (22)$$

In equation (22), ρ_{sw} is the mass density of the salt water in the pool calculated from the salinity (32 PSU) and temperature (12.77°C) equal to 1024 kg/m^3. The volume of the aggregates (V_{ag}) was calculated to be 0.0119 m^3. With volume of the aggregates, the mass density of the kelp (ρ_{kelp}) was calculated to be 1043 kg/m^3 using

$$\rho_{kelp} = \frac{m_{dry}}{V_{ag}}. \quad (23)$$

Even though instruments were not deployed during this biomass sampling period, the effort did reinforce the techniques to develop geometric and material properties.

During the 2020-2021 growing season, the 5 line array was deployed and seeded as part of the NCE. With Covid-19 restrictions eased, a more rigorous sampling plan was defined as shown on Figure 89. Nine locations were chosen as:

- Line #1 West (1W)
- Line #1 East (1E)
- Line #2 Middle West (2MW)
- Line #2 Middle East (2ME)
- Line #3 Middle (3M)
- Line #4 Middle West (4MW)
- Line #4 Middle East (4ME)
- Line #5 West (5W)
- Line #5 East (5E)

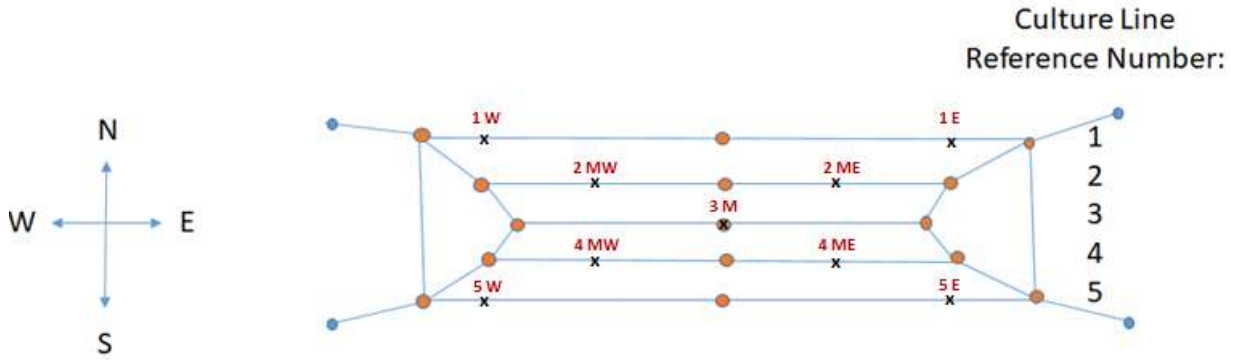

Figure 89: Sampling locations for the on the 5-line array.

The datasets from the extensive sampling of the array system during the grow out period between April and May of 2021 were processed from multiple locations. Sampling was conducted on each of the five lines from as shown on Figure 89. Samples were taken during instrument deployment and recovery days to bracket the level of growth associated with the instrumentation datasets corresponding to 4/15/21 – 4/28/21 and 5/7/2021 – 5/20/2021. Sampling including wet weight and kelp length of 1 m sections of grow line for each of the 9 locations. Biomass was determined by weighing wet-but-not-dripping bundles of kelp immediately after removing them from the grow line. Blade lengths were derived using photo analysis with a tape measure extended to a reference length (Figure 90).

Figure 90: Team members Barry Costa-Pierce, Zach Miller-Hope, and Kelson Marine intern Nate Baker preparing to measure blade length on May 20, 2021.

Samples were taken from April 15 to May 21 (harvest) at points across the farm to quantify both the temporal and spatial variation of kelp growth. Results for the 2021 season are shown in Table 15. Figure 91 shows the biomass yield by line, Figure 92 shows the average biomass on the farm over time.

Kelp datasets were processed to obtain a representation of biomass for the numerical modeling effort. During this sampling period, the AWAC and load cell instruments were deployed from April 16-28, 2021 and again from May 8-16, 2021. Processing the kelp datasets provide yields (Y_{kelp}) between 3.0-4.8 kg/m (ave = 3.9 kg/m) and 6.2-8.1 kg/m (ave = 7.4 kg/m) for each instrumentation deployment, respectively. The length of the kelp (L_{kelp}) was 1.22-1.26 m (ave = 1.24 m) and 1.37-1.40 m (ave = 1.39 m). Kelp mass density (ρ_{kelp}) measurements were made, but will be verified using static model simulations and visual buoy waterline information. The sampled kelp datasets provided the basis for an initial numerical model kelp representation assuming a mass density of 1050 kg/m^3. The number of blades per m of grow line were determined on May 20, 2021 from three samples at 90, 89 and 85.

Table 15: Ram Island biomass measurements based on 1 m line samples in 2021.

Date Measured Datenum	Age Days	Average Length m	Biomass per m kg/m	Line Number	Long. Position	Weight in air Rapella kg/m
4/15/2021	157	1.06	2.13	1	W	
4/15/2021	157	0.93	0.75	1	E	0.74
4/15/2021	157	1.14	2.77	5	E	2.74
4/15/2021	157	1.36	1.73	5	W	1.72
4/15/2021	157	1.39	2.38	3	M	2.35
4/15/2021	157	1.14	3.70	2	MW	3.7
4/15/2021	157	1.17	4.30	2	ME	4.29
4/15/2021	157	1.43	4.72	4	MW	4.34
4/15/2021	157	1.33	4.64	4	ME	4.56
4/28/2021	170	1.32	2.39	1	E	2.37
4/28/2021	170	1.26	3.46	1	W	3.47
4/28/2021	170	1.53	3.20	5	W	3.18
4/28/2021	170	1.46	3.90	5	E	3.89
4/28/2021	170	1.01	4.32	3	M	4.34
4/28/2021	170	1.05	5.12	2	MW	5.1
4/28/2021	170	1.20	6.18	2	ME	6.18
4/28/2021	170	1.23	4.85	4	MW	4.8
4/28/2021	170	1.25	9.47	4	ME	9.44
5/7/2021	179	1.44	5.60	1	E	5.6
5/7/2021	179	1.35	5.40	1	W	5.4
5/7/2021	179	1.41	6.30	2	MW	6.3
5/7/2021	179	1.26	7.60	2	ME	7.6
5/7/2021	179	1.29	7.60	3	M	7.6
5/7/2021	179	1.73	7.90	4	ME	7.9
5/7/2021	179	1.58	8.20	4	MW	8.2
5/7/2021	179	1.12	4.90	5	E	4.9
5/7/2021	179	1.13	2.50	5	W	2.5
5/20/2021	192	1.50	6.40	1	W	6.4
5/20/2021	192	1.17	7.15	1	E	7.2
5/20/2021	192	1.26	7.00	5	E	6.9
5/20/2021	192	1.01	7.65	5	W	7.6
5/20/2021	192	1.74	8.15	2	MW	8.2
5/20/2021	192	1.33	6.00	2	ME	6
5/20/2021	192	1.78	8.20	3	M	8.3
5/20/2021	192	1.48	12.90	4	MW	12.9
5/20/2021	192	1.48	12.65	4	ME	12.5
5/21/2021	193		10.28	2	W	10.15
5/21/2021	193		11.08	2	MW	11.05
5/21/2021	193		10.95	2	M	10.9

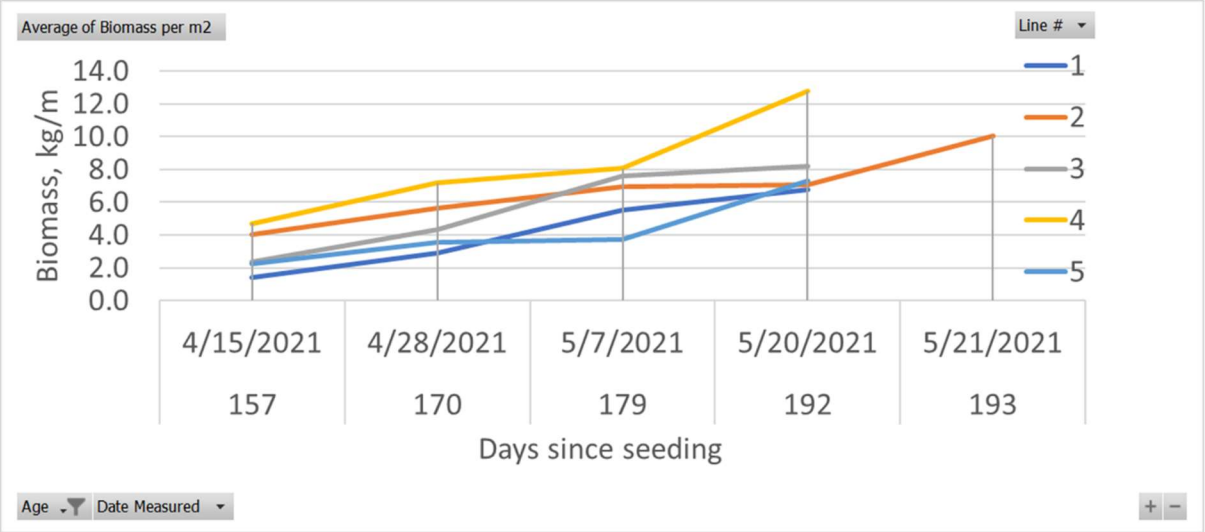

Figure 91: Wet weight per m of grow line, average by line by date (date axis not to scale).

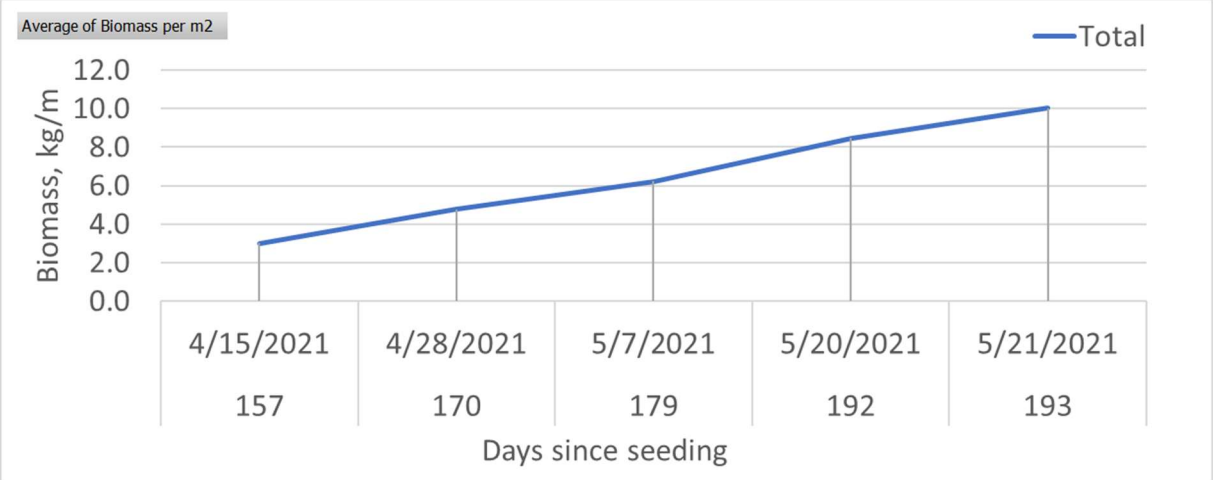

Figure 92: Wet weight per m of grow line, farm average by date (date axis not to scale).

2.3.5. Milestone 3.5: Second biomass sampling (08/14/20)

As discussed in the previous section, the biomass was successfully obtained from the array system during covid-19. Since instruments were not deployed, the entire field operation had to be repeated as part of the NCE.

2.3.6. Task 3.6: Develop macroalgae representation (1/15/22)

The macroalgae representation assumes that kelp is growing densely on a line and characterized in the numerical model as a 1 m aggregate. The properties are ideally determined from in-situ measurements of length (L_{kelp}), mass per 1 m length or yield (Y_{kelp}), number of blades per m, the width of the blade (b_{kelp}) and kelp mass density (ρ_{kelp}). Since the aggregate consists of 1 m of

grow line, the mass (m_{kelp}) is equal to Y_{kelp}. The volume of the aggregate (V_{ag}) is then calculated from

$$V_{ag} = \frac{m_{kelp}}{\rho_{kelp}}, \quad (24)$$

with an arbitrary cross-section of

$$A_{ag} = \frac{V_{ag}}{L_{kelp}}. \quad (25)$$

The kelp aggregate can then be represented in the finite element model as a beam element with a cross-sectional area (A_{ag}) discretized per unit length. This maintains the volumetric characteristics matching weight and buoyancy and used to find inertia and added mass forces described in Morison equation.

The material response of the kelp element is determined from the modulus of elasticity (E) with the cross-sectional area (A_{ag}) and its second area moment (I_{ag}) to obtain EA_{ag} and EI_{ag}. This represents the axial and bending resistance, respectively. The modulus of elasticity of kelp can estimated from cantilever beam tests with well-defined field samples. The bending resistance of the aggregate is taken from the sum of all the blades,

$$EI_{ag} = (Number\ of\ blades\ per\ meter)\left(EI_{kelp}\right), \quad (26)$$

as done with the model tests described in Fredriksson et al. (2020). The second area moment of the individual blade (I_{kelp}) was based on a rectangular cross-section with bending about the axis of least resistance,

$$I_{kelp} = \frac{1}{12} b_{kelp}\left(t_{kelp}\right)^3. \quad (27)$$

In equation (27), t_{kelp} is the thickness of the individual kelp blade determined by knowing the number of blades in the 1 m aggregate and b_{kelp}.

With this approach, the normal and tangential drag area values used in Morison equation were obtained from Fredriksson et al. (2020) based on a 1 m aggregate of material (178 LDPE strips) per unit length of strip. Therefore, the normal ($s_{D_{x,y}}$) and tangential ($s_{D_{z_a,z_p}}$) drag area values per unit length are adjusted by L_{kelp} and applied as discretized elements in the numerical procedure.

Using the available measurements from the deployment between 2018 to 2021, the techniques described with equations (24) through (27) were applied to characterize the geometric and material properties of the kelp in the form of a 1 m aggregate for the project. The results are provided in Table 16. This complied dataset is revisited for each of the load cases developed for the model validations efforts to coincide with load cell and ADCP deployment and measurements.

Table 16: Geometric and material properties to represent a 1 m aggregate of aquaculture grown kelp for the Wood and Ram Island sites from 2018 to 2021.

Parameter	Physical Model[1]	Wood Is 2018[2]	Wood Is 2019[3]	Ram Is 2019[3]	Ram Is 2020[4]	Ram Is 2021[5]
Blade length (m)	3	0.97	1.15	1.38	1.48	1.26
Blade width(m)	7.4 (10^{-2})	10.1 (10^{-2})	8.61 (10^{-2})	13.5 (10^{-2})	7.0 (10^{-2})	-
Blades per m	178	405	-	350	74	85
Yield (kg/m)	16.1	6.87	13.26	12.97	2.47	4.76
Ag. mass (kg)	16.1	6.87	13.36	12.97	2.47	4.76
Mass density (kg/m^3)	1.379 (10^3)	1.050 (10^3)	1.167 (10^3)	1.106 (10^3)	1.043 (10^3)	1.047 (10^3)
Ag. volume (m^3)	1.17 (10^{-2})	0.654 (10^{-2})	1.14 (10^{-2})	1.63 (10^{-2})	0.237 (10^{-2})	0.571 (10^{-2})
Aggregate cross-section (m^2)	3.89 (10^{-3})	0.677(10^{-2})	0.987 (10^{-2})	1.173 (10^{-2})	0.160 (10^{-2})	0.455 (10^{-2})
Modulus of elasticity (MPa)	367	5.6	3.4	4.7	-	-
Blade cross-section (m^2)	2.19 (10^{-5})	1.67 (10^{-5})	-	3.35 (10^{-5})	2.165 (10^{-5})	5.35 (10^{-5})
Blade thickness (m)	2.13 (10^{-4})	1.66 (10^{-4})	-	2.49 (10^{-4})	3.10 (10^{-4})	-
Blade second area moment (m^4)	5.96 (10^{-14})	3.82 (10^{-14})	-	1.72 (10^{-13})	1.74 (10^{-13})	-
Blade flexural rigidity (Nm^2)	2.19 (10^{-5})	2.14 (10^{-7})	-	8.16 (10^{-7})	-	-
Ag. flexural rigidity (Nm^2)	3.89 (10^{-3})	0.867 (10^{-4})	-	2.86 (10^{-4})	-	-
Ag. axial stiffness (Nm^2/m^2)	1.43 (10^{-6})	3.79 (10^4)	-	5.55 (10^4)	-	-

[1]Fredriksson et al. (2020)
[2]Zhu et al. (2021)
[3] Values estimated on 5/16/19
[4]Values at harvest
[5]Based on values from 4/28/21

2.4. Task 4.0: Instrumentation planning and deployments

2.4.1. Task 4.1: Develop instrumentation sampling and protocols (10/15/18)

An instrumentation field program was developed to determine forcing and loads on deployed kelp farm systems as a function of the biomass described in Task 3. In general, the plan included the use of Acoustic Wave and Current (AWAC) and custom fabricated load cell instruments.

The protocol required the measurement of water wave kinematics combined with steady current velocities to create deployed system response motions and loads. The AWAC instrument (Figure 93 a) has the capabilities of measuring both waves and velocity-profiles, but not simultaneously. Typically, the instrument is set to collect a velocity-profile, then switches to measure a wave burst for 20 minutes. After the wave burst, it switches back to velocity-profile mode at 10 (or 5) minute intervals. Since the instrument cannot measure velocity-profiles and waves bursts at the same time, it misses critical wave-current interaction nonlinearities. Another drawback is that the memory storage of the AWAC instrument is limited when used for both velocity profiles and waves. Therefore, the initial protocol was to deploy two AWAC instruments, one to measure velocity-profiles and the other to measure wave bursts with each instrument synchronized to the same UTC clock.

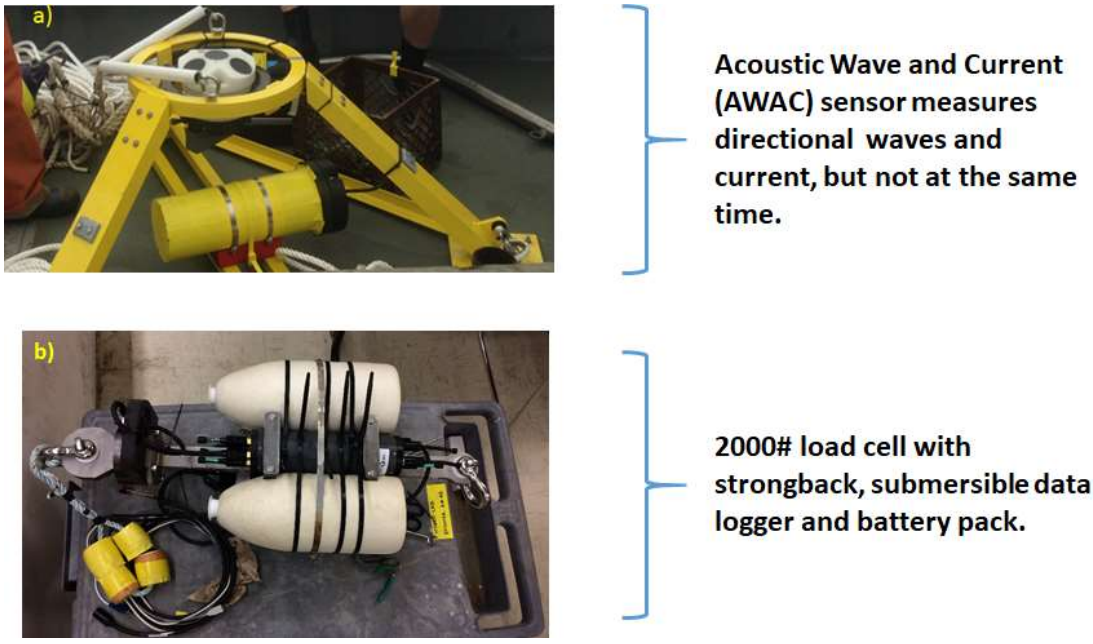

Figure 93: a) Two AWAC instruments will be deployed, one to measure velocity-profiles and the other for measuring directional waves. b) The first load-cell data acquisition system funded by a previous NSF project.

In addition to the two AWAC instruments, the field program required multiple load-cell systems attached inline components of the kelp aquaculture system. As part of a previous NSF-EPSCoR project, The UNE-USNA team developed a self-contained submersible, 2000 lbf load cell system. It included a submersible data acquisition system and battery pack attached to a strong back with flotation elements to make it close to neutrally buoyant. This first unit is shown on Figure 93 (b). The system was deployed twice on the Wood Island system in 2018 for in-field testing along with an AWAC measuring velocity profiles. The datasets are provided in Task 5.

The instruments were then prepared and configured for the winter 2018-2019 field deployment. Based on the experience from the 2018 season, it was decided to have short 1- to 2-week deployments for the following reasons.

- Individual weather events can be better characterized.
- More accurate power (e.g. battery) management.
- If instrument failure occurs, there is more time for re-deployment.
- Dataset would focus on developing the following numerical model load cases:
    - November 2018 to obtain data set to describe the response of the culture system without any growth.
    - February-March 2019 (weather permitting) to obtain data sets with moderate growth.
    - April-May 2019 to obtain data sets with harvest level growth.
    - May 2019 to obtain data sets data sets having harvest level growth with only one mooring line.

The following sections describe the initial sampling protocols for the velocity profile and wave burst measurement. A summary of the protocol is provided in Table 17. Note that it was originally planned to deploy accelerometer, but resulting datasets proved not to be useful.

Table 17: Initial sampling protocol for the four instruments to be deployed.

	Minute	0	1	2	3	4	5	6	7	8	9	10	11	12	13	14	15	16	17	18	19	20	21	22	23	24	25	26	27	28	29	30	31	32	
AWAC #1	Currents only	Currents						Currents						Currents						Currents						Currents						Currents			Continues
AWAC #2	Current/Waves	Currents		Waves: 1024 secs (17 minutes) at 2 Hz																			Repeats the following hour												
Load Cell	Tensions	Tensions: 20 minutes at 2 Hz																					Repeats the following hour												
Accelerometers	Motions	Motions: 20 minutes at 16 Hz																					Repeats the following hour												

AWAC #1 - Current velocity profiles: The initial protocol was to have the current velocity profiles measured with a single AWAC configured specifically for this application. The instrument setup was to have the current profiles measured at 0.5 m bins, sampling 3 minute averages every 6 minutes. This would provide 10 samples per hour. The intent of this sampling scheme was having it coincide with AWAC #2 measuring wave bursts.

AWAC #2 - Waves: The initial protocol for AWAC #2 was to measure waves for 17 minutes every hour at a rate of at least 2 Hz. This was to overlap AWAC #1 to have the wave burst coinciding with 3 current velocity data sets per hour. AWAC #2 was also set to measure current profile for 3 minutes every hour at 0.5-m bins before the wave bursts. AWAC #1 also measured the directional component of the waves from wave orbital velocity vector components. Time series and spectral results to be obtained from the instrument would be used as input data files for the numerical model.

Tensions: The project plan also included the use of two load cell instrument systems deployed on the mooring legs of the kelp farm. The initial plan was to have the instruments setup to measure tensions at a rate of at least 2 Hz for 20 minutes every hour. This overlaps with AWAC #1 for 3 data sets and will be nearly identical with AWAC #2 measuring waves. At this time, only the 2000 lbf capacity the load cell was in used. Part of the preparation details including having the

individual load cell calibrated by the manufacturer and checked at the Naval Academy with the data logger attached. The calibration results are shown on Figure 94.

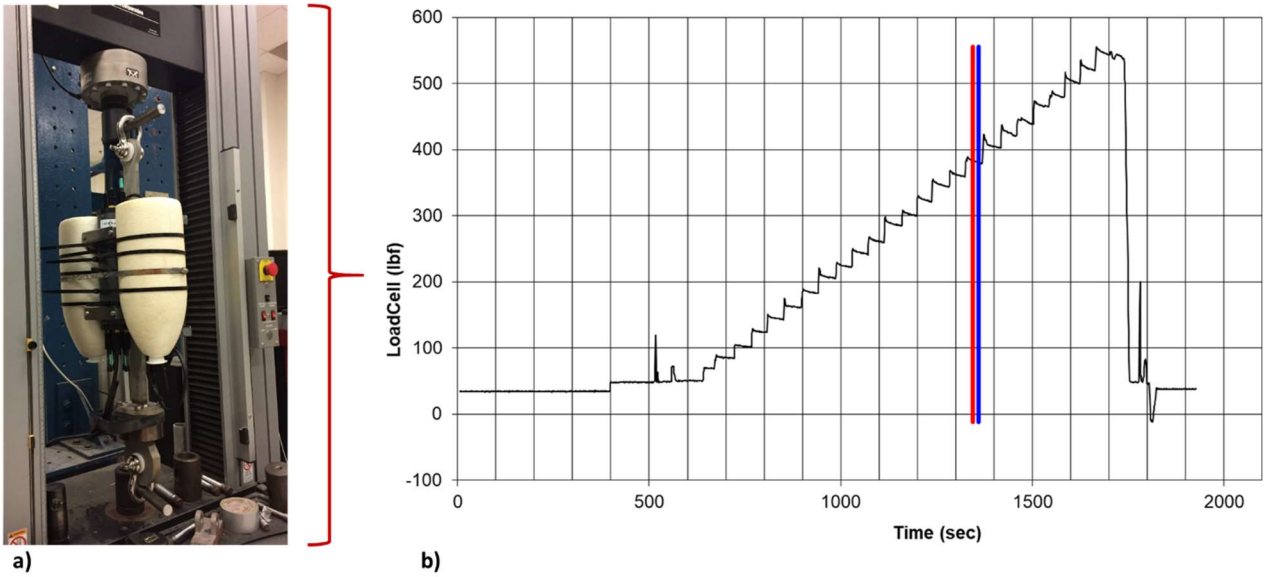

Figure 94: The 2000 lbf capacity load cell was calibrated up to 500 lbf in the strength materials laboratory to check the manufacturer calibration prior to the May 2018 deployments.

Two new load cell instrumentation packages were then designed and fabricated. The load cell capacity was based on an extreme value 8000 lbf as calculated using the horizontally integrated Morison equation as described in Task 2 for 122 m of culture line with 3 m long blades and a growth density of about 13 kg/m. To be within this range, two 10,000 lbf capacity load cells were refurbished, obtained from a previous project. Two new strong backs were then designed (Figure 95 a) and fabricated (Figure 95 b). In Figure 95 (b), the pancake type load cell is shown attached to the strong back. These stainless-steel strong backs were designed to have a capacity of about 18,000 lbf. The higher capacity strong back was chosen so that it could be potentially on larger grow-out systems.

In addition to the new load cell systems, UNE purchased a new Nortek Signature 1000 instrument (Sig1000) in February 2019. The Sig1000 has the advantage of being able to measure both currents and waves simultaneously (unlike the AWAC instruments). The purchase of this instrument enables the UNE Team to have a dedicated unit for measuring current and wave parameters that force the macroalgae system. In addition to purchasing the Sig1000, a new instrument frame was also acquired.

Prior to the March 2019 deployment the AWAC instruments were cleaned and battery packs replaced. AWAC instruments were also labeled as “yellow” and “blue” as shown on Figure 96. The 2k (2000 lbf) load cell batteries were also replaced. One of the new 10k (10,000 lbf) load cell systems with data acquisition and battery pack was configured with flotation on the strongback (Figure 96). The three load-cells systems are shown on Figure 97. Both of the two 10k load cell systems were then calibrated at the U.S. Naval Academy. The calibration datasets are provided on Figure 98.

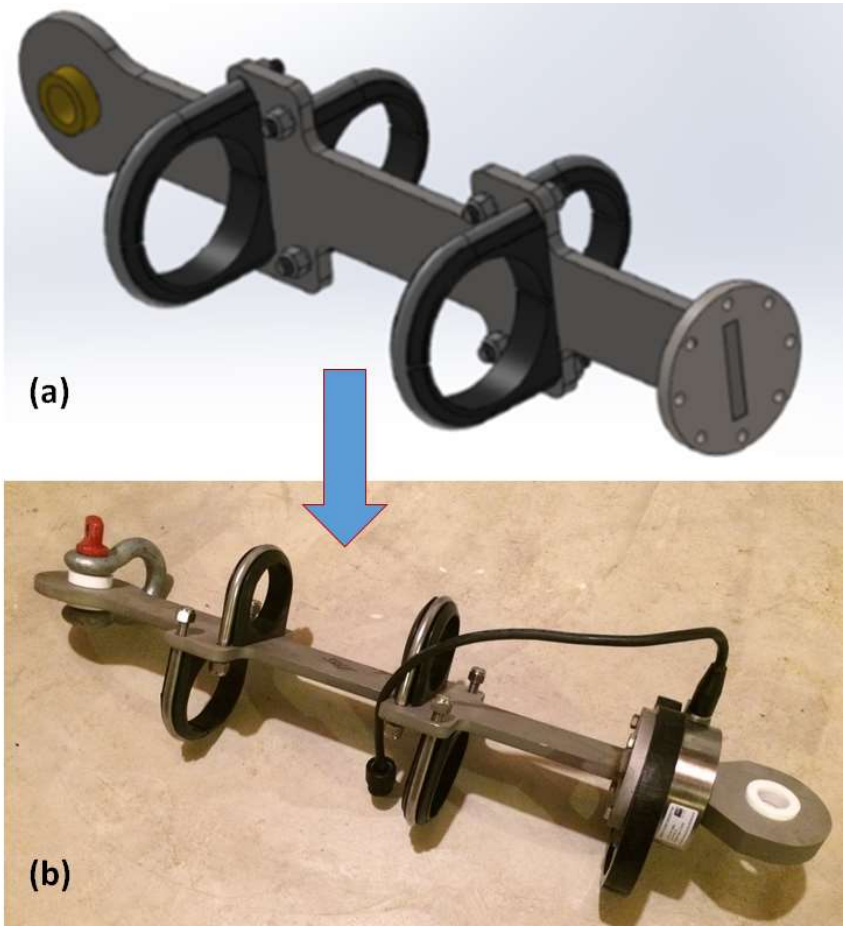

Figure 95: (a) A new load cell strong back was designed to handle higher capacity mooring systems during in June 2018. (b) The two strong backs were then built for the refurbished two 10,000 lbf capacity load cells.

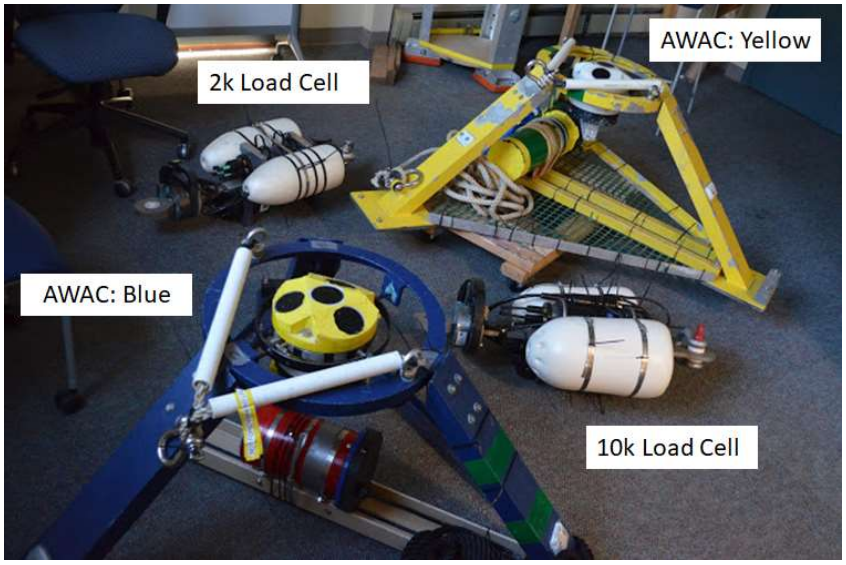

Figure 96: The two AWAC and load-cell instrumentation packages ready for deployment. These instruments were deployed three times during the 2019 season.

By May 2019, the project had three load cell systems completed and calibrated

Figure 97: Three load cell systems were completed and calibrated by May 2019.

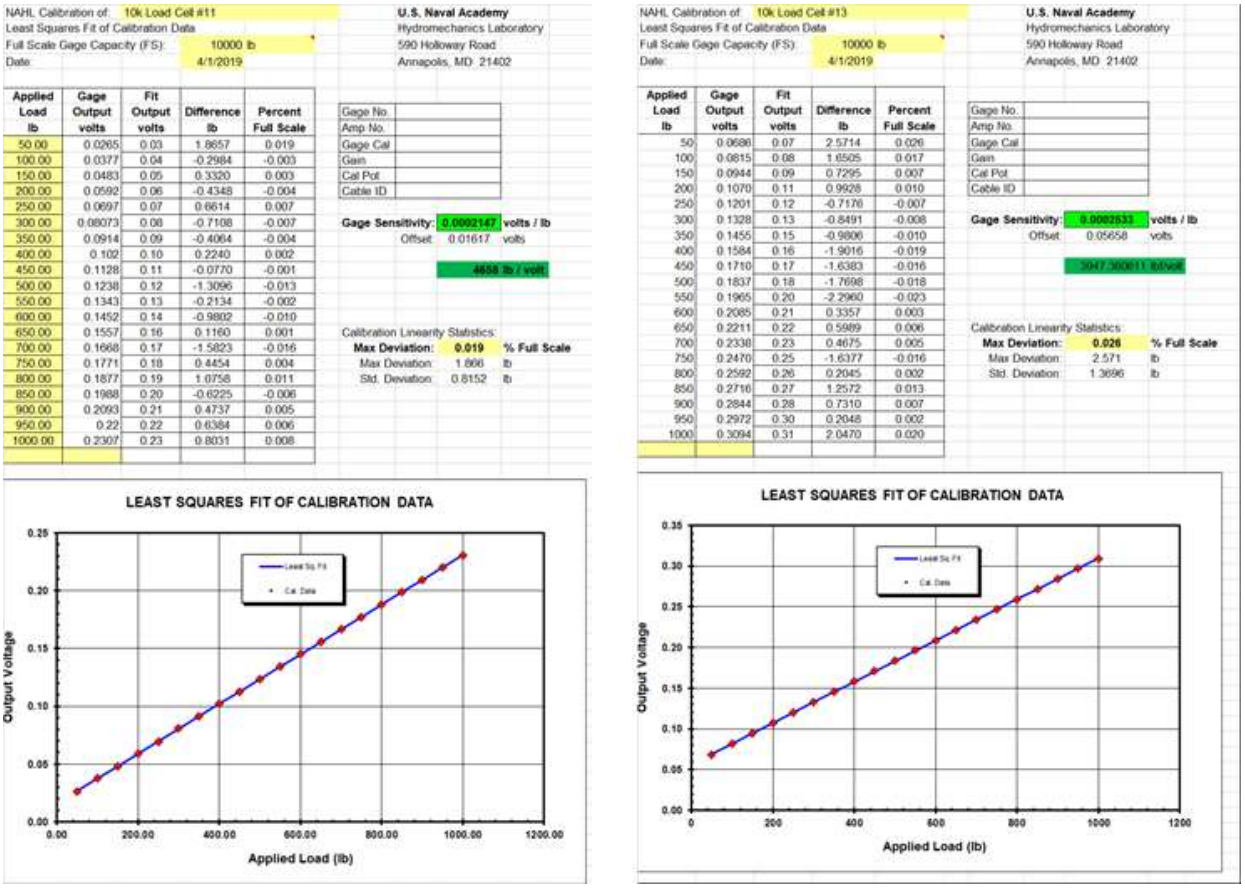

Figure 98: Calibration datasets for the two 10k load-cell instruments.

By December 2019 a fourth load cell system was completed. The load cell was specified at 5000 lbf with an integrated amplifier. The load cell, battery pack and data logger (Figure 99a) were assembled and the calibration verified (Figure 99b) at the U.S. Naval Academy. The full suite of instruments is shown on Figure 100 including 4 load cells and two AWACs and a Sig1000.

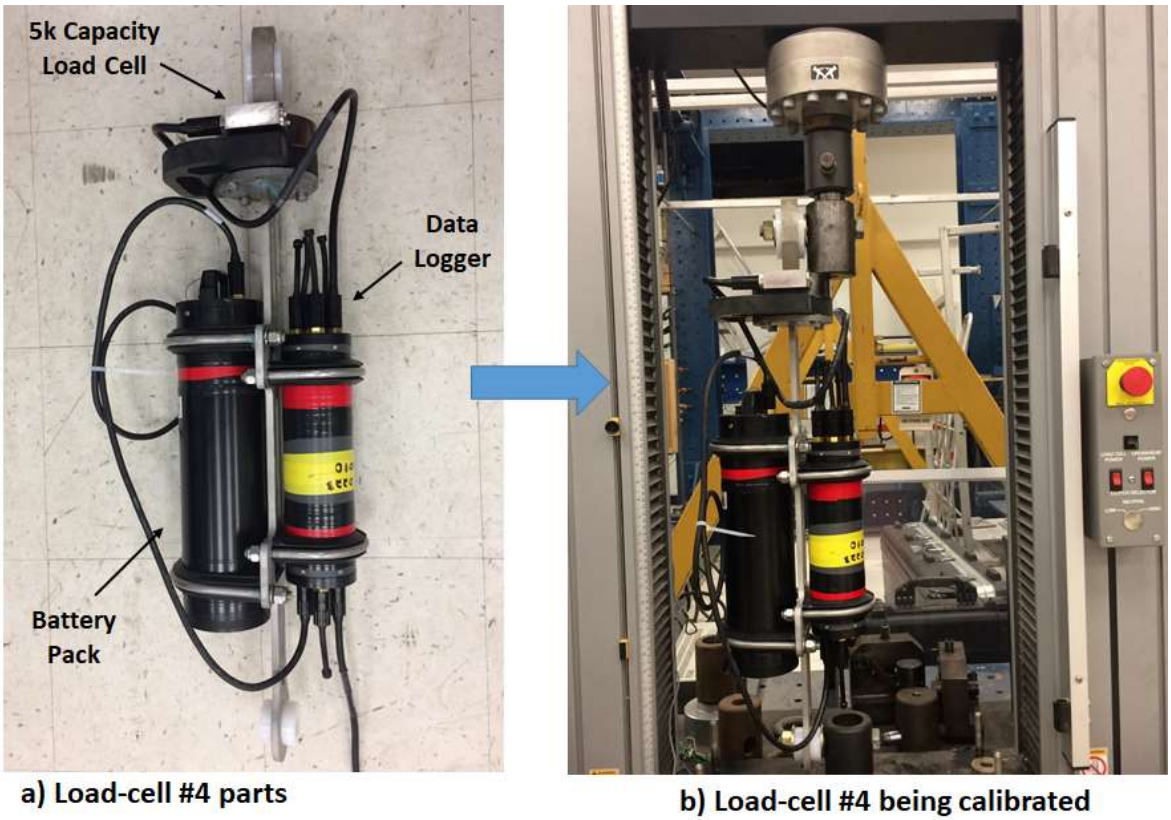

Figure 99: a) The parts of load-cell system #4 included a battery pack and data logger mounted on a strongback. b) Load-cell system #4 was assembled at the U.S. Naval Academy and the calibration verified.

Figure 100: The suite of instruments now includes 4 load cell systems, and 3 acoustic Doppler instruments.

In February 2019, it was decided to change the sampling protocol to have both AWACs measure waves based on the experience of the previous deployment in November 2018. Details of the updated sampling schemes are provided on Table 18. The sampling protocol was updated for two primary reasons including (1), to have both AWACS measuring waves and currents and (2) to accommodate strain gage warm-up drift in the load cells. Calibration of the load cells showed that each could take up to 10 minutes to stabilize. Therefore, the sampling protocol focused on correlating all datasets to load cell data collection from 15-30 minutes past the hour.

Table 18: Updated sampling protocol for the instruments to be deployed in April-2019.

	Minute	0 1 2 3 4 5 6 7 8 9 10 11 12 13 14 15 16 17 18 19 20 21 22 23 24 25 26 27 28 29 30 31 32
AWAC Yellow	Currents/Waves	Currents | Waves: 600 s (10 minutes) - 2 Hz | Currents | Waves: 600 secs (10 minutes) at 2 Hz | Repeats
AWAC Blue	Current/Waves	Currents | 256 s - 2 Hz | Currents | 256 s - 2 Hz | Currents | 256 s - 2 Hz | Repeats
Load Cells	Tensions	Tensions: 30 minutes at 4 Hz | Repeats the following hour
Accelerometers	Motions	Motions: 8 minutes at 16 Hz | Motions: 8 minutes at 16 Hz | Motions: 8 minutes at 16 Hz | Repeats

With the sampling configuration provided in Table 18, it was discovered from the first instrument deployment, that AWAC Blue could not record waves with the Acoustic Surface Track method. Waves were measured, however, using the onboard pressure sensor and with wave velocity methods. It was also decided from reviewing the deployment dataset that it would be advantageous to have both AWACs configured to be identical and to deploy each adjacent to the load cells on each of the mooring legs. With this spatial configuration, current velocity and wave datasets could be compared to examine differences on either side of the system. Therefore, AWAC yellow and blue were configured to be identical as shown on Table 19.

Table 19: Updated sampling protocol for the instruments for the April-June 2019 reporting period.

	Minute	0 1 2 3 4 5 6 7 8 9 10 11 12 13 14 15 16 17 18 19 20 21 22 23 24 25 26 27 28 29 30 31 32
AWAC Yellow	Currents/Waves	Currents | Waves: 600 s (10 minutes) - 2 Hz | Currents | Waves: 600 secs (10 minutes) at 2 Hz | Repeats
AWAC Blue	Current/Waves	Currents | Waves: 600 s (10 minutes) - 2 Hz | Currents | Waves: 600 secs (10 minutes) at 2 Hz | Repeats
Load Cells	Tensions	Tensions: 30 minutes at 4 Hz | Repeats the following hour
Accelerometers	Motions	Motions: 8 minutes at 16 Hz | Motions: 8 minutes at 16 Hz | Motions: 8 minutes at 16 Hz | Repeats

2.4.2. Milestone 4.2: Finalize data set load case protocols (11/14/18)

Even though this milestone was previously reported to be complete, modifications to the sampling protocols were adjusted based on dataset review and experience. However, the sampling scheme provided in Table 19 seemed to have worked well for the instrumentation deployments that were conducted between April 24 - May 1 and from May 16-26.

2.4.3. Task 4.3: First instrumentation deployment (05/28/19)

The reasons for deploying the load cell system on the Wood Island culture system in 2018 was to perform in water tests of the instrument package, assess the resulting datasets, refine sampling protocols and obtain potential validation information for the Hydro-FE model. The preliminary datasets were obtained with the 2000 lbf load cell system on May 17, 2018 and on May 22, 2018. The deployment configurations are shown on Figure 101. The schematic on the Figure 101(a)

shows the Wood Island system as deployed in an east-west orientation. The system was deployed in an east-west configuration to be aligned with the major axis of the tidal ellipse. During the grow-out period, only 30 of the 60 m of the culture line was seeded filling only the western half of the longline. Kelp samples were obtained with the general characteristics provided in Table 16. On May 17, 2018, the load cell system was deployed on the eastern side of the culture line and configured to sample at 2 Hz continuously for 24 hours. At the same time, the AWAC was deployed and configured to measure velocity profiles producing 3-minute averages every five minutes. After 24 hours, the instruments were recovered and the data sets examined. Both instruments were redeployed on May 22, 2018 for another 24 hours. This time, however, the load cell was installed on the western anchor of the longline. Figure 101(b) shows a photograph of the load cell system when it was deployed on the western anchor leg.

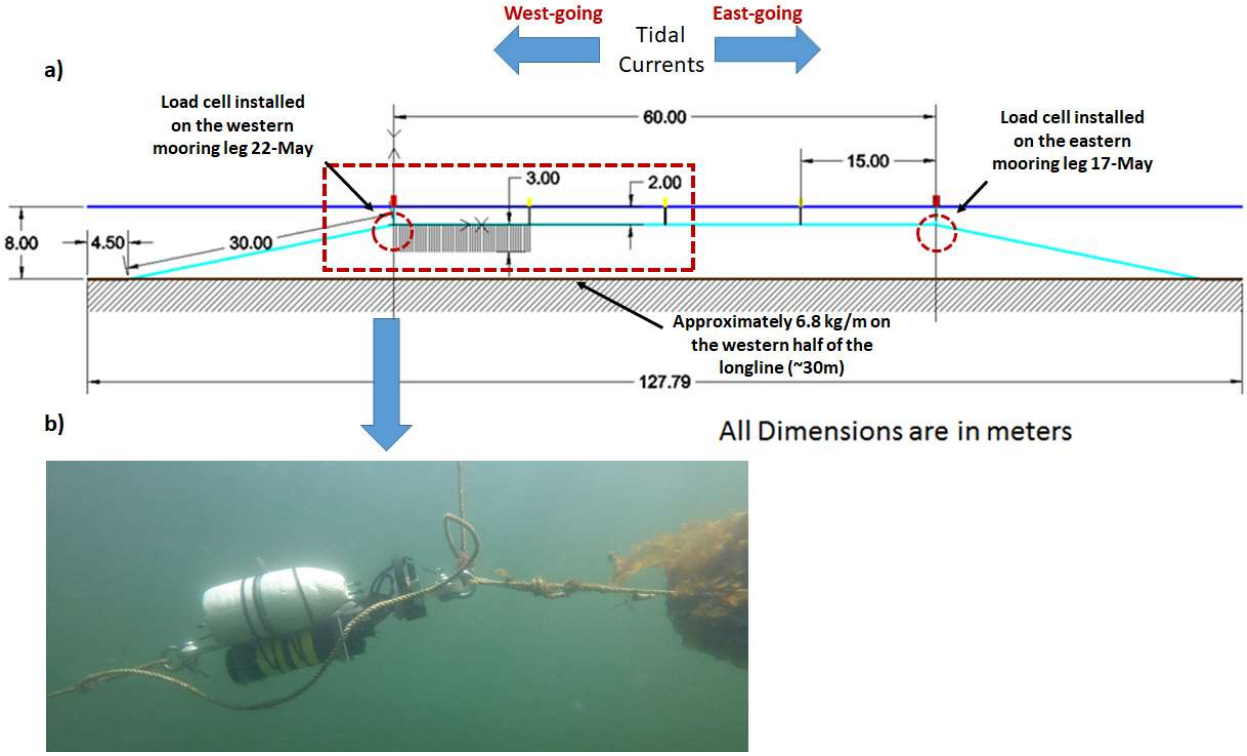

Figure 101: a) A schematic of the Wood Island culture line deployed in an east-west configuration. The load cell system was deployed on the eastern anchor leg on May 17, 2018 and on the western anchor leg on May 22, 2018, each for 24 hours. The AWAC was also deployed to measure velocity-profiles for each of the deployments. b) A photograph of the load cell system when it was deployed on the western anchor leg.

After each 24 hour deployment, the instruments were recovered and the data downloaded. The processed AWAC and load-cell datasets for the May 17, 2018 and May 22, 2018 are shown on Figure 102 and Figure 103, respectively as three, stacked plots. The first stack plot shows the surface elevation mostly due to the semi-diurnal (M_2) tide. The second stack plot shows the depth-averaged east- and north-going velocities. The third stack plot show the tension measured with the load cell.

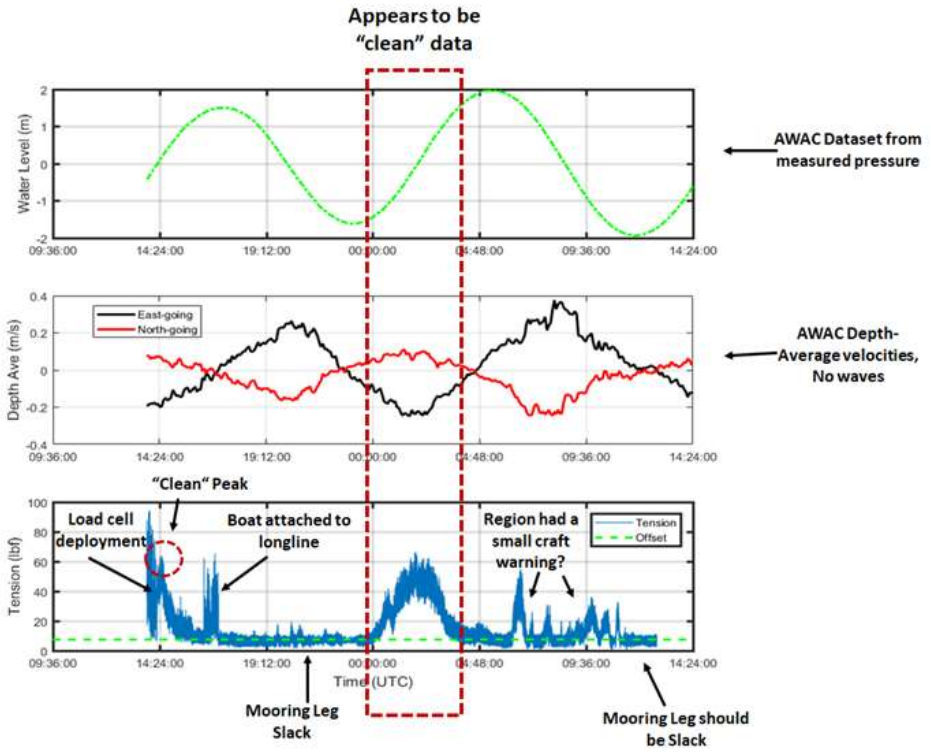

Figure 102: AWAC and load cell data set from May 17, 2018.

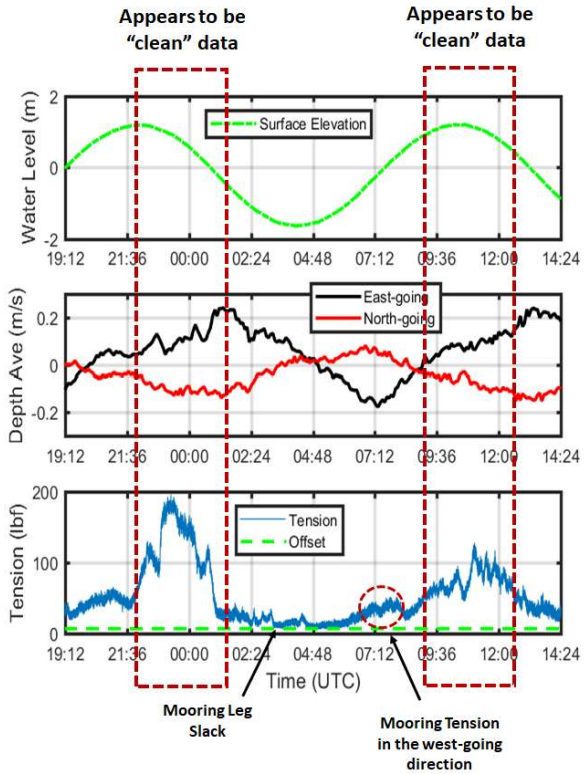

Figure 103: The load cell was deployed again on May 22, 2018, but on the western anchor leg to measure tensions in the west-going direction.

The preliminary field datasets obtained from 2018 culture line showed useable results for the two 24 hour deployments. With the successful deployments, a similar field effort was conducted at both the Wood and Ram Island site in 2019. During this year, a 61 m culture line was deployed at the Wood Island site and a 122 m at the Ram Island site.

Two load cells and two AWACS were deployed Wood Island site from April 11-17, 2019. Note that the instruments deployed on the east side were labeled as blue and those on the west side as yellow. On April 11, 2019, both the AWACs were deployed on the southern side of the culture line with the instrument setup as provided in Table 18. The blue AWAC was placed on the eastern side, while the yellow AWAC was placed on the western side of the kelp-line as shown on Figure 104. On the same day, the 2k load-cell (yellow) was deployed on the western side of the kelp-line and the 10k load-cell was deployed eastern side (blue). On April 17, 2019, the instruments were recovered and the datasets downloaded. General tide level and depth average velocity results of the AWACs are shown in Figure 105, with blue and yellow denoting the east and west sides, respectively. Also shown on the Figure are the raw data results from the two load cells with the same color combination. General wave dataset results (significant and maximum wave heights) are shown on Figure 106 for the east and west sides along with the same load cell results.

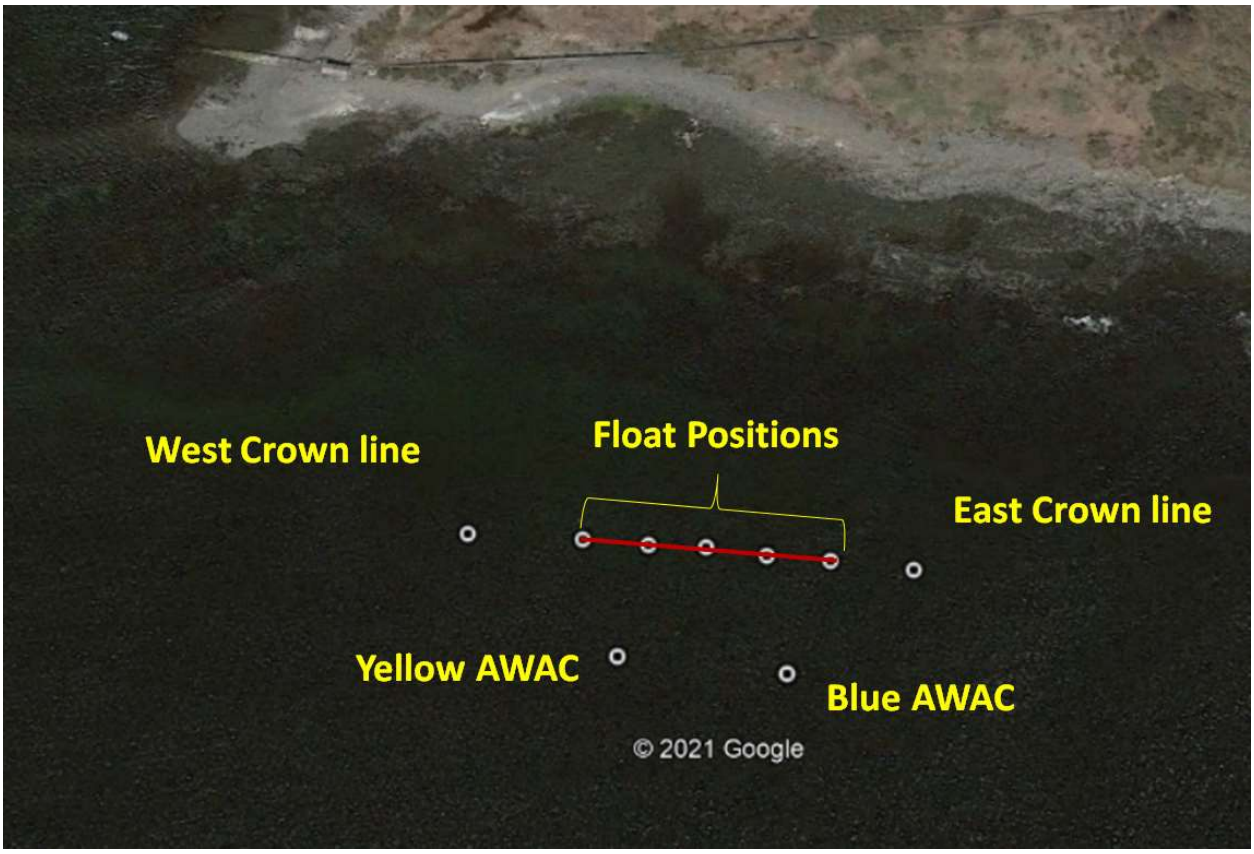

Figure 104: Positions of the Wood Island kelp line and the deployed AWACs for instrument deployment from April 11-17, 2019.

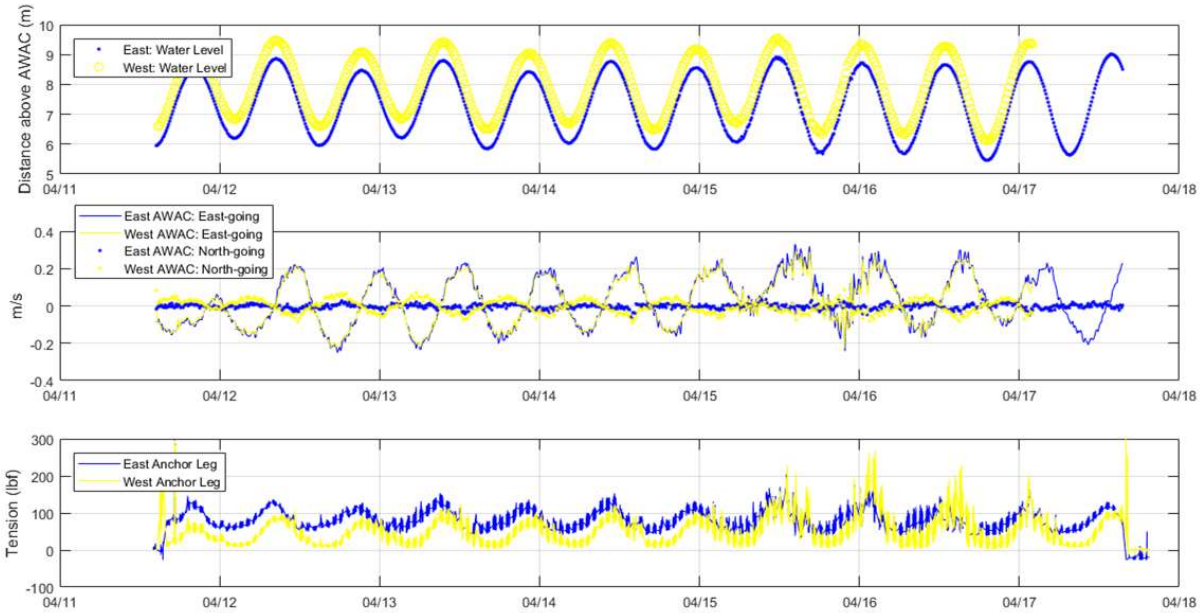

Figure 105: Wood Island dataset results April 11-17, 2019. The east/west AWAC water elevation (tides) and velocity components plotted with the east/west load cell datasets.

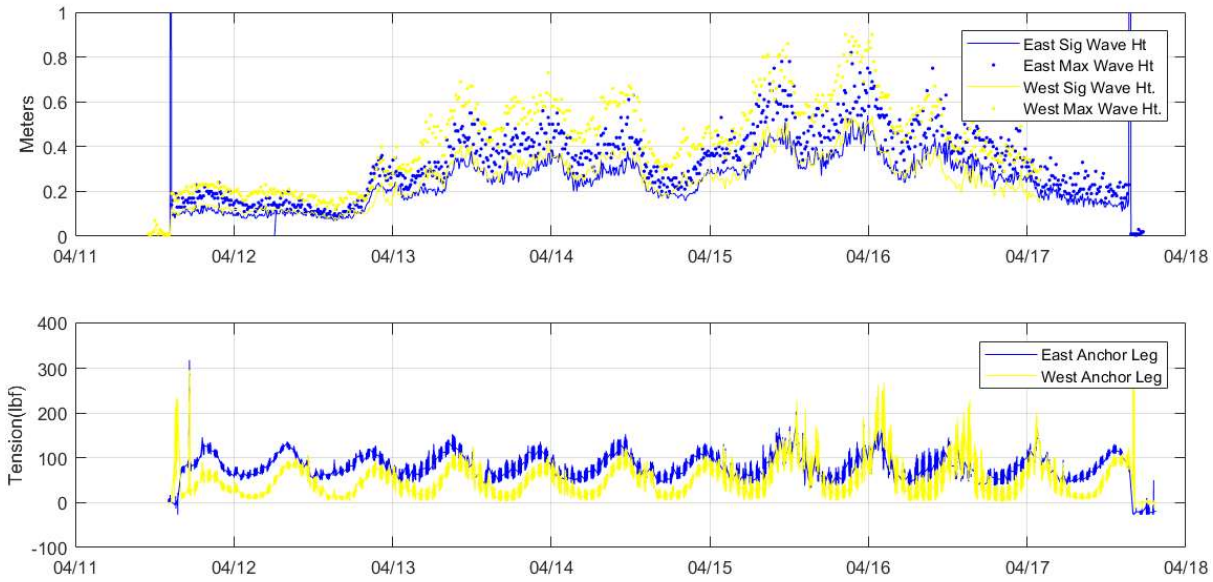

Figure 106: Wood Island dataset results April 11-17. The east/west AWAC significant and maximum wave heights plotted with the same east/west load cell datasets. The corresponding tensions are also shown.

Once the instruments were recovered from the Wood Island site on April 17, 2019, each unit was cleaned, data downloaded and reconfigured for deployment at the exposed, Ram Island site. All of the instruments were redeployed on April 24, 2019 and recovered by May 1, 2019. In a similar fashion, both the blue and yellow AWACs were deployed on the southern side of the kelp-line, but with the instrument setup as provided in Table 19 and shown on Figure 107.

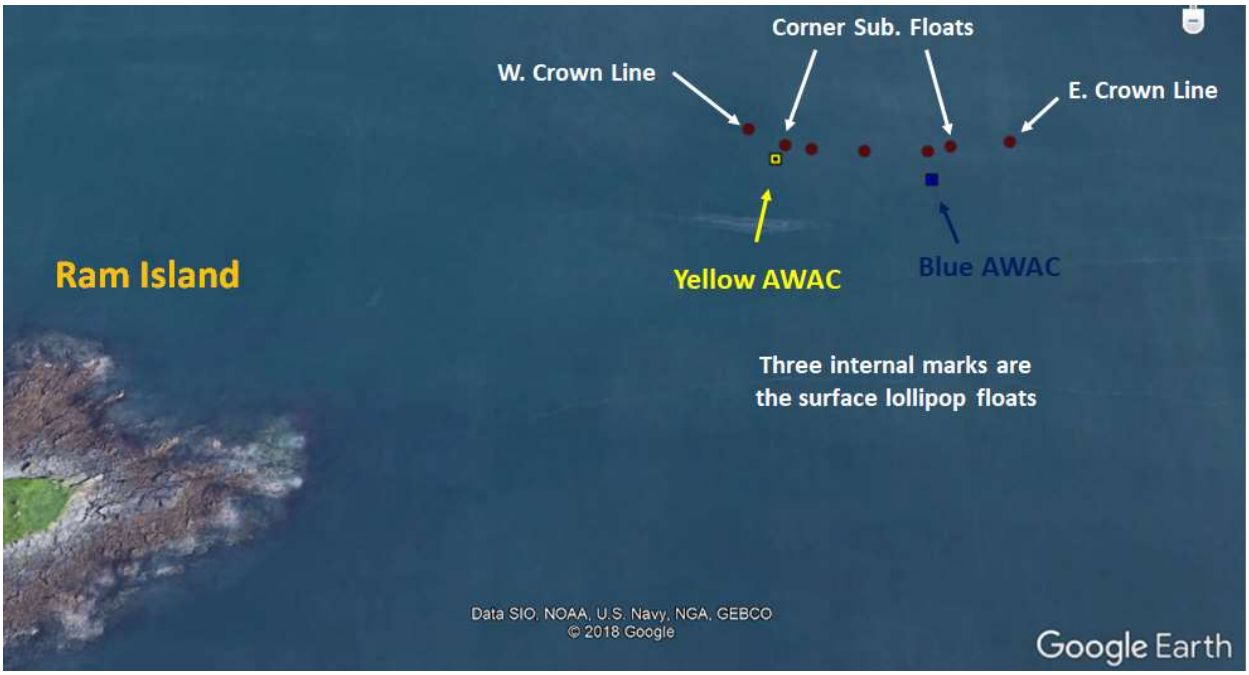

Figure 107: Positions of the Ram Island kelp line and the deployed AWACs for instrument deployment from April 24, 2019 to May 1, 2019.

Following the same protocol as at the Wood Island site, the blue AWAC was placed on the eastern side, while the yellow AWAC was placed on the western side of the culture line. On the same day, the 2k load cell (yellow) was deployed on the western side of the kelp-line and the 10k load-cell was deployed eastern side (blue). On May 1, the instruments were recovered and the datasets downloaded. General tide level and depth average velocity results of the AWACs are shown in Figure 108, with blue and yellow denoting the east and west sides, respectively. Also shown on the Figure are the raw data results from the two load cells with the same color combination. General wave dataset results (significant and maximum wave heights) are shown on Figure 109 for the east (blue) and west (yellow) sides along with the same load cell results.

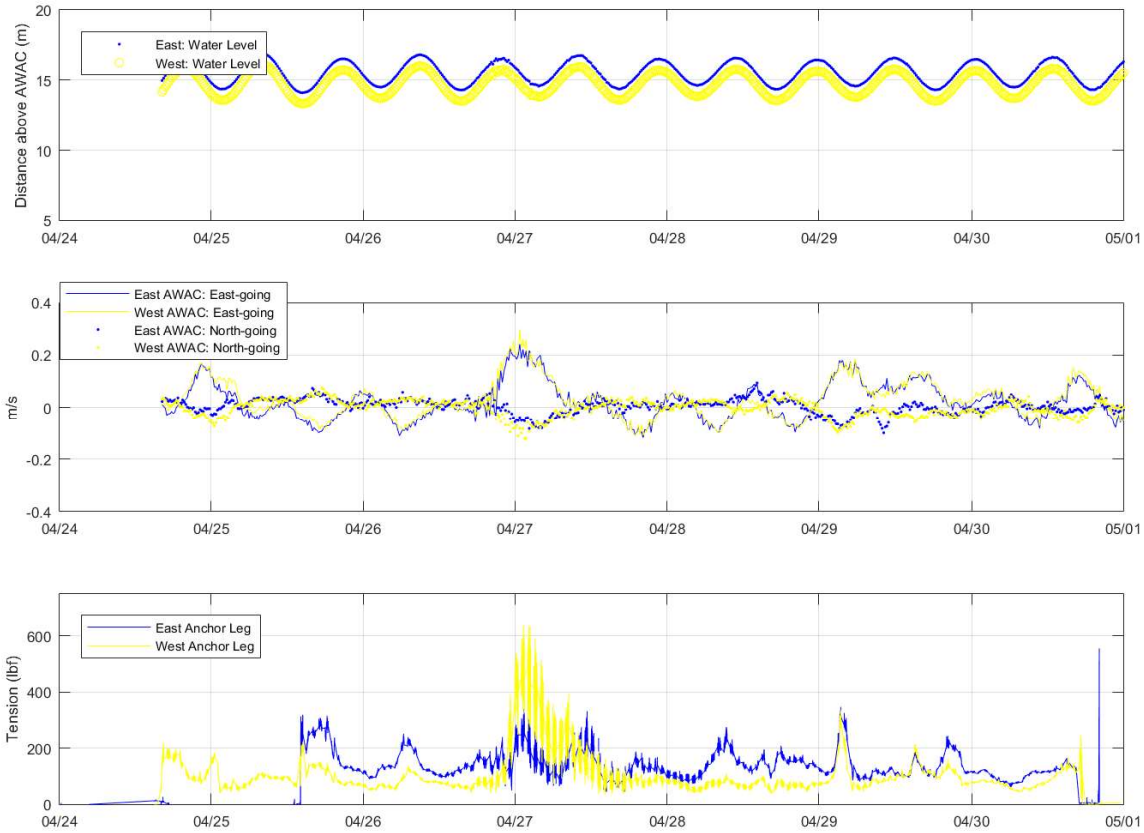

Figure 108: Ram Island dataset results April 24 – May 1. The east/west AWAC water elevation (tides) and velocity components are plotted with the east/west load cell datasets.

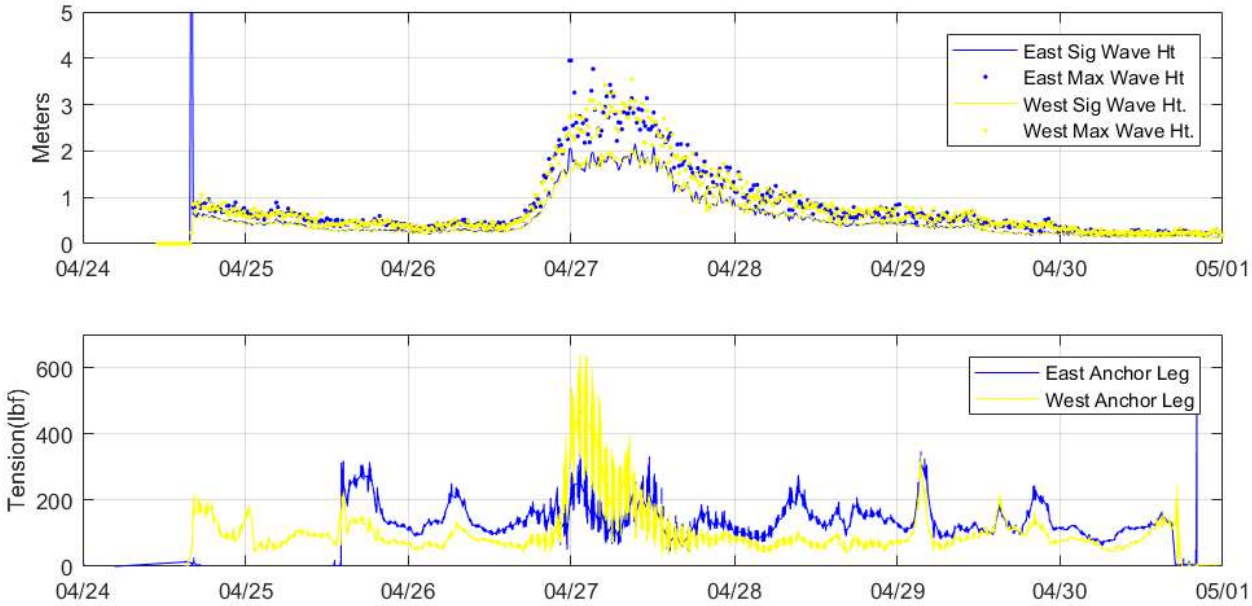

Figure 109: Ram Island dataset results April 24 – May 1. The east/west AWAC significant and maximum wave heights are plotted with the same east/west load cell datasets.

After the instruments were recovered from the Ram Island site on May 1, 2019, each unit was again cleaned, data downloaded and reconfigured. All of the instruments were redeployed on May 16, 2019 at the sheltered Wood Island site to coincide a jet-yak survey with Woods Hole Oceanographic Institution. Consistent with the other two deployments, both the blue and yellow AWACs were deployed on the southern side of the culture line, but with the instrument setup as provided in Table 19. On the same day, the 2k load cell (yellow) was deployed on the western side of the kelp-line and the 10k loadcell was deployed eastern side (blue). On May 28, the instruments were recovered and the datasets downloaded. General tide level and depth average velocity results of the AWACs are shown in Figure 110, with blue and yellow denoting the east and west sides, respectively. Also shown on the Figure are the raw data results from the two load cells with the same color combination. General wave dataset results (significant and maximum wave heights) are shown on Figure 111 for the east (blue) and west (yellow) sides along with the same load cell results. From review of the plots, it became evident that the battery pack on the 2k load cell ran out of power, though six days of data were acquired.

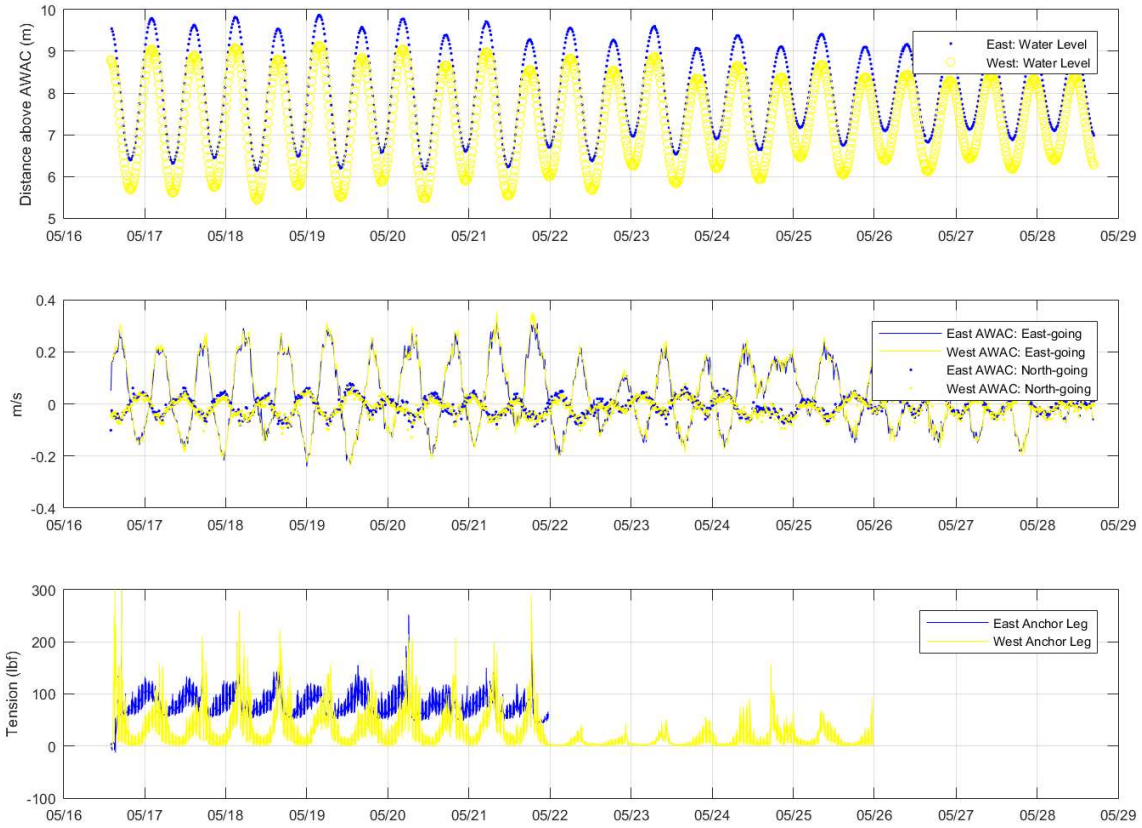

Figure 110: Wood Island dataset results May 16-28. The east/west AWAC water elevation (tides) and velocity components are plotted with the east/west load cell datasets.

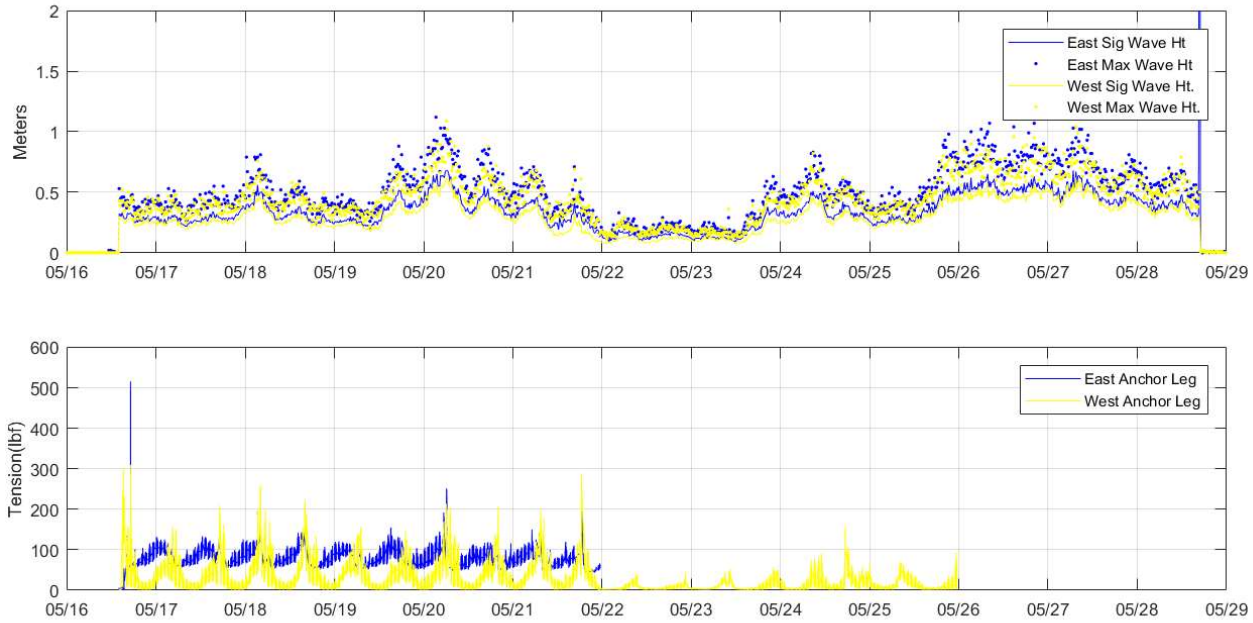

Figure 111: Wood Island dataset results May 16-28. The east/west AWAC significant and maximum wave heights are plotted with the same east/west load cell datasets.

2.4.4. Milestone 4.4: First instrument recovery (05/14/19)

Instruments have been deployed and recovered as a part of this milestone. Deployments of load cells and AWACs were conducted on the following dates.

- 17-May-18: Wood Island site
- 22-May-18: Wood Island site
- 30-Oct-18: Ram Island site
- 11-Apr-19: Wood Island site
- 24-Apr-19: Ram Island site
- 16-May-19: Wood Island site

2.4.5. Task 4.5: Load-case development for single-line system (11/14/19)

A preliminary load case for the single line system was obtained on May 18, 2018. On this day, the maximum depth-averaged tidal velocity occurred halfway between low and high tides. The load cell was deployed as the tide was increasing with the strongest west-going velocities shown as negative east values on the Figure (1424 UTC). As the high tide peaked, the tidal velocities became slack and then switched to an east-going direction. Since the load cell was on the eastern anchor leg, this part of the mooring became nearly slack (1912 UTC). As the tidal current switched (0000 UTC) again to the west, the tension measured by the load cell increased to approximately 60 lbf, subsiding once high tide was reached. The data set also shows the sensitivity of the load cell with several spikes occurring during deployment. Additional spikes were measured during a kelp sampling period when the boat was attached to the culture line. Toward the end of the 24

hour duration, winds were blowing strong enough to institute a small craft warning. It is suspected that these winds caused the tension readings to approach 50 lbf. Throughout the sampling period, High frequency oscillations were also evident. It is suspected that these oscillations were the result of surface buoy motions from the winds, waves and currents.

As discussed in Task 4.3, the May 18, 2018 dataset served as an initial load-case to examine the performance of the numerical model. Since only about 6.8 kg/m of kelp were grown on 30 m of longline and with the maximum loads on the order of 50 lbf (with offset removed), performing accurate model simulations required meticulous input forcing parameters. Therefore, this dataset was examined with more detail by focusing on two specific current profiles with the continuous stream of load cell data. The datasets are shown on Figure 112 with the two profiles acquired on May 18, 2018 at 0120 UTC (depth = 5.69) and at 0125 UTC (depth = 5.74) as the depth-averaged points on the right side of Figure 112. Recall that the AWAC was measuring depth profiles at 0.5 m bins producing 30-minute averages every 5 minutes.

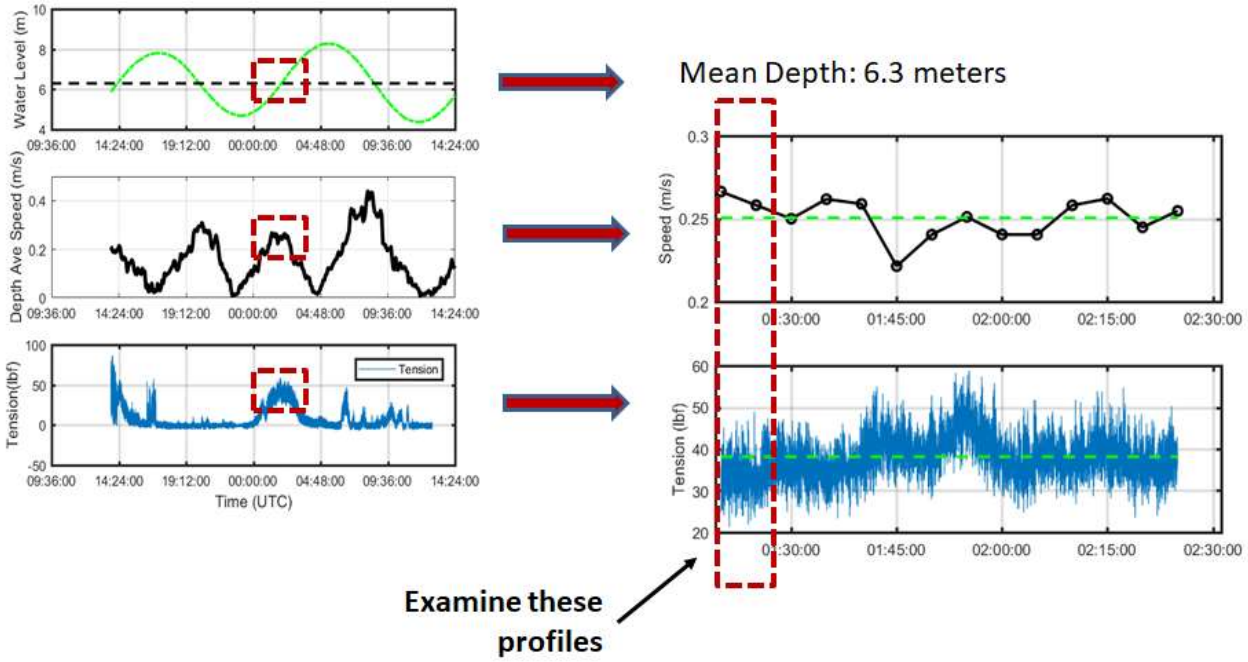

Figure 112: Two specific profiles were examined with continuous tensions.

The dataset details are provided in Figure 113 with the two east- and north-going profiles. As shown on the Figure, the red profiles were obtained at 0120 and the blue profiles were obtained at 0125, each for 3-minutes. Each profile was similar indicating a consistent flow during the 8 minutes of data that were examined. The resulting measured tension was also similar during this time and showed influence of surface wave action and buoy movements. The profiles were combined into a composite speed profile and used as input to the numerical model.

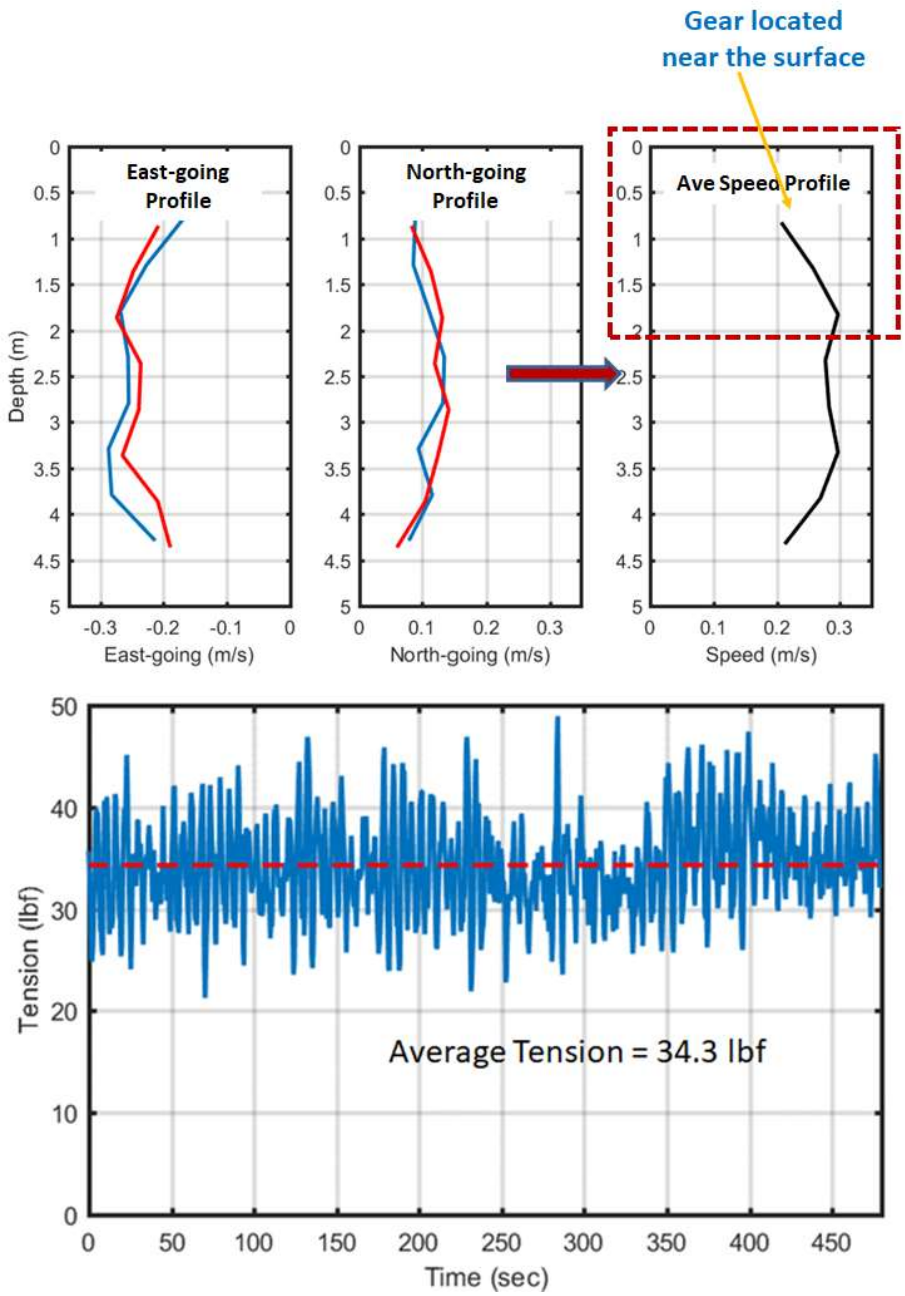

Figure 113: The May 18, 2018 dataset details. The red profiles were obtained at 0120 and the blue profiles were obtained at 0125, each for 3-minutes.

Another potential load case dataset was obtained on May 22, 2018, also from the Wood Island site. This dataset obtained AWAC information and tensions on the western anchor leg as the tidal currents were moving in the eastern direction. The surface elevation, depth-averaged tidal currents and resulting western anchor leg tension are shown on Figure 103. The surface elevation and depth averaged tidal currents are 90 degrees out of phase as expected. The maximum tension, however, appears to lag the maximum tidal currents. This could be due to the placement of the AWAC not being exactly coincident with the load cell. The tension values are nearly 3 times on the western anchor leg since the east-going tidal currents were stronger.

As described in Task 2, the 122 m culture line system (Figure 20) was deployed at the exposed Ram Island site on October 30, 2018 in a slack configuration (Figure 21) with a mean sea level (MSL) of 15 m. At the time it was decided to deploy the AWAC and load cell instruments that along with the aquaculture gear to measure tensions without any significant biomass. For this deployment, the instruments were configured with the original sampling scheme with one of the AWACs measuring waves and currents and the other AWAC measuring only currents. With the AWACs, only the 2000 lbf capacity load cell was deployed on the eastern anchor leg with the sampling plan provided in Table 17. Recall that due to the weather conditions (small craft warning) the system could not be tensioned. On October 31, 2018, the weather improved and therefore instruments were recovered prior to setting the mooring. Therefore, a data set was acquired of the 122 m culture line with no kelp in a slack configuration.

When the instruments were recovered, the information was downloaded and evaluated. It was discovered that one of AWACs was deployed such that the transducers were permanently set at an angle of about 20 degrees. It is suspected that the gimbal mechanism had been stuck during the deployment and therefore the dataset was not used. The other AWAC, however, was configured to measure both current profiles and waves. The current profiles were set at an interval of 30 minutes recording 3 minute average measuring at 0.5 m bins up from the AWAC. Wave bursts were measured for 1024 seconds (at 2 Hz) starting once the profiles were completed. The wave bursts were also measured at an interval of 30 minute.

The pressure and current profile data from the AWAC were downloaded from the instrument. The surface elevation from the pressure measurements are shown on Figure 114(a). The bin velocities were depth-averaged with the east- and north-going velocities shown Figure 114(b) along with the corresponding speed. Maximum speeds were approximately 0.15 m/s.

In addition to the datasets from the AWAC, information was also obtained from the load cell mounted on the eastern anchor leg. The load cell was configured to measure tensions at a rate of 2 hz for 20 minutes every hour. The raw data set was processed by removing the offset obtained from a data burst acquired when the instrument was recovered and sitting on the deck of the vessel. The average and standard deviation of this burst was 11.18 and 0.38 lbf, respectively. The offset was removed as shown on Figure 114(c).

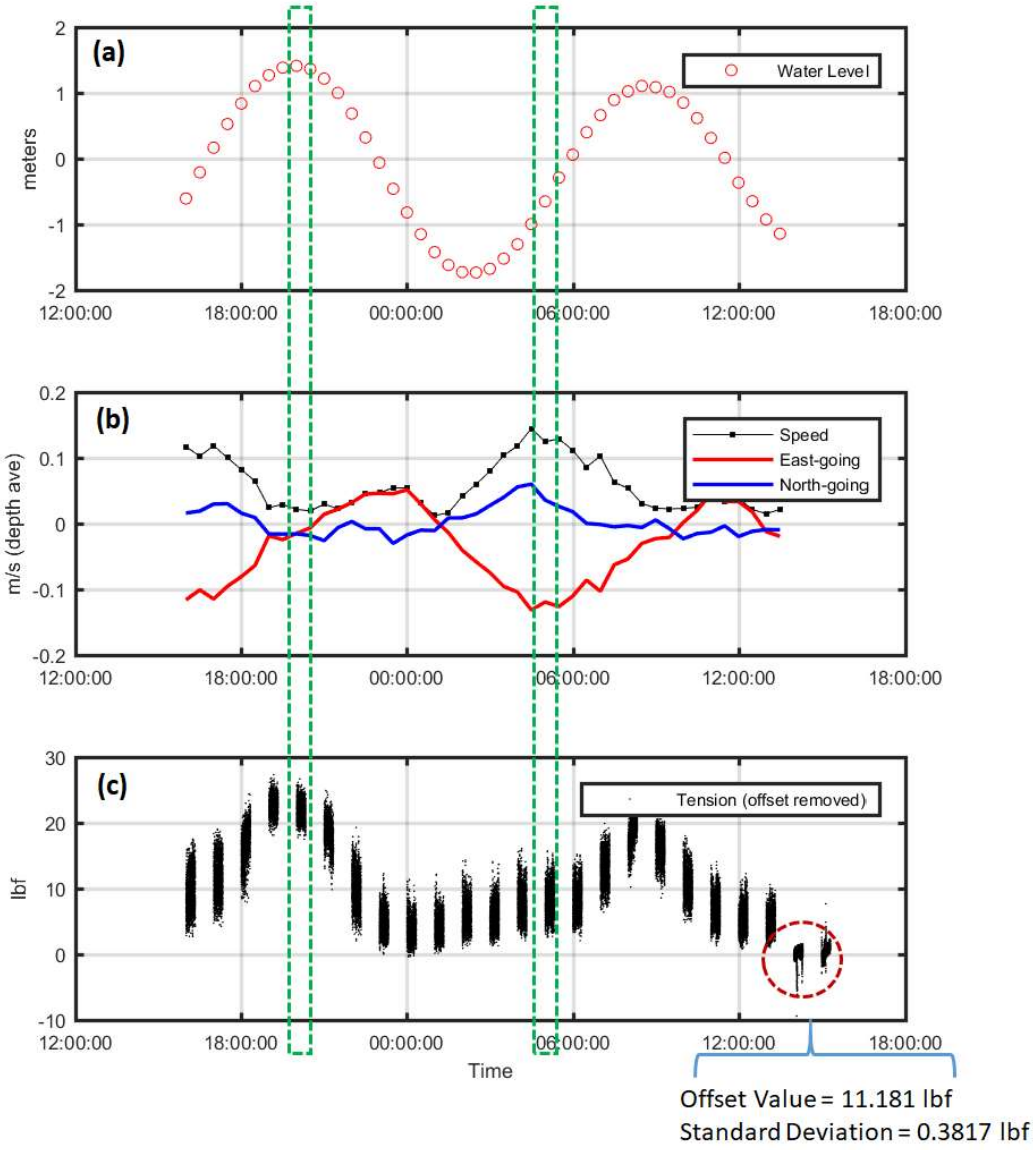

Figure 114: The water level, east- and north-going depth average velocities.

Two load-cases for this dataset were chosen for this dataset. The first load-case was chosen to be at the high-water mark. From Figure 114, the slack longline showed the highest tension of only 23 lbf. This is due to tensioning of the slack mooring with increasing water level pulling the surface buoy down. The second load-case was chosen to be near the mid-water level when the east-going velocities were the highest at approximately 0.13 m/s. This dataset shows that with the slack (but fixed) mooring system, changes in float buoyancy are greater than drag induced when no macroalgae is present.

To create datasets for these specific load-cases, the AWAC data was process to determine the profiles. A contour plot of the east-going velocities is shown on Figure 115(a) as a function of tidal elevation. The corresponding profiles for the high- and mid-water load-cases are shown on Figure 115(b) and Figure 115(c).

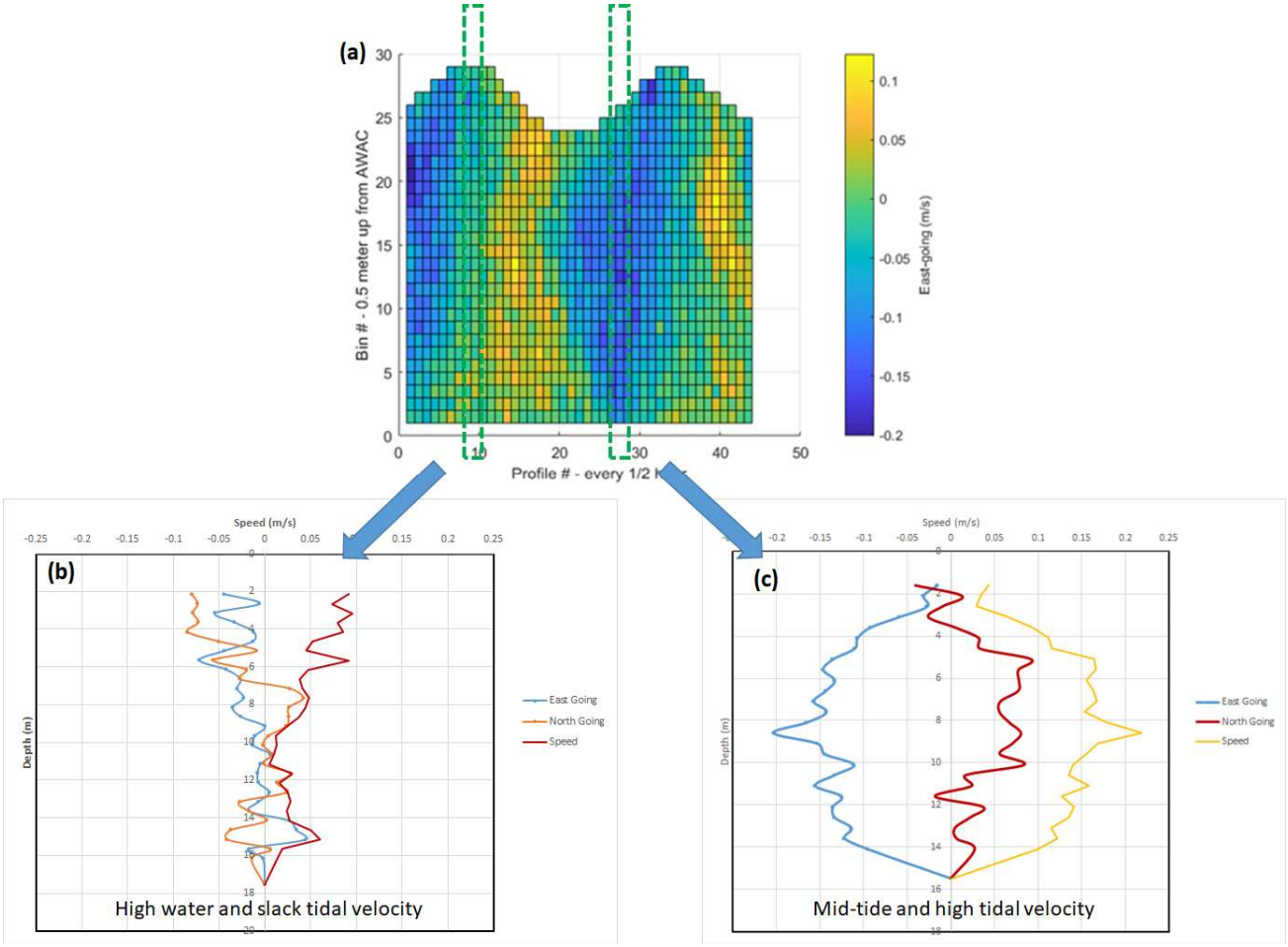

Figure 115: (a) The east-going profile data set. (b) Profile data set for the high water, slack tidal velocity condition. (c) Profile data for the mid-tide, high tidal velocity condition.

The acoustic surface track data sets from the AWAC were also downloaded and shown on Figure 116 (a) showing the influence of the waves (high frequency) and tides (low frequency). The green boxes on the Figure indicate the corresponding load-case for the high- and mid-water conditions. The corresponding pressure time-series for the two load-cases are shown on Figure 116 (b)

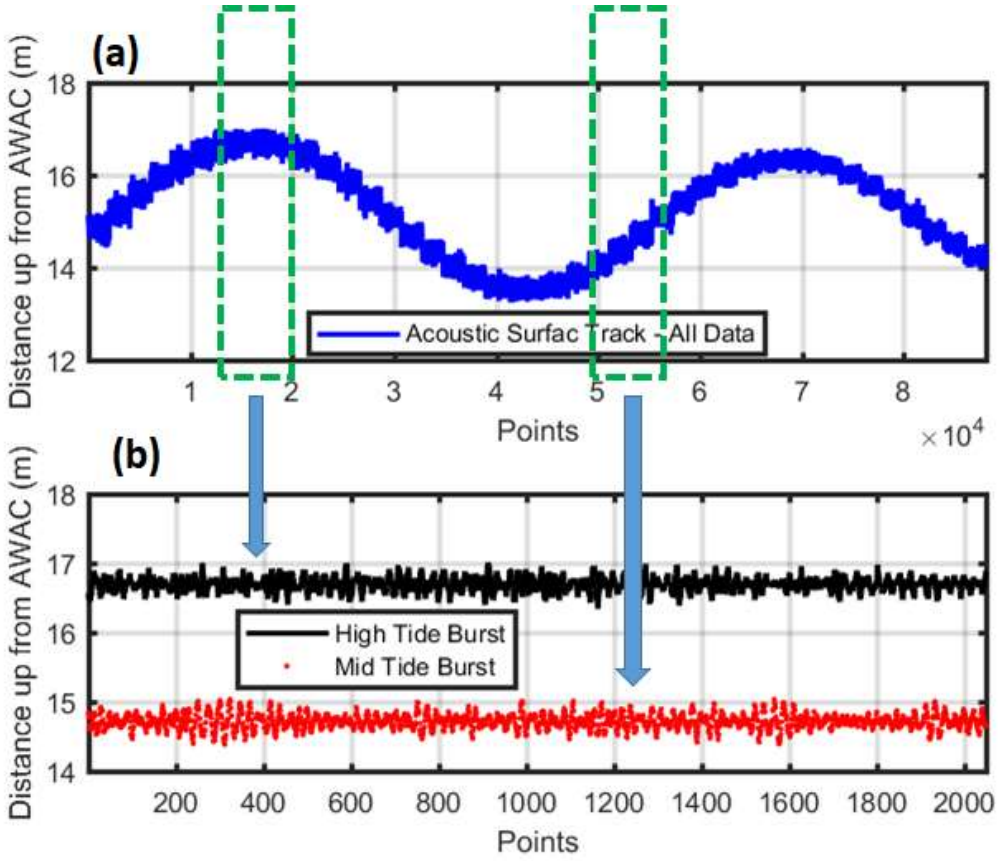

Figure 116: (a) The overall acoustic surface track data sets from the AWAC deployment showing the high (waves) and low frequency (tides) components. (b) The specific bursts for the two load-cases.

Software provided by Nortek enables processing of the wave burst data into the H_s (significant wave height), H_{m0} (zeroth moment wave height), H_{max} (maximum height), T_p (peak period) and wave direction. The results are provided in Table 20 with the details for the two load-cases highlighted with green. The specific time-series for the load-cases are shown on Figure 117.

Table 20: Wave Statistics for LPA deployment October 30-31, 2018.

		Date Time	H_s (m)	H_{m0} (m)	H_{max} (m)	T_p (s)	Wave Dir. (degT)
1	1a	30-Oct-2018 16:03:01	0.4200	0.4700	0.6900	12.9600	66.20
2	1b	30-Oct-2018 16:33:01	0.4400	0.4800	0.6800	8.7600	78.20
3	2a	30-Oct-2018 17:03:01	0.3800	0.4600	0.6800	11.4800	56.97
4	2b	30-Oct-2018 17:33:01	0.3700	0.4200	0.6500	8.0200	86.32
5	3a	30-Oct-2018 18:03:01	0.4300	0.5000	0.8200	11.4400	88.83
6	3b	30-Oct-2018 18:33:01	0.3600	0.4500	0.7100	8.4100	93.52
7	4a	30-Oct-2018 19:03:01	0.3900	0.4500	0.7400	8.4200	90.85
8	4b	30-Oct-2018 19:33:01	0.3200	0.3900	0.6500	11.3300	71.59
9	5a	30-Oct-2018 20:03:01	0.3800	0.4400	0.6100	11.5800	70.83
10	5b	30-Oct-2018 20:33:01	0.3300	0.3800	0.6700	11.3800	63.45
11	6a	30-Oct-2018 21:03:01	0.3800	0.4400	0.7100	11.5000	74.27
12	6b	30-Oct-2018 21:33:01	0.3500	0.4100	0.6200	11.7700	66.82
13	7a	30-Oct-2018 22:03:01	0.3300	0.4000	0.8300	11.3500	82.07
14	7b	30-Oct-2018 22:33:01	0.3500	0.4200	0.7300	11.6100	75.06
15	8a	30-Oct-2018 23:03:01	0.3500	0.4000	0.6600	10.5400	68.84
16	8b	30-Oct-2018 23:33:01	0.3500	0.4100	0.5400	11.4400	76.77
17	9a	31-Oct-2018 00:03:01	0.3600	0.4200	0.6000	10.8500	72.09
18	9b	31-Oct-2018 00:33:01	0.4100	0.4400	0.7300	11.4700	70.61
19	10a	31-Oct-2018 01:03:01	0.3900	0.4100	0.5800	10.6700	80.24
20	10b	31-Oct-2018 01:33:01	0.4000	0.4100	0.7000	11.2900	77.65
21	11a	31-Oct-2018 02:03:01	0.3700	0.3900	0.5500	11.4200	66.43
22	11b	31-Oct-2018 02:33:01	0.3600	0.3800	0.5300	11.0700	84.05
23	12a	31-Oct-2018 03:03:01	0.3900	0.4200	0.6300	11.2900	67.80
24	12b	31-Oct-2018 03:33:01	0.3800	0.4300	0.6200	11.2300	74.75
25	13a	1-Oct-2018 04:03:01	0.3800	0.4100	0.6600	11.2400	78.65
26	13b	31-Oct-2018 04:33:01	0.4000	0.4300	0.6200	11.0700	68.28
27	14a	31-Oct-2018 05:03:01	0.4100	0.4400	0.6400	11.5400	65.54
28	14b	31-Oct-2018 05:33:01	0.3500	0.3900	0.6600	11.4400	67.96
29	16a	31-Oct-2018 06:03:01	0.3400	0.3800	0.5300	11.4200	78.34
30	16b	31-Oct-2018 06:33:01	0.3000	0.3400	0.5100	11.1000	67.26
31	17a	31-Oct-2018 07:03:01	0.3300	0.3700	0.5100	11.4500	62.71
32	17b	31-Oct-2018 07:33:01	0.3100	0.3600	0.5200	11.6500	74.64
33	18a	31-Oct-2018 08:03:01	0.3100	0.3500	0.5500	11.2500	75.95
34	18b	31-Oct-2018 08:33:01	0.2800	0.3200	0.4600	11.3300	58.83
35	19a	31-Oct-2018 09:03:01	0.3100	0.3400	0.5500	11.5100	73.37
36	19b	31-Oct-2018 09:33:01	0.2700	0.3000	0.4400	11.3700	75.36
37	20a	31-Oct-2018 10:03:01	0.2900	0.3100	0.4500	11.5000	73.81
38	20b	31-Oct-2018 10:33:01	0.3000	0.3200	0.4700	11.1300	81.09
39	21a	31-Oct-2018 11:03:01	0.3300	0.3500	0.4500	11.3600	76.93
40	21b	31-Oct-2018 11:33:01	0.3800	0.3900	0.6800	11.1700	84.27
41	22a	31-Oct-2018 12:03:01	0.3600	0.3800	0.5700	10.9200	77.81
42	22b	31-Oct-2018 12:33:01	0.3400	0.3600	0.5200	10.9700	78.20
43	23a	31-Oct-2018 13:03:01	0.3100	0.3300	0.5000	11.0900	80.63

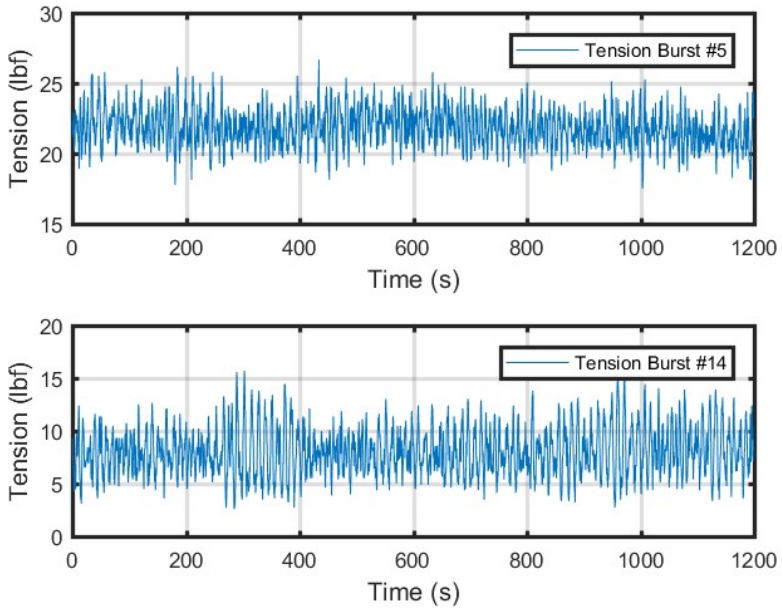

Figure 117: Detailed tension data from the high- and mid-water datasets (burst #5 and #14).

Load cases were also considered from the April 11-17, 2019 datasets from the Wood Island site. The datasets on Figure 118 show the current velocities from each AWAC bin for both the east and west instruments. On the Figure, the north-going (V2) component is plotted as a function of the east-going (V1) component showing the nature of the tidal currents. Results from the two ADCPs were then averaged to best estimate the velocities acting on the farm. Velocity measurements were then vector-averaged over the portion of the water column nominally occupied by the biomass, that is, over the range between $z_{minimun}(t) = h(t) - 3m$ and $z_{maximum}(t) = h(t) - 1m$. Here z is the distance from the seafloor, h is the depth, which depends on tidal elevation. Time, t, is the start time for each measurement burst.

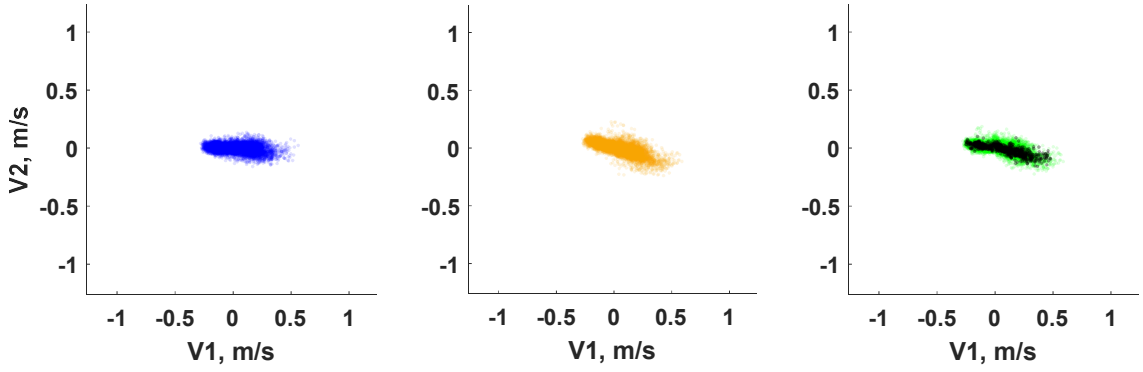

Figure 118: Current speeds shown as east-going (V1) and north-going (V2) components at the Wood Island site. Blue, yellow, and green dots show results for individual bins measured by the east ADCP, the west ADCP, and the average of the two ADCPs, respectively. Black dots are the velocity measurements vector-averaged over the portion of the water column nominally occupied by the biomass.

The vertically-average current velocity samples were then sorted into 36 directional bins and 9 speed bins. The resulting "current rose" is shown in Figure 119.

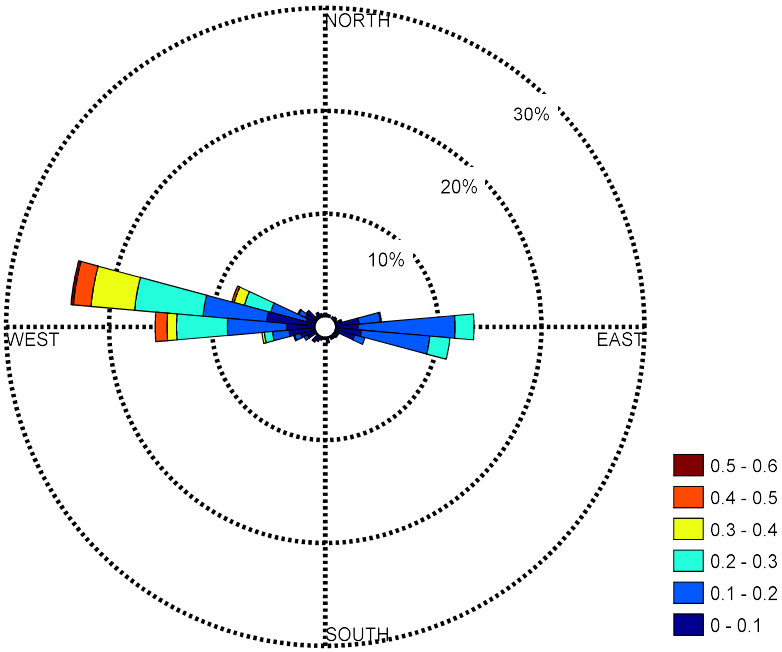

Figure 119: Current rose for Wood Island site using measurements from validation campaign. Angle indicates the direction current is coming *from*, relative to true north.

At the time, it was decided to preserve the integrity of the validation effort, the tension dataset was normalized by the maximum value. Thus, the data shown in Figure 120 is dimensionless. The load cells were configured to sample in 30 minute "bursts" every hour during the deployment. For each of these bursts, the results were distilled into the mean and the variance, σ^2 (standard deviation squared). These results, along with the environmental forcing data, are shown in Figure 120. Figure 121 shows the dataset with a focus on April 13, 2019.

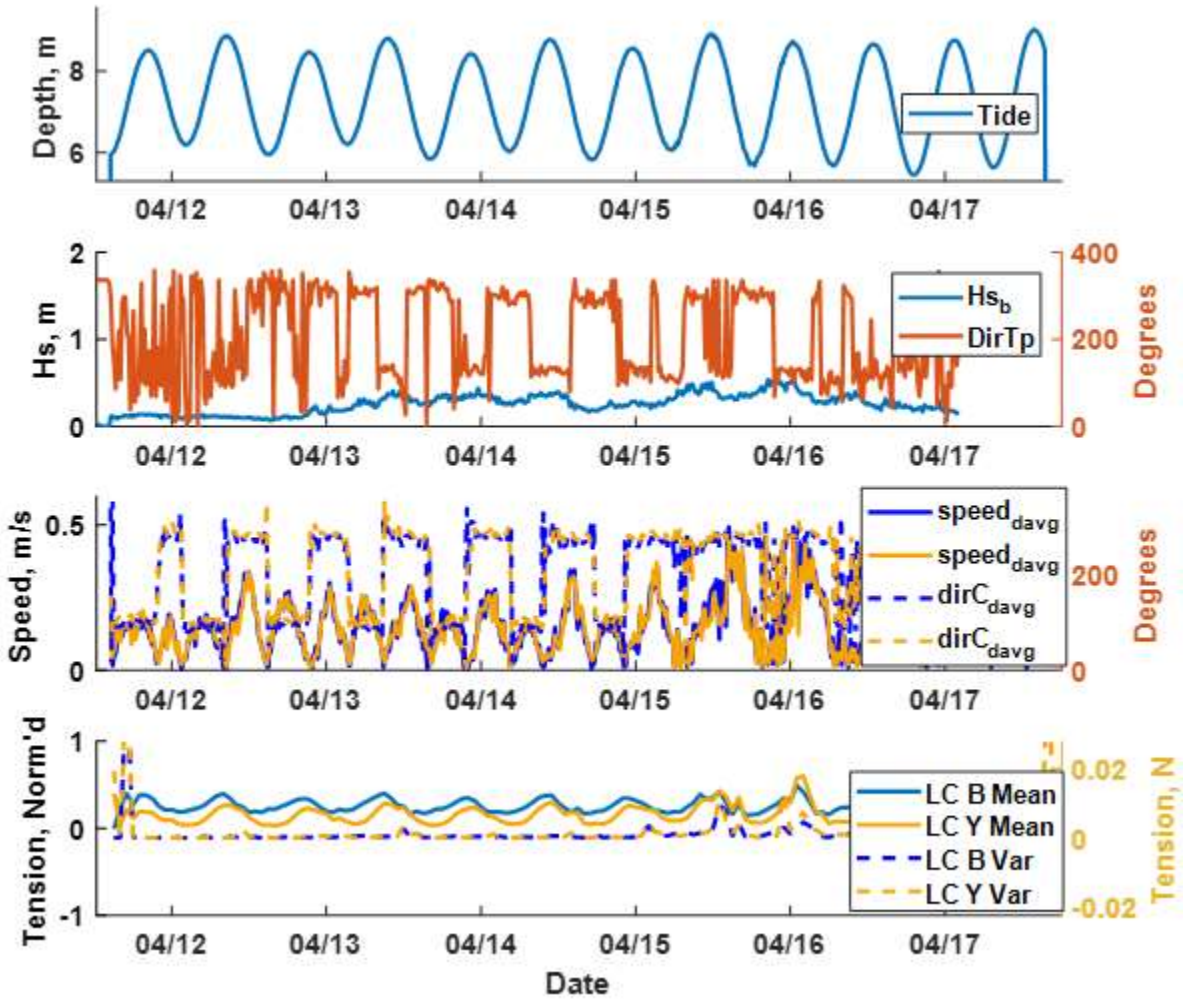

Figure 120: Water depth, significant wave height and direction, vertically-averaged current speed and direction, and mean and variance of measure tensions from each load cell at the Wood Island site. Results from instruments on the eastern end of the farm are in blue; results from the western end are in yellow.

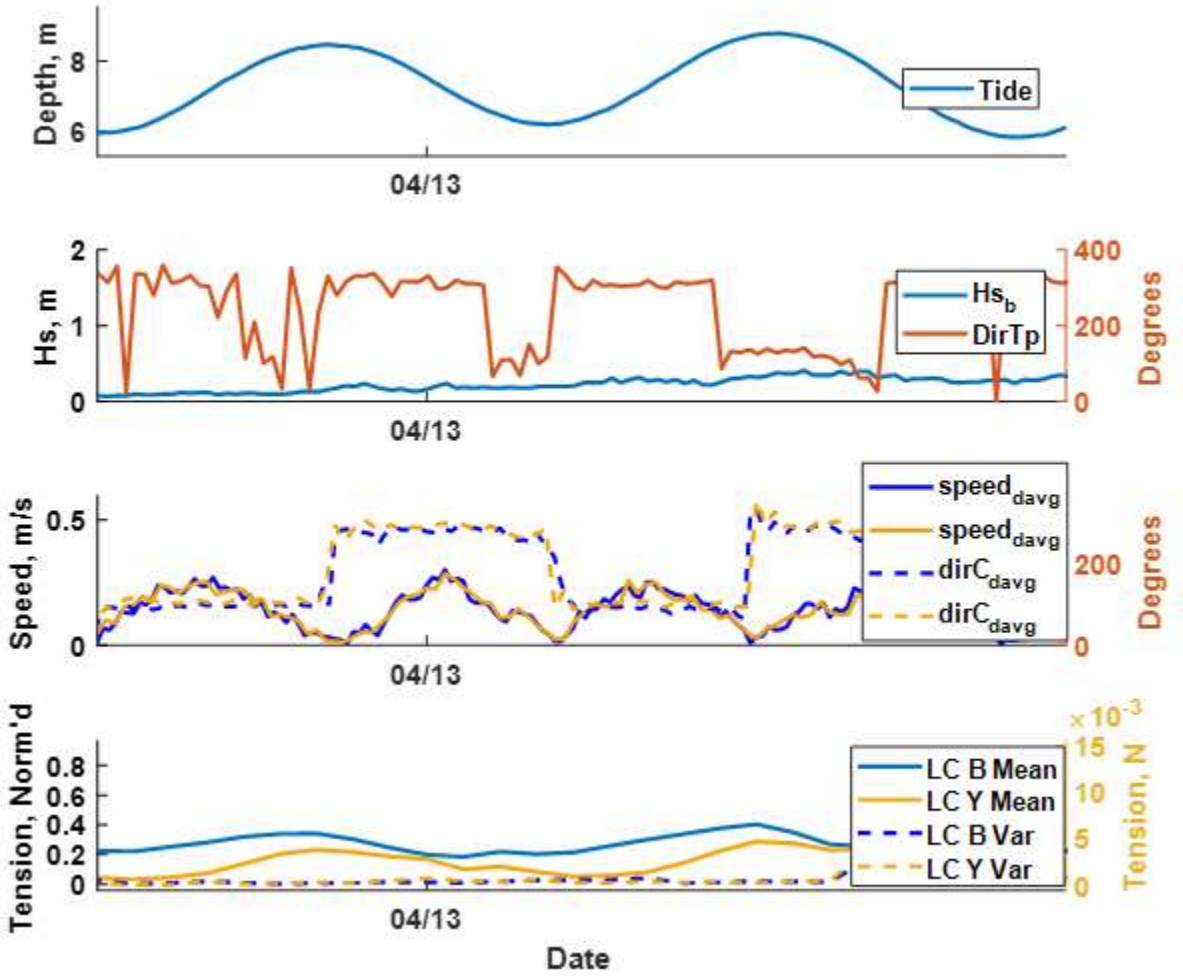

Figure 121: Water depth, significant wave height and direction, vertically averaged current speed and direction, and mean and variance of measure tensions from each load cell at the Wood Island site for a full tidal cycle. Results from instruments on the eastern end of the farm are in blue; results from the western end are in yellow.

To enable the comparison of data across multiple instruments, meta statistics (e.g. time-average velocity, variance in tension) from each burst for each instrument were linearly interpolated onto a common time vector. This time vector spanned the time range during which all instruments were sampling and had a time step of 1 hour. The Wood Island datasets were examined for load-cases with five potential options from low to high tide over a range of current velocities as shown on Figure 122 and Table 21 .

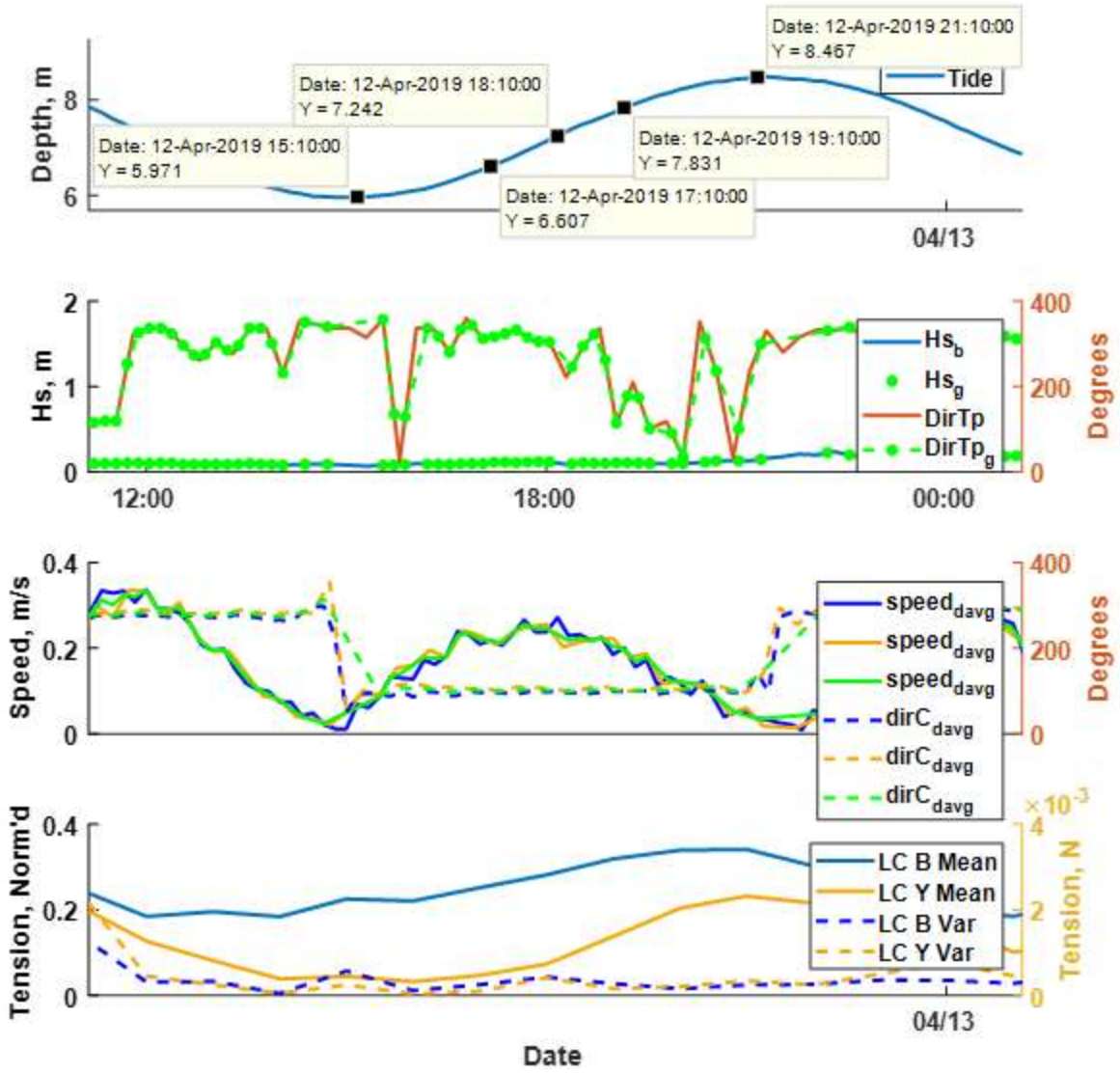

Figure 122: Selected validation cases for 2019 Wood Island Deployment.

Table 21: Selected validation cases for 2019 Wood Island Deployment.

	Current		Waves		Tide
Date	Cur. Speed (m/s)	Cur. Dir (deg.)	Hs (m)	Tp (s)	Depth (m)
4/12/2019 14:10	0.06	272	0.09	9.54	6.1
4/12/2019 16:10	0.18	105	0.09	-9.00	6.1
4/12/2019 17:10	0.22	100	0.11	8.13	6.6
4/12/2019 19:10	0.20	100	0.11	8.84	7.8
4/12/2019 21:10	0.03	134	0.15	3.43	8.5

An assessment was also made to identify load cases from the Ram Island dataset obtained from April 24–May 1, 2019. The current velocities from each AWAC bin for both the east (blue) and west (yellow) AWACs are shown on Figure 123 with the north-going component (V2) plotted as a function of (V1) characterizing the tidal velocities. Results from the two AWACs were averaged to best estimate the velocities acting on the farm (green). The velocity measurements were vector-averaged over the portion of the water column nominally occupied by the biomass. The biomass was estimated to be over the range between $z_{minimun}(t) = h(t) - 3m$ and $z_{maximum}(t) = h(t) - 1m$. As with the Wood Island dataset, z is the distance from the seafloor, *h* is the depth, which depends on tidal elevation. Time, *t*, is the start time for each measurement burst. The vertically-average current velocity samples were sorted into 36 directional bins and 9 speed bins. The resulting "current rose" is shown in Figure 124.

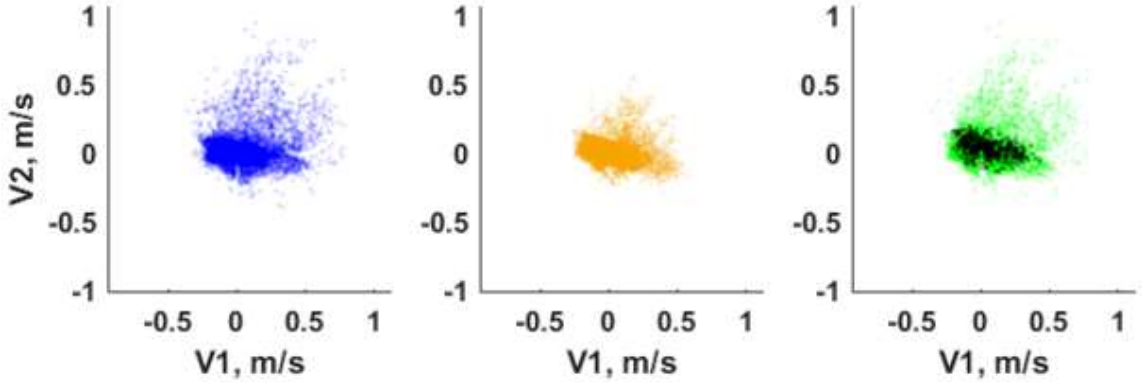

Figure 123: Measured current speeds shown as east-going (V1) and north-going (V2) components at the Ram Island site. Blue, yellow, and green dots show results for individual bins measured by the eastern AWAC, the western AWAC, and the average of the two AWACs, respectively. Black dots are the velocity measurements vector-averaged over the portion of the water column nominally occupied by the biomass.

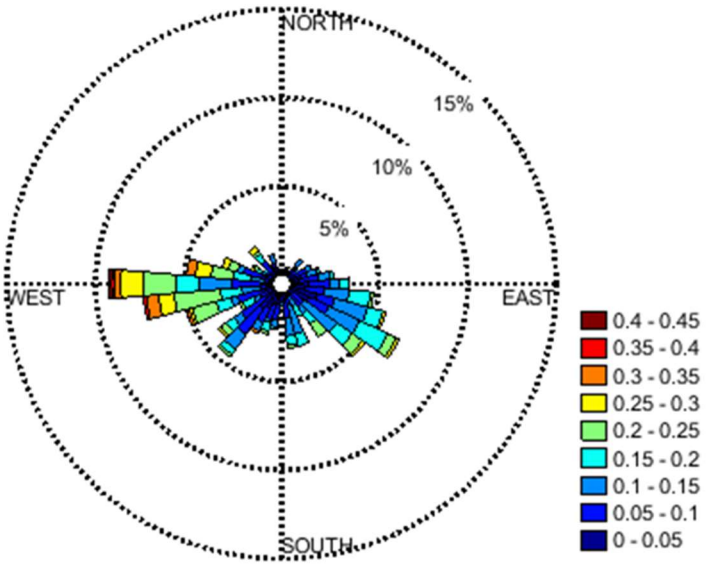

Figure 124: Current rose for Ram Island site using measurements from validation campaign. Angle indicates the direction current is coming *from*, relative to true north.

The load cell datasets were again normalized by the maximum value measured before the validation process to prevent bias. Thus, the data shown in Figure 125 is dimensionless. The load cells were configured to sample in 30 minute bursts every hour during the deployment. For each of these bursts, the results were distilled into the mean and the variance, σ^2. These results, along with the environmental forcing data, are shown in Figure 125. Figure 126 shows the same data but only for the storm observed on April 27. During this event, strong currents were observed coming from the WNW (onshore). As a result, the largest mean tensions were observed on the westward mooring leg (in yellow). Because the western mooring leg experienced higher mean tensions, the variance in tension was also much larger for the western mooring line than the eastern mooring line during this storm, even though the waves came steadily from the east.

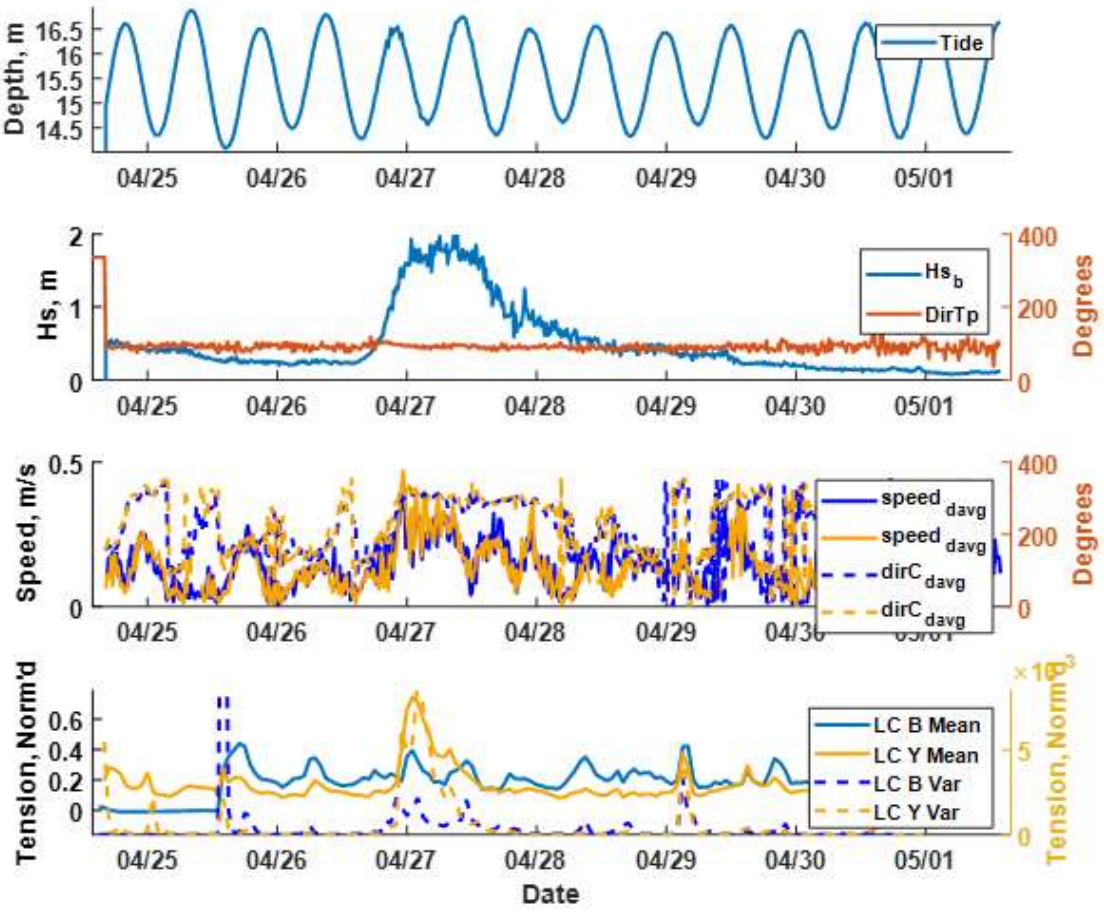

Figure 125: Water depth, significant wave height and direction, vertically-averaged current speed and direction, and mean and variance of measure tensions from each load cell at the Ram Island site. Results from instruments on the eastern end of the farm are in blue; results from the western end are in yellow.

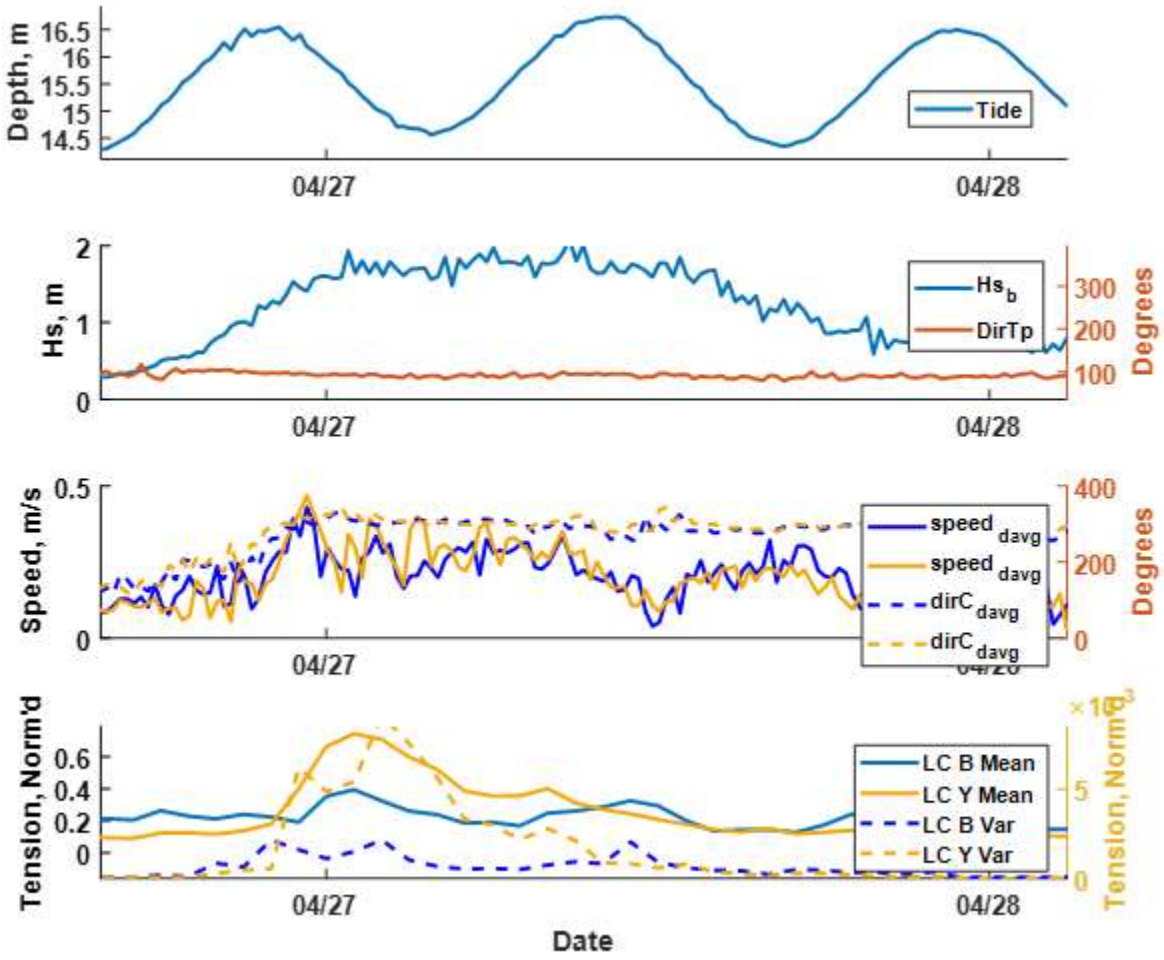

Figure 126: Water depth, significant wave height and direction, vertically-averaged current speed and direction, and mean and variance of measure tensions from each load cell at the Ram Island site during the April 27 storm. Results from instruments on the eastern end of the farm are in blue; results from the western end are in yellow.

To enable the comparison of data across multiple instruments, meta-statistics (e.g. time-average velocity, variance in tension) from each burst for each instrument were linearly interpolated onto a common time vector. This time vector spanned the time range during which all instruments were sampling and had a time step of 1 hour. This enabled comparison showing the effect of current speed on mooring tension under wide range of combinations of wave height, direction, and tidal elevation (Figure 127).

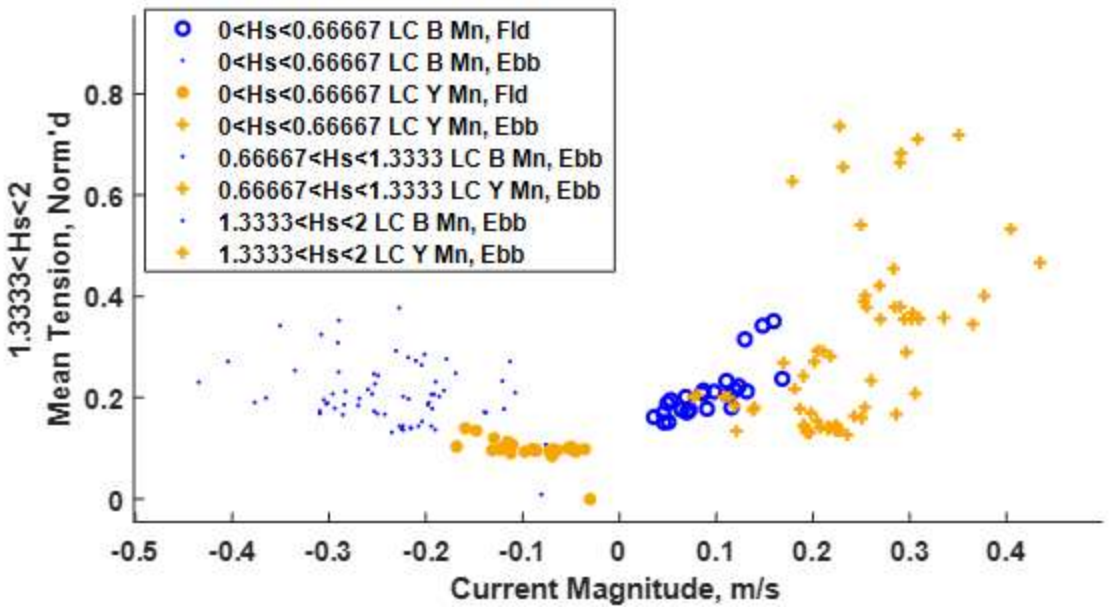

Figure 127: Mean tension as a function of current magnitude when current direction is within 20 degrees of nominal longline axis. Eastern load cell is in blue. Western load cell is in yellow.

The variance of mooring line tension versus significant wave height is shown in Figure 128. While the variance of tension is clearly associated with significant height, this figure demonstrates that it is not only proportional to wave height. Wave direction, current speed and direction, and tidal elevation all influence the dynamic response.

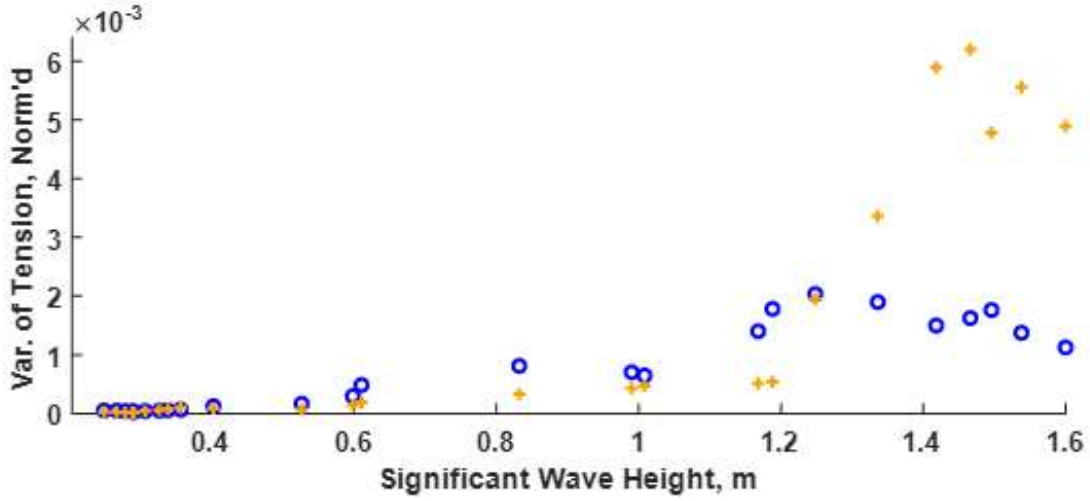

Figure 128: Variance of tension as a function of significant wave height during the April 27 storm (April 26, 2019 1500 to April 27, 2019 0000). Eastern load cell is in blue. Western load cell is in yellow.

After full review of the dataset from the Ram Island deployment, a final set of load cases were established. The five load cases were chosen considering a range of tidal elevations, currents speeds and directions and significant wave height values. Processing of the datasets assumed that the dominating forcing were considered as weak, stationary and ergodic processes during specific measured durations and spatially within the region of the deployed gear. Since variability is inherent in the oceanic environment, load case criteria were established to assess steady-state conditions. Current speed values from 15-18 and 30-33 minutes past each hour from the east and west AWACS were examined to have a less than 10% relative difference. A similar approach was applied with significant wave height values obtained during the second burst past the hour. The final selected load cases are shown in Figure 129 and with details in Table 22.

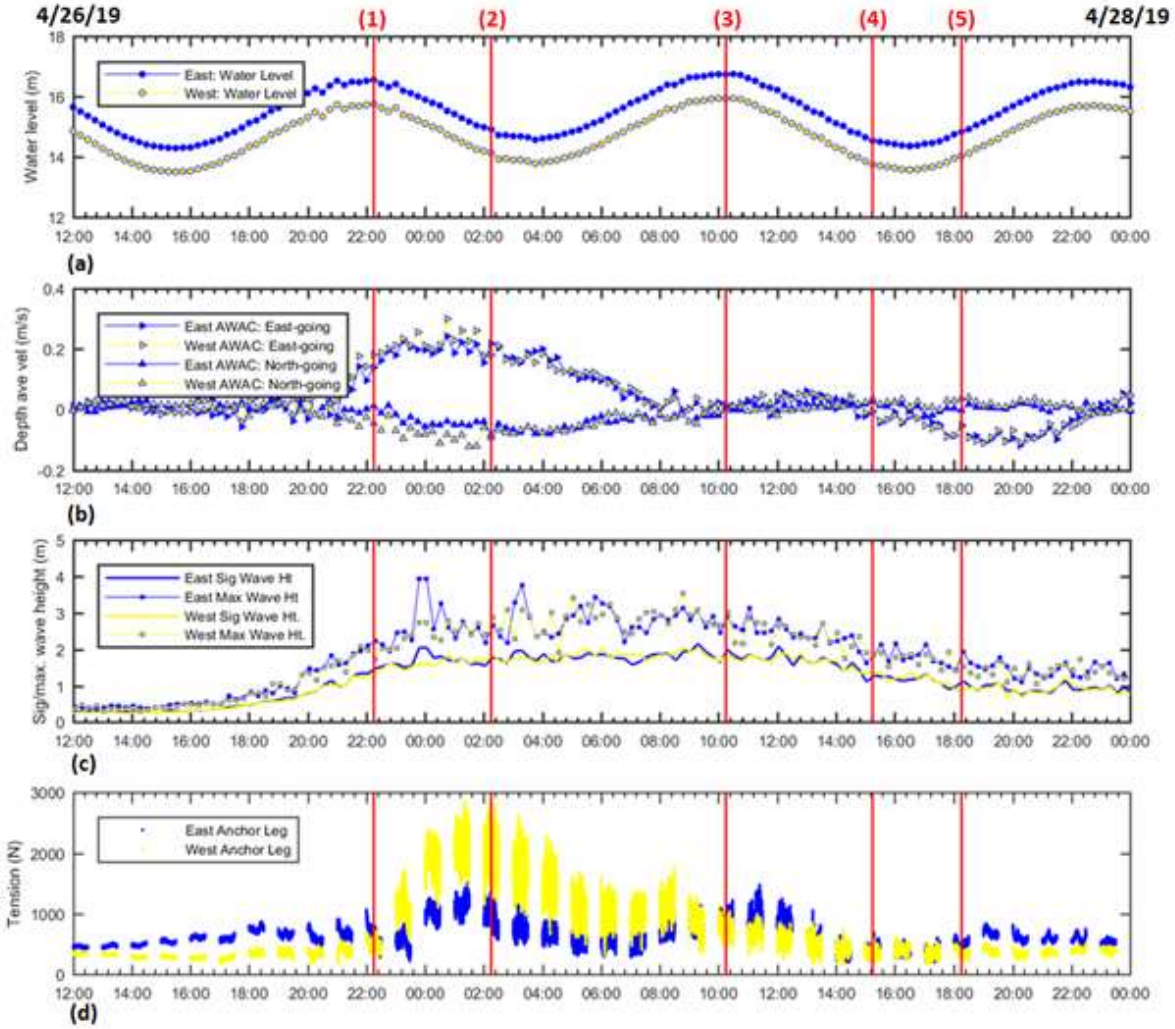

Figure 129: The five selected validation cases for 2019 Ram Island Deployment including surface elevation (a), depth average velocities (b), significant wave height (c) and mooring line tension (d).

Table 22: Selected validation cases for 2019 Ram Island Deployment.

	Date/Time	Current Speed (m/s)	Current Dir. (degT- coming from)	Hs (m)	Tp (s)	Dir (degT)	Tide Depth (m)
1	26-Apr-19; 2215	0.26	250	1.3	6.0	97	16.5
2	27-Apr-19; 0215	0.29	277	1.7	6.8	91	14.9
3	27-Apr-19; 1015	0.19	242	1.8	7.4	92	16.7
4	27-Apr-19; 1515	0.23	254	1.3	7.7	86	14.6
5	27-Apr-19; 1815	0.20	268	1.0	7.5	89	14.8

As discussed previously, the AWAC was configured to obtain an average velocity profile from 3 minutes of data every 15 minutes. The instrument was then setup to make an AST burst at 4 Hz directly following the profile measurement. The AST burst contained 2048 counts equal to 512 seconds of data (8 minutes, 32 seconds) in order to fit within the 15-minute cycle. Back-to-back profile measurements were used in the validation process to choose load cases for steady-state conditions on either side of the wave burst. While 512 seconds of surface wave data at 4 Hz is shorter than many wave sampling strategies, a 7 second wave, for example, can still occur 75 times within the burst. The sampling scheme for load case #2 is shown on Figure 130 for both the east and west side AWAC instruments. The Figure also shows the corresponding surface wave profiles.

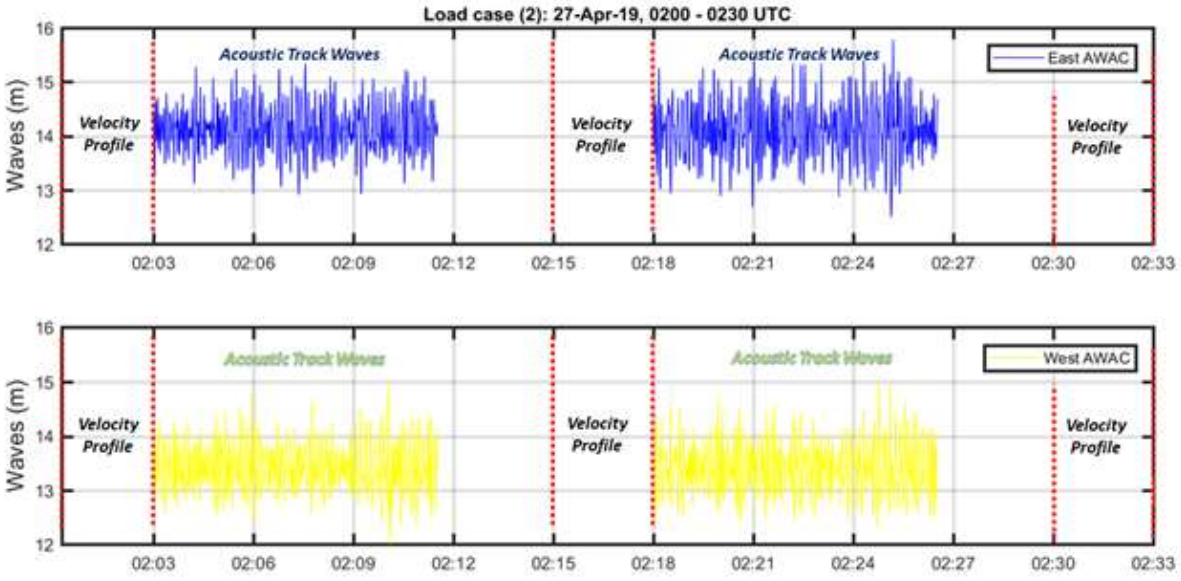

Figure 130: AWAC measurement details for load case #2 showing how the velocity profiles were configured before and after the wave bursts.

For each of the load cases, current velocity profile input was taken as an average between each depth bin point. The profile resolution for each velocity dataset was 0.5 m from the near surface to a point 1.4 m up off the bottom. Both east- and north-going components were averaged in this manner to maintain the distinct direction at each bin. For load case #2, the time average of each depth bin were taken from the 0215-0218 and 0230-0233 profiles and used at input to the Hydro-FE model. The east- and north-going profile for each time set are shown on Figure 131 (a) and (b) with the speed on (c) for the west side AWAC. These profiles show a positive east-going

and negative north-going direction in the top portion of the water column. It is important to note the bin locations are relative to a changing water level associated with the tides. This representation was taken since the relative location of the kelp grow line in the water column was also changing with the water level being located between a depth of 2 to 4 m. Since the tide was decreasing, there were less profile points in the 0230-0233 measurement. Comparison of both profile component at each measurement time, show little change indicating that the current speeds and direction were mostly constant on either side of the wave burst.

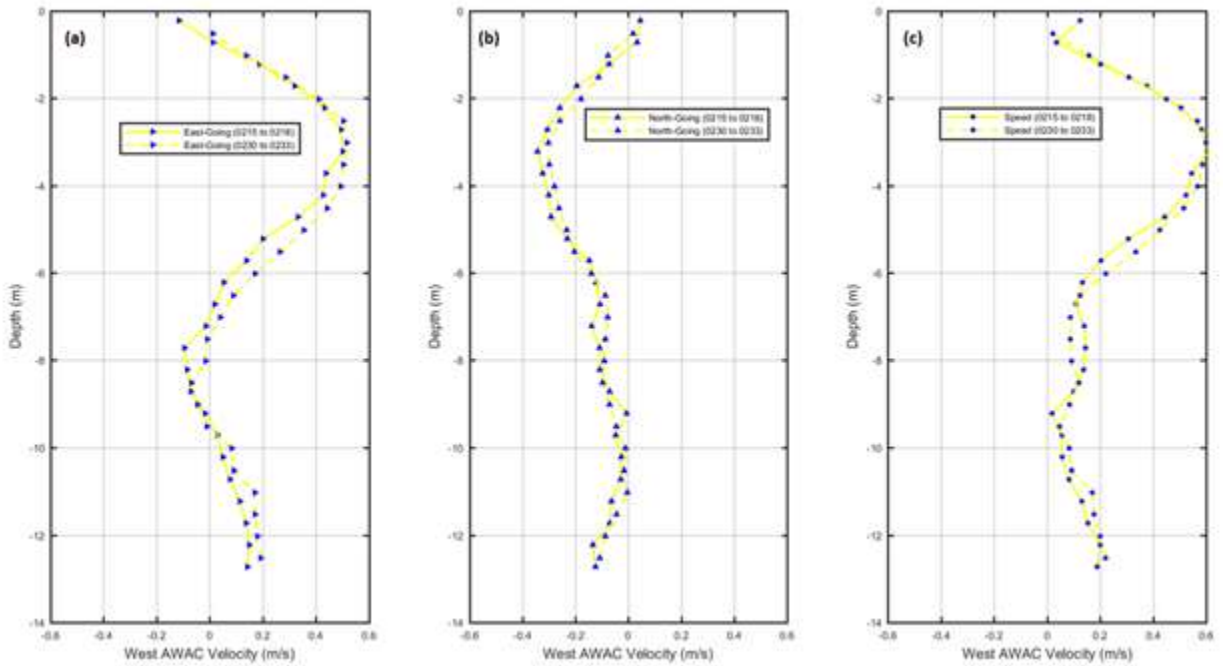

Figure 131: (a) The east-going AWAC profile for load case #2 from 0215-0218 and 0230-0233. (b) The north-going AWAC profile for load case #2 from 0215-0218 and 0230-0233. (c) The speed AWAC profile for load case #2 from 0215-0218 and 0230-0233.

Wave dataset for load case #2 was taken from the east AWAC since the prevailing direction was from the east. The dataset is a wave burst for 8 minutes and 32 seconds starting at 0218 UTC following the 0215-0218 and before the 0230-0233 profile measurements. The AST information for this load case is shown on Figure 130. The spectral representation is shown on Figure 132 with an H_{m0} of 1.87 m and a T_p = 7.14 seconds and a frequency resolution of 0.01 Hz.

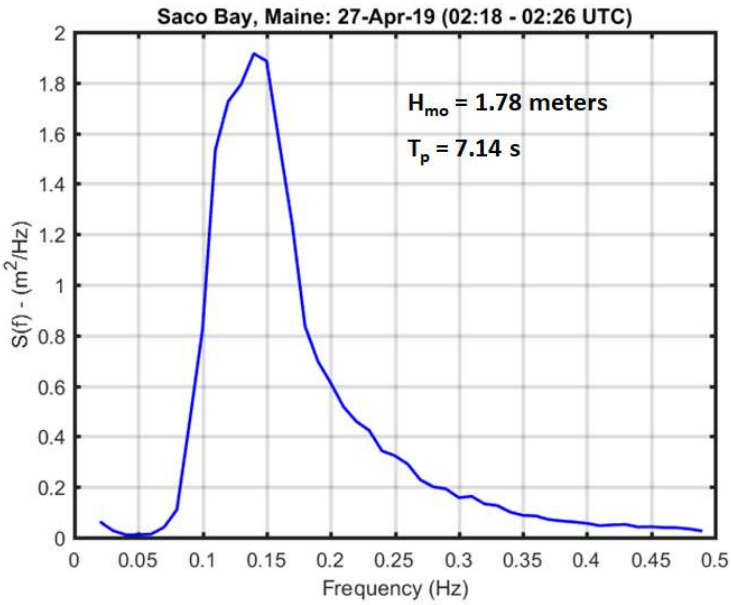

Figure 132: The wave spectral characteristics from the east AWAC used for load case #2.

In addition to the AWAC information, datasets from the load cells on each of the east and west anchor legs were also obtained for the Ram Island validation using the five load cases. The results for load case #2 are shown on Figure 133. As previously described, both load cells were configured to measure 30 minute bursts at 4 Hz each hour. This coincides with the two current profiles and wave burst measurements. The measurement strategy allowed for the option of obtaining two load cases each hour without having to run the load cells continuously. The mooring tension details for load case #2 taken from 0215-0230 to coincide with the AWAC profile and wave burst measurement scheme are also provided in Figure 133.

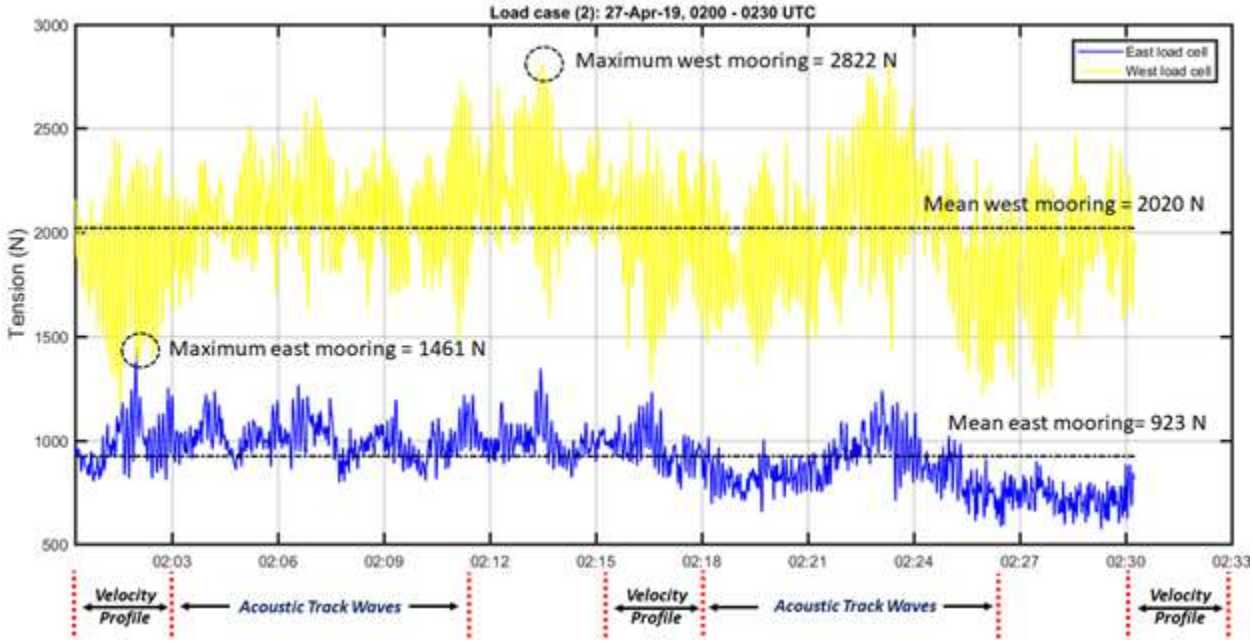

Figure 133: The east and west load cell measurements obtain for load case #2.

The third potential validation dataset was obtained at the Wood Island site from May 16-29, 2019. The datasets were processed in a similar manner to first examine the north- and east-going components as shown on Figure 134. In the Figure, the current velocities are provided from each AWAC bin for both the eastern (blue) and western (yellow) instruments with the components plotted with respect to each other. Results from the two ADCPs were averaged to best estimate the velocities acting on the farm (green). The datasets were then vector-averaged over the portion of the water column nominally occupied by the biomass, that is, over the range between $z_{minimum}(t) = h(t) - 3m$ and $z_{maximum}(t) = h(t) - 1m$. Once again, z is the distance from the seafloor and *h* is the depth, which depends on tidal elevation. Time, *t*, is the start time for each measurement burst. The vertically-averaged current velocity samples were sorted into 36 directional bins and 9 speed bins. The resulting "current rose" is shown in Figure 135.

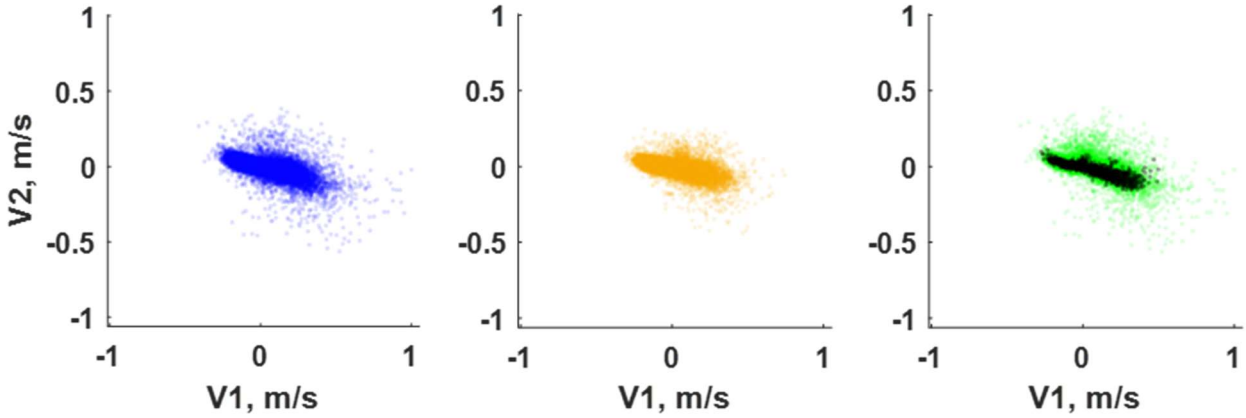

Figure 134. Measured current speeds shown as east-going (V1) and north-going (V2) components at the Wood Island site. Blue, yellow, and green dots show results for individual bins measured by the eastern ADCP, the western ADCP, and the average of the two ADCPs, respectively. Black dots are the velocity measurements vector-averaged over the portion of the water column nominally occupied by the biomass.

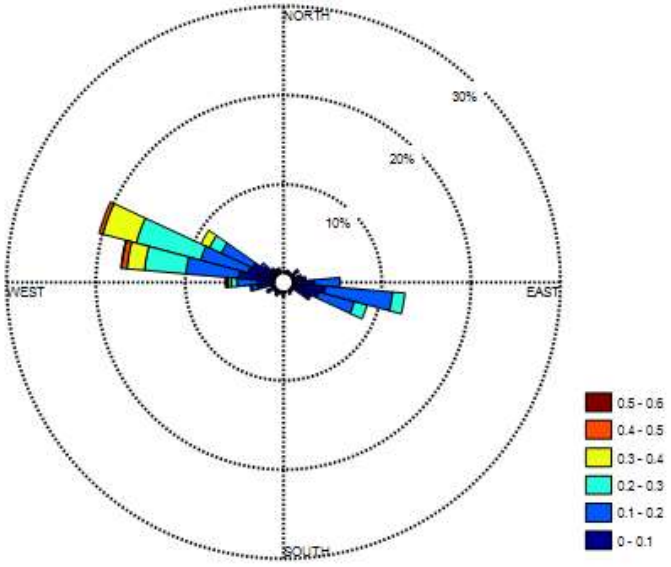

Figure 135. Current rose for Wood Island site using measurements from validation campaign. Angle indicates the direction current is coming *from*, relative to true north.

The load cell datasets were normalized by the maximum value measured in an effort to preserve the integrity of the blind validation experiment. Thus, the tension data shown in Figure 136 are dimensionless. The load cells were configured to sample in 30-minute bursts every hour during the deployment. For each of these bursts, the results were distilled into the mean and the variance, σ^2. These results, along with the environmental forcing data, are shown in Figure 137.

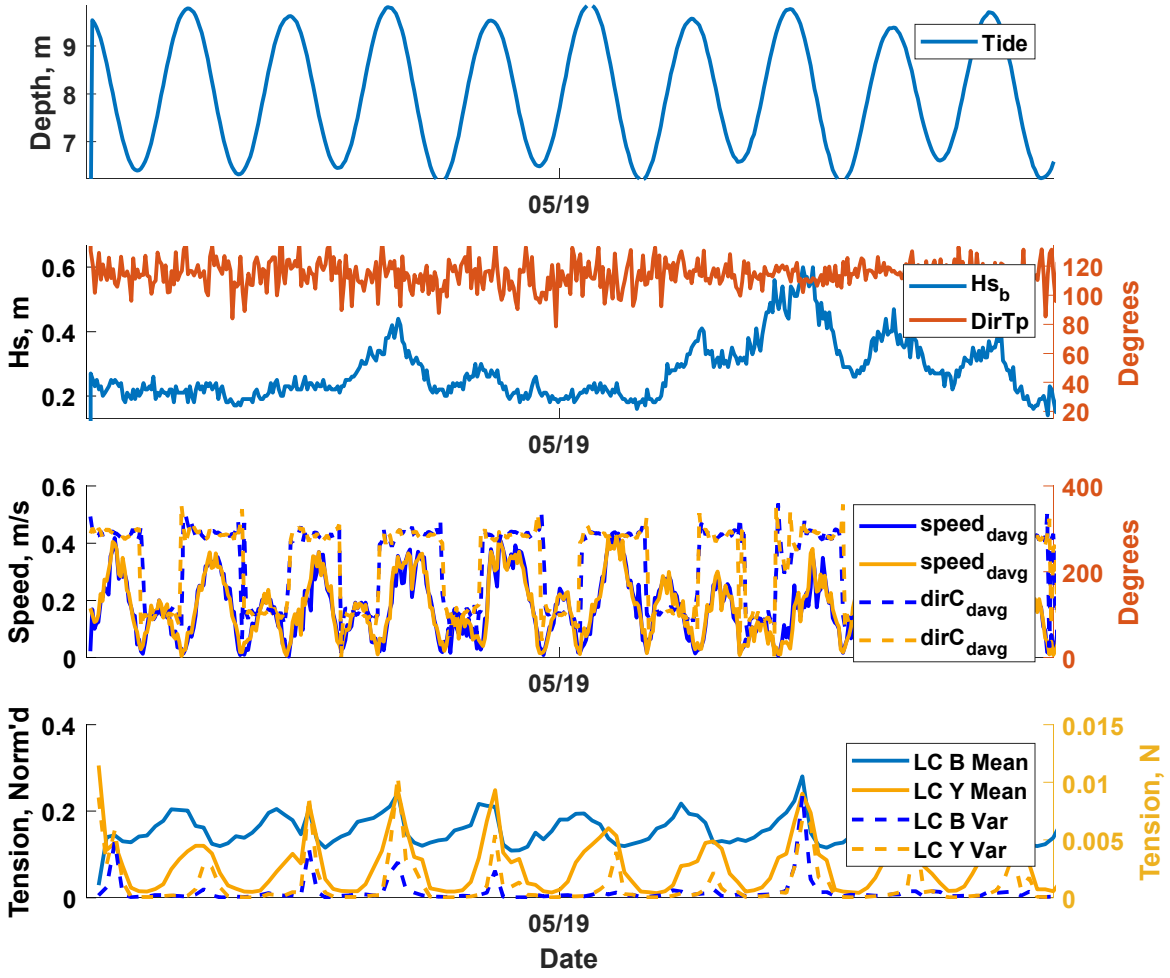

Figure 136: Water depth, significant wave height and direction, vertically averaged current speed and direction, and mean and variance of measure tensions from each load cell at the Wood Island site. Results from instruments on the eastern end of the farm are in blue; results from the western end are in yellow.

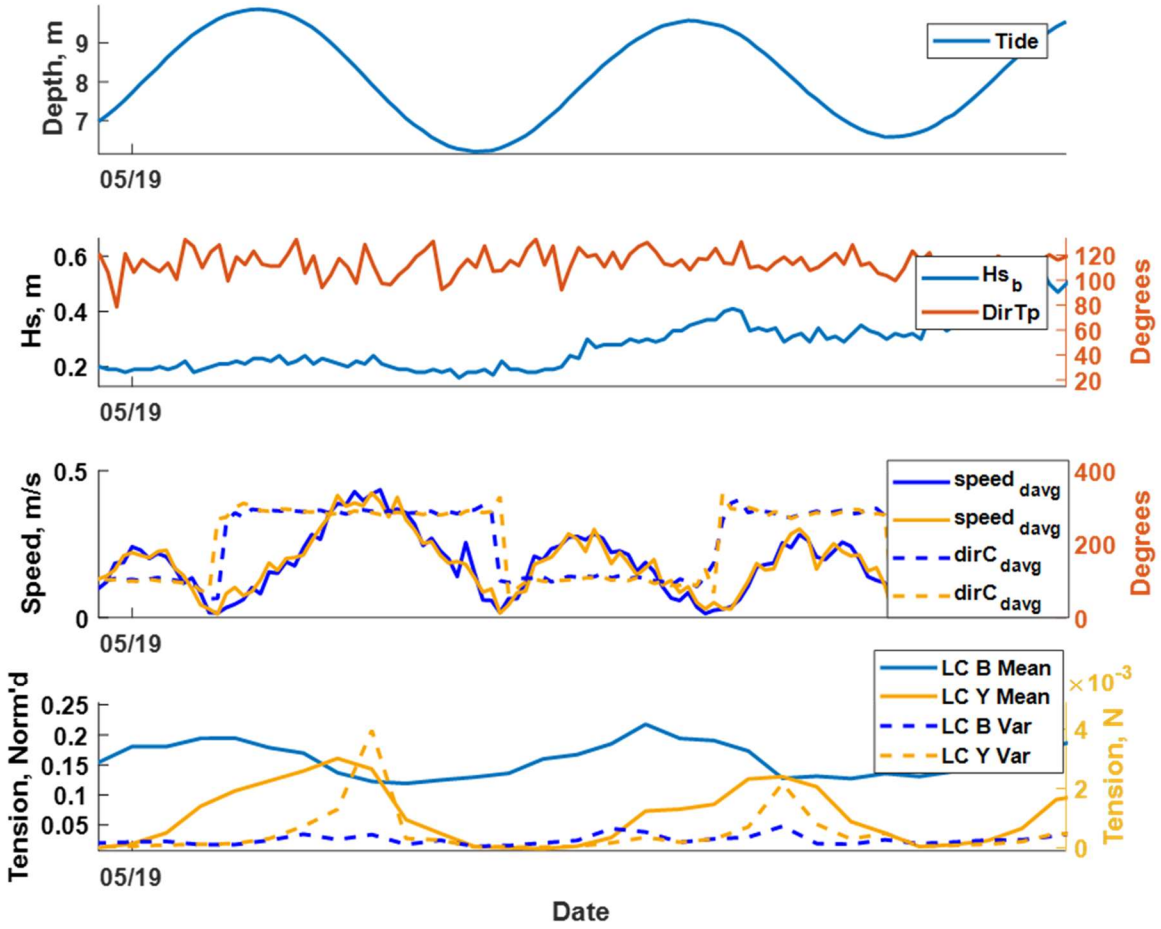

Figure 137: Water depth, significant wave height and direction, vertically averaged current speed and direction, and mean and variance of measure tensions from each load cell at the Wood Island site for a full tidal cycle. Results from instruments on the eastern end of the farm are in blue; results from the western end are in yellow.

To enable the comparison of data across multiple instruments, meta-statistics (e.g. time-average velocity, variance in tension) from each burst for each instrument were linearly interpolated onto a common time vector. This time vector spanned the time range during which all instruments were sampling and had a time step of 1 hour. This enabled comparisons such as Figure 138, which shows the mean mooring line tension versus current speed in the flood direction (toward shore).

This figure shows an offset between the measured tensions in the east and west mooring legs even when the fluid forcing is near zero. The horizontal components of the measured force acting in equal and opposite directions must be close to equal when no external force is applied. Thus, the difference between east and west mooring line tensions at near-zero current speed indicate that the mooring is not symmetrical. Furthermore, Figure 138 shows almost no perceptible dependence on current speed. However, this is not because tension is independent of current speed. Rather, because of the relationship between tidal elevation and current speed in this

tidally driven site, the current speed is increasing while the tidal elevation is decreasing, and vice-versa. The fact that these two effects nearly cancel each other in this experiment cannot be generalized to all macroalgae farms. The relative influence of tidal elevation, speed, and other environmental forcing factors on mooring tension is a function of the farm geometry, surface buoyancy, line elasticity, mooring pretension, and other design factors. This highlights the need to incorporate the environmental conditions and design parameters when simulating systems in Hydro-FE and when designing macroalgae farms.

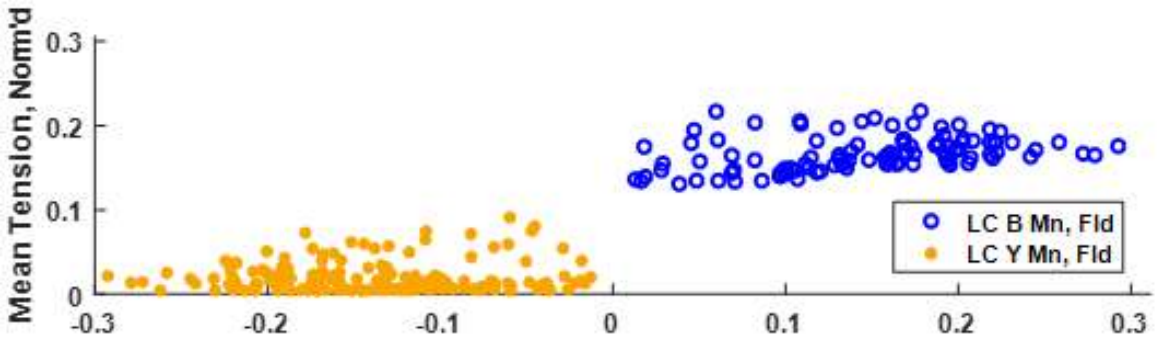

Figure 138: Mooring leg tension versus flood current speed. Eastern load cell is in blue. Western load cell is in yellow. Negative current speed corresponds to flow traveling west to east.

2.4.6. Task 4.6: Second instrumentation deployment (05/20/21)

With covid-19 restrictions in 2020, the five-line array was redeployed and seeded spring of 2021. As the kelp grew early in 2021, the four load cell systems were prepared for deployment on each of the mooring legs. Since the array system was deployed in a predominant east-west orientation, the anchor legs were designation with a color code like previous instrument locations described as the following.

- Northeast: blue
- Southeast: red
- Southwest: yellow
- Northwest: green

One of the initial preparation steps was to investigate the status of load cells by taking zero measurements. The zero measurements were done in a temperature stable room with the instruments sitting on the floor with the shackles removed from the threaded eye screwed into the pancake instrument. The instrument zero values for the blue, green, yellow and red load cells are shown on Figure 139. The AWACs were also configured for the same deployment scheme that proved suitable during the spring 2019 datasets.

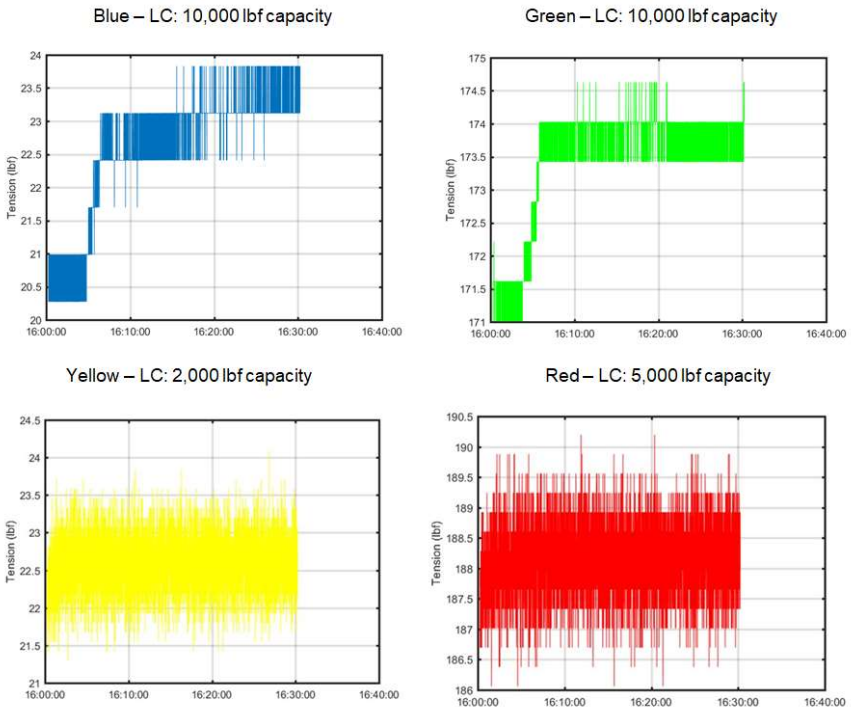

Figure 139: Zero values for each of the blue, green, yellow, and red load cells.

Once the load cell zero values were checked, the instruments were deployed from April 16-28, 2021 and then again from May 7-16, 2021 at the NE, SE, SW and NW locations shown on Figure 140. The Figure also shows the positions of the blue (east) and west (yellow) AWAC instruments. A summary of the AWAC dataset results is shown in Figure 141. The AWAC datasets include water elevation, depth-average currents, wave height statistics, and wave direction information from both the blue and yellow instruments. In addition to the AWACs, the load cell datasets from the NE, SE, SW and NW mooring legs are also provided. The datasets for the 07-May-21 to 16-May-21 are shown in Figure 142.

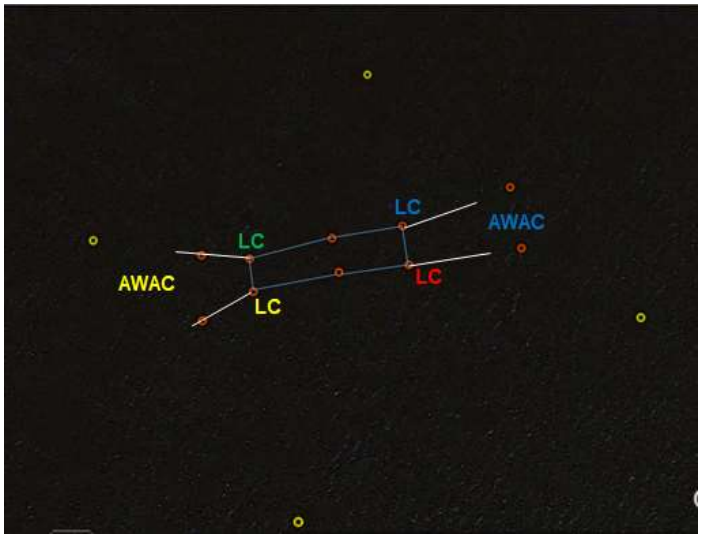

Figure 140: The locations of the blue (NE), red (SE), yellow (SW) and green (NW) load cells on the array system. The locations for the blue (east) and yellow (west) AWACs are also shown on the Figure.

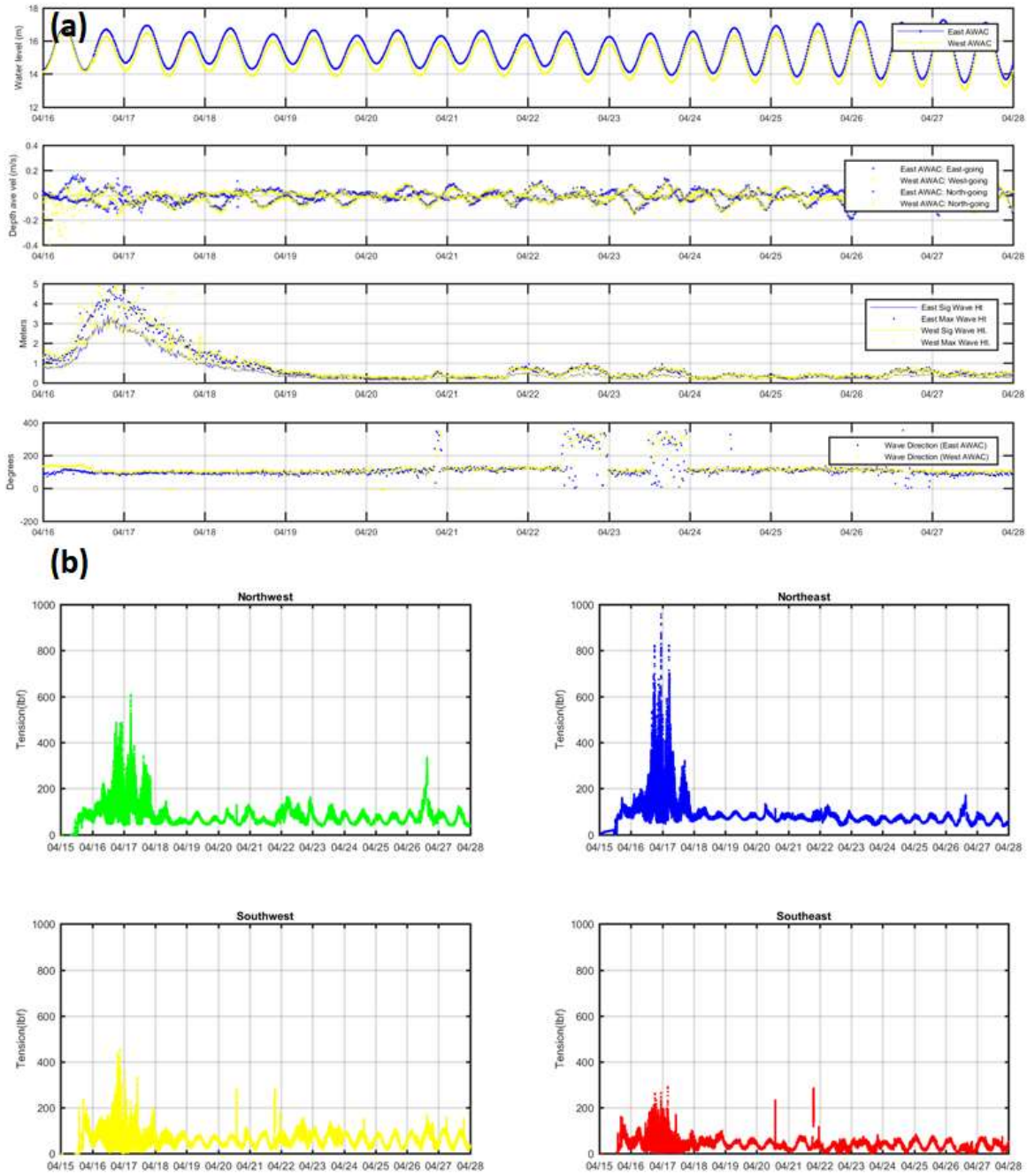

Figure 141: (a) The two AWAC dataset results and the (b) the four load cell dataset results for April 16-28, 2021.

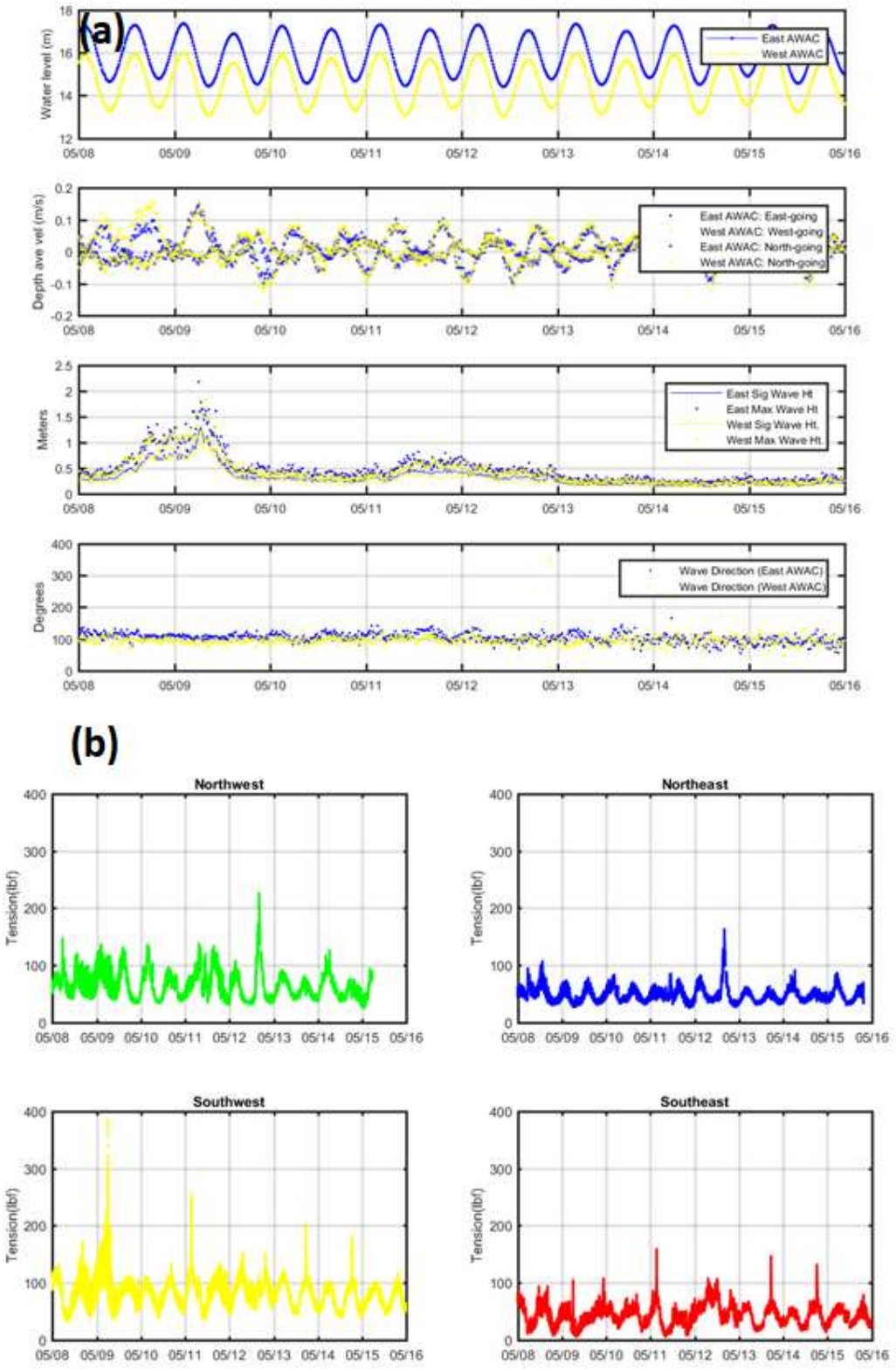

Figure 142: (a) The two AWAC dataset results and the (b) the four load cell dataset results for May 8-16, 2021.

2.4.7. Milestone 4.7: Second instrumentation recovery (5/20/2021)

Both AWAC instruments and all four load cell systems were recovered completing the instrumentation effort for the project. The yellow and blue AWACS are shown on Figure 143 after recovery.

Figure 143: The yellow and blue AWACs after recovery on May 20, 2021.

2.4.8. Task 4.8: Load case development for planar-type system (1/15/2022)

The first step in the development of load cases for model validation was to examine the most extreme event that occurred during the spring 2021 season. From examining Figure 141 and Figure 142, a subsample plot of the datasets was created for the timeframe between April 16-18, 2021. The datasets included water levels, depth average velocities, wave height characteristics and the four mooring leg load cells. The subsample dataset is shown on Figure 144. The highest load cell tension event was identified on April 16, 2021 between 2300 and 2303 UTC (see green box).

The datasets from the four load cells were then plotted for April 16, 2021 for the 4 Hz burst between 2300-2330 (Figure 145) associated with the green box shown on Figure 144. From examining the subsample dataset, the maximum tension value was identified to occur just after 23:00 UTC on April 16, 2021. The highest tension value occurred on the northeast load cell (blue) at a value of about 4250 N.

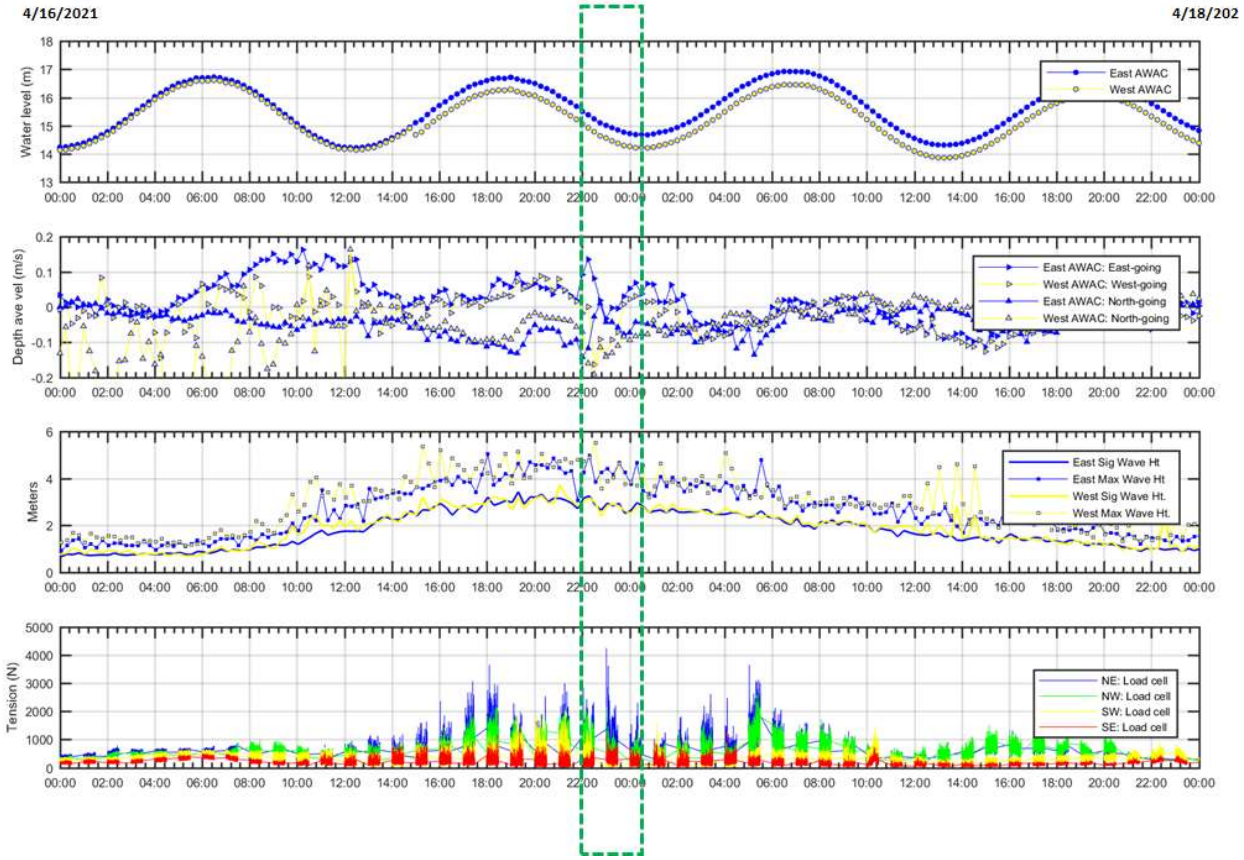

Figure 144: A subsampled dataset from April 16-18, 2021 that includes the maximum tension value from the four load cells.

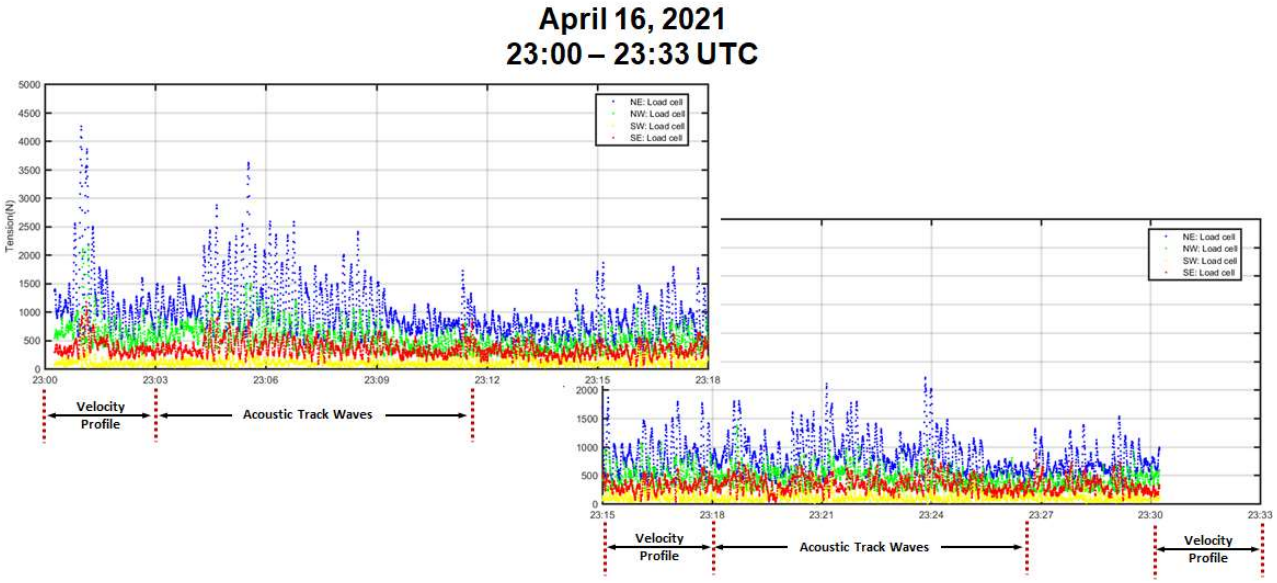

Figure 145: Load cell times series from the blue (northeast), red (southeast), yellow (southwest) and green (northwest) instruments.

Recall that each of the four load cells were set to collect data from for 30 minutes every hour. During that time, the east and west AWACs cycled from collecting velocity profiles at 2300-2303, 2315-2318 and 2330-2333 and waves at 2303-2311 and 2318-2326. From the dataset on Figure 145, the northeast load cell (blue) showed the highest tensions from 2300-2318. Datasets from the east and west AWACs were examined for waves (Figure 146) and velocity profiles (Figure 147) during the time of the peak tensions. Wave spectra from each of the AWACs from 2248 – 2256 were less than those from 2303-2311 with significant wave height values approaching 3 m at the former time range. The current velocity profiles from 2300-2303 and 2315-2318 from each of the AWACs show values less than 0.2 m/s for both east- and north-going components indicating that the extreme tensions were driven by the waves.

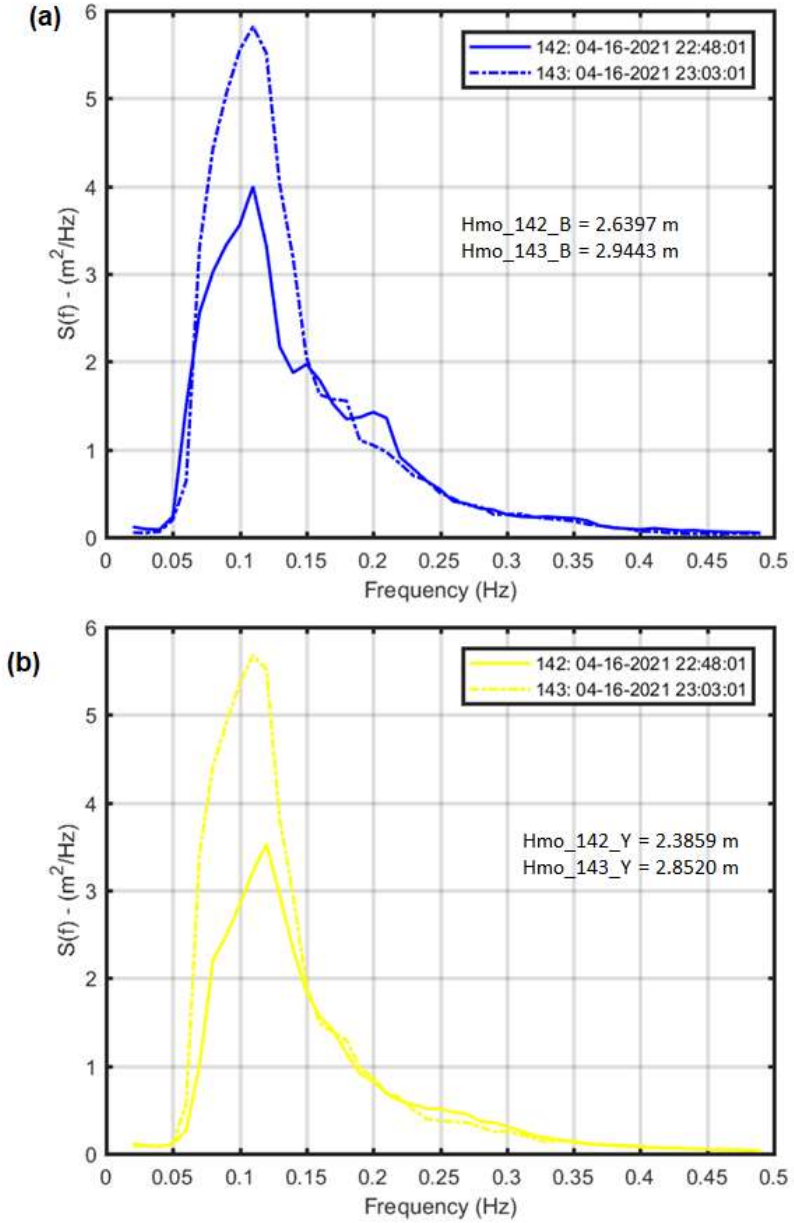

Figure 146: Wave spectra information from 2248 – 2256 and 2303-2311 for the blue (a) and yellow (b) AWACs, respectively.

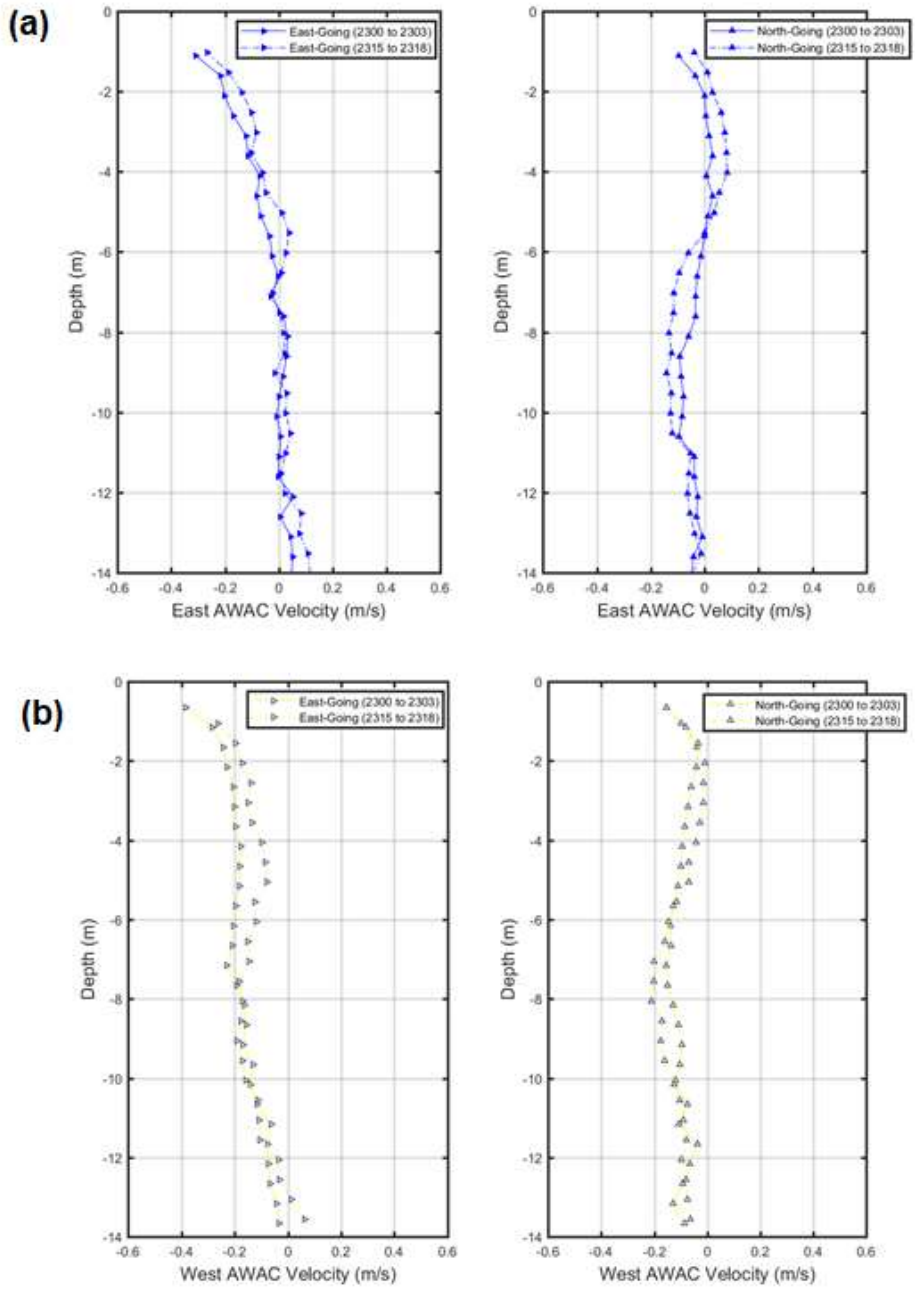

Figure 147: Velocity profile information from 2300 – 2303 and 2315-2318 for the blue (a) and yellow (b) AWACs, respectively.

After review of the datasets with some detail, a set of potential load cases was determined with the same criteria applied for the singe line validation effort. Current speed values from 15-18 and 30-33 minutes past each hour from the east and west AWACS were examined to have a less than 10% relative difference. A similar approach was applied with significant wave height values obtained during the second burst past the hour. The preliminary load cases are shown on Figure 148.

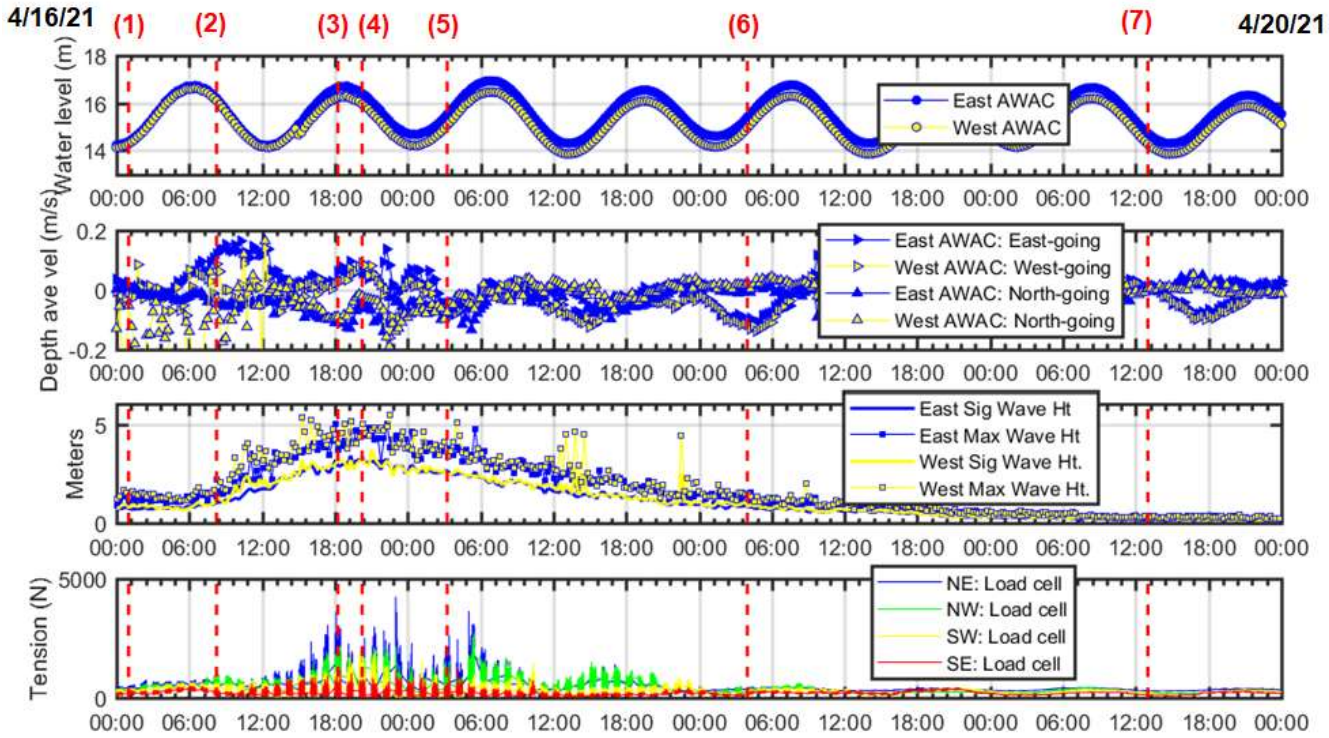

Figure 148: Preliminary load cases for the array system validation effort.

The specific date and time for the load cases are:

1. April 16, 2021 0103
2. April 16, 2021 0818
3. April 16, 2021 1818
4. April 16, 2021 2018
5. April 17, 2021 0318
6. April 18, 2021 0403
7. April 19, 2021 1303

2.5. Task 5.0: Hydro-FE model validation

2.5.1. Task 5.1: Perform Hydro-FE comparisons with experiments (12/01/2019)

An extensive set of physical model experiments were conducted to investigate the drag characteristics of large amount of kelp grown on a longline as described in Fredriksson et al. (2020). The physical model characteristics were based on a section of *S. latissima* grown on a 61 m longline at the site in Saco Bay, Maine (Figure 149). The seeded longline was deployed in November 2015 and harvested in early May 2016. At the time of harvest, the *S. latissima* was estimated to be about 3 m in length with 13-15 kg of biomass per m of longline. Along with these nominal characteristics, it was clear from this experience that the model would have to incorporate multiple, individual blades per unit length of longline.

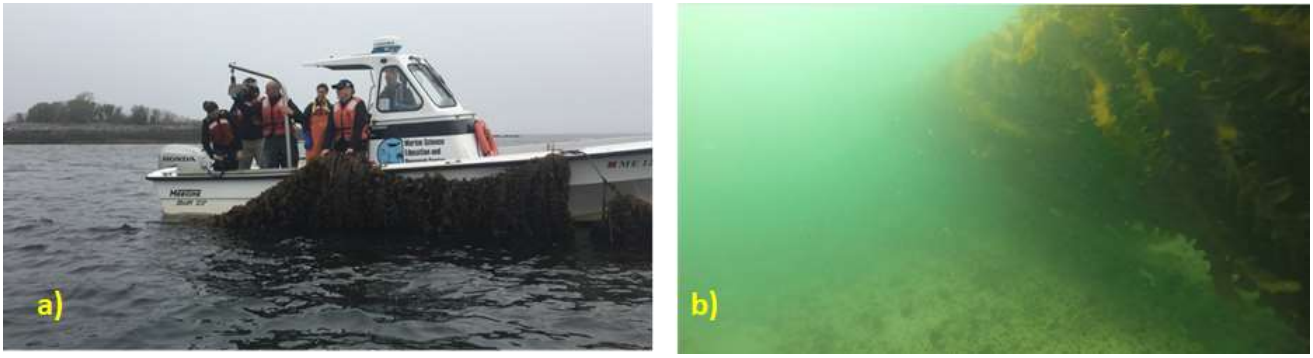

Figure 149: The physical model was based on the characteristics of the harvested longline shown at the surface on a) and submerged on b).

The experiments were conducted in the Hydromechanics (Hydro-Lab) Laboratory at the U.S. Naval Academy. One of the facilities in the Hydro-Lab includes a test basin that is 116-m x 7.9-m x 4.9-m with a tow carriage, wave maker and planar motion mechanism (PMM). With the large test basin, a full-scale model was built to represent a longline section of dense kelp. It was decided that the primary characteristics to match with the physical model was (1) the individual blade flexural rigidity, (2) the exposed length, (3) the individual blade mass density, (4) the mass/length of biomass on the longline and (5), as practical as possible, the number of blades per unit length.

For item (1), LDPE tube was found to be similar to samples measured at that time. The dimension for item (2) was 3 m, based on measurements from the longline shown on Figure 149. To achieve the appropriate mass density (3), three stainless steel washers were added to the top, middle and bottom sections of the 3 m strips of LDPE such that the composite mass density was 1380 kg/m^3. Point masses were considered to minimize the influence of the flexural rigidity of the LDPE. A total of 178 strips of plastic were needed on the 1 m model to achieve (4) with a final value of 16.11 kg/m (in air). The model required over 534 m of plastic strips wrapped over a 1.88 cm rod (the practical result for item 5) and clamped in place. The clamp also included a mount for a force-block gage. The 1-m x 3- m model, with 178 hanging strips is shown hung from a crane in Figure 150. In addition to the full-scale mounted-kelp model (with attachment bar), a second model representing a mounted-tare was also built with the same bar, clamp and force block mount with 178 shortened plastic strips. Measurements from the mounted-tare model were removed from the mounted-kelp-model to obtain a kelp only data set.

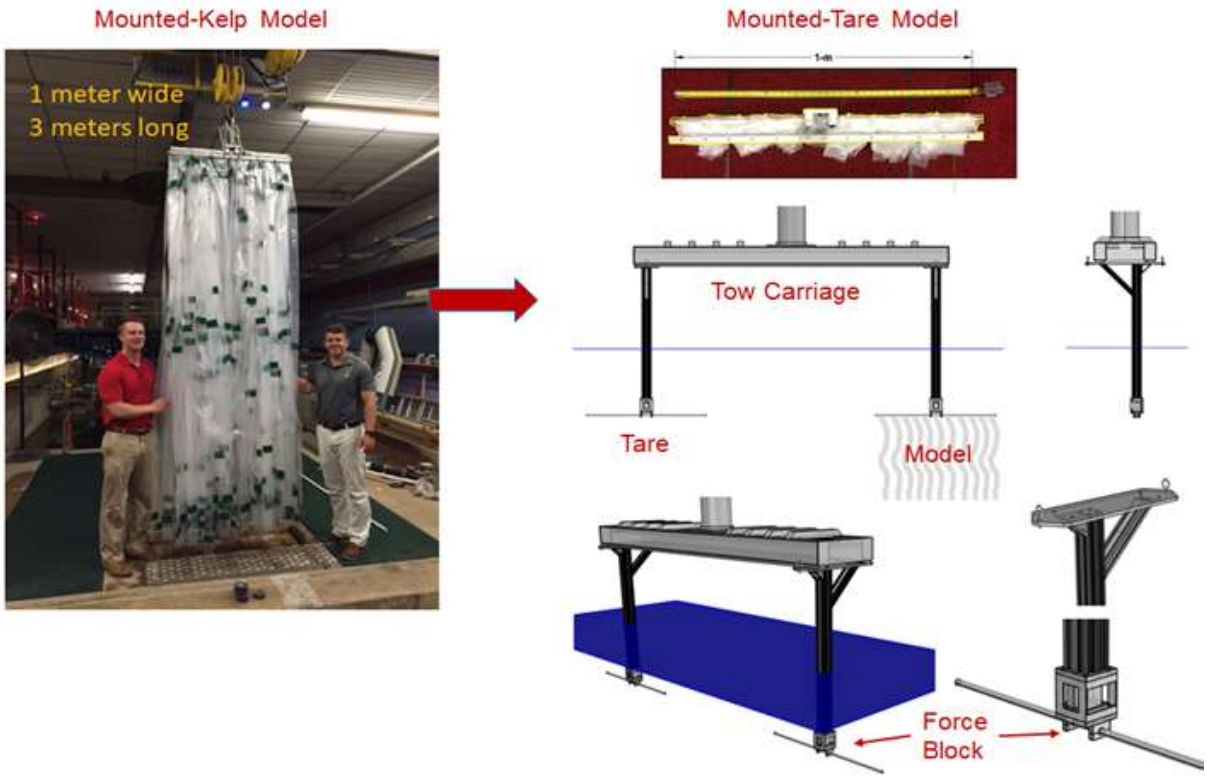

Figure 150: The kelp and tare model attachment on the tow carriage.

During the tow tests, horizontal and vertical reaction forces were measured with the force blocks at each model attachment shown in Figure 151 (a) and (b). To resolve the normal and tangential drag components on the flexible structure from the measured forces, coordinate transformations and force balance calculations were conducted. In this procedure, a global coordinate system was set at the attachment location such that the X-axis was aligned with the attachment bar and the Y-axis perpendicular to the attachment bar with the forces measured along each axis defined as F_X and F_Y, respectively. This orientation was chosen to be similar to the definition by Faltinsen (1991) with respect to moving ships. During the tow tests, three replicates were obtained from the force block mounted at a 90 degree angle to measure vertical forces upwards. This was defined as the Z-axis. Since a set of vertical forces were measured for both the aligned and perpendicular orientation, the datasets were defined as F_{Za} and F_{Zp}, respectively (also shown in Figure 151 (a) and (b).

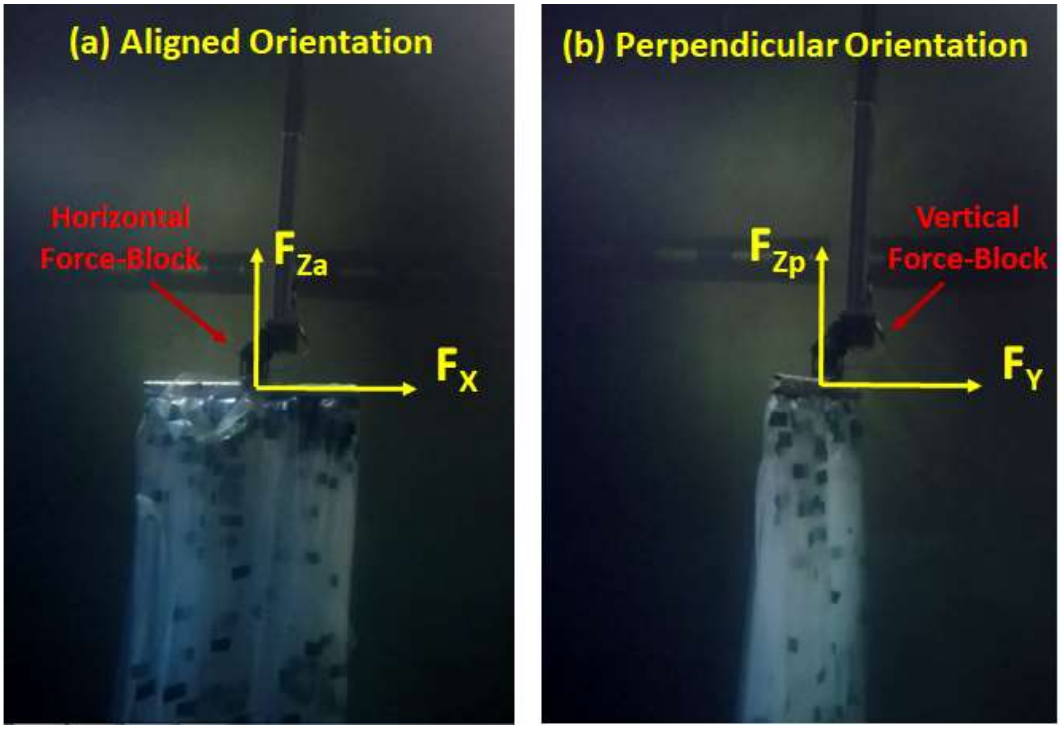

Figure 151: Tests were conducted in aligned (a) and perpendicular (b) orientations with respect to the centerline of the tank. The coordinate system of X, Y and Z were defined by the orientation of the kelp-model attachment bar with the aligned axis as X and the perpendicular axis as Y to obtain the F_X and F_Y. The corresponding vertical components were defined as F_{Za} and F_{Zp} for the aligned and perpendicular sets of measurements.

Force balances were then defined (Figure 152) for a local section of the kelp model away from the attachment point and the free end in steady flow. Since no curvature was observed at this midpoint section during the tests, the shear force (V) and bending moment (M_b) in this region of the aggregate were assumed to be zero. Defining the diagram with a local coordinate system having the x-axis normal and the z-axis tangential to the aggregate (x-z plane), the force balance resolves the normal component of drag (f_{Dx}) per unit length as

$$f_{Dx} = \left(\rho_{aggregate} A_c g - f_B\right) cos(\theta_x). \quad (28)$$

with $\rho_{aggregate}$ as the mass density of the composite aggregate material, f_B is the buoyant force per length and θ_x as the angle from the horizontal. Since the normal drag force is distributed, per unit length on a section of the model, A_c is the cross-sectional area of the aggregate based only on volume. The same approach was applied in the y-z plane,

$$f_{Dy} = \left(\rho_{aggregate} A_c g - f_B\right) cos\left(\theta_y\right), \quad (29)$$

with θ_y as the corresponding angle from the horizontal.

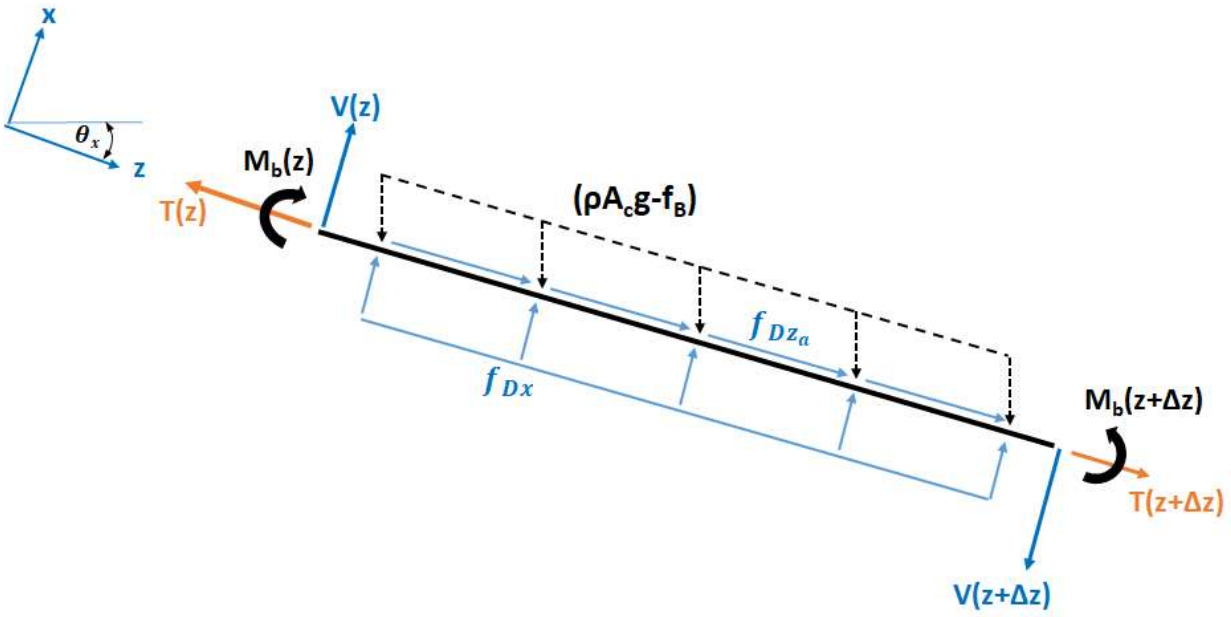

Figure 152: Force balance diagram of a beam section of the physical model away from the attachment point and the free end. At steady state, resolving the force balance in the local x-direction yields the normal drag force per unit length. The force balance in the y-z plane is orthogonal and identical.

This force balance approach, however, could not resolve the tangential per unit length components (f_{Dz_a} *and* f_{Dz_p}) since the local tension (T) along the aggregate could not be measured. Instead, the total tangential drag forces (F_{Dz_a} and F_{Dz_p}) were determined with a force transformation (Figure 153) from the resultants (F_{Ra} and F_{Rp}) of the force block measurements and corresponding angles (ω_X and ω_Y),

$$F_{Ra} = \sqrt{F_X^2 + F_{Za}^2} \quad (30) \qquad \text{and} \qquad \omega_X = arctan\left(\frac{F_{Za}}{F_X}\right) \quad (31)$$

$$F_{Rp} = \sqrt{F_Y^2 + F_{Zp}^2} \quad (32) \qquad \text{and} \qquad \omega_Y = \arctan\left(\frac{F_{Zp}}{F_Y}\right). \quad (33)$$

Then coordinate transformation was done with

$$\xi_x = \frac{\pi}{2} - \omega_X - \theta_x \quad (34) \qquad \text{and} \qquad \xi_y = \frac{\pi}{2} - \omega_Y - \theta_y, \quad (35)$$

also shown in Figure 153. The tangential forces (F_{Dz_a} and F_{Dz_p}) were then calculated and converted to per unit length of kelp model (L_{kelp} = 3 m) along the blade axis for the aligned and perpendicular orientations with

$$f_{Dz_a} = \frac{F_{Dz_a}}{L_{kelp}} = \frac{F_{Ra}sin(\xi_x)}{L_{kelp}} \quad (36) \qquad \text{and} \qquad f_{Dz_p} = \frac{F_{Dz_p}}{L_{kelp}} = \frac{F_{Rp}sin(\xi_y)}{L_{kelp}}. \quad (37)$$

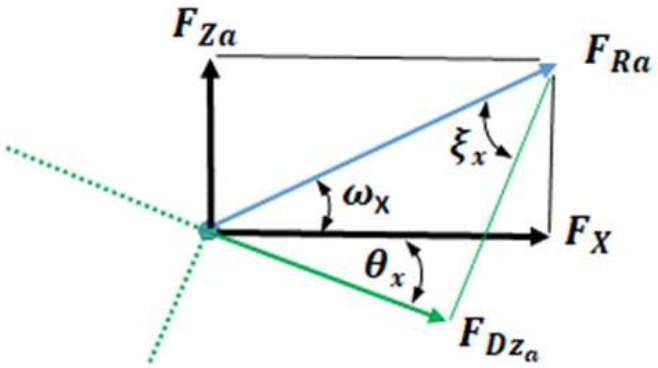

Figure 153: Transformation of coordinates to calculate F_{Dz_a} from the measured F_X and F_{Z_a} forces. The coordinate transformation in the Y-Z plane is orthogonal and identical.

Each tow test included the five speeds running the length of the tank for about 110 seconds. Time series datasets for each speed were obtained for approximately 20 seconds. Acceleration of the tow carriage between each speed took about 2 seconds, from which steady state conditions from the force block measurements were achieved after 4 seconds. For each setting, force and tow speed pairs were obtained by time averaging approximately 10 seconds of the steady-state values assuming the tow segment was a stationary process. Representative values at each speed were then ensemble averaged assuming ergodicity. With the ensemble averages, the mounted-tare values were subtracted from the mounted-kelp values to obtain kelp-only F_X, F_Y, F_{Za} and F_{Zp} in the aligned, perpendicular and vertical orientations, respectively. The force blocks were set to zero at the beginning of each tow so the wet weight of the mounted-kelp and -tare values were removed from the F_{Za} and F_{Zp} datasets. This was done to isolate the hydrodynamic forces, especially in the vertical direction since the wet weight had been measured.

In addition to the force datasets, digitized video was also captured to quantify the deflected angle of the compliant kelp model. Individual frames at each speed were used to measure the deflected angle scaled within a computer aided design (CAD) program when steady state conditions were achieved. The deflected angle was measured down from the horizontal axis of the global coordinate system to a line parallel to the leading edge of the kelp model aggregate.

With the datasets obtained from the force blocks, normal and tangential drag force components on the model kelp aggregate were determined. Drag force representations can take multiple forms for submerged, compliant macrophytes (Statzner et al., 2006) similar to *S. latissima*. In this case, normal and tangential drag forces were used to calculate the corresponding drag-area (Hoerner, 1965) for each component. This approach was taken because reference areas were ambiguous since not all blades were 100% exposed to the flow, similar to observations of cultured kelp in Saco Bay. The drag-area values, per unit length of kelp model, were calculated as

$$s_{Dx} = \frac{(f_{Dx})}{\frac{1}{2}\rho_w {U_x}^2} \quad \text{and} \quad (38) \qquad s_{Dz_a} = \frac{(f_{Dz_a})}{\frac{1}{2}\rho_w {U_{z_a}}^2}, \quad (39)$$

$$s_{Dy} = \frac{(f_{Dy})}{\frac{1}{2}\rho_w {U_y}^2} \quad \text{and} \quad (40) \quad s_{Dz_p} = \frac{\left(f_{Dz_p}\right)}{\frac{1}{2}\rho_w {U_{z_p}}^2}, \quad (41)$$

with units of length. If a reference area and length can be defined, non-dimensional drag coefficients can be calculated from the drag-area values.

In equations (38) – (41),

$$U_x = Usin(\theta_x) \quad \text{and} \quad (42) \quad \mathrm{U}_{z_a} = \mathrm{U}\cos(\theta_x) \quad (43)$$

are obtained from the aligned orientation, while

$$U_y = Usin\left(\theta_y\right) \quad \text{and} \quad (44) \quad \mathrm{U}_{z_p} = \mathrm{U}\cos\left(\theta_y\right) \quad (45)$$

are obtained from the perpendicular orientation. Representing drag in this manner with relative component velocities is consistent with approaches described in Casarella and Parsons (1970) which is necessary for calculating drag in unsteady flows and for use with configurations not tested in the tank.

The model kelp aggregate angle at each speed was estimated from a captured video frame during the steady-state portion of the tow and quantified with a CAD program. The results (θ_x and θ_y) are shown in Figure 154 and Figure 155 for the aligned and perpendicular orientations respectively. Each of the figures shows the angles formed at each origin (defined in Figure 152 and Figure 153) from the horizontal axis to a line parallel to the leading edge of the aggregate. Deflected angle values, θ_x and θ_y, were similar with differences of 0.7, 0.3, 1.8, 0.5 and 0.8 degrees at each of the increasing speeds between the orientations. The Figures also show the reconfiguration of the kelp aggregate model with increasing speed with the largest change occurring between 0 and 0.25 m/s.

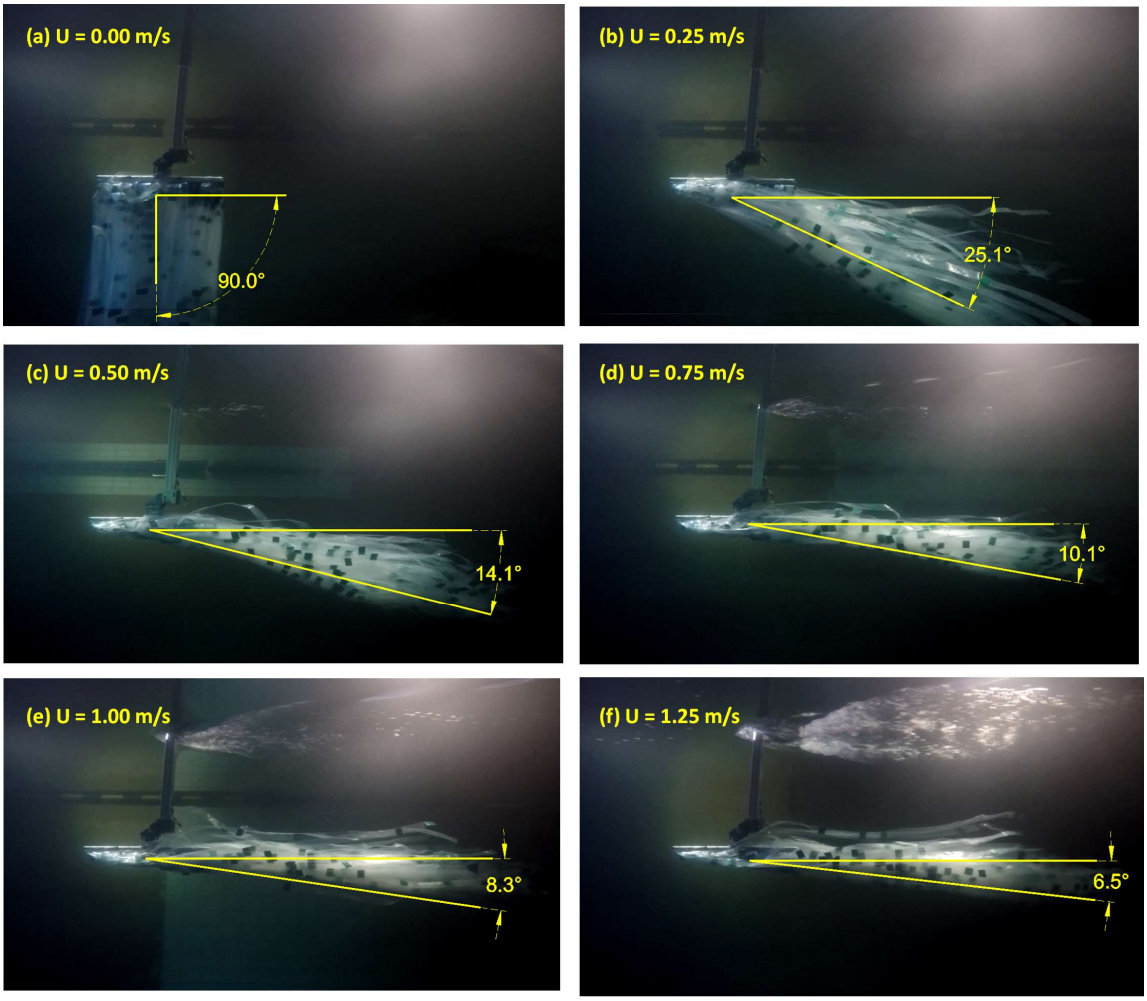

Figure 154: Deflected angle θ_x for the aligned orientation at each of the five towing speeds.

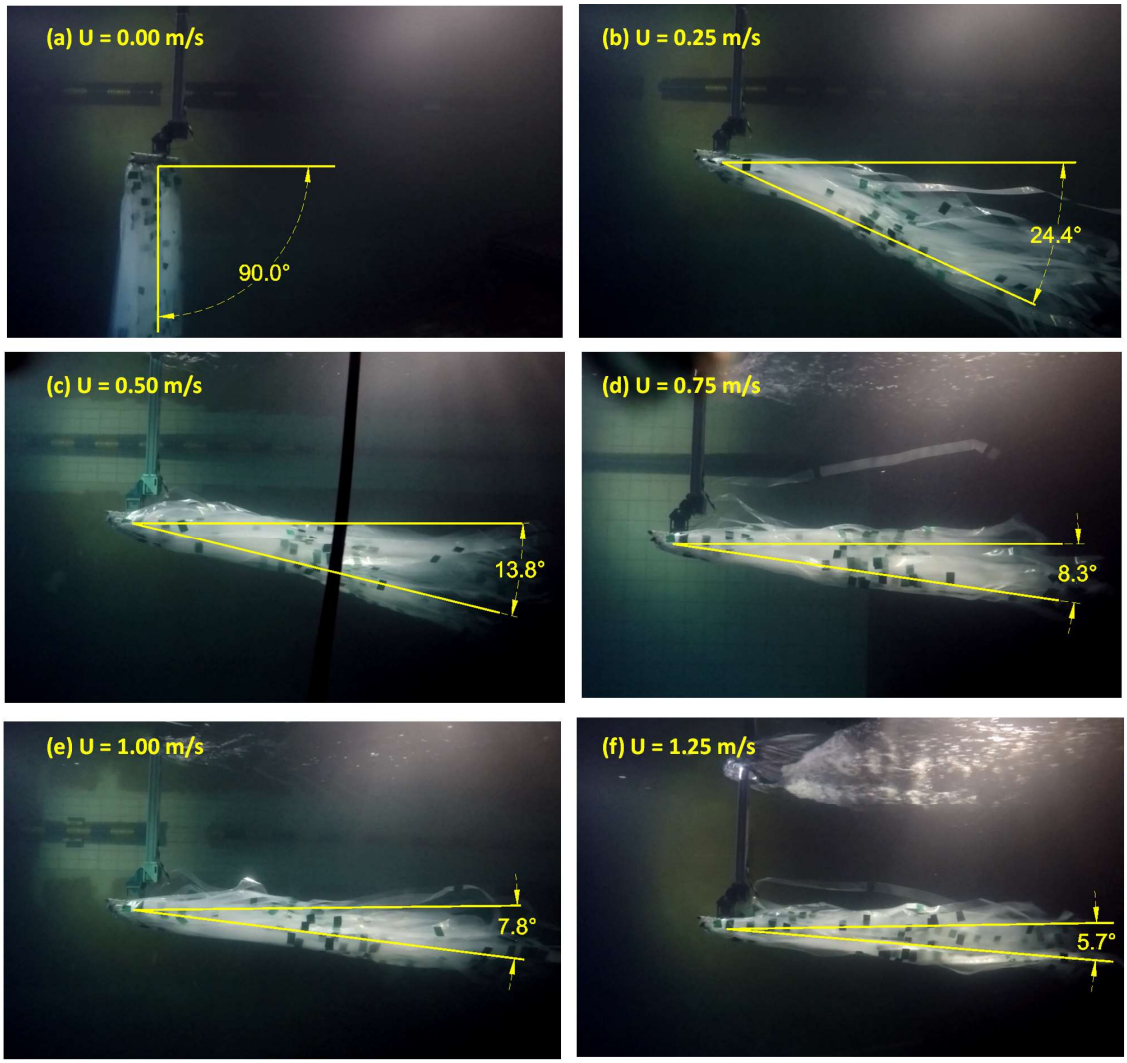

Figure 155: Deflected angle θ_y for the perpendicular orientation at each of the five towing speeds.

From the horizontally mounted force blocks, ensemble averages were calculated from the 10 and 11 replicate datasets for the aligned and perpendicular orientations to obtain the mounted-kelp and –tare results as shown in Figure 156 (a) and (b). The mounted-kelp and –tare datasets were then processed to obtain kelp-only, F_X and F_Y results representing both orientations as shown in Figure 156 (c).

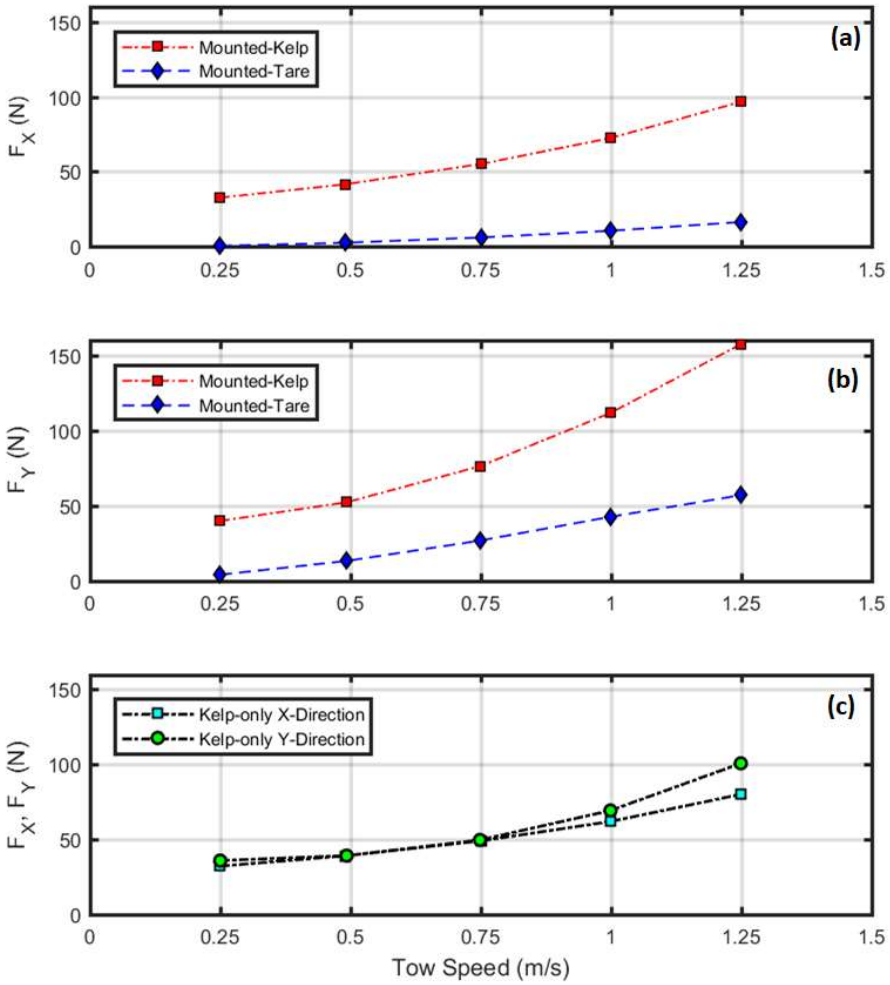

Figure 156: The horizontal force results in the X- (a) and Y- directions (b) associated with the aligned and perpendicular orientations, respectively. The kelp-only datasets are shown in (c). Both datasets in (c) show a transition from 0 to 0.25 m/s due to the kelp aggregate becoming more streamlined.

Table 23: Horizontal force mean value results for the mounted-kelp and -tare configurations.

	Aligned Orientation		Perpendicular Orientation	
Nominal tow speed (m/s)	Mounted-kelp (N)	Mounted-tare (N)	Mounted-kelp (N)	Mounted-tare (N)
	Mean	Mean	Mean	Mean
0.25	32.72	0.56	39.77	3.90
0.50	41.60	2.61	52.23	13.05
0.75	55.19	6.16	76.25	26.64
1.00	72.53	10.59	111.82	42.54
1.25	96.66	16.51	157.67	56.93

The mounted-kelp and –tare datasets for each orientation show force differences due mostly to the frontal area of the mount. When this component is removed, the kelp-only datasets in for each orientation show similarities at speeds between 0.25 and 0.75 as shown in Figure 156 (c). At speeds greater than 0.75, the results in the perpendicular orientation (F_Y) increase more than in the aligned orientation (F_X). One possible explanation is that the aligned shape becomes more streamlined with less area from 178 blades exposed to the flow. The blades associated with the perpendicular orientation, seem to maintain side-view shape and exposed area with increasing speed. The results from both orientations in Figure 9 (c) indicate that there must exist an inflection point below 0.25 m/s for the drag to reach zero at 0 m/s.

As previously described, a second force block was installed on both the mounted-kelp and –tare models for three of the towing tests in each orientation. The two additional force blocks were utilized to measure the vertical forces during the towing tests. Prior to initializing each tow, the vertical force blocks were also set to zero to remove the wet weight of the model to isolate the vertical hydrodynamic forces. The vertical forces were processed in the same manner as the horizontal forces. The mounted-kelp, mounted-tare and kelp-only results are shown in Figure 157 (a) and (b). The Figures also include the estimated wet weight of the model (43.65 N) as a positive value for comparison with the measured vertical force. The difference between the measured vertical force and the wet weight shows that hydrodynamic force approaches, but never reaches a point of completely supporting the wet weight.

The hydrodynamic properties of the kelp model were obtained from the results of the tank tests by applying the force balance principles with the geometric and material properties. With the deflected angles, the normal force components per unit length for the mounted-kelp model, f_{Dx} and f_{Dy}, were calculated based on the force balances in equations (28) and (29). The F_{Za} and F_{Zp} forces for the mounted-kelp model were converted to the tangential components, f_{Dza} and f_{Dzp} by coordinate transformation from equations (34) and (35) with the length of the kelp aggregate model. Drag-areas per length were then calculated from these force components using equations (38) - (41). The force and drag-area results per unit length of kelp model are provided in Table 24.

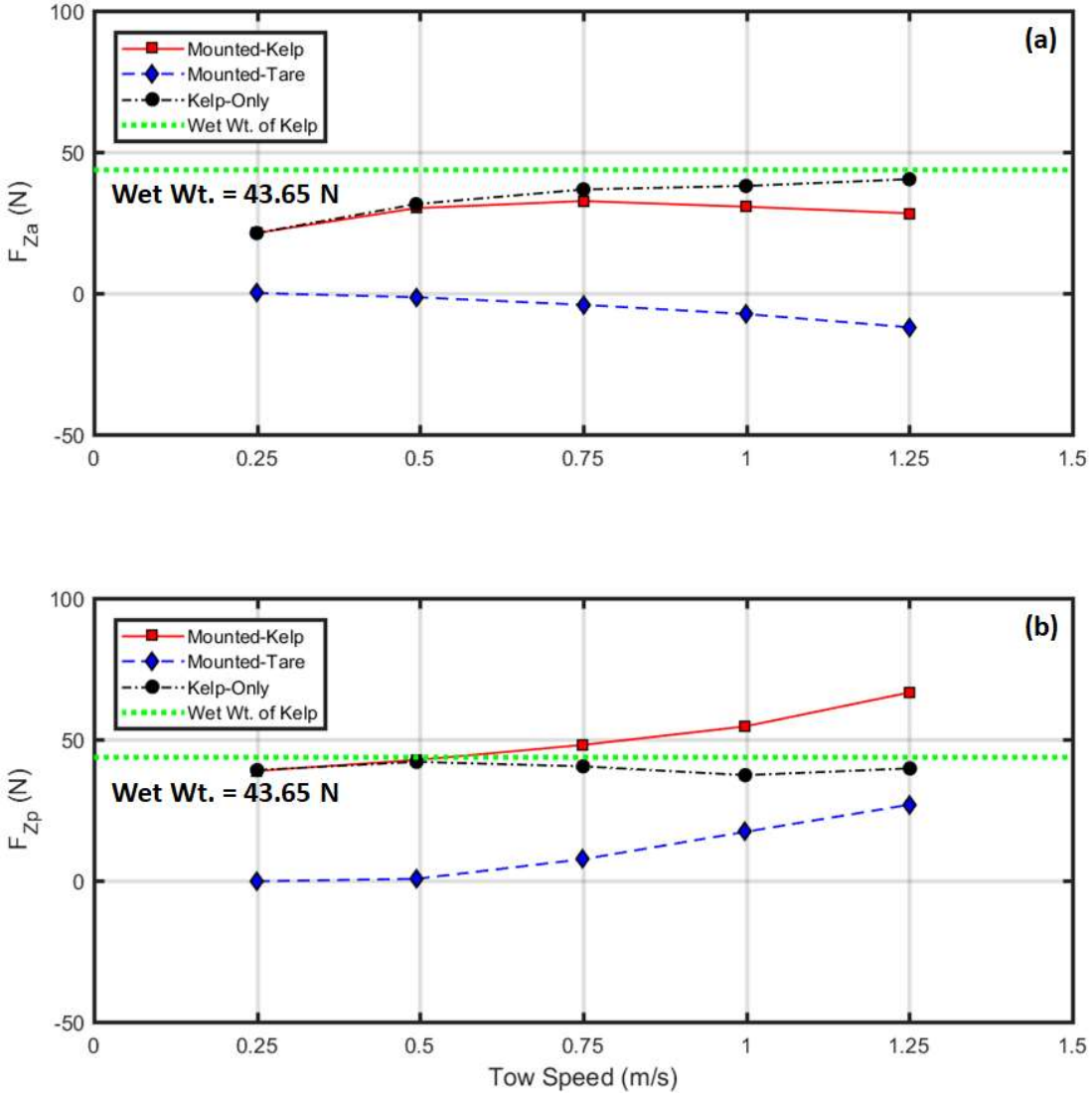

Figure 157: The vertical force results in the aligned (a) and perpendicular (b) orientations. Also shown is the wet weight of the kelp-model as a positive value calculated as the difference between the dry weight and buoyancy equal to 43.65 N.

Table 24: Force and drag-area results per length of kelp model (L_{kelp}= 3 m).

Tow Speed (m/s)	f_{Dx} (N/m)	s_{Dx} (m²/m)	f_{Dy} (N/m)	s_{D_y} (m²/m)	f_{Dz_a} (N/m)	s_{Dz_a} (m²/m)	f_{Dz_p} (N/m)	s_{Dz_p} (m²/m)
0.25	13.18	2.35	13.25	2.49	5.77	0.225	5.04	0.195
0.50	14.11	1.95	14.13	2.03	9.22	0.0803	7.98	0.0693
0.75	14.33	1.66	14.40	2.46	12.99	0.0478	13.08	0.0476
1.00	14.40	1.39	14.42	1.57	19.53	0.0401	19.56	0.0401
1.25	14.46	1.45	14.48	1.88	25.13	0.0326	30.46	0.0394

The first step in the validation was to compare the tow and force oscillation tank results with Hydro-FE. The plastic strip model was built in the Hydro-FE program to have the same geometric and material properties including the length, width, thickness, modulus of elasticity and mass density. The numerical model was used to run multiple simulations at the same environmental conditions as the physical model tests.

The 1 m by 3 m physical model was represented as a single line of beam elements in Hydro-FE. The effective cross-sectional properties of the 1 m wide model are shown in Table 25. The model was rigidly connected at the top end to a zero-displacement boundary condition (no rotation or translation). To validate the physical model tests, the weight and buoyancy was matched with a cylindrical finite-element model having a volume = 0.01168 m^3 applied with a kelp model mass density of 1379 kg/m3. With the length of the aggregate as 3 m, the cross-section of the cylindrical element was then calculated from the volume as 0.00389 m^2 with an effective diameter (Deff) of 0.0704 m. The flexural rigidity and second area moment of the individual model blades were taken as 1.78 (10-5) Nm^2 and 4.8 (10-14) m^4, respectively so that the modulus of elasticity is 371 MPa. The flexural rigidity of the aggregate was determined as the superposition of the 178 plastic blades assuming that (1) each bends independently, (2) the effect of friction and sticking between blades is neglected and (3) the modulus of elasticity is maintained. Superimposing the second area moment values of the aggregate cross-section, Iy = 8.54 (10-12) m^4 and with the same modulus of elasticity, EI of the aggregate was calculated as 3.17 (10-3) Nm^2. For the symmetric cylindrical model, Iy =Ix. With the volumetric characteristics of the cylindrical element matching that of the physical model, drag coefficients integrated into the Hydro-FE model had to be adjusted to match the empirical drag areas towing tests.

Table 25: Structural properties of the 1 m wide kelp model.

Parameter	Value	Units
Modulus of Elasticity	3.7 (10^8)	Pa
Mass Density	1.38 (10^3)	Kg/m^3
Diameter	7.04 (10^{-2})	m
Equivalent Cross Section	3.389 (10^{-3})	m^2
Second Area Moment of Cross Section	8.54 (10^{-12})	m^4

The drag area values from Table 24, with the structural properties resulting from Table 25, were implemented in the Hydro-FE model. The discretization sensitivity to element length was evaluated by performing numerous simulations each with a different number of elements from 1 to 233 according to Fibonacci's sequence. Results of the sensitivity analysis showed that a 3 m long kelp numerical model could be discretized into as few as eight elements without affecting the results With the Hydro-FE model, the horizontal, vertical and angle of the aggregate were calculated for the aligned and perpendicular orientations. Results for both the aligned and perpendicular orientations are provided in Figure 158 (a) and (b), respectively. Root mean square error between the physical and numerical models are also shown on the Figures with all values less than 7%.

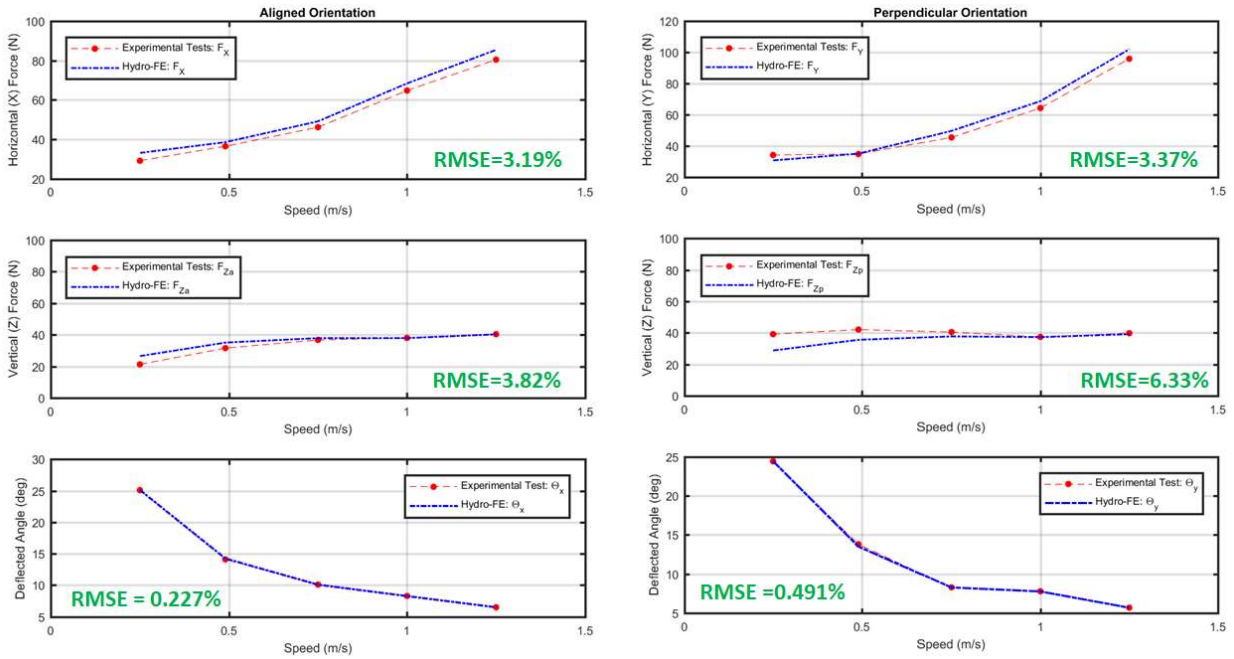

Figure 158: (a) Validation of Hydro-FE with steady tow test experiments in the perpendicular orientation and (b) in the parallel orientation.

The tow carriage and tank facility in the Hydromechanics Lab also has a planar motion mechanism (PMM) typically used in Naval Architecture to simulate sway and yaw motions of a ship during towing experiments. In this application, however, the PMM was used with the same kelp model to investigate oscillatory drag components and added mass coefficients. The oscillatory drag coefficient is compared to the steady drag coefficients and the added mass coefficient. The PMM is shown above the tank water surface in Figure 159(a) and the kelp is shown attached to the PMM during one of the tests in Figure 159(b). In this series of tests, the PMM was operated at the range of periods of 4, 5, 6, 7, 8, 9, 10, 11 and 12 seconds. A force block was attached to the rig measure the oscillatory forces.

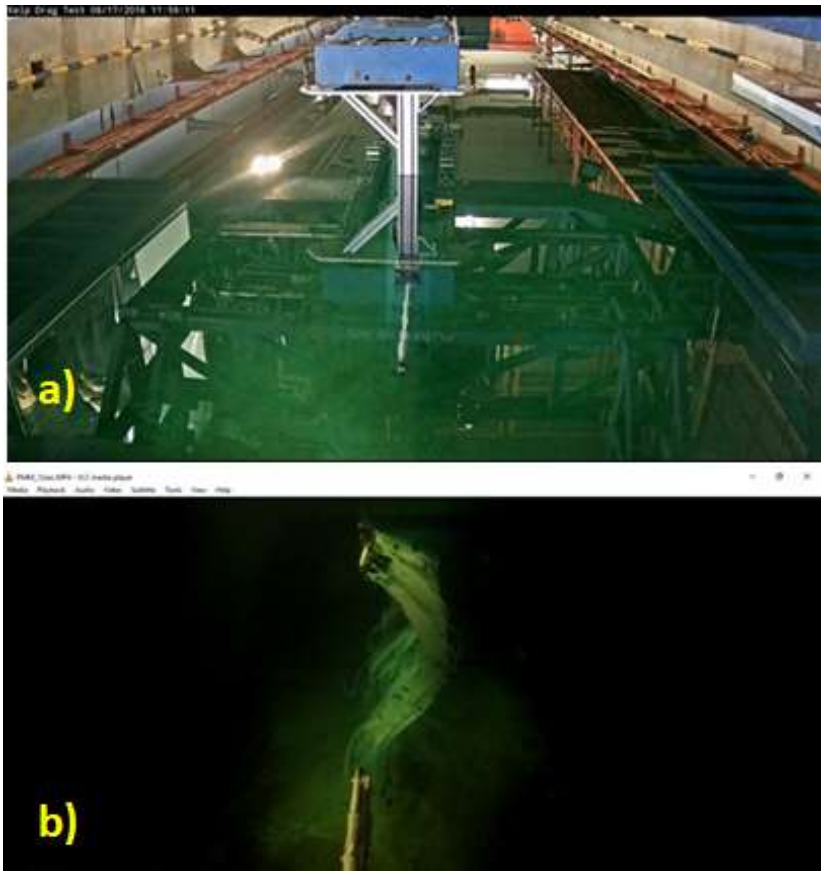

Figure 159: The kelp model was attached to the PMM to investigate oscillatory drag and added mass characteristics.

The PMM was operated with the attached model configured in the same aligned and perpendicular configurations as conducted with the tow tests. Example force and displacement data sets are shown on Figure 160. As an initial step, the PMM force data, f(t) was processed by resolving the time series as a summation of sine and cosine components,

$$f(t) = \sum_{i=1}^{n} a_n cos(\omega_n t) + b_n sin(\omega_n) \quad (46)$$

where a_n are the amplitudes of the cosine components, b_n are the amplitudes of the sine components and ω_n are the radian frequencies of the PMM. In this case, the displacement of the PMM was taken as a function of sine once the carriage was up to full speed. In this phase arrangement, the maximum velocity occurs 90 degrees from the displacement (i.e. cosine) and therefore, if the model was a rigid structure, the amplitude of the drag force will be equal to a_n. Maximum accelerations, however, are in-phase with the displacements (sine) and therefore the amplitude of the inertia force will be equal to b_n (once again, if the model was a solid object). The datasets are processed to obtain these amplitudes according to

$$a_n = \frac{2}{t_d} \int_0^{t_d} f(t) cos(\omega_n t)\, dt \quad (47)$$

and

$$b_n = \frac{2}{t_d}\int_0^{t_d} f(t)sin(\omega_n t)\,dt \qquad (48)$$

for the drag and inertia forces, respectively. Finding *a* and *b* for each test can either be done using fast Fourier Transform techniques or discretely using sum-product versions of equations (47) and (48) above.

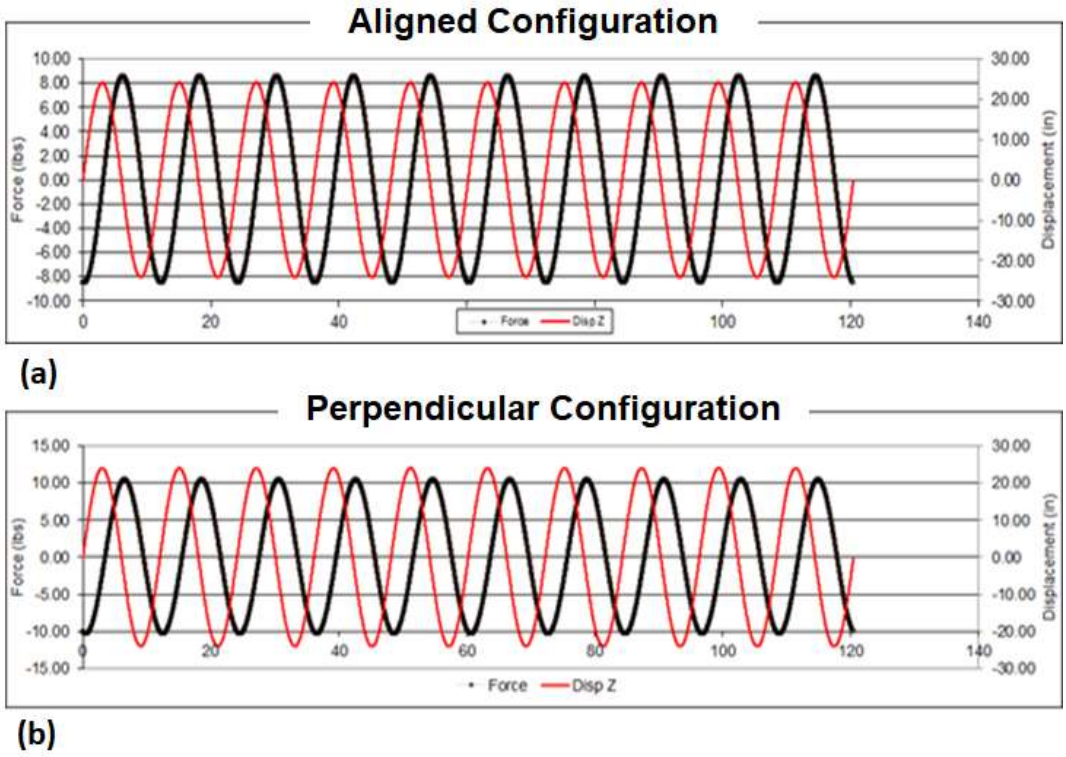

Figure 160: An example dataset showing the relationship between the PMM displacement and the measured force on the kelp model for the (a) aligned and (b) perpendicular configurations. In the force datasets, values for tare are removed.

Thirty-one PMM data sets were conducted for the aligned and perpendicular configurations to examine forces associated with oscillatory velocities and accelerations. The PMM was operated at periods ranging from 4 to 12 seconds to represent the typical range in the Gulf of Maine with at least 10 cycles for each tests. The settings for the tests are provided in Table 26 and Table 27. Six of the tests were performed as replicates (exact settings) and three of the tests were done to examine amplitude dependence. From each time series results, the maximum force, velocity and acceleration were obtained as provided in Table 26 and Table 27.

Table 26: PMM aligned dataset particulars.

						(a_n)	(b_n)		
Data File	Period (s)	Freq (rad/s)	No. of Cycles	PMM Amp (m)	Max Force (N)	Cos Force (N)	Sine Force (N)	Max Vel (m/s)	Max Accel (m/s)
60	4.00	1.572	14	0.038	7.751	-7.305	2.593	0.060	0.0939
61[1]	6.99	0.899	11	0.228	21.174	-21.135	-1.293	0.205	0.1841
62[2]	5.00	1.257	11	0.076	9.934	-9.674	2.258	0.095	0.1199
63[1]	6.99	0.899	11	0.228	20.363	-20.328	-1.196	0.205	0.1841
64	5.99	1.049	11	0.152	14.997	-14.989	0.483	0.159	0.1672
65[1]	6.99	0.899	11	0.228	20.363	-20.296	-1.644	0.205	0.1843
66	8.00	0.786	11	0.304	25.117	-25.011	-2.305	0.239	0.1878
67[1]	6.99	0.899	11	0.228	19.692	-19.634	-1.508	0.205	0.1842
68	9.01	0.698	10	0.381	29.123	-28.956	-3.113	0.266	0.1855
69[1]	6.99	0.899	11	0.228	19.412	-19.336	-1.721	0.205	0.1842
70	10.00	0.628	10	0.458	32.055	-31.896	-3.190	0.288	0.1809
71[1]	6.99	0.899	11	0.228	19.929	-19.875	-1.465	0.205	0.1843
72	10.99	0.572	10	0.535	36.363	-36.150	-3.935	0.306	0.1748
73	12.04	0.522	10	0.612	38.012	-37.756	-4.401	0.319	0.1665
74[2]	5.00	1.257	10	0.127	14.058	-14.040	0.717	0.159	0.2003
75[2]	5.00	1.257	11	0.026	3.245	-2.868	1.519	0.032	0.0405

[1]Test denoting replicates, [2]Tests investigating amplitude dependence

Table 27: PMM perpendicular dataset particulars.

						(a_n)	(b_n)		
Data File	Period (s)	Freq (rad/s)	No. of Cycles	PMM Amp (m)	Max Force (N)	Cos Force (N)	Sine Force (N)	Max Vel (m/s)	Max Accel (m/s)
14	6.99[1]	0.90	6	0.227	29.96	-28.96	-7.67	0.204	-0.184
17	6.99[1]	0.90	8	0.227	31.28	-30.38	-7.46	0.204	-0.183
18	5.00[2]	1.26	7	0.076	14.18	-14.04	-1.97	0.095	-0.120
19	6.99[1]	0.90	10	0.227	31.27	-30.24	-7.93	0.204	-0.184
20	5.99	1.05	11	0.151	23.18	-22.60	-5.13	0.159	-0.167
21	6.99[1]	0.90	10	0.227	30.93	-29.68	-8.72	0.204	-0.183
22	8.00	0.79	10	0.303	36.06	-34.81	-9.40	0.238	-0.187
23	6.99[1]	0.90	10	0.227	30.40	-29.23	-8.35	0.204	-0.184
24	6.99[1]	0.90	13	0.227	30.17	-29.07	-8.08	0.204	-0.184
25	9.01	0.70	10	0.380	39.77	-38.40	-10.36	0.265	-0.185
26	6.99[1]	0.90	10	0.227	30.05	-28.99	-7.93	0.204	-0.184
27	10.00	0.63	10	0.457	42.52	-41.26	-10.29	0.287	-0.180
28	10.99	0.57	10	0.533	44.67	-43.16	-11.53	0.305	-0.174
30	12.04	0.52	10	0.610	46.26	-44.53	-12.51	0.318	-0.166
31	5.00[2]	1.26	11	0.126	21.55	-21.05	-4.60	0.159	-0.200

[1]Test denoting replicates, [2]Tests investigating amplitude dependence

To examine this dataset, the oscillatory force amplitudes associated with the cosine and sine components were estimated from applying equations (47) and (48) above and provided in Table 26 and Table 27. These amplitudes are plotted on Figure 161 as a function of Keulegan-Carpenter (KC) number,

$$KC = \frac{U_{max}T}{L}. \quad (49)$$

In equation (49), U_{max} is the velocity amplitude, T is the period of oscillation and L is the characteristics dimension taken in this case as the width of the model of 1 m. The KC number is a non-dimensional parameter that is typically used to characterize the relative importance of drag and inertial forces as a function of oscillation velocities and accelerations, respectively, when examining rigid ocean structures. The full-scale kelp model, however, is not rigid so the cosine and sine components of the total force are not necessarily equal to drag and inertia.

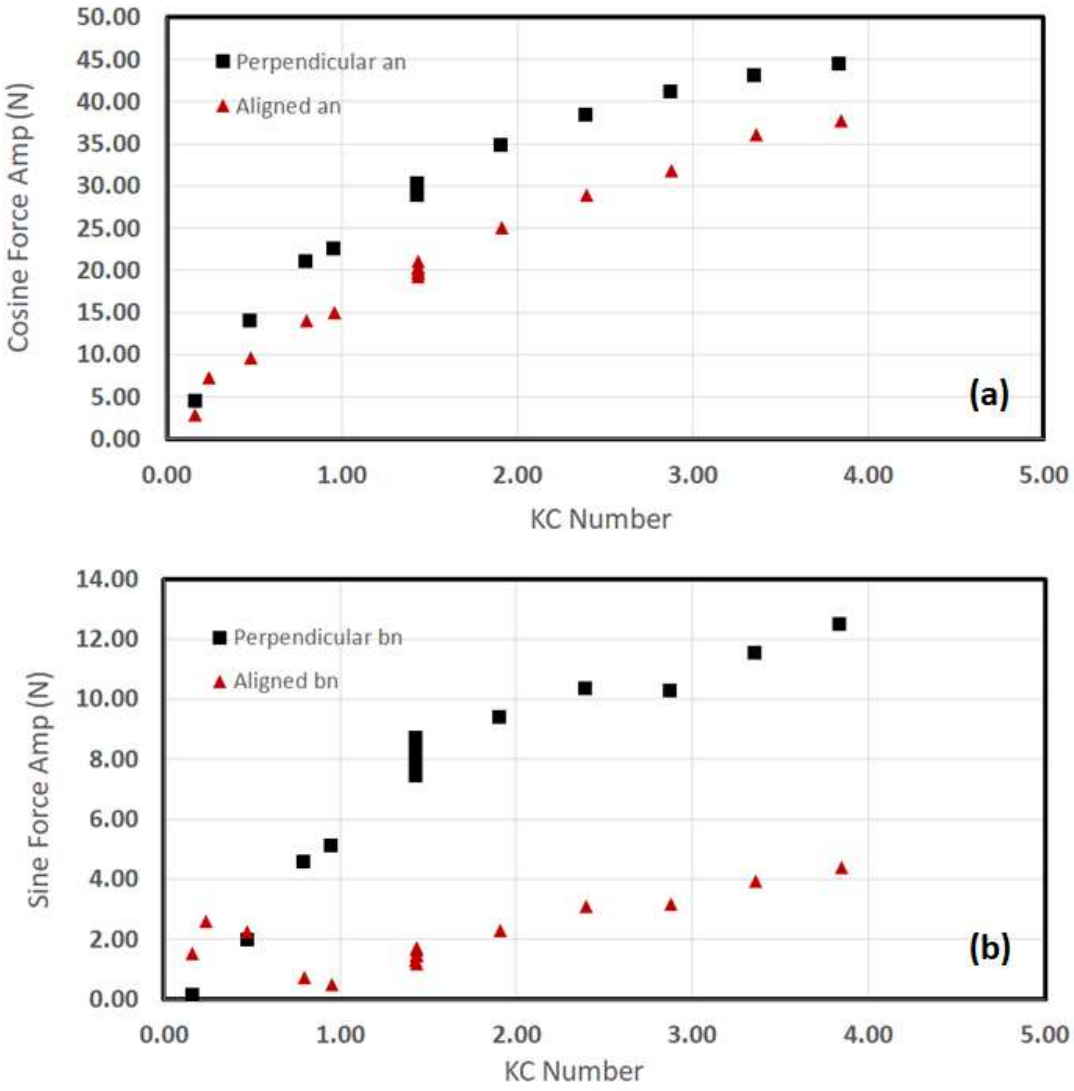

Figure 161: (a) The cosine and (b) sine forces for the perpendicular and aligned orientations.

However, the PMM tests are being considered as a technique to validate the Hydro-FE model for oscillating forces by examining the cosine and sine components of the measured forces. For a rigid structure, the first step to process the PMM data would be to perform discrete Fourier analysis to extract the force components due to drag and inertia. Processing these datasets with the discrete Fourier transform approach for the flexible model, however, may not yield the same results as it would for rigid bodies. This was discovered when the Hydro-FE model was built and is demonstrated on Figure 162.

	Max. attachment point velocity	Max. attachment point acceleration
Drag force vector		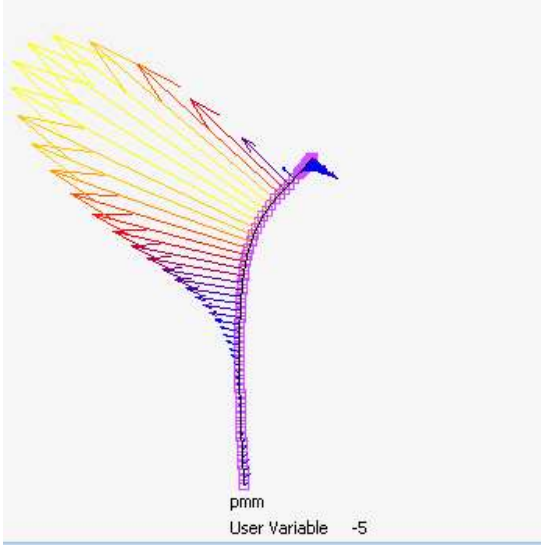
Inertial force vector	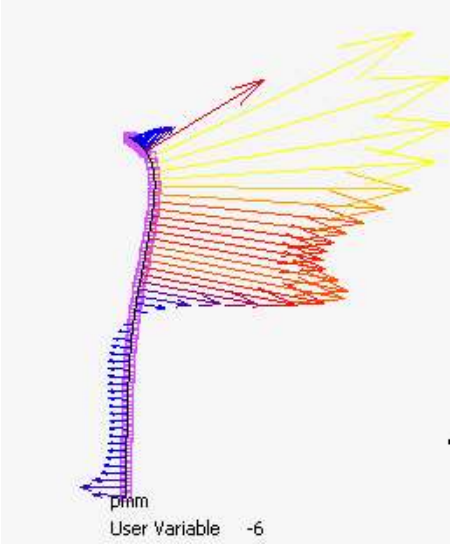	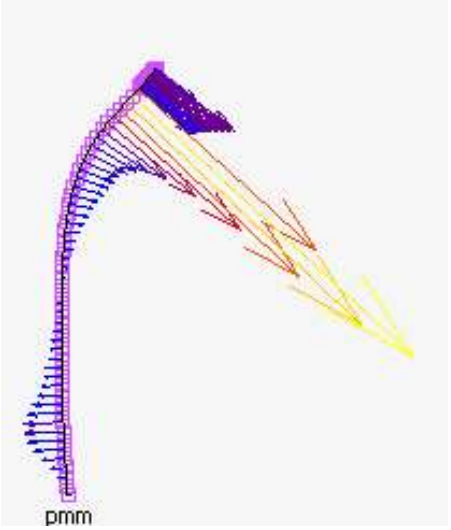

Figure 162: Drag and added mass force vectors at two different instants in the 12 s PMM test. The first column shows the force vectors when the velocity of the attachment point is maximal (zero acceleration). The second column shows the force vectors when the acceleration of the attachment point is maximal (zero velocity).

As shown on the Figure, force vectors indicate that significant drag forces are present even when the velocity of the attachment point is zero. Similarly, non-negligible added mass forces are present even when the attachment point acceleration is zero. This is because of the flexibility of the system. Therefore, the hydrodynamic coefficients for the forced oscillation tests are being determined from a multi-variate sensitivity analysis, rather than an analytical solution.

The objective of representing the physical test section with a series of finite elements is complicated by the variation in behavior of the blades along the length of the physical model. It was found that near the attachment point, the blades are closer together and behave as a solid

sheet (Figure 163). In the lower half of the test section, however, the blades spread out and behave as individual high-aspect ratio sheets. The potential implications of this variation are demonstrated with respect to added mass in Figure 164.

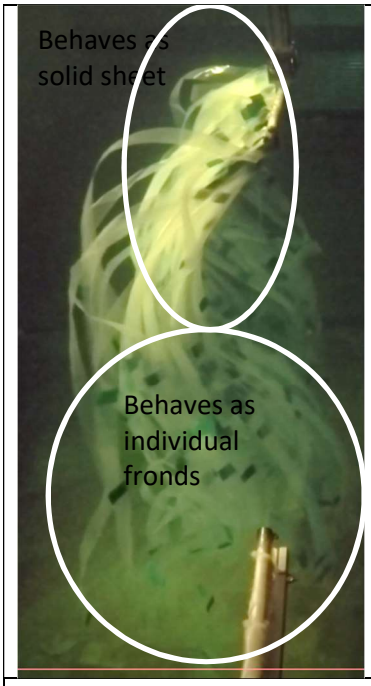

Figure 163: PMM test of physical model oscillating with a period of T=12 s. Near the top of the blades, the header bar constrains the blades to move as a solid sheet. Near the bottom of the blades, they oscillate freely as individual blades, changing their hydrodynamic properties.

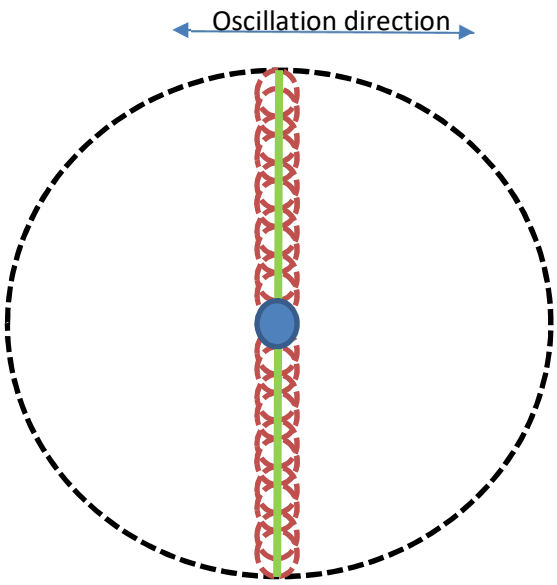

Figure 164: Schematic showing different treatments of added mass on a plan-view of the 1 m wide physical model. The physical model is represented by the solid green line. The model is represented in the FEA simulation as a cylindrical element whose cross-sectional area (solid blue circle) is equal to that of the physical model. The physical model is made up of 7.55 m-wide blades. If each blade acts individually, the total added mass per length of blade, according to potential theory for high aspect ratio strips, is comparable to the sum of the small orange circles. However, if the physical model behaves as a solid sheet, potential flow theory suggests that the added mass would be equivalent to the mass of water enclosed in the large black dashed circle.

For a rigid flat plate with a width of 1 m and an aspect of ratio 3:1, the theoretical added mass per unit length is 375 kg/m. For 178, 7.55 cm wide rigid flat plates with high aspect ratios, the collective added mass per unit length is 199 kg/m. These values correspond to added mass coefficients between 59 and 110 based on the mass per unit length of the physical model. Based on Figure 163, it seems that the actual behavior will be between these two extremes. Similarly, the projected area used in the drag calculations depending on whether the model is moving as a solid sheet or as a collection of independent blades.

A design-of-experiments approach was used to assess the impact of specific design parameters on the performance of the device. (See, for example, Oehlert 2010). The input parameters chosen for this study are provided in Table 28.

Table 28: Low and high values of design parameters for sensitivity study.

Parameter	level0	level1	units	Notes
Ca	1.0000	60.000	#N/A	
Bending, EI	3.16E-03	3.16E-02	mult.	
Drag area/length	1	13.4	m	
Cdx	0.486	1.514	mult.	Ratios of Min. and Max to Mean from methods 1 - 4 in steady tow
Cdz	0.3429	1.6571	mult.	Ratios of Min. and Max to Mean from methods 1 - 4 in steady tow

Note that these are initial values to be updated with the results from Fredriksson et al. (2020).

A fractional factorial experiment was chosen for efficiency. A resolution of IV was specified, meaning that no two-factor interactions were aliased with any main effects. A Franklin-Bailey algorithm was used to find generators for the smallest two-level fractional-factorial design. This resulted in a fractional factorial experiment in which 2^{5-2} representations were simulated for each combination of oscillation period and amplitude.

The design-of-experiments approach yields the estimated effect of each design factor on each objective function of interest. Figure 165 – Figure 167 show the estimated mean effect of each input factor on the amplitude of the horizontal force. Steeper gradients indicate that the forces are more sensitive to the parameter in question. These results show that uncertainties due to the treatment of the projected area have a much larger effect on the force magnitudes than those due to the range of hydrodynamic coefficients, for this particular test setup. Oscillating tests in even a small steady current may yield very different force amplitudes.

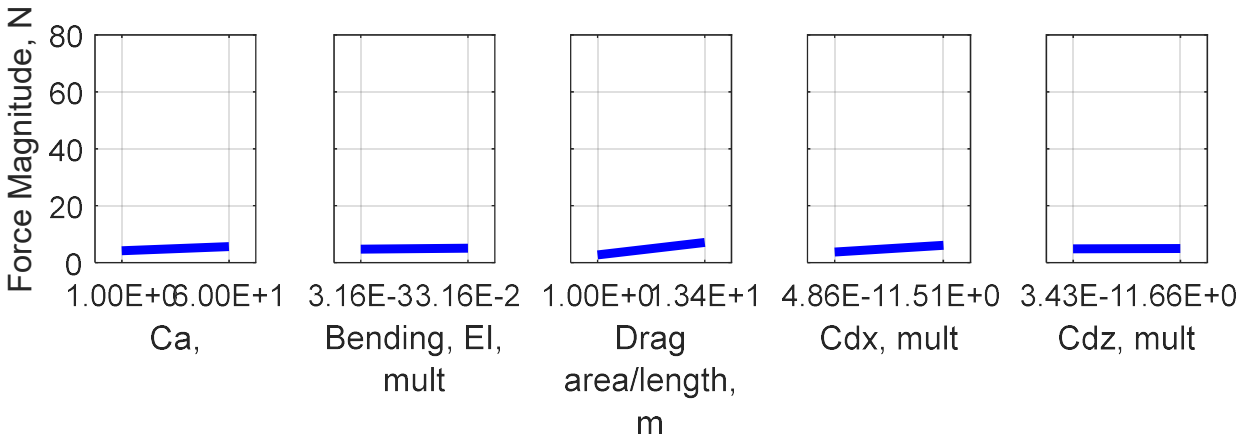

Figure 165: Sensitivity of horizontal force magnitude input parameters for T = 4s.

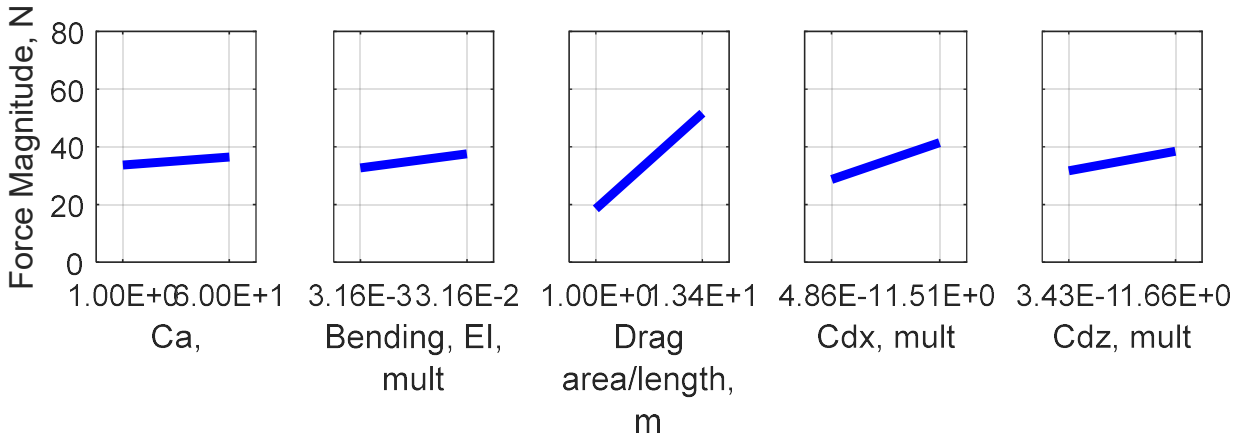

Figure 166: Sensitivity of horizontal force magnitude input parameters for T = 8s.

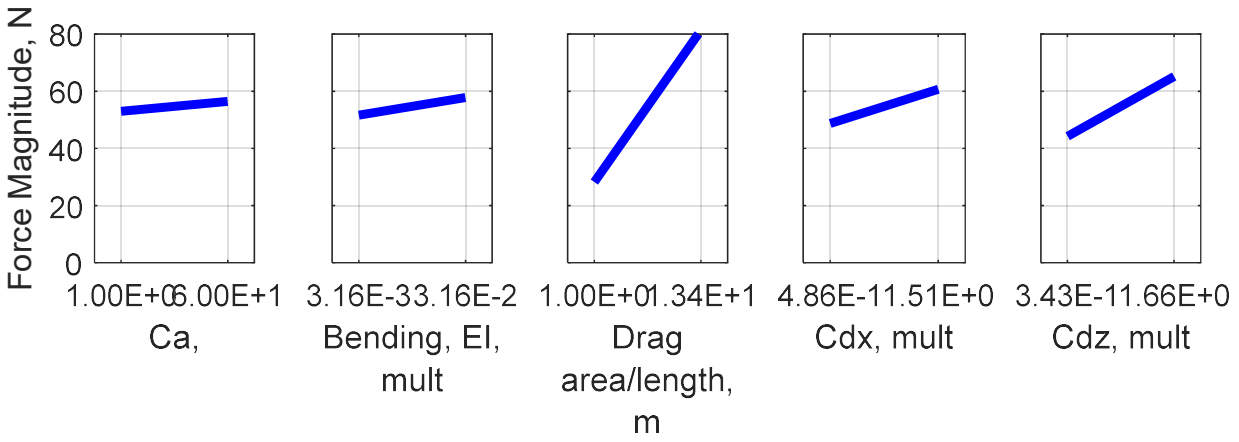

Figure 167: Sensitivity of horizontal force magnitude input parameters for T = 12s.

To ensure the practicality of hydrodynamic coefficients derived in this project, the set of drag coefficients validated by the steady tow tests were assumed a function only of relative velocity. That is, drag coefficients were assumed to vary only with Reynolds number, and not Keulegan–Carpenter number. Drag coefficients derived from the steady tow tests were interpolated onto the RMS velocity of the PMM for each combination of frequency and amplitude using a polynomial interpolation method (PCHIP). Due to the uncertainties represented in Figure 163 and Figure 164, a range of added mass coefficients and drag diameters was explored. The numerical results using the combination that produced the best match with the set of tank data are shown in Figure 168.

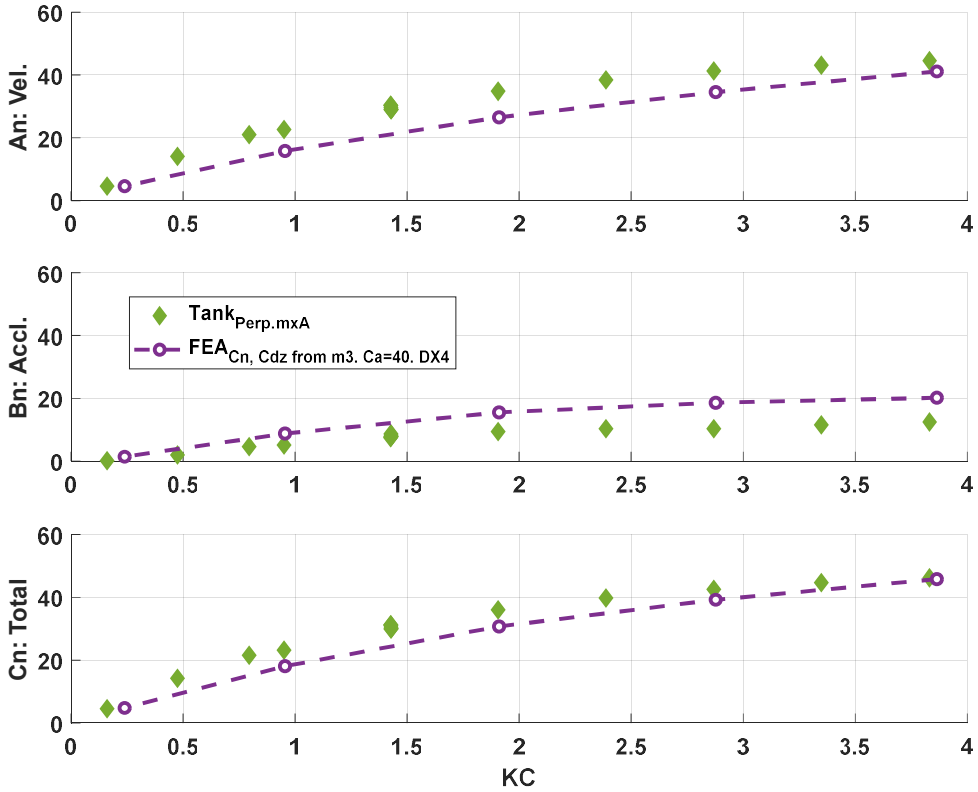

Figure 168: Validation of numerical model of forced oscillations tests in still water. Velocity- and acceleration-dependent components, along with the total magnitudes of the horizontal force, are given as a function of Keulegan–Carpenter number.

The drag area results per unit length from the physical model tests (Table 24) are employed in the Hydro-FE software for the oscillation tests. In dynamic representations based on Morison's Equation, elements are generally assumed cylindrical. When using cylindrical elements to represent non-cylindrical aggregates of kelp, the definitions of hydrodynamic coefficients must be considered and explicitly communicated. The drag-area values in Table 24 are represented as per unit length of a 1 m aggregate for both the normal and tangential orientations. When the physical kelp model oscillates in still water, the portions of the individual blades far from the clamped end spread apart from each other. This effect greatly increases the effective drag diameter and the added mass coefficient. If each blade in the physical model were independently exposed to the undisturbed fluid, the total drag diameter for a 1m-wide test section would be (178 blades) ×(7.55 cm/blade) = 13.4 m. An effective drag diameter of 4.0 m was found to produce the most valid comparison with the tank data. An added mass coefficient of 40 resulted in the best correlation with the experimental measurements. This value is defined as the added mass of the test section, per length, divided by the mass of water displaced by the test section, per length. This definition is used in most dynamic FEA codes. If the physical model were to approach an infinitely thin sheet, the added mass coefficient using this definition would approach infinity.

More precise agreement with tank observations could be obtained by varying the drag diameters and added mass coefficients as a function of Keulegan–Carpenter number (KC) in the software.

Furthermore, the normal and tangential drag coefficients could be assumed different in oscillating flow than in steady flow. While a physical case can be made for each of these approaches, the present approach was used because it ensures that validation results are not the result of excessive "fitting", and because it results in an approach that can be practically applied by engineers modeling full-scale kelp cultivation systems in waves and currents.

It should be noted that the values of drag diameter and added mass derived from the oscillating tests may change if the system is simultaneously subjected to a steady current and waves. The steady current could force the blades to align, resulting in less area being exposed to the undisturbed fluid flow. This possibility should be investigated either with further tank tests or with field experiments.

2.5.2. Milestone 5.2: Validate Hydro-FE at experimental model scale (2/15/18)

With the Hydro-FE model configured with the geometric, material and hydrodynamic properties of the physical model, simulations were conducted to make the physical model tests with 6.5% RMSE values (see Figure 158). The milestone set in the SOPO was to be able to produce results within 15% for three increasing scales. Matching the physical model tests within 6.5% satisfies M5.2 at steady speeds.

2.5.3. Task 5.3: Develop a scalable model for single line systems (12/16/20)

Based on the present analysis, it is recommended that 1 m aggregates of kelp be represented as a series of beam elements in the dynamic, Hydro-FE model. The technique applies the approach described for the physical model tests with the structural characteristics provided in Table 25.

The drag-area values were then obtained as a function of the relative velocities. The drag-area values were empirically determined using equations (38) – (41) as per length of aggregate with L_{kelp} = 3 m. In general, the Hydro-FE model computes the per unit length, normal drag as

$$\frac{\partial \overrightarrow{F_n}}{\partial l} = \{DC_n\}\frac{1}{2}\rho_w|U_{Rn}|\vec{U}_{Rn} \quad (50)$$

and the per unit length, tangential drag as

$$\frac{\partial \overrightarrow{F_t}}{\partial l} = \{\pi DC_t\}\frac{1}{2}\rho_w|U_{Rt}|\vec{U}_{Rt} \quad (51)$$

for cylindrical beam elements with C_n and C_t as published empirical values and D as the diameter. In equation (50), a normal, projected area is assumed and in equation (51), a tangential, surface area is assumed. For both of these equations, the terms in the brackets are equivalent to drag-area per unit length with $\vec{U}_{Rn}$ and $\vec{U}_{Rt}$ as the normal and tangential components of the fluid particle velocity relative to the element velocity, respectively.

For the case of the 178 blade, kelp aggregate model, drag-area values were for normal and tangential velocities in both the aligned and perpendicular orientations. Since the 178 blades can move independent of each other, the resulting nominal shape was left inherent in the drag-area coefficients, s_{Dx}, s_{Dy}, s_{Dza} and s_{Dzp}. Therefore, the drag-area coefficients could directly replace the $\{DC_n\}$ and $\{\pi DC_t\}$ values for the kelp aggregates depending upon orientation to the flow with the geometric and material properties are matched. The 1 m aggregate model was applied in

Hydro-FE to the 122 m kelp system that was deployed at the exposed Ram Island site during the 2018-2019 grow out season (Figure 169).

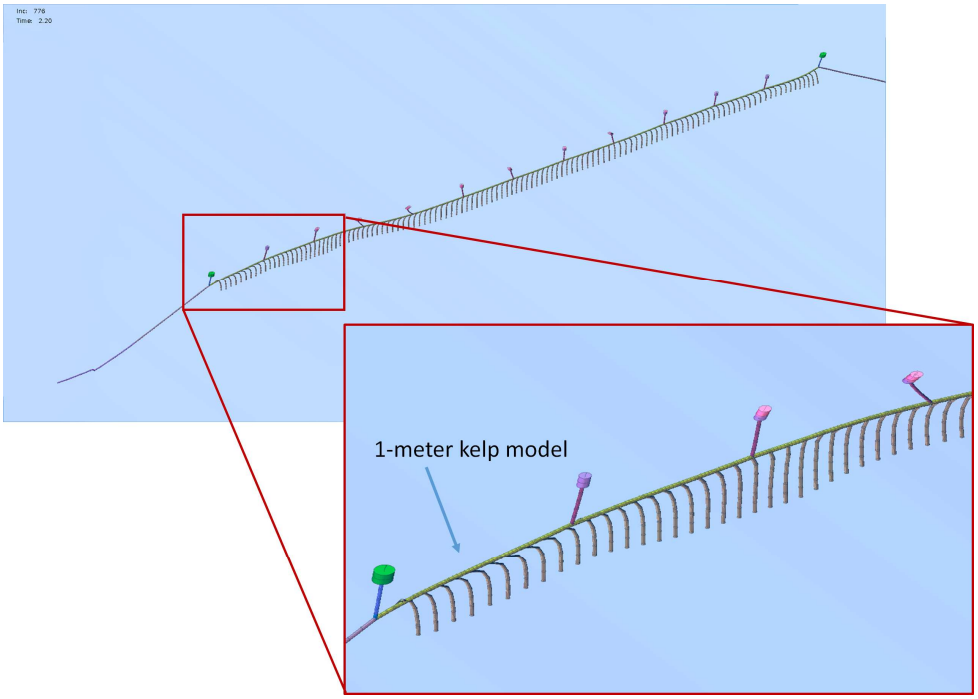

Figure 169: An example of the 1m kelp aggregate model applied on the 122 m system deployed at the Ram Island site during the 2018-2019 growing system.

Being able to match the geometric, material and hydrodynamic properties of kelp aggregate is an important first step in the development of the Hydro-FE model. The Hydro-FE model, with empirical drag-area input, does not represent flow reduction created by work done on aggregates of kelp. Therefore, a velocity reduction scheme was developed.

Therefore, as a first step to represent flow reduction, a scheme like described in Rosman et al. (2010) was implemented with Hydro-FE. The approach considers the change in velocity as a 1-dimensional momentum balance between horizontal advection and the total drag per unit length (f_{D_X}) considering both normal and tangential global X-components such that:

$$u\frac{\partial u}{\partial x} = \frac{f_{D_X}}{A_X \rho_w}, \tag{52}$$

where A_X is the horizontal projected area for which momentum is extracted from the flow. The classic approach is to integrate equation (6) to isolate drag as a function of velocity squared and incorporate an empirical drag coefficient for specific examples. In this case, however, empirical drag force data (f_{D_X}) were obtained from the full-scale, physical model tests. Equation (52) was applied in the numerical procedure as a discretized form of momentum extraction from the ambient flow (U_0) by "integrating" drag over the entire line stepwise for each successive aggregate position (x_n) as,

$$U_n = U_{n-1} - \left(\frac{f_{D_X}}{A_X \rho_w U_n}\right)(x_{n-1} - x_n). \tag{53}$$

In equation (53), U_n is the velocity following the aggregate at n = 1, to the total number of aggregates along the length of the grow line. This relationship is solved iteratively for each aggregate location within the farm for U_n. It marches along the grow line producing a set of reduced horizontal velocities applied as modified drag area values in the numerical procedure at each aggregate location. This model is applied with the field data.

Work was also done to build a feature that enables support for one-way coupling with coastal hydrodynamic models. A version of the interface was implemented that allows to process the output from FVCOM model, perform data interpolation and smoothing (to avoid aliasing artifacts and high-frequency noise), and to use instead of the predefined sets of velocity inputs. In addition to this effort, the Hydro-FE model was modified to make multidimensional approximations of current velocity fields. An example of the circulation model 4D velocity fields is shown on Figure 170 and Figure 171. This modification allows for predetermined velocity reduction due to fluid-structure interactions. It can also take input from high-fidelity circulation (and wave models to be used in the forcing function imposing loads on the aquaculture structure. Much of this work has been submitted as part of a manuscript (Knysh et al., 2022), but using data from the single line, Wood Island deployed AWAC instruments.

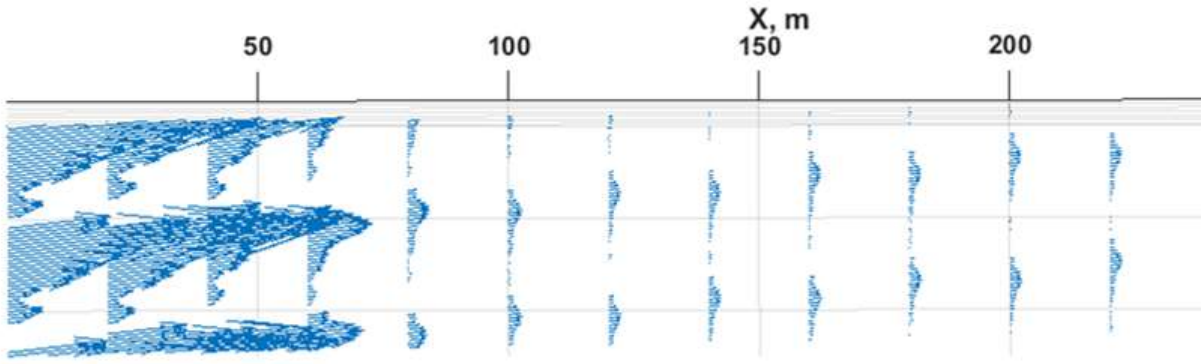

Figure 170: 1-Dimensional Momentum Balance for Current Reduction, Hydro-FE Upgrades—User-defined velocity in 4D (X, Y, Z, and t).

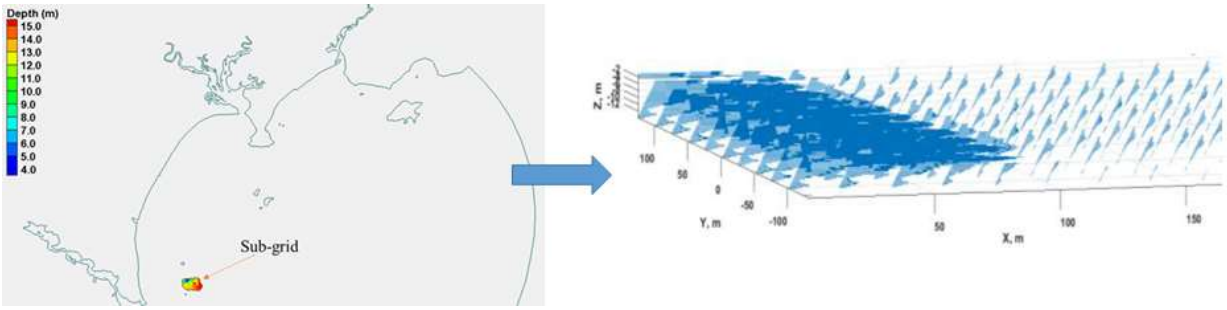

Figure 171: Integration of high-fidelity velocity and wave data from field measurements and ocean circulation and wave simulations.

2.5.4. Task 5.4: Perform Hydro-FE comparisons with field data (12/16/20)

This section summarizes the steps taken to compare Hydro-FE modeling results with field data. The first dataset utilized came from Wood Island instrument deployments in May 2018. With this dataset, Hydro-FE was used to conduct a nonlinear, time-domain dynamic simulation. The model geometry was based on the schematic of the Wood Island site shown in Figure 172. A mean water depth of 5.69 m was measured at the time of interest and was used in the model. During the field experiment, kelp was growing only on the western half of the longline. The kelp was modeled as 100 aggregated strands 0.46 m in length, 30 cm apart. No velocity reduction was applied in this situation and a slightly different set of drag-area coefficients were used. The different set of coefficients were used since the work of Fredriksson et al (2020) was still being finalized.

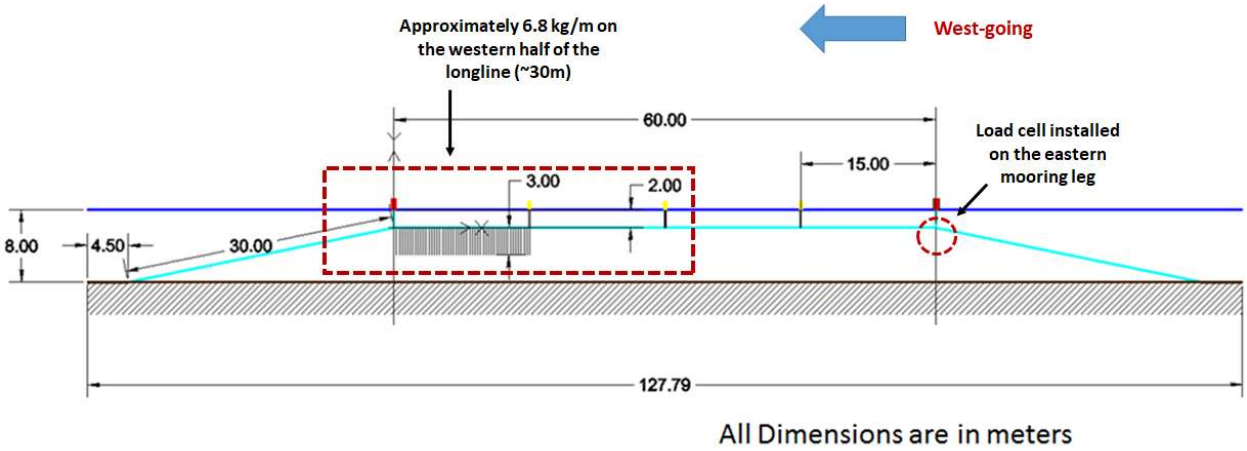

Figure 172. Wood Island Longline Setup. Differences between this schematic and the model included a water depth of 5.69 m (vs 8.0 m) and kelp length of 0.4623 m (vs 3.0 m), and the distance between anchors was 116.0 m (vs 127.8).

The boundary conditions consisted of applying gravity, buoyancy, and the Morison equation based hydrodynamic forces to all elements in the system. Zero displacement boundary conditions were applied to the nodes at the extreme ends of the anchor chains. The environmental conditions for this load case are provided in Table 29.

Table 29: Current Profile for validation load-case, 18-May-2018 01:20:00

Distance up	Depth	East-going	North-going	
5.7	0	-0.169	0.089	m/s
4.9	0.791	-0.169	0.089	m/s
4.4	1.291	-0.227	0.086	m/s
3.9	1.791	-0.268	0.111	m/s
3.4	2.291	-0.256	0.135	m/s
2.9	2.791	-0.255	0.133	m/s
2.4	3.291	-0.287	0.094	m/s
1.9	3.791	-0.282	0.116	m/s
1.4	4.291	-0.213	0.079	m/s

Figure 173 shows component 11 of stress (in Pa) in the deformed structure for the simulated case. Node 2025, corresponding to the load cell location, was queried for the 11 component of stress and converted to tension. The steady-state tension observed was 175 N (40 lbf). This value is compared with the mean measured tension in Figure 174. The agreement between the simulated and measured tensions. Further efforts will quantify the sensitivity of the predicted tensions to uncertainties in the as-deployed system configuration. This load-case provided valuable insight to the longline response for off-axis loading.

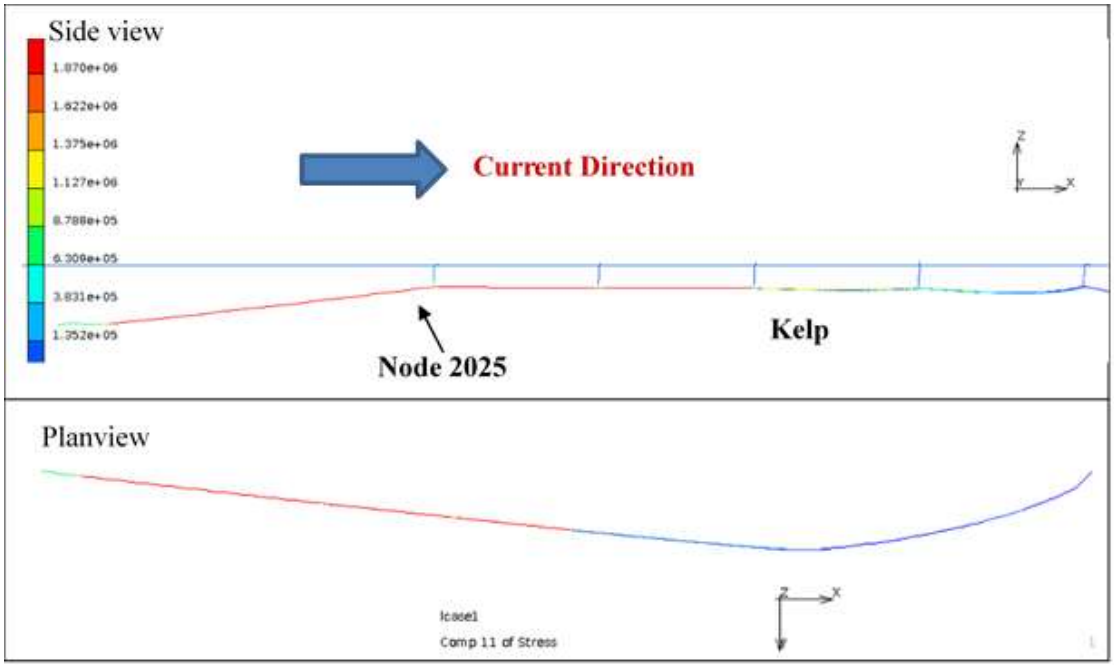

Figure 173: Contours of component 11 stress (Pa) in longline structure for the validation load case. The current is applied from left to right. Peak tension occurs in the mooring line on the eastern side of the structure.

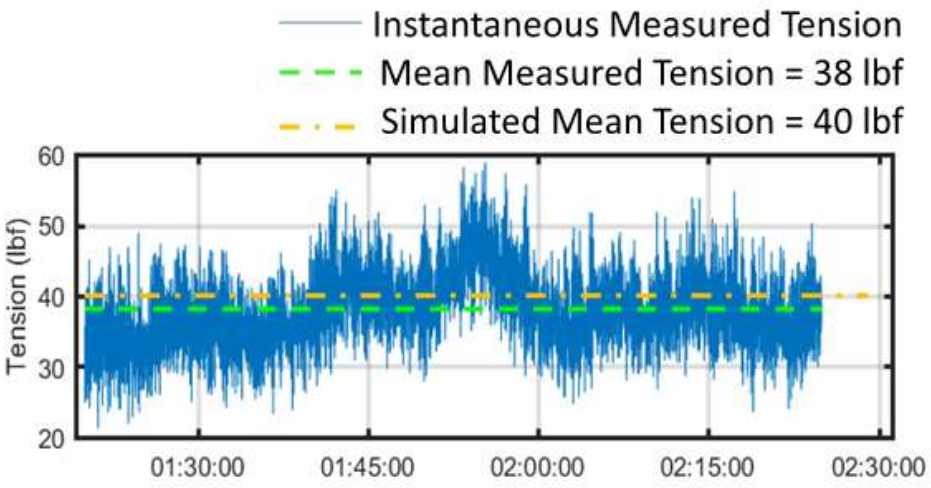

Figure 174: Hydro-FE simulated anchor line tension compared with mean measured tension.

These preliminary results show that the 1 m aggregate representation indicates promise of the modeling technique since the calculated values were close to those measured. The tension values, however, were extremely small, almost within the accuracy of the load cell. The effort did provide valuable experience with the field instrumentation sampling and the preliminary modeling approaches.

With the publication of Fredriksson et al. (2020), a more refined effort was pursued to validate the Hydro-FE modeling with the field data obtained from the single line system deployed at the Ram Island site and harvested in 2019. In general, the modeling approach utilized the drag coefficients derived from the tow tank experiments that varied with relative velocity. In this validation effort, simulations were conducted using the specific drag coefficients associated with the characteristic velocity for the five load cases. Recall, that field data from the load cells was collected in 30 min bursts, therefore the first 15 minutes was discarded due to potential warm-up effects that may appear when the system turns on. Thus, each validation load case was simulated for 15 minutes.

Mooring line tensions are influenced by both waves and currents. Waves are oscillatory and have both drag and inertia components as a function of wave velocity and acceleration, respectively. Wave inertia components are related to volume of the structure and are typically smaller than forces induced by wave drag for kelp aggregates. Oceanographic currents are steadier. Since drag is modeled as a function of velocity squared, it contains nonlinear oscillatory wave and steady current component that include interaction. While distinguishing these drag components in the numerical can be addressed (Fredriksson et al., 2005), it is however, difficult with field datasets.

Therefore, to compare the field datasets with the numerical model for the 5 load cases, an approach was taken to compare both mean and statistical maximum values. The statistical maximum values are defined as,

$$Statistical\ Maximum = mean + 2(standard\ deviation) \tag{54}$$

assuming a normal distribution. A percent difference calculation was performed with the measured dataset as the expected values.

The mean and statistical maximum results for the in-situ data and model results are compared in Figure 175. The results are superimposed on the west load cell time series burst from April 26-27, 2019. For comparison, also shown are two previously proposed methods of estimating loads on the culture line system. One method ("Rigid Rough Plate") is to treat the entire longline of kelp as a single, rigid, rough plate, and estimate the average drag using literature values for flat plates that account for surface roughness. These drag coefficients are for Reynolds number whose characteristic length scale is the length of the culture line. In this method the reference area is the length of the longline times the average length of the kelp blades. That is, the reference area is the outline area. This method critically underestimates mean mooring tensions also shown on Figure 175. The second method considered is similar, but the reference area in the drag calculation is the total surface area of all kelp blades on the line. This method dramatically overestimates mean mooring tensions. Finally, Hydro-FE was run without accounting for the momentum loss in the steady current. This approach tends to overestimate

mooring tensions. However, when the current speed reduction is accounted for using the 1-dimensional momentum balance approach described previously, the agreement between the numerical model and the field results is improved (Figure 176).

Notably, the statistical maximum mooring tensions and the field data include both low-frequency and wave-frequency contributions. Hydro-FE contains no ad-hoc or empirical physics to describe low-frequency oscillations. Therefore, the excellent agreement between the model predictions and the field observations suggests our approach of representing the hydro-/structural dynamics of the kelp and farm components in their most basic physics feasible and gives us broad predictive capabilities in assessing the performance of novel macroalgae cultivation systems.

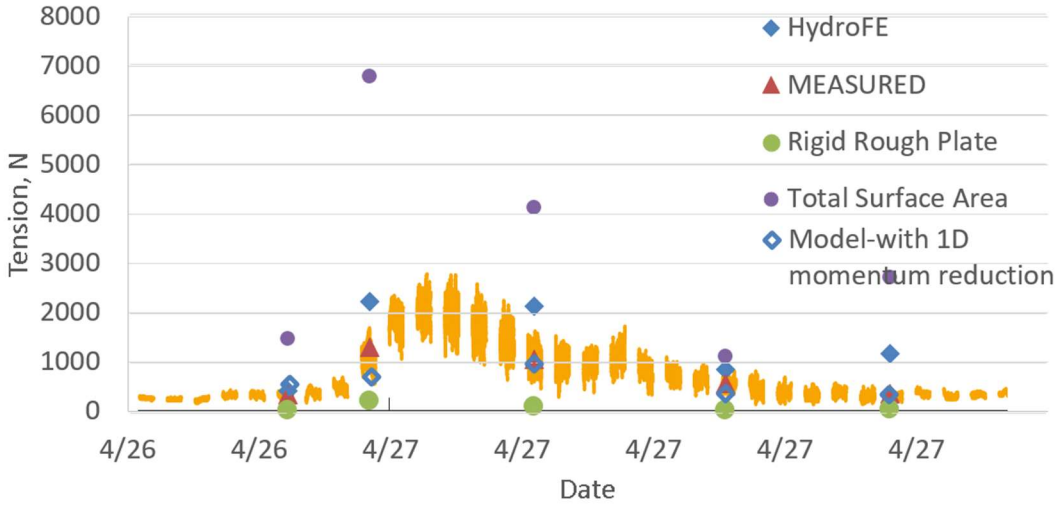

Figure 175: Mean mooring tension in Yellow (westward) mooring leg. Comparison of field data ("MEASURED"), with numerical model data ("Model-with 1D momentum reduction").

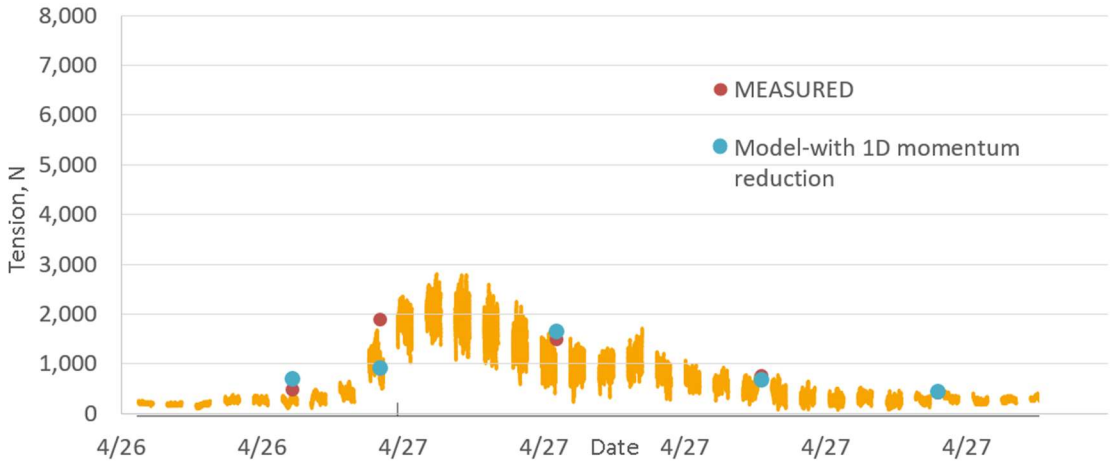

Figure 176: Statistical Maximum mooring tension in Yellow (westward) mooring leg. Comparison of field data ("MEASURED"), with numerical model data ("Model-with 1D momentum reduction").

The results of load case #2 are presented as detailed example since it is characterized as the highest current velocity condition and the highest load on the west side of the mooring. In this load case, the strong currents were flowing in the southeast direction with the waves coming from the east. One of the time steps of the Hydro-FE model for this load case is shown on Figure

177. An arbitrary box is also shown on the Figure representing the domain of fluid reduction applied in the model. With the currents going to the southeast, the model predicts sag on the east side of the system.

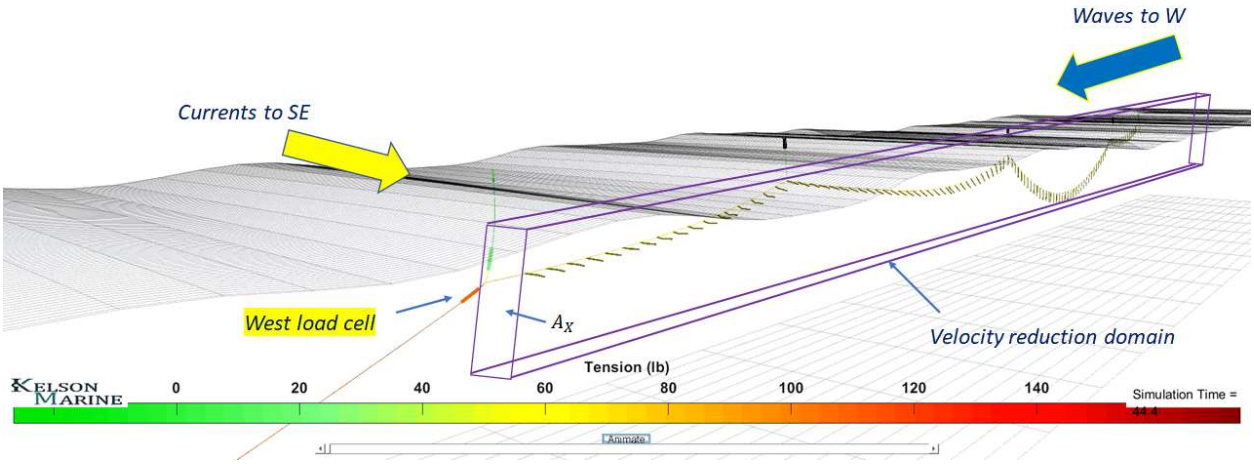

Figure 177: The Hydro-FE model for load case #2. For this load case, waves were going to the west and current to the southeast. A box representing the velocity reduction domain is also shown on the Figure. Note that tension units are present here as lbf.

The time series results comparing the load cell datasets with the Hydro-FE calculations for load case #2 are shown on Figure 178 (a) and (b), respectively. The mean, maximum and standard deviation values measured from the western side of the mooring matched well with those calculated. Some distinct differences, however, were evident. For example, the eastside mooring values from the in-situ datasets show a much higher mean tension than those obtained from the Hydro-FE. As shown on Figure 177, the eastside had subtantial sag, indicating how sensitive this aquaculture farm configuration is to geometry. Mean tensions measured on the actual farm had higher pretension values, as it was most likely stretched out more than the simulated version. Another distinct difference was found between the west side load cell and mooring time series results. The load cell measurments show the strong influence the 7 second waves, while the Hydro-FE model did not.

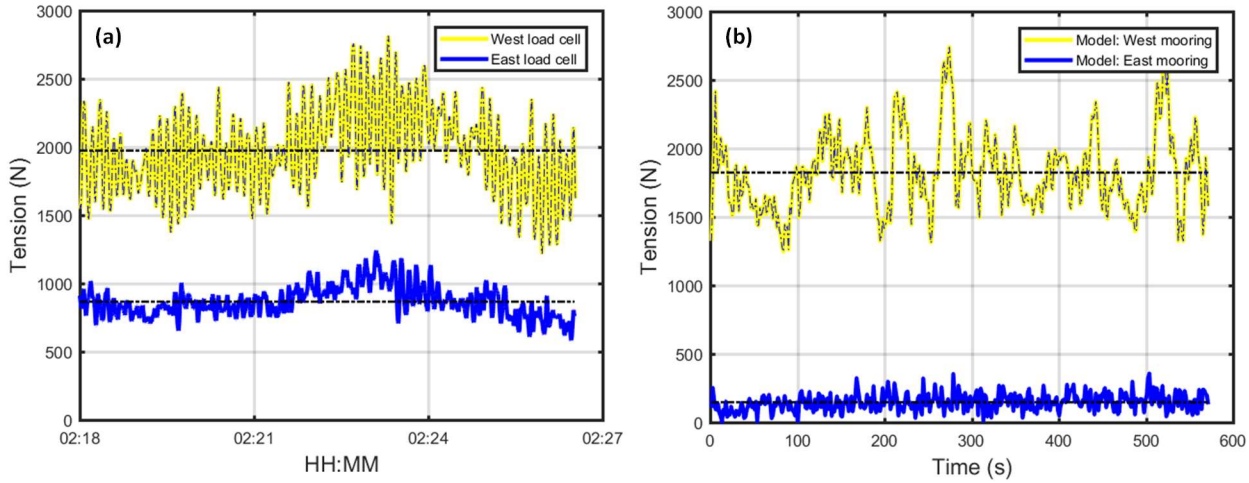

Figure 178: (a) The west and east side tension measurements for load case #2. (b) The west and east side tension results for load case #2.

2.5.5. Milestone 5.5: Validate Hydro-FE for single-line system scale (12/16/19)

The single-line validation effort was done comparing the mean and statistical maximum results for the five load cases. The results are summarized in Table 30. Since the purpose of Hydro-FE was to provide a design tool, maximum mooring line tensions were a key metric of interest. As the results show, the Hydro-FE with the 1D momentum balance predicted the loads in the western load cell under selected load cases within 15%.

Table 30: Measured tensions and tensions predicted with Hydro-FE.

	Current		Waves			Tide	Max Tension, N (Mean $+2\sqrt{m_0}$)			
Date	Cur. Speed, m/s	Cur. Dir, deg.	Hs, m	Tp, s	Dir., deg	Depth, m	Rigid Rough Plate	Total Surface Area	Model-HydroFE w MmtmBalance	OrcaFlex w MmtmBalance
4/26/19 22:15	0.26	250	1.3	6.0	97	16.5	108	3774	644	453
4/27/19 2:15	0.29	277	1.7	6.8	91	14.9	135	4323	2,468	2,630
4/27/19 10:14	0.19	242	1.8	7.4	92	16.7	60	2591	913	635
4/27/19 15:14	0.23	254	1.3	7.7	86	14.6	83	3196	526	403
4/27/19 18:14	0.20	268	1.0	7.5	89	14.8	62	2658	499	374
	Current		Waves			Tide	% Error			
Date	Cur. Speed, m/s	Cur. Dir, deg.	Hs, m	Tp, s	Dir., deg	Depth, m	Rigid Rough Plate	Total Surface Area	**Model-HydroFE w MmtmBalance**	OrcaFlex w MmtmBalance
4/26/19 22:15	0.26	250	1.3	6.0	97	16.5	-88%	303%	-31%	-52%
4/27/19 2:15	0.29	277	1.7	6.8	91	14.9	-95%	65%	-6%	1%
4/27/19 10:14	0.19	242	1.8	7.4	92	16.7	-94%	168%	-6%	-34%
4/27/19 15:14	0.23	254	1.3	7.7	86	14.6	-83%	542%	6%	-19%
4/27/19 18:14	0.20	268	1.0	7.5	89	14.8	-87%	445%	2%	-23%
								RMS Error:	**14.6%**	**30.8%**

Also shown in Table 30 are comparisons using a rigid rough plate model, a total surface area model and a comparison with OrcaFlex using the same momentum balance approach. The Hydro-FE model as this stage is performing better than the off-the-shelf OrcaFlex model. The Hydro-FE modeling details are being formulated into a follow-on manuscript to Fredriksson et al. (2020).

2.5.6. Task 5.6: Develop scalable model for planar-type system

With the field sampling of the kelp biomass for the 2021 growing season complete, a numerical model of the 5-line array was built to match the as-installed, in-situ conditions. The model is shown on Figure 179. The validation datasets obtained from the AWACs and load cells are also complete and seven load cases were processed for validation. This Task will be completed as part of the project, “A validated finite element modeling tool for hydrodynamic loading and structural analysis of ocean deployed macroalgae farms, using open-source tools."

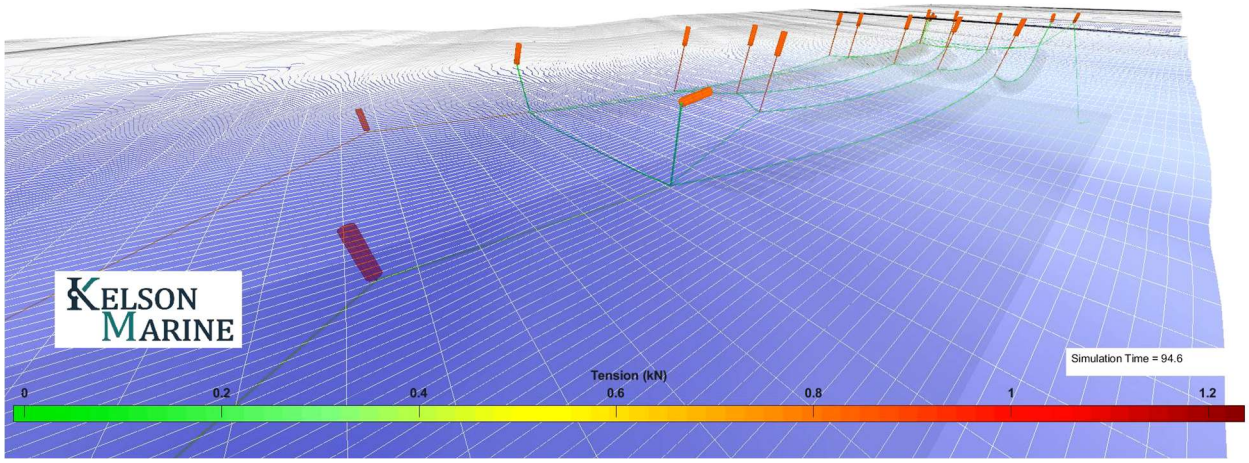

Figure 179:Numerical model of 2020 – 2021 five-line array at Ram Island site.

2.5.7. Task 5.7: Perform Hydro-FE comparisons of the array system with field data

This Task will be completed as part of the project, “A validated finite element modeling tool for hydrodynamic loading and structural analysis of ocean deployed macroalgae farms, using open-source tools" by Kelson Marine.

2.5.8. Milestone 5.8: Validate Hydro-FE for planar-type systems

This Task will be completed as part of the project, “A validated finite element modeling tool for hydrodynamic loading and structural analysis of ocean deployed macroalgae farms, using open-source tools" by Kelson Marine.

2.5.9. Milestone 5.9: Develop modeling techniques for hectare-sized systems

Work has been done to develop modeling techniques for hectare-sized system. Part of the strategy was to utilize Task 7 to become involved with the Category 1 projects for designing these larger systems by leveraging the work in the Category 3 project. While screenshots are provided, the modeling techniques are not. Again, this Task will be completed as part of the project, “A validated finite element modeling tool for hydrodynamic loading and structural analysis of ocean deployed macroalgae farms, using open-source tools" by Kelson Marine. Screenshots of the Ocean Rainforest, Marine Bioenergy, Trophic, and University of Alaska farm systems are shown here.

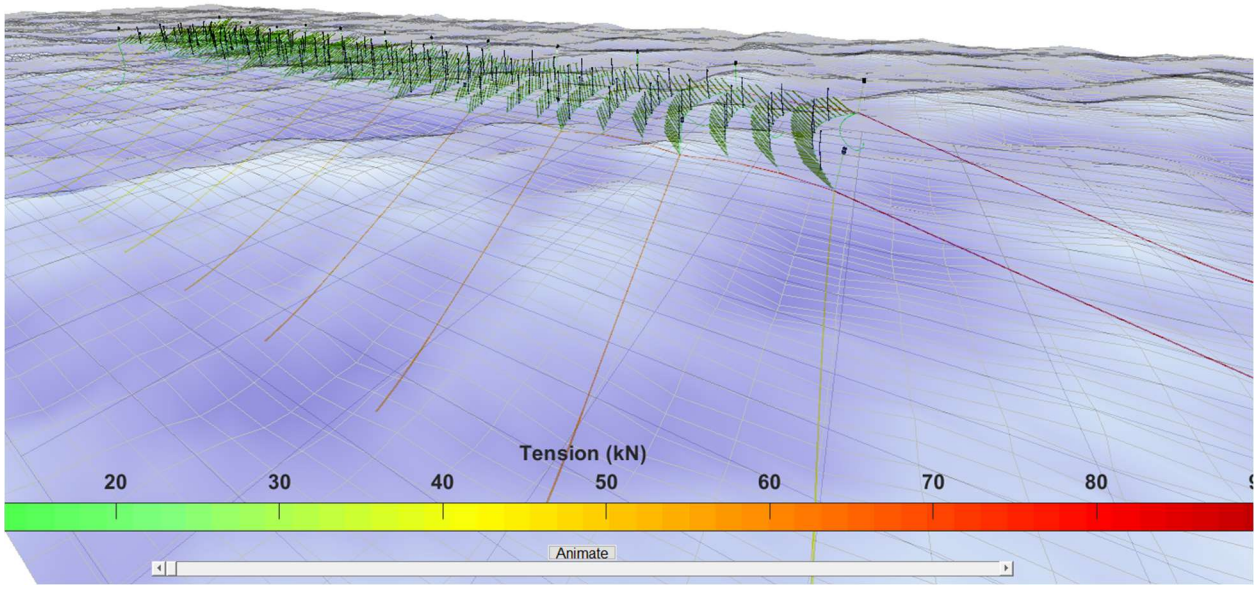

Figure 180: Ocean Rainforest farming system.

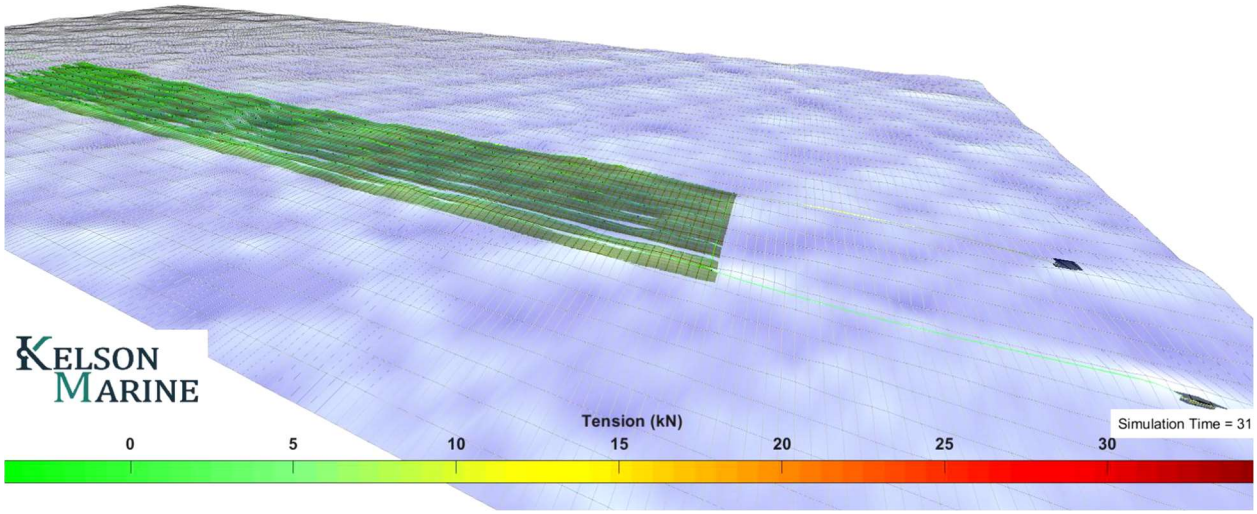

Figure 181: Marine Bioenergy farming system.

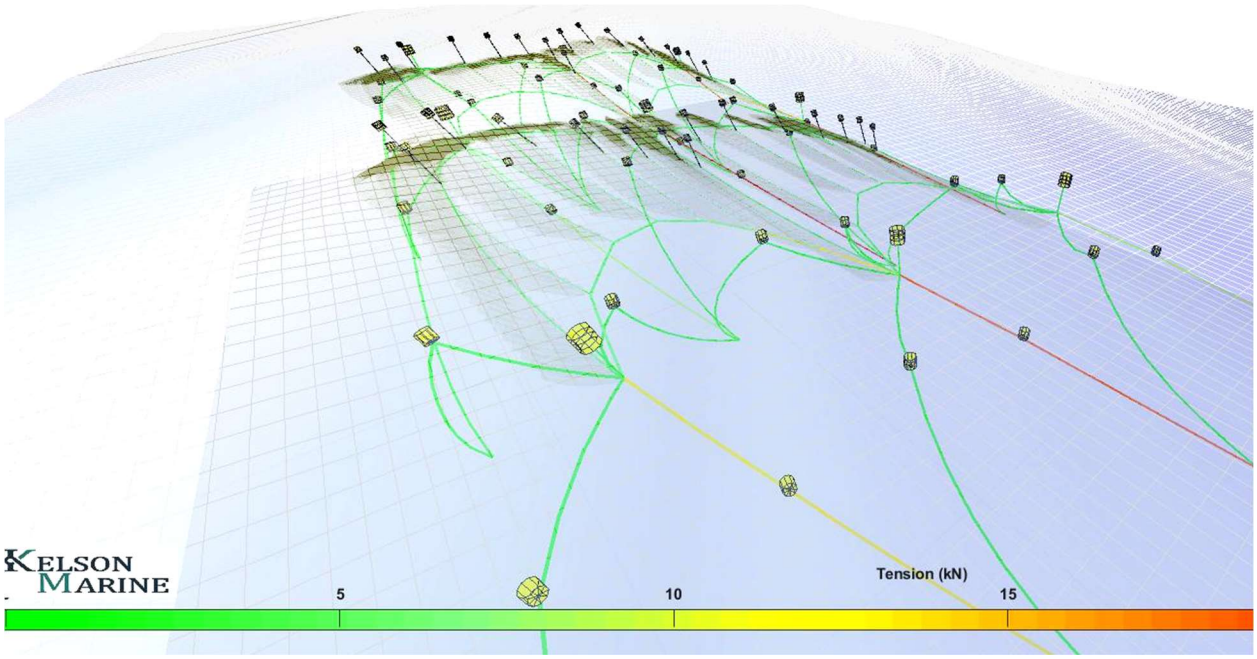

Figure 182: Trophic farming system.

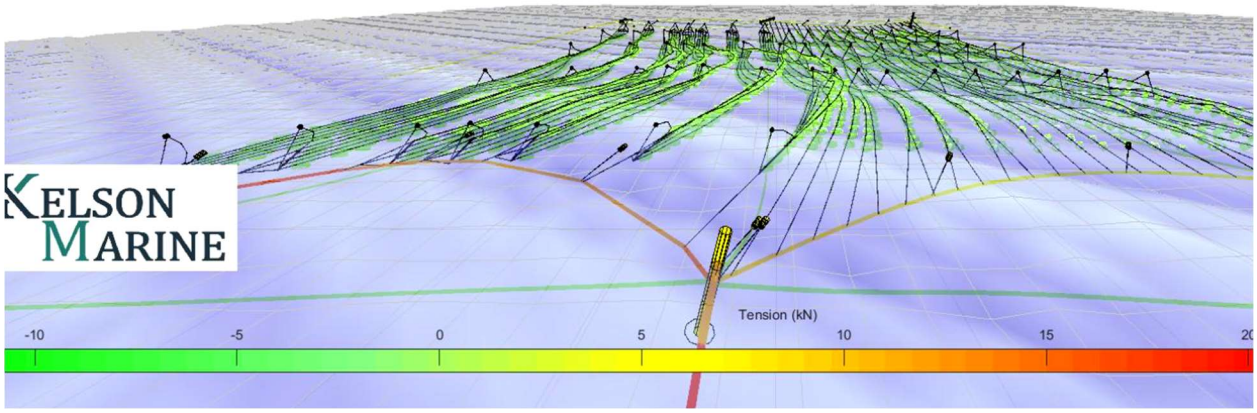

Figure 183: University of Alaska farming system.

2.6. Task 6.0: Interact with NOAA on permitting

This task was included as an opportunity to communicate efforts being conducted with NOAA, Office of Aquaculture to develop technical guidance for culture systems in Federal waters. During this project, team members completed a set of technical guidelines for finfish aquaculture for the Gulf of Mexico was completed and published as a NOAA Technical Memorandum (Fredriksson and Beck-Stimpert, 2019). This document is available at https://repository.library.noaa.gov/view/noaa/19836.

Also, during this project, a group of Mariner engineers convened to discuss applicant safety factor and risk levels to be used in the design process for macroalgae systems. A report was submitted to the ARPA-E program titled: Design Criteria for Offshore Macroalgae Growing Systems by David W. Fredriksson (USNA), Tobias Dewhurst (MMC), Zach Moscicki (UNH) and Corey Sullivan (UNH). Our intent was to build upon the draft technical guidelines for the Gulf Plan to have addition information for macroalgae type systems.

Collaborative work with the NOAA Office of Aquaculture has leveraged datasets acquired through this Cat 3 project. Members of this team have started to work with NOAA to examine potential whale impacts with kelp grow-out gear. Datasets obtained during the May 2019 field effort (Task 4) was presented at an Entanglement Workshop at the NOAA Southwest Fisheries Science Center. The MARINER dataset (Figure 184) shows how the mooring line tension time-series can be resolved showing the influence of tides, tidal currents, waves and the attachment of the 36 ft research vessel. The research vessel could be analogous to a large marine mammal. By understanding how the source of the forcing mechanisms, the team is pursuing developing an instrument that could perhaps detect a whale impact. The work associated with this task is ongoing.

Work done with the Category 1 Trophic/UNH team showed the numerical modeling approach developed and validated by this Category 3 team was used to help design the Trophic Phase II prototype. Besides evaluating design alternatives to find suitable mooring line lengths, anchor leg configurations, and longline and structural line geometries, the numerical model was applied within a design-of-experiments approach. Whereas the initial design resulted in the anchor capacity being exceeded during a worst-case 25-year storm (safety factor of 0.8) this design approach resulted in a system with a predicted anchor safety factor of 2.0 for the same anchors, while keeping eight of the twelve desired grow out lines (Table 31). The intent was to formulate these techniques to further develop engineering guidelines.

Members of the team have also collaborated with a NOAA Entanglement Prevention group assisting in the development of the Whale Simulator model. Part of this work was to examine the response of rope aquaculture systems to the impact of large marine mammals. The interaction is being investigated by examining the kinetic energy of the whale to the potential energy response of the mooring system. Impact tank tests are being conducted at the USNA to understand the horizontal stiffness of the mooring system using a range of submersible flotation elements. The aquaculture system used in the tests was representative of the single line system show in Figure 20. A screen-shot of the model whale during impact on the cross-tank line is shown in Figure 185.

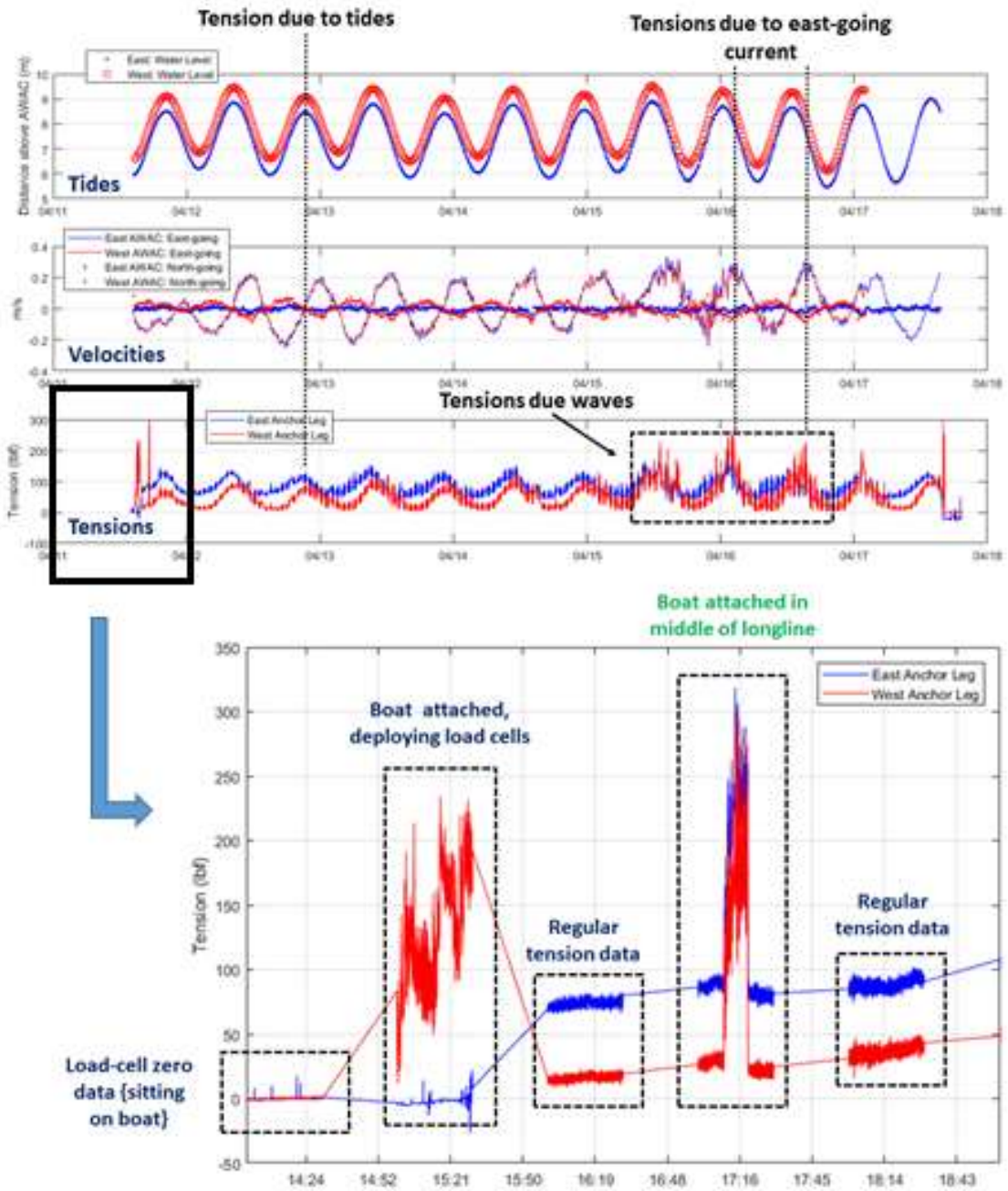

Figure 184: An example of how the mooring line tension time-series can be resolved showing the influence of tides, tidal currents, waves and the attachment of the 36 ft research vessel. The research vessel analogous to a large marine mammal.

Table 31: Performance of the Trophic Phase II prototype before model-based design (November 2019) and after (March 2020).

	Nov. 2019	March 2020
Operations		
All node buoys visible in 95% conditions	Yes	Yes
Safe tensions for harvest operations at low and high tide	No	Yes
Slack lines eliminated	Yes	Yes
Survival		
Extreme scenario defined from statistical analysis of ocean data	Estimated	Yes
Mooring lines meet specified safety factors	Yes	Yes
Anchors meet specified safety factors Safety Factor	No 0.8	Yes 2.0
Prevent cascading failure	No	Yes
Performance		
Number of grow-out lines supported	12 lines	8 lines

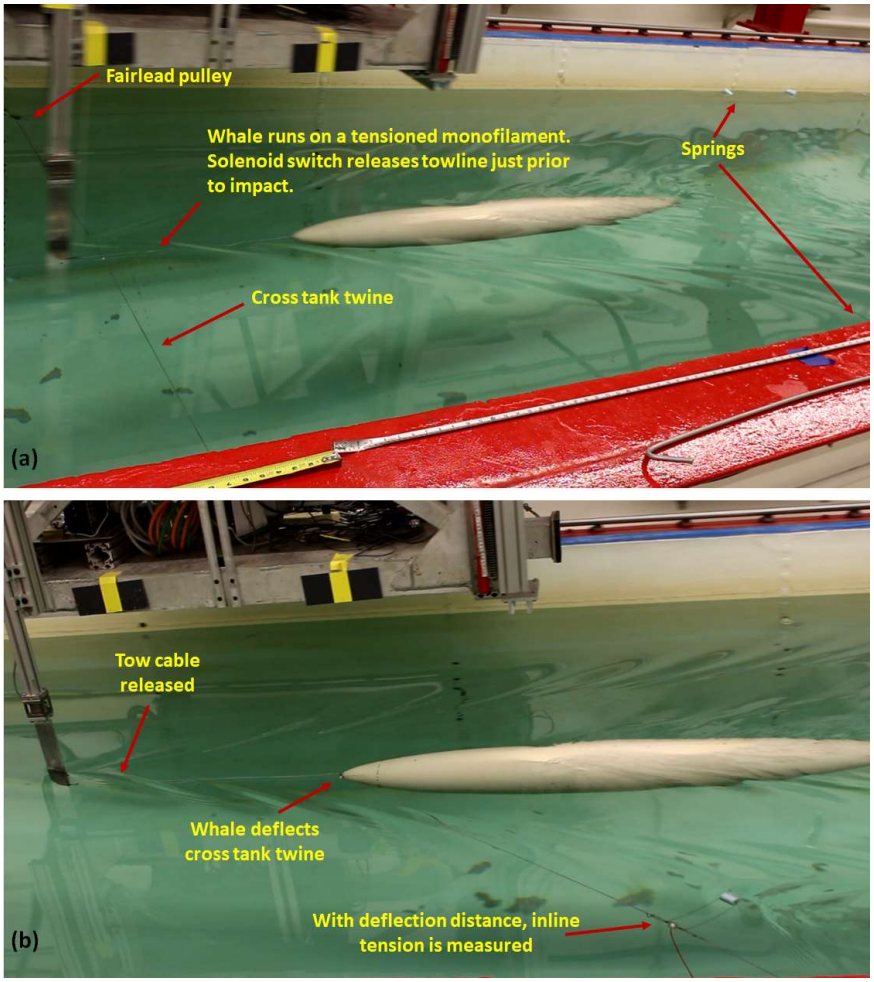

Figure 185: (a) Conducting an impact test prior to the whale hitting the cross-tank twine. (b) After impact, the whale deflects the twine with inline tension measured with a submersible load cell.

2.7. Task 7.0: General Outreach

In the four years of this project, numerous outreach efforts were made communicating the knowledge that has been acquire. This section highlights, many of these initiatives.

On November 14, 2018, as a representative of the Mariner Team and UNE School of Marine Programs, Liz Johndrow visited the Frank H. Harrison Middle School in Yarmouth, ME to assist students in the seventh grade in launching their own kelp nursery. Students were introduced to techniques used to initiate nursery cultures including the preparation of wild sorus tissue, the extraction of active kelp spores and the settlement of the spores on the cultivation spools. The lesson emphasized important topics involving kelp's life cycle, how water quality can affect marine organisms, and the many benefits of kelp. After the initial kelp spores were generated, Liz was a source of contact for all of the student's husbandry needs. With the help from Mariner project and support from UNE, the class was successful in cultivating their first spool of kelp and out planted it with the help of industry partner Madeleine Point Oysters in Yarmouth, ME.

Later the same month (November 20, 2018), Liz deployed a small-scale kelp farm off Peaks Island, ME to help support the Kelp4Kids initiative program. Kelp seed from the Mariner program was donated to supplement the program for elementary school students from this island community. The Kelp4kids program teaches concepts about kelp aquaculture, marine ecology, and water quality. On this project, Liz worked with high school student Darcy Ross from the Baxter Academy in Portland, to designed a three-tiered system utilizing 100ft of seed in 15ft of water. The system was harvested in June 2019.

On April 17, 2019, after applying for the Experimental lease from DMR, there was public interest from members of the City of Saco for more information on the field efforts. The City Board Planner and Director of the Parks & Rec. Department desired a better understanding of seaweed aquaculture and the goals of the MARINER project. The Mariner team invited the Saco city members to take a trip to the Ram Island Farm to recover 2 AWACs and 2 Load-cells as well as collect biological samples. Both visitors were fascinated by the instrumentation and potential positive effects the project could create. There were no other inquiries or hindrances in the leasing process.

A Maine Public Broadcasting Network, Maine Spring Live: Wildlife, Nature, and You episode on April 26, 2019 featured Liz Johndrow taking part in educational outreach with the Yarmouth Middle School. See video below.

https://video.mainepublic.org/video/maine-spring-live-wildlife-nature-and-you-o8kboo/

During the eventful Seaweed Week (May 1, 2019) hosted throughout the state, UNE campuses participated by collaborating with Sodexo food distributors. To highlight the combined efforts, Liz Johndrow collected mature Sugar Kelp from the Saco Bay Farms and set up a booth in the Biddeford campus dining hall. Fresh kelp was available for the community to experience and taste, as a raw product and in a number of kelp smoothies made for the event.

On May 15, 2019, the UNE team collaborated with Woods Hole Oceanographic Institution collaborated in Saco Bay with various kinds of instrumentation. The UNE team focused on

deploying 2 AWACS, 2 Loadcells, 1 TCM-1 and 2 accelerometers while WHOI deployed their JetYak and Blue ROV over the Wood Island Farm.

Liz Johndrow (again) worked with industry partner Bangs Island Mussels to harvest three longlines of skinny kelp in Casco Bay, ME on May 23, 2019. With a total of 4 crew members including President Matt Moretti, a total of 14,600 lbs was harvested, cool stored, and transported to shore. Immediately upon arrival at the wharf Atlantic Sea Farms was there to accept the crop and start processing the fresh product for future kelp products. Collaborating with growing aquaculture businesses in Casco Bay, ME provides the MARINER team with better insight towards current industry struggles and obstacles faced by farmers in our surrounding waters.

2.7.1. Task 7.1: Meet with Cat 1 projects (8/15/18)

One of the primary goals of this Category 3 project was to develop numerical modeling techniques to enhance the design of hectare size kelp farms. Therefore, as part of this task, the UNE team interacted with five of the Category 1 teams to understand the difference approaches being pursued for each project. The Category 1 teams are listed below.

- Category 1: University of Alaska/Woods Hole Oceanographic Institution
- Category 1: University of S. Mississippi – Adustadepth
- Category 1: University of S. Mississippi – SeaweedPaddock
- Category 1: Trophic
- Category 1: Catalina/Ocean Rainforest

In addition to the Category 1 teams, we also interacted with the Category 4 team from the Woods Hole Oceanographic Institution and the Category 3 team from the Pacific Northwest National Laboratory.

2.7.2. Milestone 7.2: Identify Cat 1 modeling requirements (3/31/19).

In this early stage of the project, the University of Alaska team performed techno-economic analysis (TEA) on multiple grow out configurations as shown on Figure 186(a) through (d). Since the capital cost are related to the configuration characteristics, numerical models of each design were built. The models were constructed to have nearly the same amount of culture line in each geometric configuration to normalized comparisons as shown on Figure 187(a) through (d). System details are provided in the Category 1 reports.

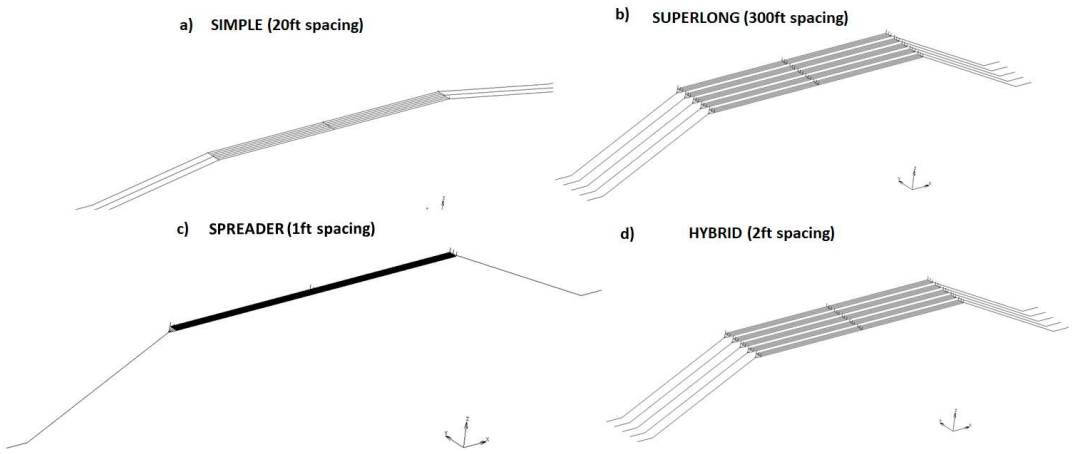

Figure 186: Numerical models were built based four geometric configurations.

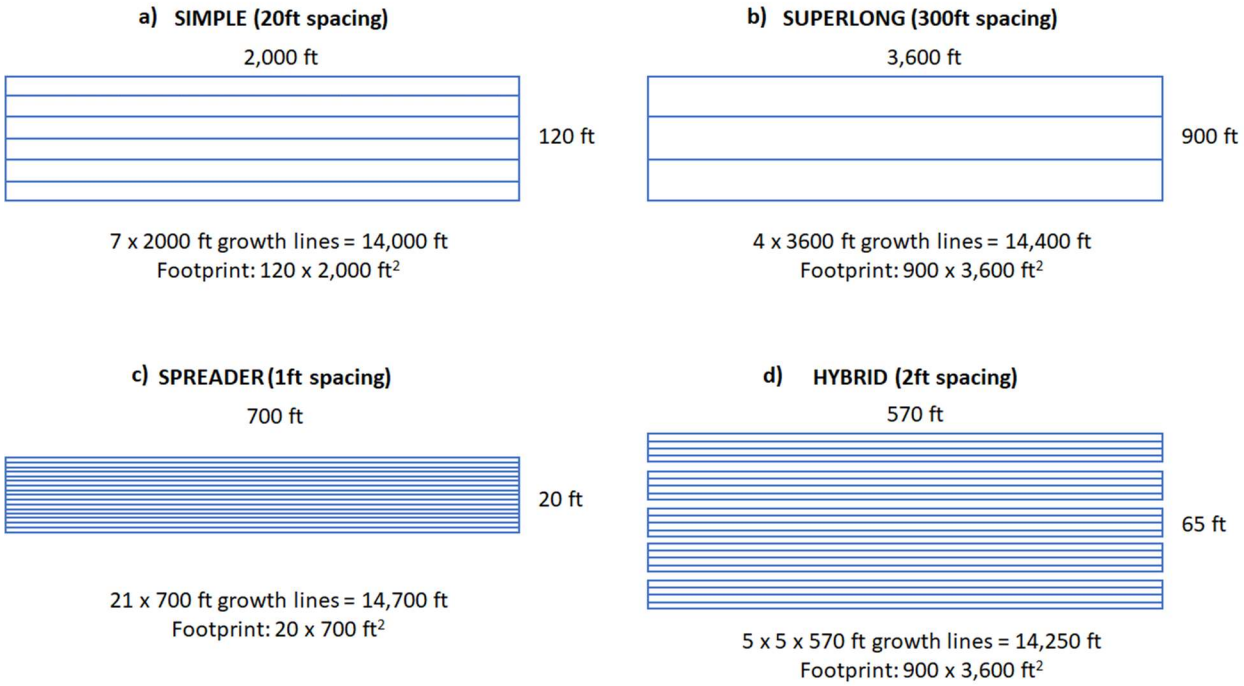

Figure 187: The models were constructed to have the same amount of culture line in each geometric configuration to normalized comparisons.

In August, 2018, collaboration with the Alaskan Category 1 team focused on identifying Hydro-FE load case scenarios in support of the TEA effort to investigate farm configurations that optimizes tradeoffs between biomass yield and component costs. A candidate array system is shown in Figure 188 where 20 modules make up an array.

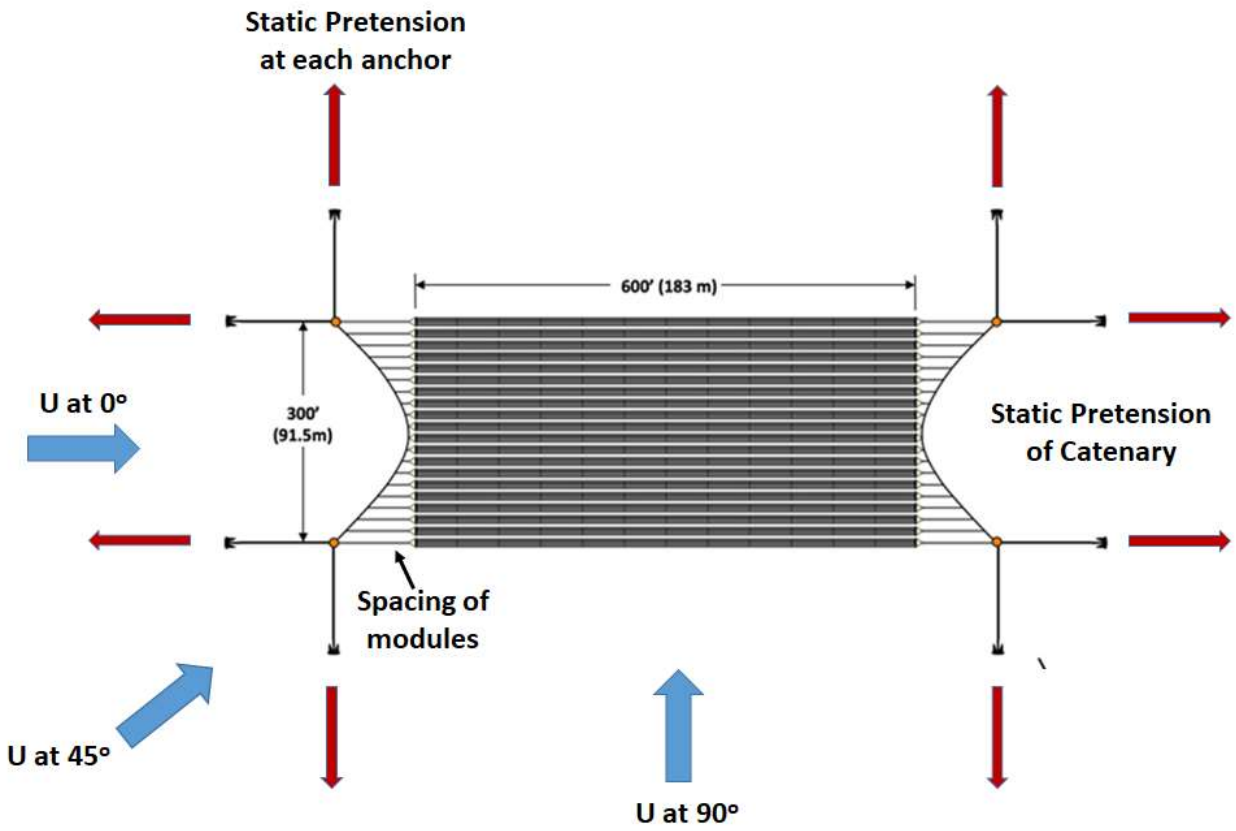

Figure 188: A candidate macroalgae farm where twenty modules form an array system.

In this particular design, each module consisted of five longlines with 0.76 meter spacing (Figure 189). It is important that the longline and module spacing is determined to minimize entanglement and macroalgae growth interaction, and to facilitate the efficient connection/disconnection of sets of longlines with the catenary during planting and harvesting. Ideally, farm boats will handle 10 longlines at a time. The parameters considered to optimized configuration include:

- Wave and/or current characteristics
- Wave and/or current direction
- Pretension of anchors (flotation at corners)
- Pretension value in the catenary determined by #3.
- Pretension in the longlines
- Length of the module (therefore longline)
- Type and characteristics of cross-member
- Bending resistance of longline (if a member other than rope is used).

With this information, an updated Hydro-FE model of the system was developed based on the configurations shown on Figure 189 and Figure 190. This prototype design included a 10ft spreader bar with 5 culture lines. The system was analyzed using Hydro-FE numerical model to estimate its behavior in a storm condition with a 1yr return period.

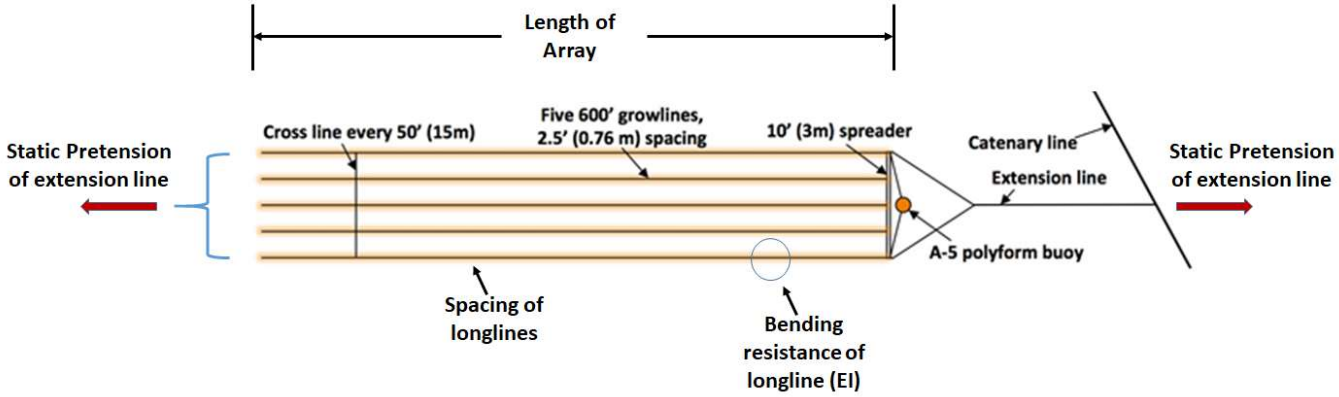

Figure 189: An example module consisted of five longlines.

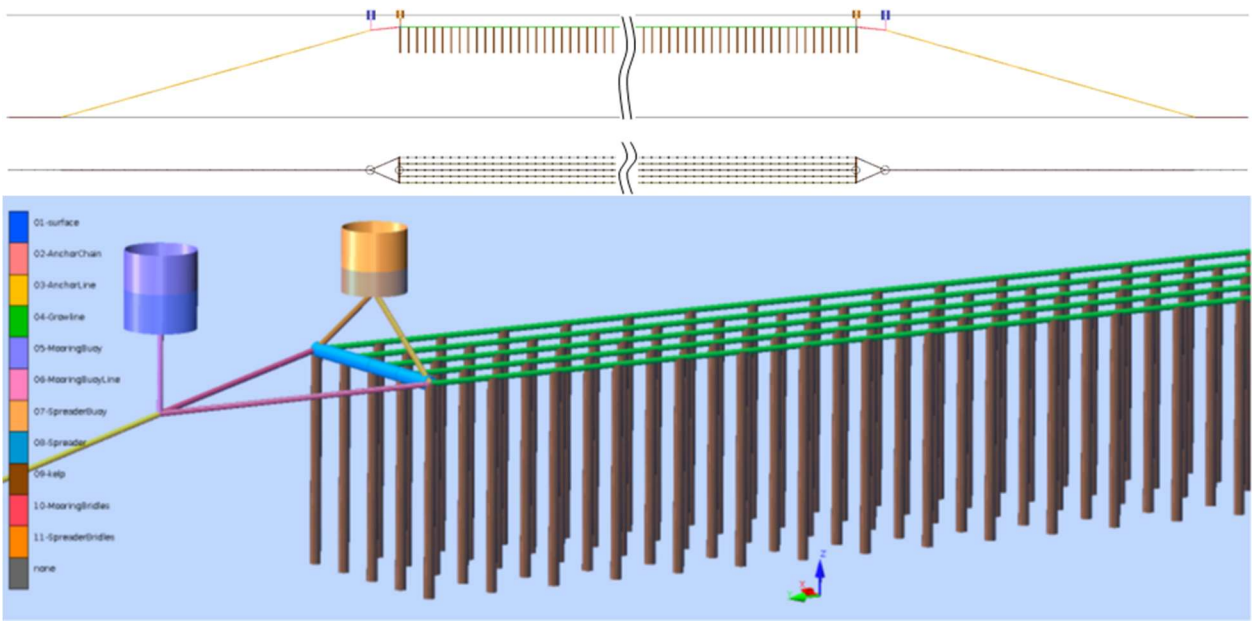

Figure 190: A Hydro-FE model of the spreader system being considered for the TEA analysis.

The first set of simulations were carried out with a goal to evaluate the hydrostatic properties of the farm in still water (depth of 12m, no waves and no currents). This step was needed to understand the interplay between the geometric layout and the selection of the flotation elements in the steady state. Three different configurations were chosen based on the proposed design specifications. Each of the configurations was simulated with no pretension, and full pretension and two mass density levels macroalgae (2.5% and 7.5% heavier than seawater). This was done to evaluate the model sensitivity to these input parameters. Overall, each configuration was run as 2x2 matrix of variants for 12 simulation cases. The configuration details are provided in Table 32.

Table 32: Hydrostatic configurations analyzed in the sensitivity study.

#	Configuration	Details	Total buoyancy	Reserve buoyancy
1	1xA7-1xA7	613 kgf corner buoys, 613 kgf spreader buoys	2454 kgf	1126 kgf (46%)
2	2xA7-2xA7	1226 kgf corner buoys, 1226 kgf spreader buoys	4944 kgf	3617 kgf (73%)
3	1xA7-2xA7-1xA7	613 kgf corner buoys, 1226 kgf spreader buoys 613 kgf midpoint buoy	4312 kgf	2984 kgf (69%)

The environmental scenarios were then chosen as storm conditions with a 1 to 2 year return period for two cases in which the 1) farming unit is deployed in E-W orientation and the 2) farming unit is deployed in N-S orientation. In each configuration, the wave profile was modeled as incoming from the S direction with 4m significant wave height and 10s period using JONSWAP spectral model (Figure 191). The current profile was modeled as incoming from the W direction with a linear ramp profile having a velocity of 0.45 m/s at the seafloor increasing to 0.6 m/s at the surface. An example of deformed configuration is presented in this section.

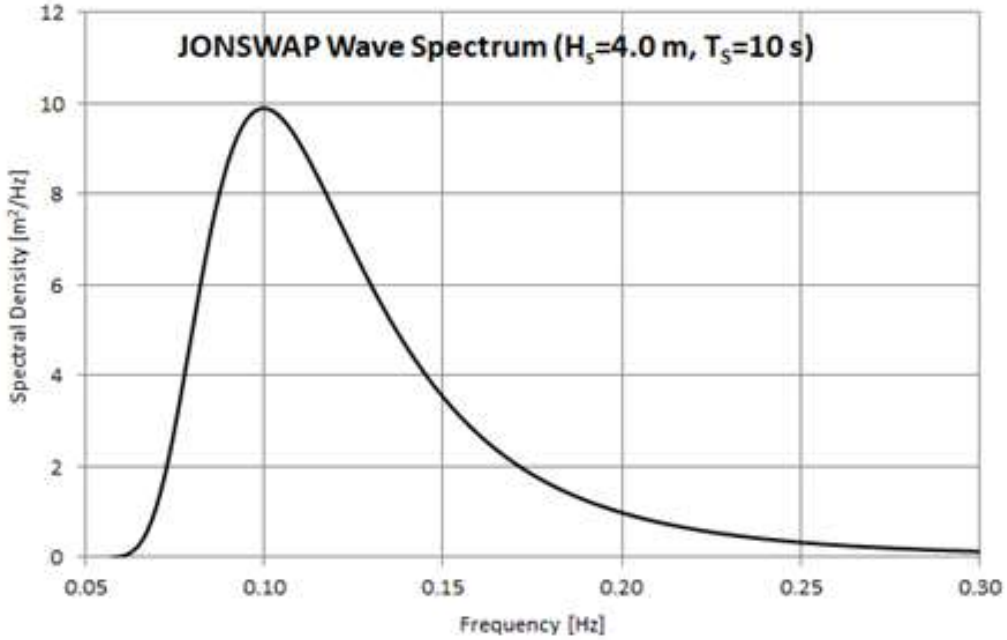

Figure 191: Visualization of the wave spectrum (JONSWAP model) used in 1-yr storm simulations.

It was observed that configurations #1 (1xA7-1xA7) and #2 (2xA7-2xA7) were sensitive to the perturbations of both model parameters and demonstrate poor performance with sagging culture lines with the midpoint too deep from the waterline in 3 out of 4 variants. Configuration #3 exhibited lower sensitivity to input parameters and overall good performance in both

tensioned variants. Based on this analysis, we chose to modify the prototype design to incorporate a midpoint buoy and used this configuration for further studies.

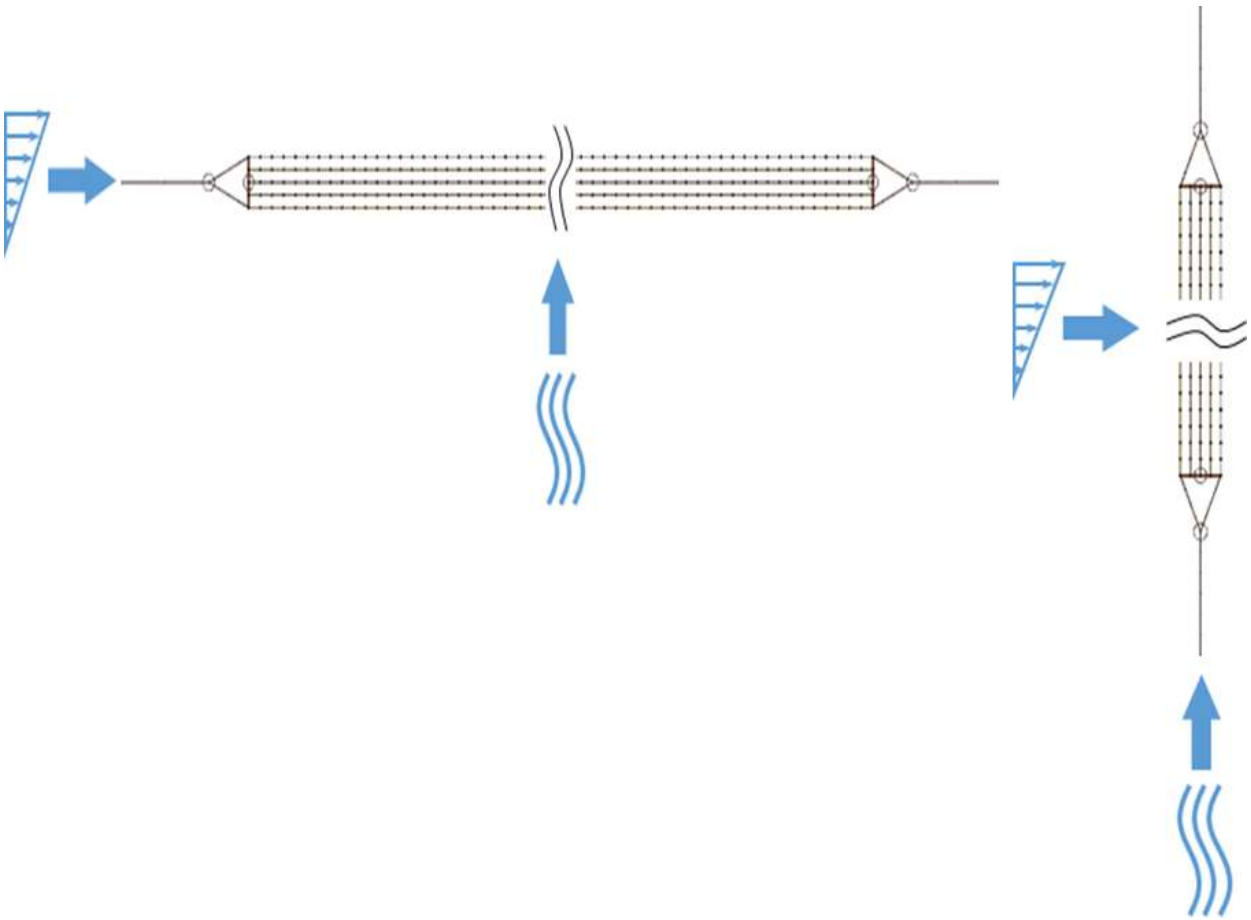

Figure 192: Simulations were performed for two-cases. Case #1 (left) had the currents in-line with anchor placement with waves at a 90-degree angle. Case #2 had the waves in-line with the anchor placement and currents at a 90-degree angle.

A summary of these project results is shown in Figure 193 that include line tension values and stresses in the header pipe.

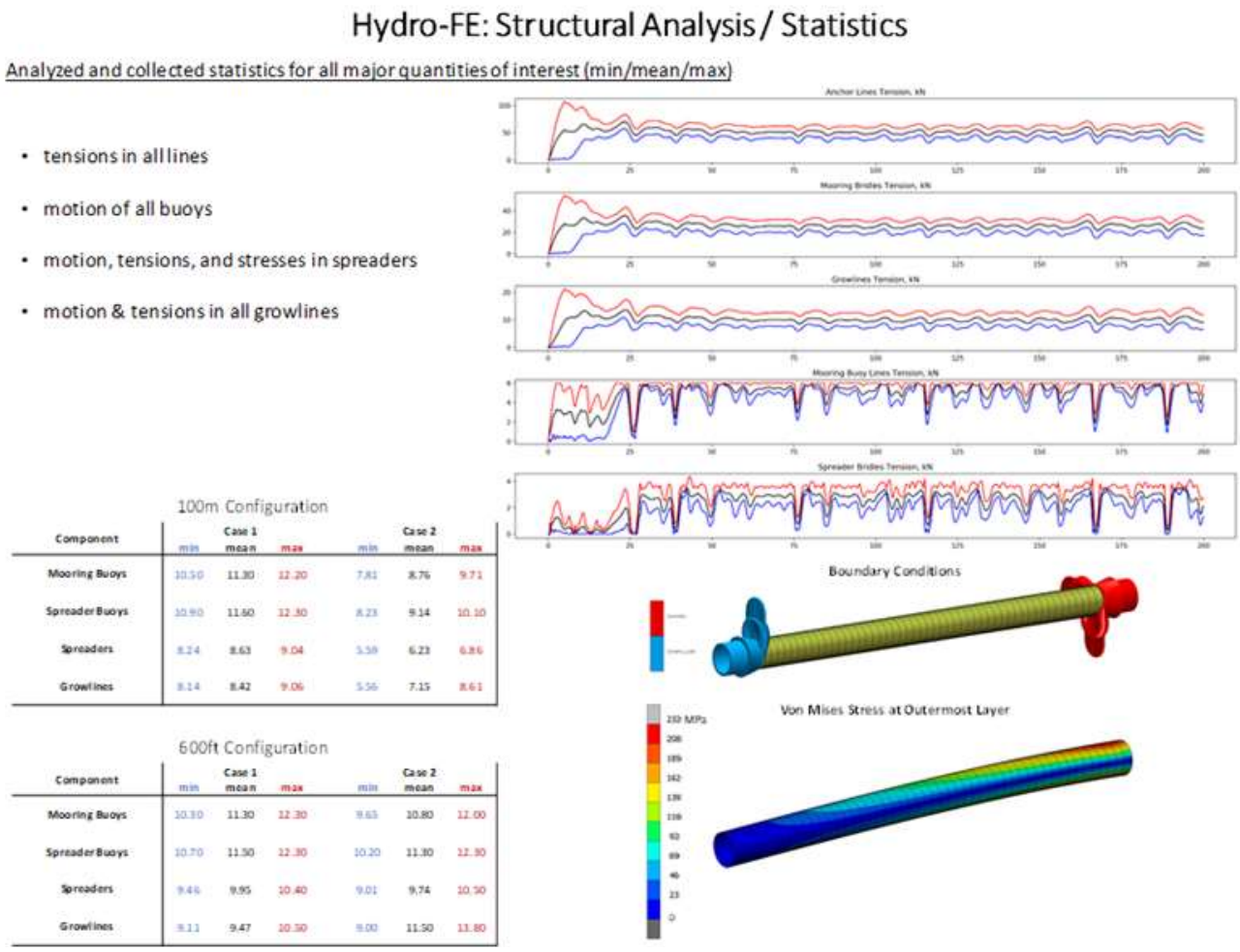

Figure 193: Summary of the simulation results and post-processing procedure to identify maximum loads/displacements/stresses in the considered system.

Work on the Category 1 project, SeaPaddock was done during the Phase 1 part of the project. During this time, the modeling team interacted multiple times a month with the researchers at the Universities of Southern Mississippi (USM) and New Hampshire (UNH) to develop numerical model of the SeaPaddock system. The preliminary engineering designs of the system were provided to build the model. The system consists of individual sections of vertical netting (Figure 194a) connected into a continuous length (Figure 194b) with the ends attached (Figure 194c). The initial finite element model of the system is shown on Figure 194d. The system has no horizontal structural members and therefore maintains its shape using external towing vehicles. At this stage, the structural model was built using the consistent net element described in Tsukrov et. al., (2003) and incorporated in the Hydro-FE program. Part of the analysis was to simulate forces due to the towing vessels in stationary and maneuvering configurations. Note that the numerical model was built without visualization additions so only the nodes and the elements are shown. In addition, when modeling with the consistent net element, not all of the individual twines are modeled for computational efficiency purposes.

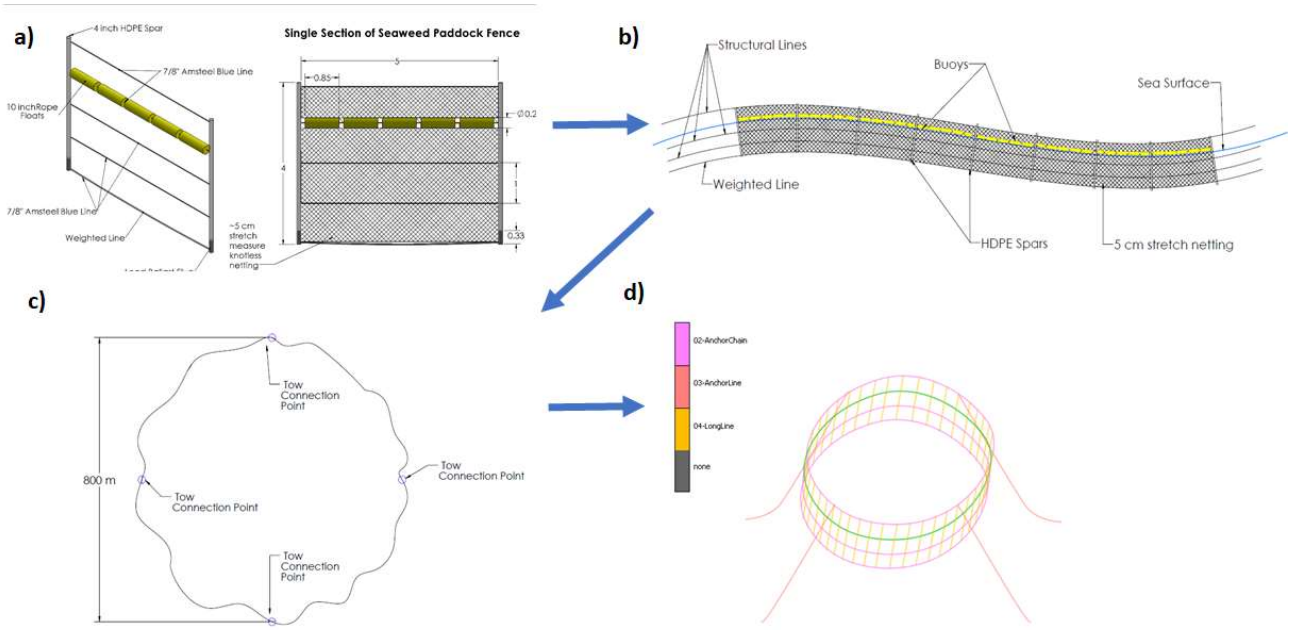

Figure 194: At the time, the Seaweed paddock design incorporated sections of vertical nets (a) combined into a continuous length (b) and connected at the ends (c). The numerical model representation is shown on (d).

The numerical model was used to simulate the system response in the storm and operational conditions with 6 load cases. The results were processed to obtain the load/displacement time series, which were analyzed to extract the extreme values. A summary of the Seaweed Paddock design results is shown on Figure 195. The system presently incorporates sections of vertical nets combined into a continuous length and connected at the ends. The optimization of the towing shape and the example of displacement/tension time series are provided in Figure 195.

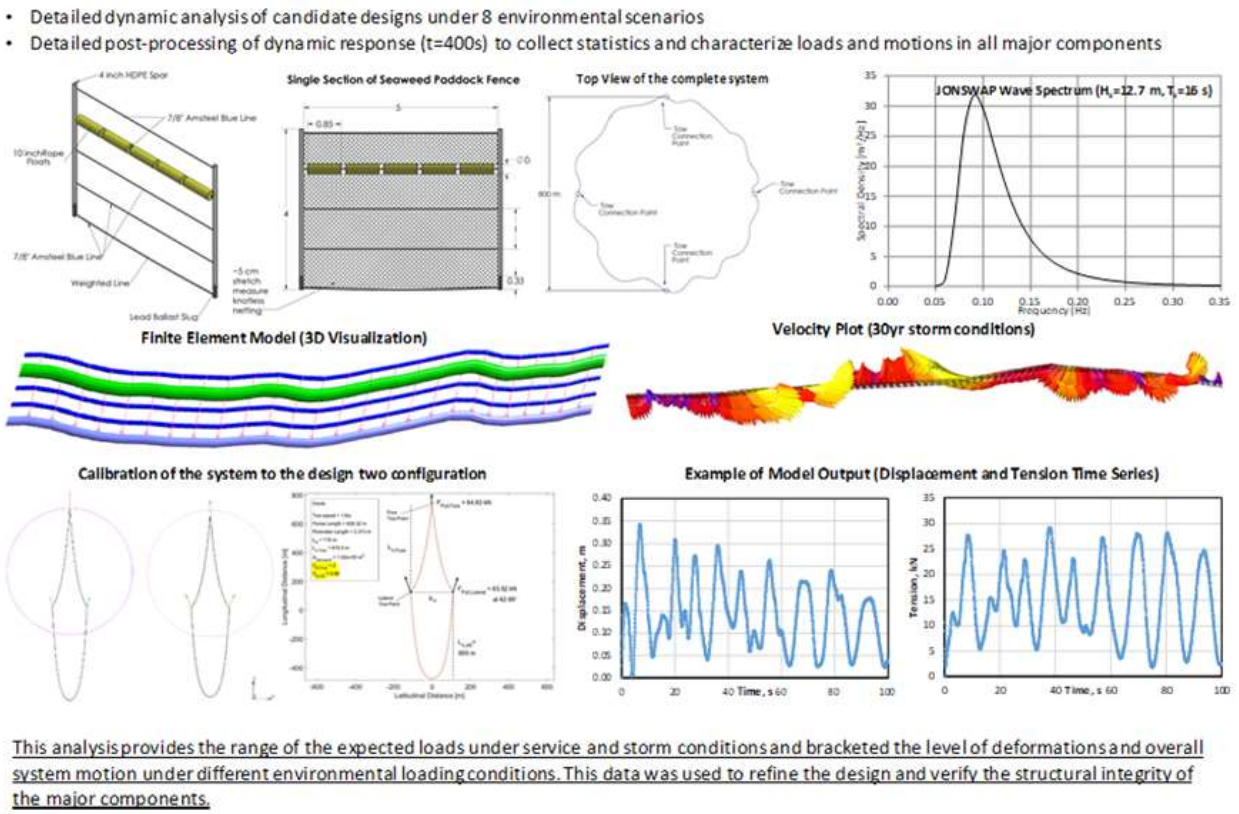

Figure 195: The Seaweed Paddock design incorporates sections of vertical nets combined into a continuous length and connected at the ends. The optimization of the towing shape and the example of displacement/tension time series are provided in the bottom half.

An extensive amount of work was conducted by the modeling team for the AdjustaDepth system during Phase 1 of its project. The geometric and material properties was specified by the UNH as shown in the diagram of the system in Figure 196. The finite element hydrodynamic simulation model of the system was developed using Hydro-FE.

The dynamic finite element model was constructed of truss elements. Anchor chains and ropes, spoke lines, tethers, and rim lines were all modeled as cylinders whose cross-sectional areas and densities matched those of the physical components. Their hydrodynamic coefficients were specified as C_{dx}=1.2, C_{dz}=0.08, and Ca=1.0 since this work was done prior to the publication of Fredriksson et al. (2020). Since models containing large numbers of nonlinear elements can require prohibitively long simulation times, the simulation approach was to consolidate the number, *n*, of small linear elements into larger elements with the same length and the equivalent hydrodynamic and structural properties. However, when representing multiple elements as a single, consolidated element, it is impossible to match both the total cross-sectional area and the total projected area of the elements. This presents a problem in hydrodynamic finite-element models, because drag forces are proportional to projected area, while buoyancy and inertia are proportional to cross-sectional area. Figure 197 illustrates this discrepancy for a consolidated element representing six individual cylinders.

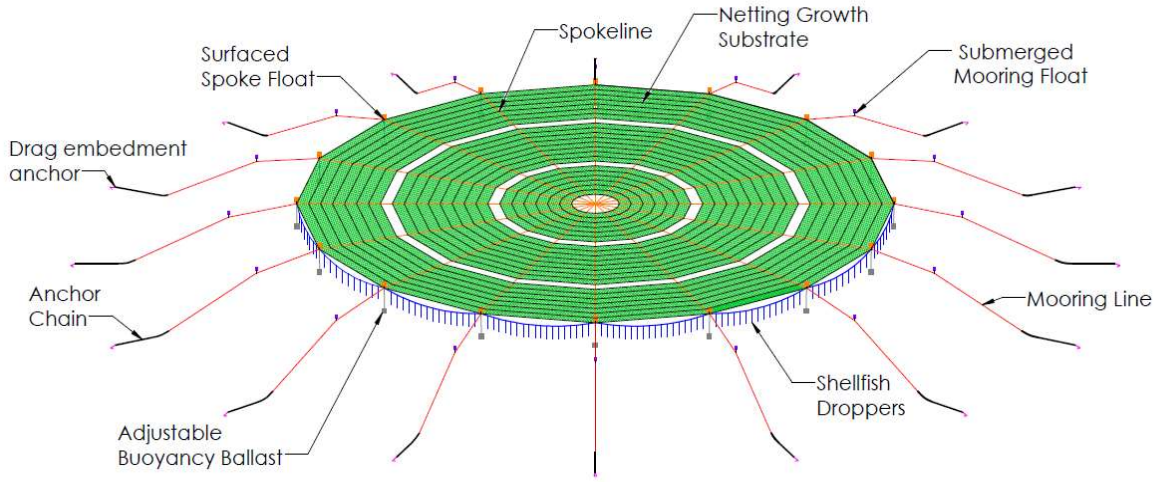

Figure 196: A schematic of the Adjustadepth system in the surfaced configuration as designed by UNH. Anchor ropes are shown in orange. Anchor chains are shown in gray. Gracilaria and its substrate are shown in green. Shellfish droppers are shown in blue. Neither the central float and ballast nor the flotation buoys along the spoke lines are shown.

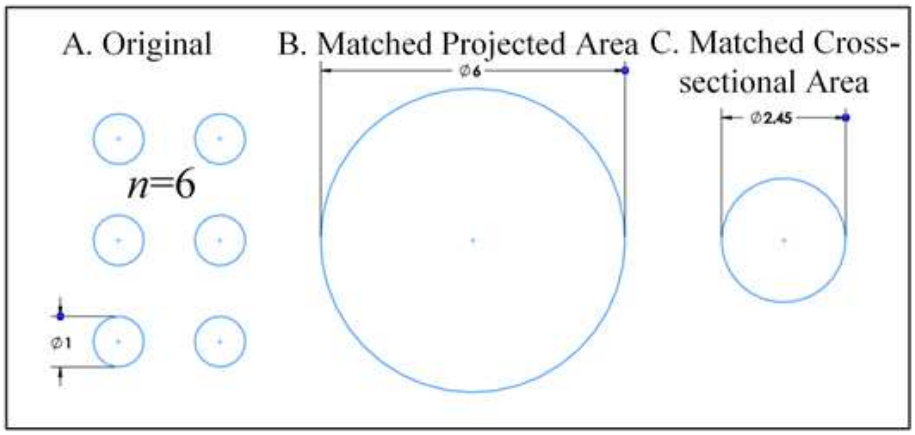

Figure 197: To model the Adjustadepth system, cylindrical elements were consolidated. In the Figure, (A) shows *n* cylindrical elements of unit diameter being represented by a single consolidated element. If the total projected area is matched (B), then the cross-sectional area is *n* times too large. If the total cross-sectional area is matched (C), then the projected area is (original projected area)/$\sqrt{n}$.

Tsukrov et al. (2003) addressed this problem by implementing a one-dimensional "consistent net element" in Aqua-FE™ to model fish cage netting. Since the drag and inertial terms are decoupled in the Morison equation, their coefficients can be modified such that the drag, buoyancy, and elastic forces on the element, as well as its inertia, can be reproduced if the cross-sectional area and the number of represented elements is specified. In the present analysis using Hydro-FE, this is accomplished by multiplying drag force in each direction by $\sqrt{n}$. Shellfish droppers and floats were modeled using this technique.

Buoys and ballasts were modeled as single-element segments with the specified lengths and net buoyancy values. The axial drag coefficients, C_{dz}, were modified to account for the finite length of the buoys when moving along their axis.

The grow out substrate, including biofouling and *gracilaria*, was modeled as a network of horizontal cylindrical elements whose aggregate hydrostatic, hydrodynamic, and structural properties matched those of a rough, impermeable, flexible disk. Buoyancy and inertia were conserved by setting the diameter of the substrate elements such the total volume equaled that of the substrate, biofouling, and *gracilaria*. As specified by UNH, the tangential drag on this flexible disk was treated using a bulk drag coefficient for a rough flat plate at a high Reynolds number. In the direction normal to the disk, drag force in the global Z direction (vertical) was scaled so that the total drag normal to the disk would be equal to that of a circular disc moving broadside through still water at high Reynolds numbers.

The dynamic model was analyzed in five load cases. These included static conditions, as well as wave and current dominated 30-year storms. Both collinear and perpendicular wave and current scenarios were investigated. Load case parameters are given in Table 33.

Table 33: Load case summary

	Description	Current speed (m/s)	Current direction (from) (deg from N)	Sig. Wave Height	Dominant Wave Period	Wave direction (from)	biomass %
	Static	N/A	N/A	N/A	N/A	N/A	100%
1	30 yr Wave extreme	1.36	140	15	15.37033	140	100%
2	30 yr Current extreme	1.7	140	10.5	12.7565	140	100%
3	30 yr storm, perp wave (dom.) and currents	1.36	50	15	15.37033	140	100%
4	30 yr storm, perp wave (dom.) and currents	1.7	50	10.5	12.7565	140	100%

The system was subjected to random waves using a Brettschneider spectrum with a random seed approach. Dynamic simulations were run for 500 seconds. Plots of stress values throughout the AdjustaDepth system are shown in Figure 198 through Figure 202. Maximum observed anchor line tensions, and the resulting safety factors, are given in Table 34.

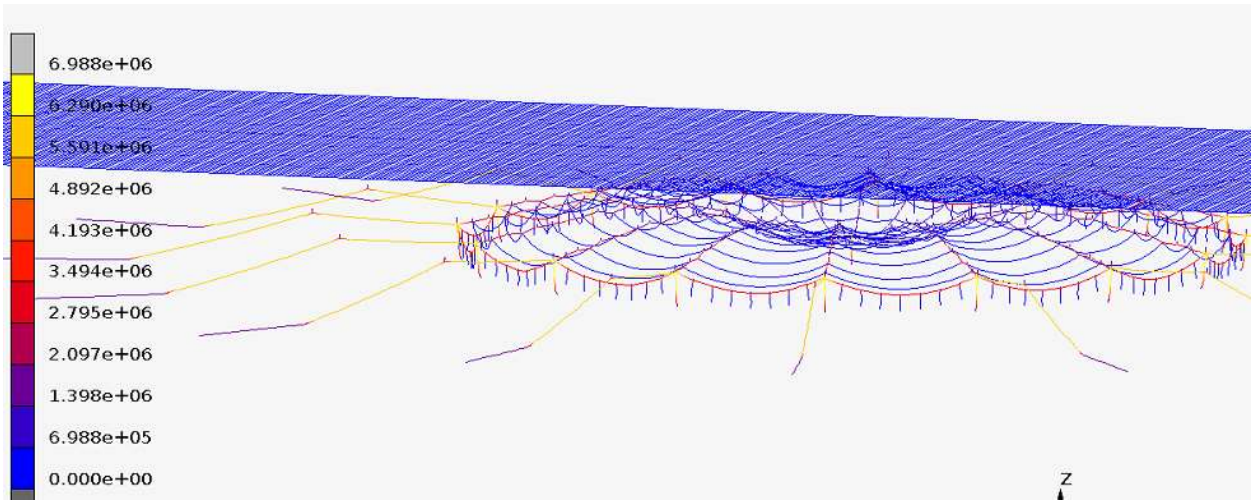

Figure 198: Maximum principal stress in structural members under static conditions.

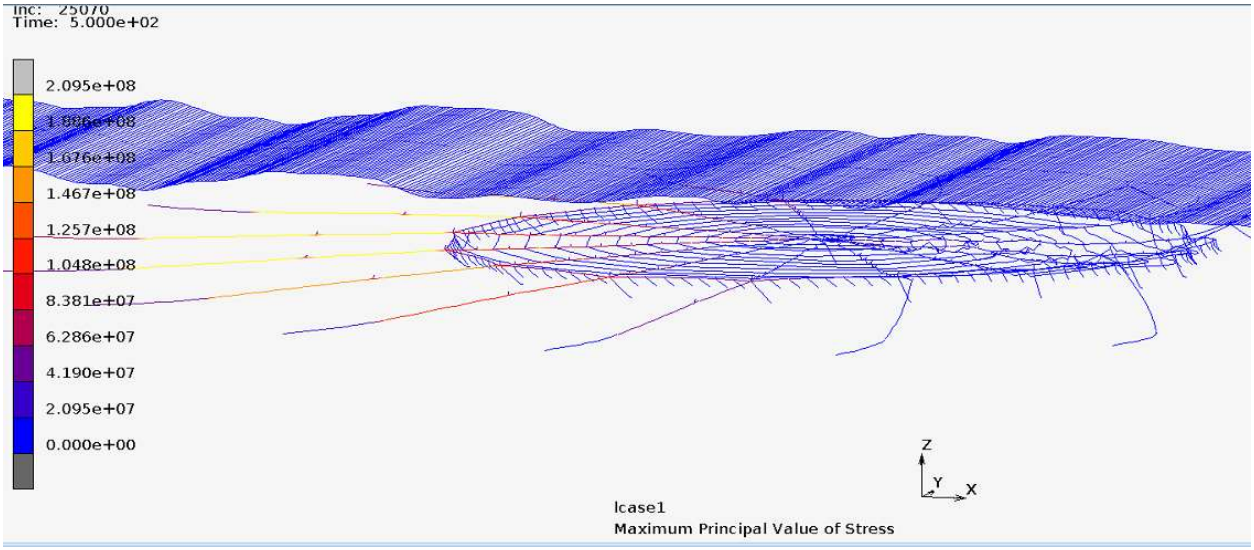

Figure 199: Maximum principal stress in structural members under dynamic scenario 1.

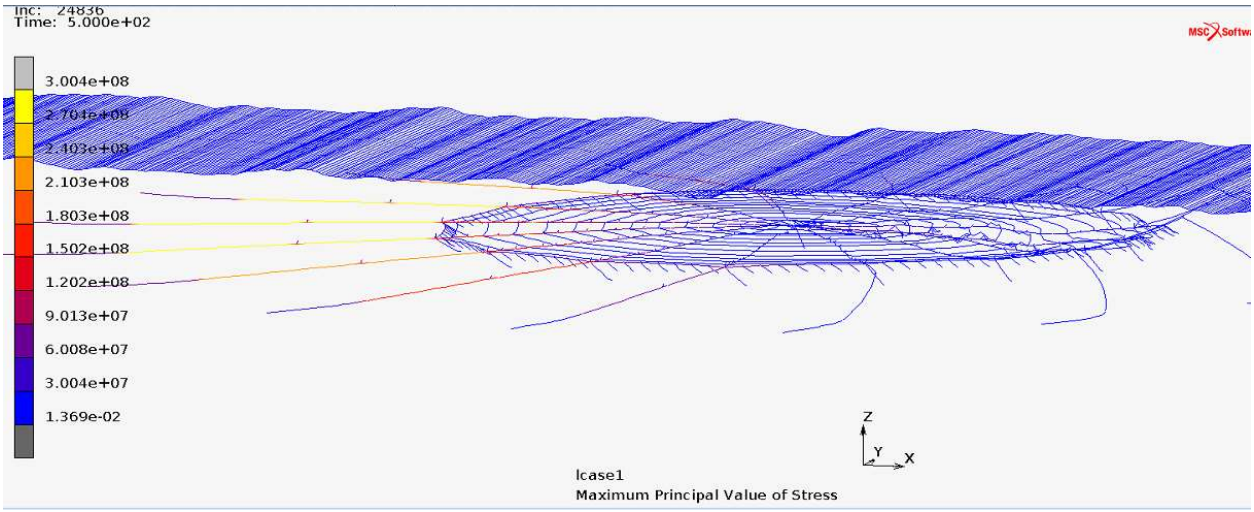

Figure 200: Maximum principal stress in structural members under dynamic scenario 2.

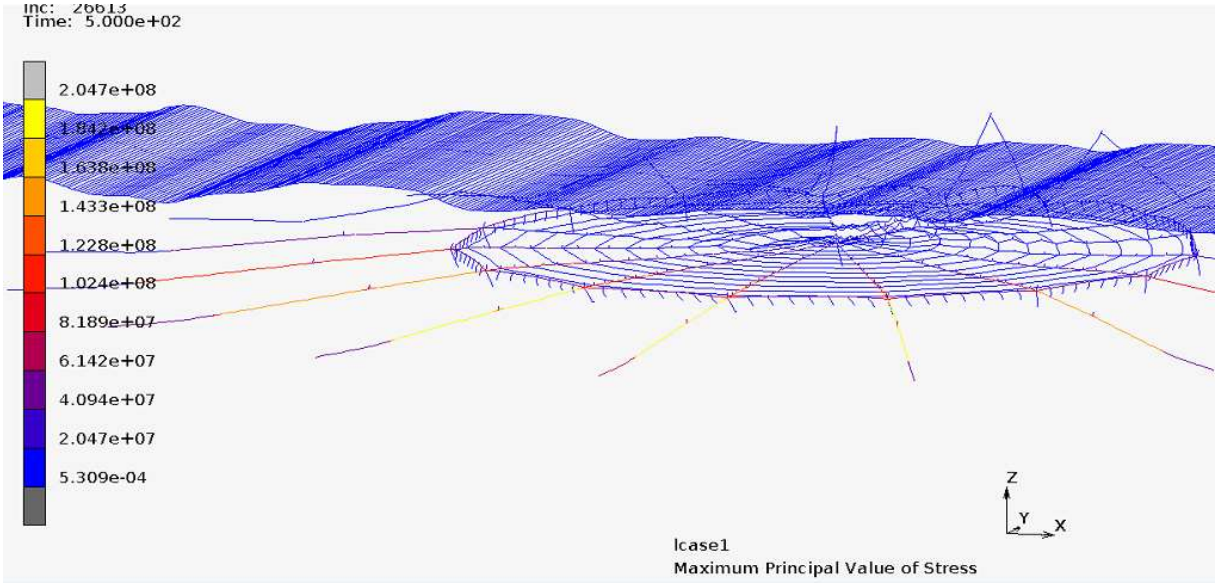

Figure 201: Maximum principal stress in structural members under dynamic scenario 3.

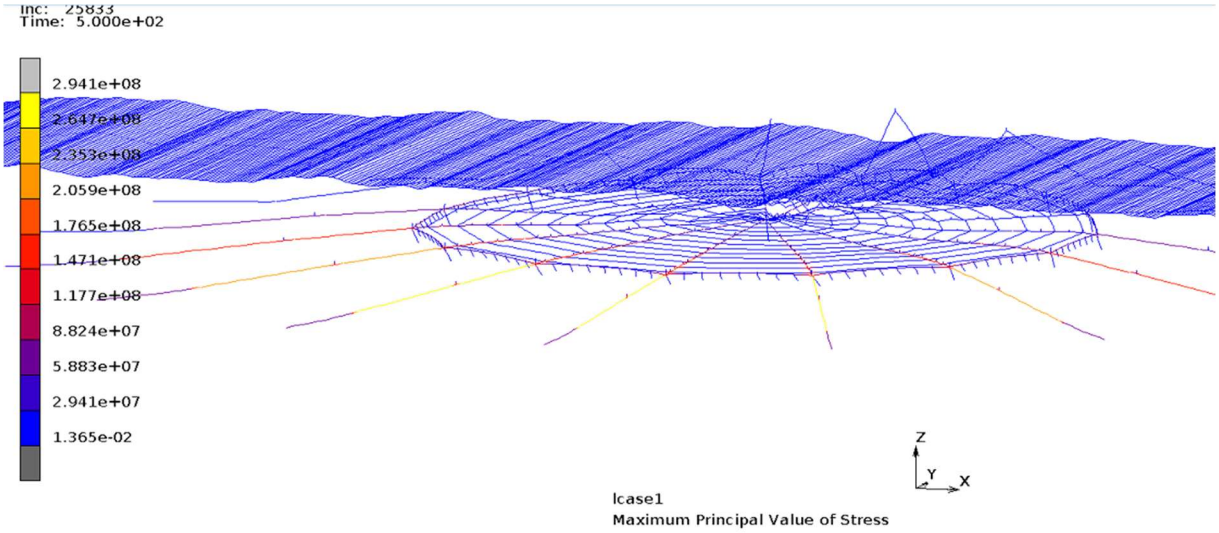

Figure 202: Maximum principal stress in structural members under dynamic scenario 4.

Table 34: Maximum anchor line tensions and safety factors

		Anchor Line area	0.005866	m^2
	Results (approximate)	Break strength	1863900	N
Scenario	Description	Stress, Pa	Tension, N	SF
0	Static	5.59E+06	3.28E+04	56.84
1	30 yr Wave extreme	1.89E+08	1.11E+06	1.68
2	30 yr Current extreme	2.70E+08	1.59E+06	1.18
3	30 yr storm, perp wave (dom.) and currents	1.84E+08	1.08E+06	1.72
4	30 yr storm, perp wave and currents (dom.)	2.65E+08	1.55E+06	1.20

The major conclusions from this effort included 1) wave loading had a visible effect on system motion even in the submerged configuration, however, current loading dominates anchor loads, 2) downstream mooring floats rise almost to the surface and interact strongly with waves and 3) anchor line safety factors are lower than typically recommended for offshore structures, but are above unity. In addition to this summary, a full analysis report was submitted to the UNH and USM team in support of this project. Results are summarized for two design iterations on Figure 203.

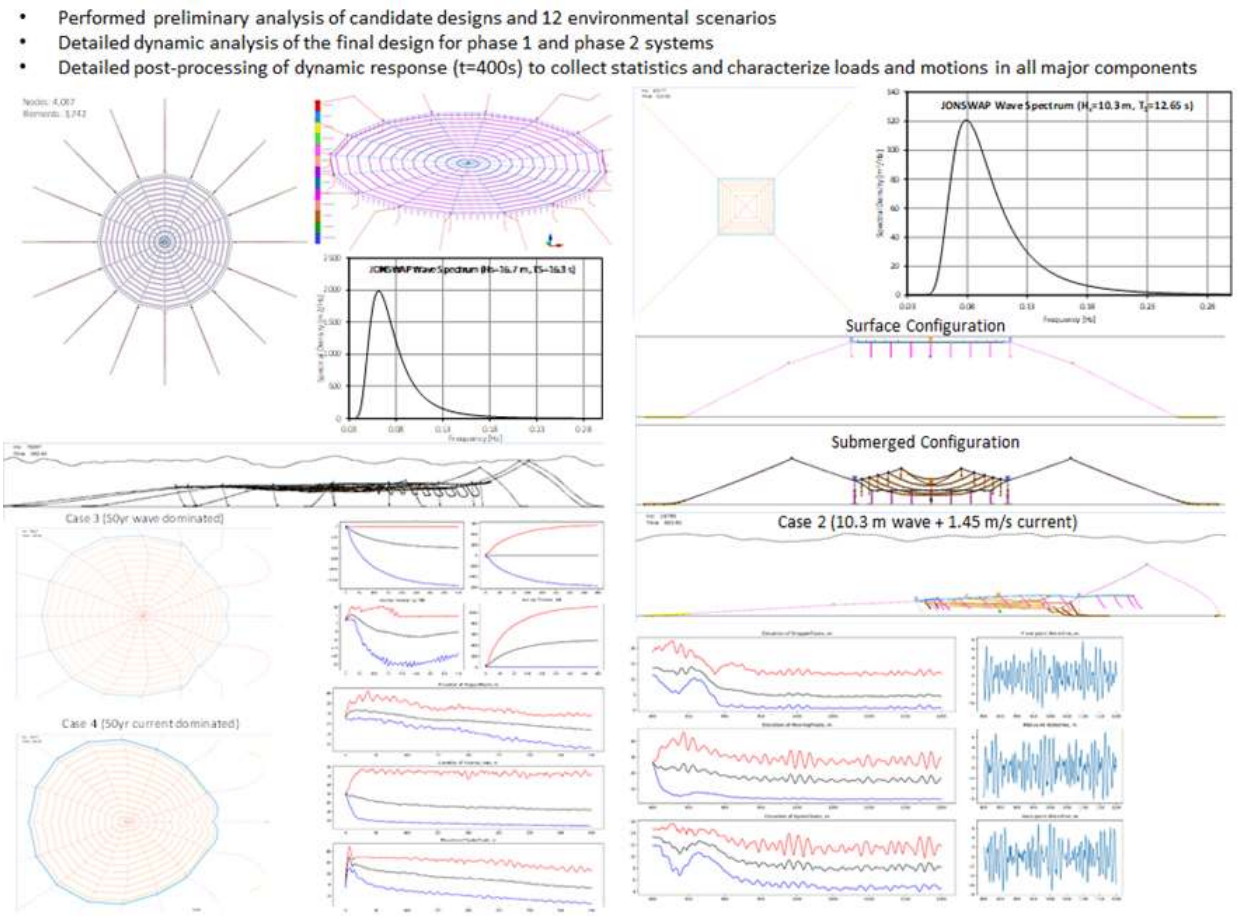

Figure 203: Summary of the Hydro-FE results conducted for the Adjustadepth project.

The modeling team also worked with the Trophic system group during Phase 1 of their project. Numerical models of the Trophic macroalgae cultivation system were developed using the same dynamic Finite Element Analysis approach is a similar manner as the other Category 1 efforts. The FEA-based numerical model was developed for a representative farm consisting of 12 “tiles” in a 4X3 array is shown on Figure 204.

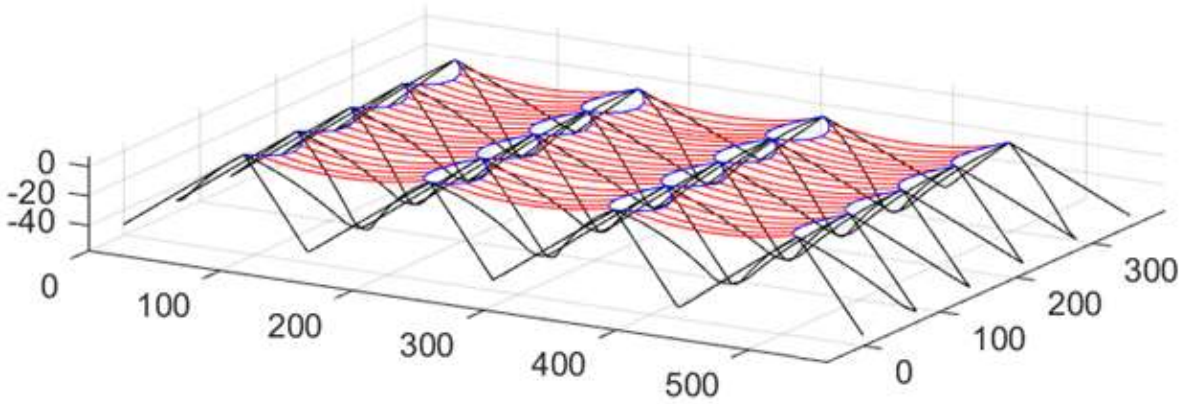

Figure 204: Perspective view of the Trophic system with the mooring Lines (black), header Lines (blue), and culture lines (red) during static simulation (no waves or current).

As described previously, models containing large numbers of nonlinear elements can require prohibitively long simulation times. Thus, a similar approach as shown on Figure 197 was taken to consolidate the number, *n*, of small linear elements into larger elements with the same length and the equivalent hydrodynamic and structural properties.

In the Trophic study, however, various aggregation ratios were investigated. During this design iteration, aggregation ratios of $n = 7$ and $n = 5$ were applied to the culture lines and kelp fronds, respectively. Culture lines were assumed biofouled, with increasing dry mass of the longlines by 0.765 kg/m. The mass density of the biofouling was taken as 1530 kg/m3. The equivalent diameter of the biofouled longline rope was calculated to be 27.1 mm using these assumptions. A slightly larger diameter of 30.8 mm was assumed for drag calculation, accounting for the fact that biofouling is non-uniform and is largely made up of open space. Kelp mass and buoyancy were calculated assuming a dry weight of 245 N/m length of longline. The static position of the main elements in the numerical model of the 4X3 array is shown in Figure 204 (note that kelp fronds are not displayed in the figure but are included in the simulation). Simulations were performed for both operational and extreme environmental conditions specified as summarized in Table 35. Seven load-cases were specified by the UNH team for the first iteration of dynamic modeling results.

Table 35: Environmental Conditions as prescribed by UNH.

Normal operating conditions (from NBDC station 44034)			
	significant wave height	1.5	m
	approximate dominant period	7.13	
	waves perpendicular to longlines		
	current speed @ 2m depth	0.4	m/s
	current speed @ 50m depth	0.25	m/s
	current parallel to longlines		
Extreme conditions (survival) (from WIS station 63013)			
	significant wave height	8.5	m
	approximate dominant period	16	sec
	waves perpendicular to longlines		
	current speed @ 2m depth	1	m/s
	current speed @ 50m depth	1	m/s
	current parallel OR perpendicular to longlines		

These cases included various combinations of operational and extreme currents and monochromatic waves. For the extreme significant wave height given in Table 36, the most probable largest single wave during a one-hour storm was computed according to,

$$\mathrm{A_{max}} = 2\mathrm{m_0}\ln\left(\frac{t}{T_2}\right)^{\frac{1}{2}}. \tag{55}$$

Here t is the storm duration of interest (t=3600 s) and T_2 is the mean wave period. Furthermore, m_0 is the zeroth moment of a narrow-banded wave spectrum, such that the significant wave height $H_s \approx 4\sqrt{m_0}$ (Faltinsen 1991). Environmental variables for each case are listed in Table 36.

Table 36: Environmental conditions for each load-case.

ID	Name	Wave Height (m)	Wave Period (s)	Wave Direction*	Current Speed, (m/s)*	Current Direction**
1	Static	-	-	-	-	-
2	Operational Parallel Current	-	-	-	0.4	0
3	Extreme Parallel Current	-	-	-	0.6	0
4	Extreme Perpendicular Current	-	-	-	0.4	90
5	Operational Wave	2.72	7.125	90	-	-
6	Extreme Wave	14.42	16	90	-	-
7	Extreme Parallel Current and Wave	14.42	16	90	0.6	0

*Within array, **Relative to longlines

Maximum tensions were quantified for each mooring line and catenary line under each load case. Figure 205 show the results of Case 7 simulation when the mooring buoys were included in the simulation.

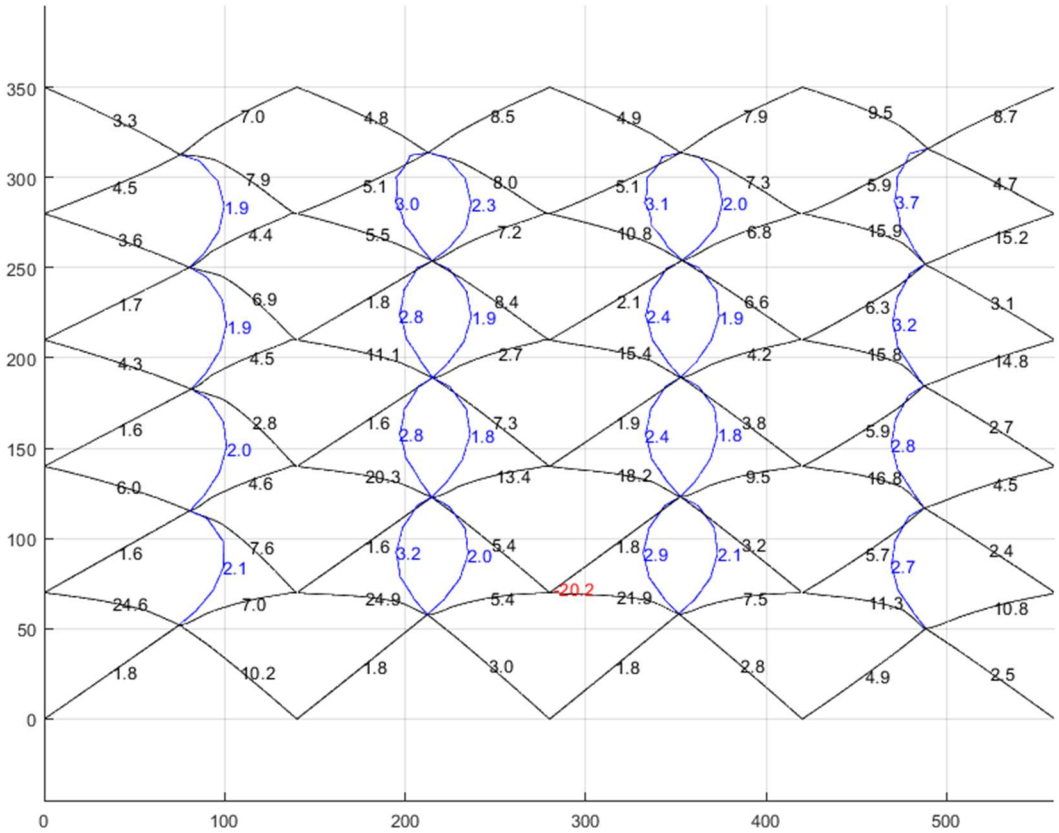

Figure 205: Plan view of array showing Mooring Lines (black) and Catenary Lines (blue) in their mean position during Case 7 simulation with mooring buoys included in simulation. Minimum safety factors on each line are shown. Maximum longline submergence is indicated in red. Axes show distance in meters. Current goes from left to right (west to east); the wave train is traveling from bottom to top (south to north).

Several conclusions and recommendations were provided to Trophic LLC, including the following:

- Safety factors in the mooring and catenary lines under the extreme cases appear to be near or above recommended values.
- Interference issues with mooring floats and longlines were identified and mitigated
- The effects of Trophic system self-diving buoys were quantified.
- Node buoys and culture lines submergence were also quantified.
- Maximum submergence of the culture lines was observed to be highly sensitive to longline length and the shape formed by the catenary lines.

Additional modeling and analysis work were done by the modeling team in support of this Trophic Category 1 project. The work included analyzing design iterations of the Trophic kelp cultivation array in both static and dynamic load cases. Initial static results showed that anchor line tensions and catenary line tensions varied significantly throughout the array. These variations were shown to be a function of the simulated array size and shape. Thus, the simulated array size was increased from 4X3 to 4X4 and 5X5 arrangement of tiles. To extend this analysis while keeping simulation times feasible, an approximate symmetry condition was applied to two adjacent sides of the simulated array. The validity of this approximation was demonstrated by comparing results for a 4X4 array with results from a 2X2 array with a symmetry condition. Observed tensions away from the symmetry plane agreed with the full 4X4 case to within 2%. On the symmetry plane, results differed by up to 10%, due to the approximation employed.

The symmetry approximation technique was employed to compare static solutions for design iterations 2.0 and 2.2 for a 10X10 grid. In these large grid simulations, anchor line and header line tensions approached those observed when the node buoys were fixed in their nominal positions. Static tensions on the outer anchor lines were more than double than those observed in the internal tiles (58.4 kN compared to 18.5 kN) at mid tide. Conversely, header line tensions near the outer edge were slightly more than half those observed on the inner tiles (28.9 kN at mid tide compared to 54.8 kN).

Design iteration 2.2 was found to decrease maximum static anchor line tensions and catenary line tensions compared to design iteration 2.0. It also showed slightly decreased node buoy displacements and increased minimum static anchor line tensions.

To select an appropriate wave modeling approach, random wave and regular wave representations of the wave dominated storm condition were compared for peak loads. The regular wave representation used nonlinear regular waves whose heights were equal to the maximum single wave height expected in either a one-hour (or three-hour) storm. The random wave representation used seed values that ensured that one wave during the simulation would have a height equal to that used for the regular waves. The regular wave representation predicted peak tensions up to 40% higher than those predicted with the random sea approach. Therefore, random waves were used for all dynamic scenarios.

The numerical model of the Trophic system was used to compare the responses to a wave-dominated versus a current-dominated extreme event and to compare the responses to waves heading parallel to versus perpendicular to the longlines. The wave-dominated extreme event with waves parallel to the longlines resulted in the largest tensions throughout the system.

The Trophic array was also analyzed with only 33% of its maximum biomass on the longlines. This could reflect a storm condition in which some of the kelp and biofouling has been stripped from the longlines by hydrodynamic forces. In this 50-year storm scenario, mooring line tensions were reduced by 30% compared to the maximum growth case.

The model was used to assess the importance of assumptions about the reduced current speed within the farm (current shadowing). The 50-year storm was simulated with no current shadowing. That is, each element was exposed to the undisturbed current. The peak anchor-line tensions were increased by only 8%. This reflects the significant role played by wave forces (both oscillating and time-averaged effects).

Besides the 50-year extreme events, the 25- and 10-year return periods were also simulated. As with the initial 50-year storm scenarios, these analyses assumed 100% biomass growth and the specified current shadowing assumption. Reductions in maximum tensions were relatively inconsequential. For example, the design load for the anchor line in the 50-year event was calculated to be 309 kN, while for the 10-year event, the design load was 296 kN.

To assess the resilience of the system to failure, a broken anchor line scenario was simulated in a 50-year storm. The broken anchor line increased the peak load in the nearby lines by up to 7% of the peak tension in the intact scenario. Sufficient safety factors should be applied in the selection of line diameters such that this increase in tension will not result in cascading failure. A summary of the results is provided in Table 37.

Table 37: Design Loads for each dynamic scenario for longline, mooring line, and catenary line.

	1	2	3	4	5	6	7	8	9
	50 year storm								
Dynamic Scenario	Max Wave	Max Current	Parallel Forcing	Perpendicular Forcing	Reduced Biomass	No Current Shadowing	25 Year Storm	10 Year Storm	Broken Mooring
Longline Design Load (kN)	16.2	12.5	17.5	17.8	12.7	18.2	17.1	14.8	18.0
Mooring Design Load (kN)	184.5	178.2	307.2	133.0	212.8	331.6	297.9	295.8	329.2
Catenary Design Load (kN)	181.1	155.2	253.3	117.3	185.1	268.3	243.3	248.9	267.0

A revised design of the Trophic kelp cultivation array was analyzed in preparation for Phase 2. A 2x2 array was analyzed with several modifications from previous iterations. The objective of this analysis is to simulate a single 2x2 configuration in static and dynamic conditions in mid tide (50 m depth) and obtain the following results:

- Anchor line tensions
- Anchor line angle to seafloor
- Catenary line tensions
- Longline tensions
- Node float depths
- Average longline depths

The static loads on the mooring lines, catenary lines, and longlines are shown in Figure 206. The peak loads are 8.1 kN, 5.7 kN, and 1.8 kN for the mooring lines, catenary lines, and longlines, respectively.

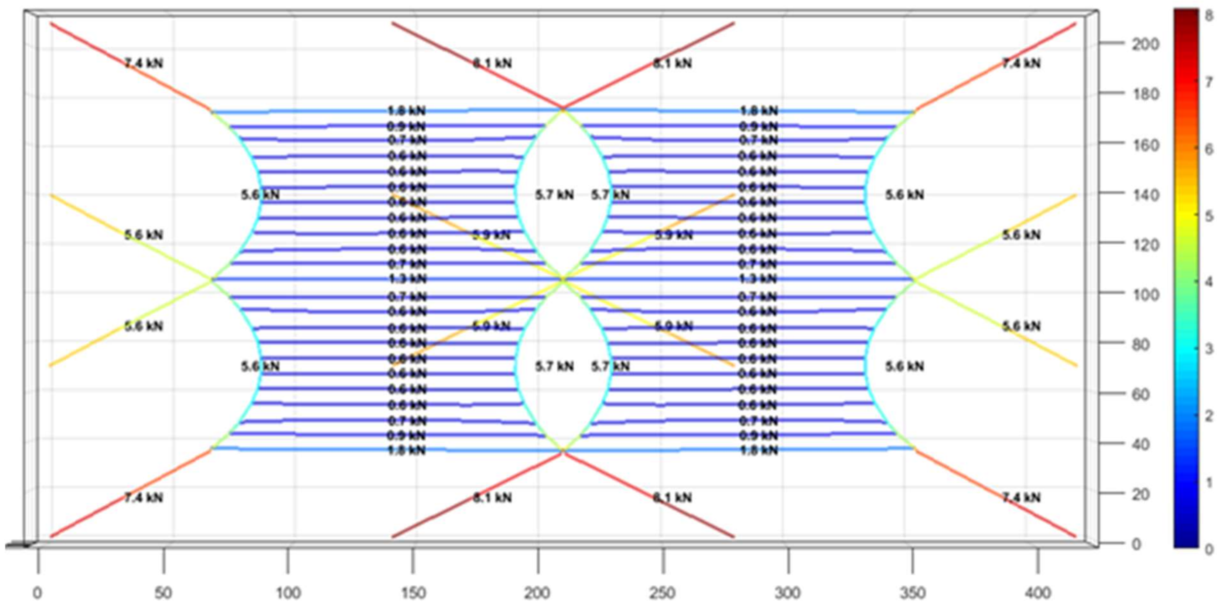

Figure 206: Static loads of mooring, catenary, and longlines in 2x2 array.

A single dynamic scenario was run on with the 2x2 grid model with a 25-year wave condition having a significant wave height of 8.0 m, a dominant wave period of 11.0 s, and a current speed of 0.50 m/s. Simulations were done with the waves and current were co-aligned and with an offset of 27 degrees from the culture line orientation. A biomass of 33% was assumed.

To avoid prohibitively long simulation times, a focused wave approach was used. Typically, wave heights in random wave simulations are randomly generated within the parameters of the wave spectrum. However, the focused wave approach chooses the phase value seeds of the frequency components to ensure that the largest wave in the simulation equals the *largest expected wave in a one-hour storm*, which was determined by assuming a Rayleigh distribution for individual wave heights (Tucker and Pitt, 2001).

The length of simulations was determined by using a modal analysis to calculate the longest undamped natural period of the system. The simulation time was set to equal six modal periods, with the first three allowing the system to reach equilibrium. Therefore, data from the first half of the simulation were discarded.

For each dynamic scenario, a Design Load was computed following methods described in Bureau Veritas Guidance Note NR 493 (BV,2015). The Design Load is equal to the average of peak loads from each random seed simulation plus the standard deviation of peak loads multiplied by a factor that is dependent on the number of random seeds simulated.

The design loads on all mooring and catenary lines are shown on Figure 207 with the maximum mooring line design load of 83.6 kN, and the maximum header line design load of 79.2 kN.

Assuming a mooring line breaking strength of 98 kN and a catenary line breaking strength of 85 kN, these design loads correspond to safety factors of 1.17 and 1.07 for the mooring and header lines, respectively.

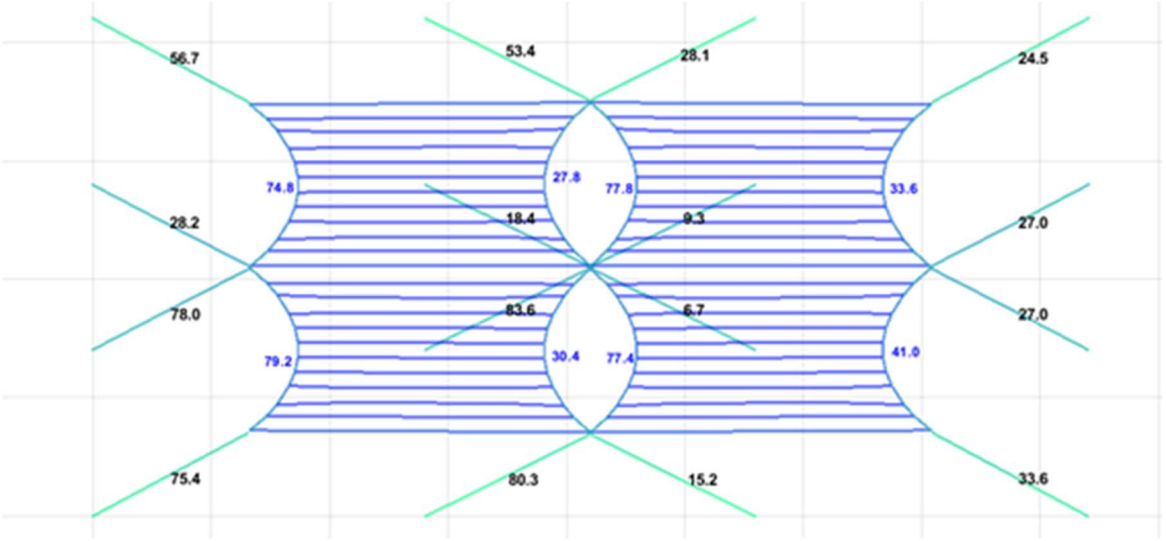

Figure 207: Design loads on mooring and header lines.

Though not shown in Figure 207, the design loads were also computed on each culture line with the maximum value equal to 16.0 kN. This corresponds to a safety factor of 1.49, assuming a breaking strength of 23.8 kN. The horizontal (lateral) and vertical design loads at the anchor are shown in Figure 208 and Figure 209, respectively. The maximum lateral anchor design load was calculated to be 76.3 kN, and the maximum vertical design anchor load equal to 34.6 kN. In addition to the design loads, the maximum depth values were also determined as shown in Figure 210.

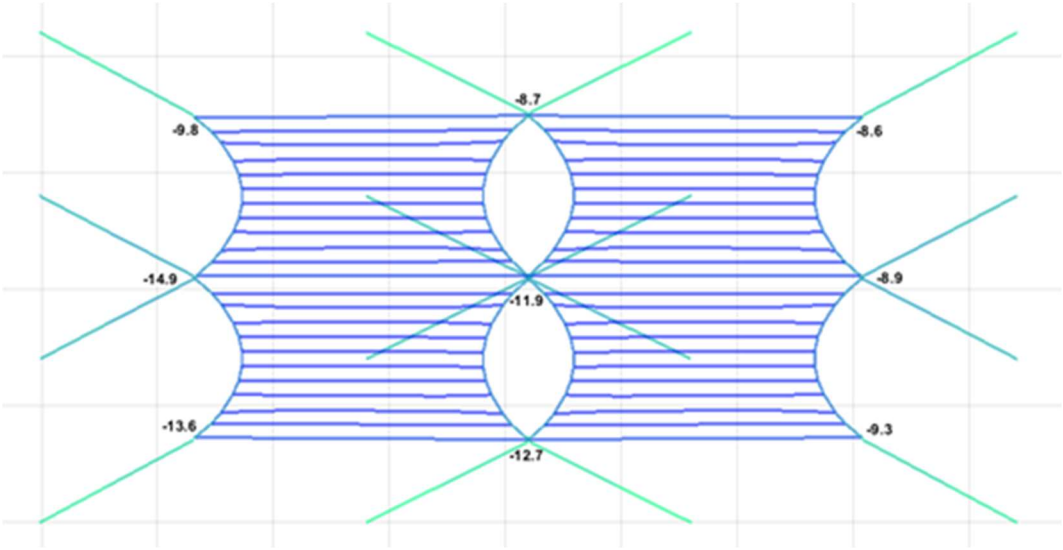

Figure 208: Lateral design loads at each anchor.

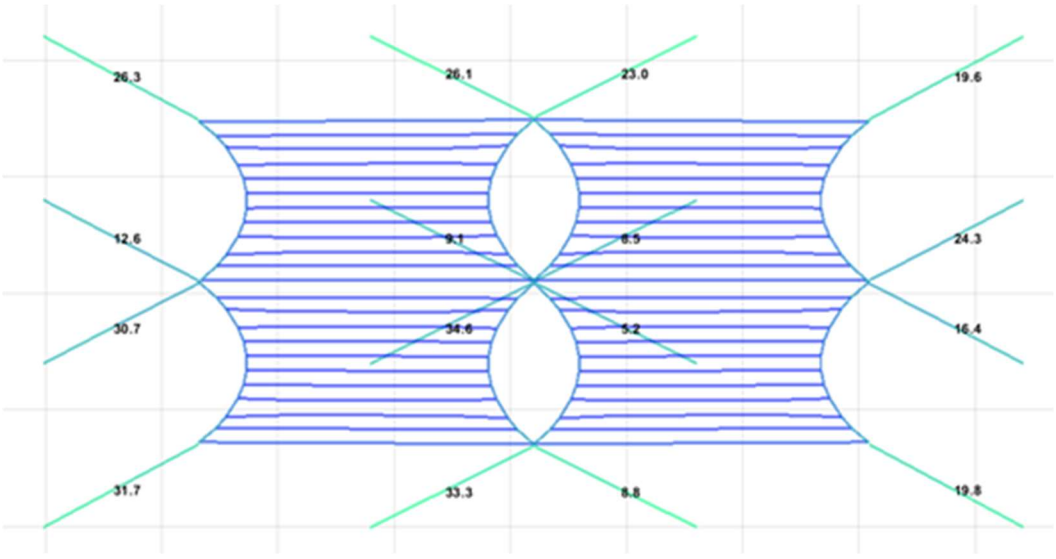

Figure 209: Vertical design load at each anchor.

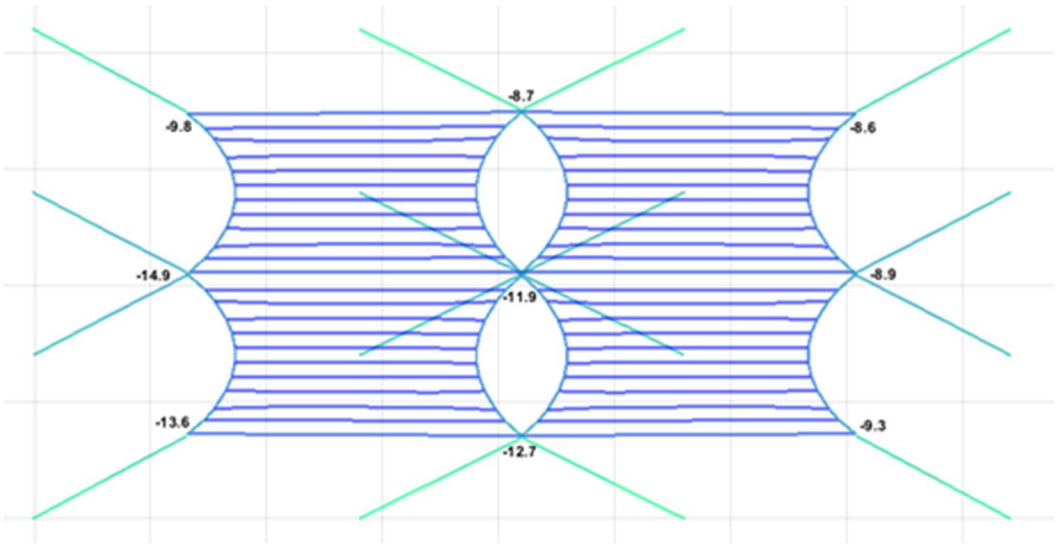

Figure 210: Maximum depth of node buoys (in meters), relative to mean water line.

Work with the Ocean Rainforest team was also done in support of both this Category 3 and in preparation with their Phase 2 proposal. Using a similar set of tools and approaches, a finite element hydrodynamic model of Ocean Rainforest macrocystis system was developed to study the loads and motions of the structural components. A diagram of the system is shown in Figure 211.

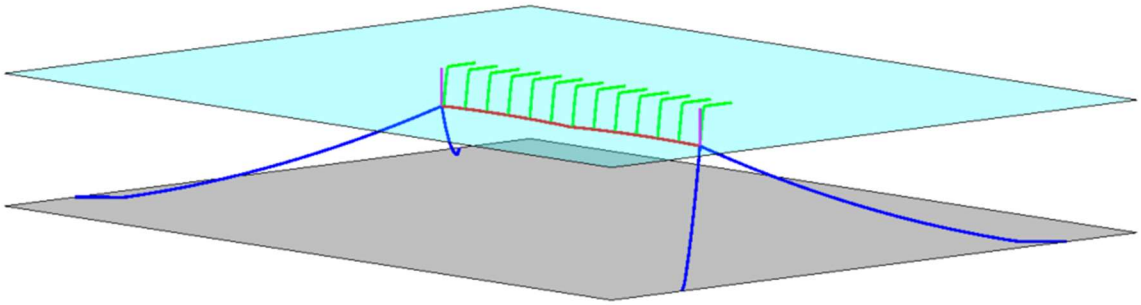

Figure 211: Diagram of simulation model of Macrocystis Cultivation Rig. Mooring anchor lines are shown in blue, horizontal line is shown in red, kelp plants are shown in green, buoy lines are shown in magenta. Note: for simplicity, not all macrocystis plants are shown in the diagram.

The Ocean Rainforest system includes two buoys at the water surface with net buoyancy of 10 kN taken as spherical shapes. The surface buoys were connected to a submerged horizontal line with studless chain anchors. All of the vertical, seeded kelp lines were attached to a 200 m long horizontal line positioned 20 m below the mean waterline. The horizontal line consists of 44 mm (1.75") diameter, 8 plait, nylon (TIPTO®LON) produced by Lankhorst Rope. A 50 kg clump weight was added to the midpoint of the horizontal line, and was modeled to have no buoyancy, added mass, or drag.

Macrocystis plants were attached in the design to the vertical seed lines. It was assumed that six plants are placed on each seed line, evenly spaced at 0.5 meters apart. Each plant was also assumed to consist of four stalks, with leaves located every one meter. For purposes of simulation, the leaves were treated as skin-friction dominated drag plates. The leaves are assumed to orient themselves in line with the fluid flow.

To reduce simulation computation time, two simplifications are made:

- Drag, mass, and buoyancy properties of the leaves are incorporated into the kelp stalks. This eliminates the need for creating separate bodies in the simulation model for each leaf.
- The kelp stalks are aggregated such that each kelp plant is represented by one strand. Aggregation is done carefully to ensure that the total drag, mass, and buoyancy of the kelp plant is unchanged.

Simulations were performed of the Ocean Rainforest system with five preliminary load cases as are summarized inTable 38. Each load case was simulated for 1000 seconds with the first 750 seconds assumed as a transient period. The maximum and minimum tensions in the structure are summarized in Table 39. The loads on the anchor are summarized in Table 40. An uplift of 27.4 m indicates that all of the chain has been lifted off the seafloor, resulting in non-negligible vertical forces on the anchor. The deflections of the midpoint of the horizontal line and the surface buoys are summarized in Table 41.

Table 38: Summary of load cases for the Ocean Rainforest modeling effort.

	Load case 1	Load case 2	Load case 3	Load case 4	Load case 5
Wave Model	Static (no waves)	Static (no waves)	Regular	Regular	Regular
Wave Height			6 m	6 m	6 m
Wave Period			10 s	10 s	10 s
Current Velocity	0.025 m/s	0.025 m/s	1.3 m/s	1.3 m/s	1.3 m/s
Macrocystis Growth	None	Full (40 m stalks)	None	Full (40 m stalks)	Harvested (17 m stalks)

Table 39: Structural loads during each dynamic simulation.

	Load case 1	Load case 2	Load case 3	Load case 4	Load case 5
Upstream Mooring					
Minimum Load (N)			20,456	80,375	46,255
Maximum Load (N)	5,061	4,884	8,606	76,396	39,595
Downstream Mooring					
Minimum Load (N)			8,206	2,635	6,319
Maximum Load (N)	5,061	4,884	3,483	1,436	2,164
Horizontal Line					
Minimum Load (N)			8,687	74,088	37,347
Maximum Load (N)	6,544	6,353	18,496	78,472	43,976
Float Line					
Maximum Load (N)	4,989	4,405	11,455	11,178	11,713
Minimum Load (N)			3,789	9,337	8,959

Table 40: Anchor chain uplift and directional loads for each load case

	Load case 1	Load case 2	Load case 3	Load case 4	Load case 5
Anchor Chain Uplift					
Upstream Mooring (m)	5.1	4.1	19.3	27.4	27.4
Downstream Mooring (m)	5.1	4.1	8.1	0.0	3.0
Anchor Load					
Upstream Mooring					
Lateral Force					
Min (N)			8,728	76,227	39,156
Max (N)	4,677	4,594	20,205	80,112	45,898
Vertical Force					
Min (N)			549	3,284	1,284
Max (N)	449	447	773	3,670	1,971
Downstream Mooring					
Lateral Force					
Min (N)			2,922	1,242	1,890
Max (N)	4,766	4,510	7,009	2,061	5,586
Vertical Force					
Min (N)			396	340	363
Max (N)	449	444	512	369	475

Table 41: Excursions of the horizontal line (measured at its midpoint) and the surface buoys.

	Load case 1	Load case 2	Load case 3	Load case 4	Load case 5
Horizontal Line Midpoint Excursion					
Lateral Offset					
Min (m)			13.9	45.2	35.0
Max (m)	0.0	0.5	16.1	45.8	36.6
Depth					
Min (m)			22.2	42.9	32.2
Max (m)	25.4	21.3	25.1	43.7	33.7
Buoy Excursion					
Lateral Offset					
Min (m)			1.1	5.0	2.1
Max (m)	0.0	0.0	8.2	8.4	6.9
Submerged Depth					
Min (m)			0.5	24.8	13.4
Max (m)	0.7	0.7	3.5	25.4	14.6

Load case 1: Load case 1 assesses how the structure sits in the water with no kelp or environmental excitation (from waves or current). In this situation, it is assumed that the buoys are half-submerged. Approximately 5 meters of anchor chain are pulled off the seabed in this condition with a pretension of approximately 5,000 N measured in the anchor lines. The schematic result for load case 1 is shown on Figure 212.

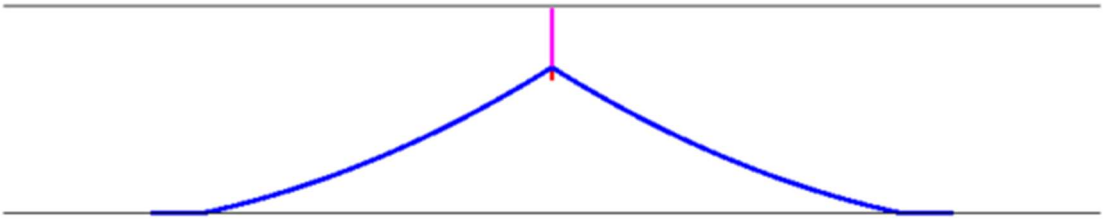

Figure 212: Side view of the Cultivation Rig in load case 1.

Load case 2: Load case 2 repeats the calm environmental conditions of Load case 1 but with the presence of fully grown macrocystis and a small current of 0.025 m/s to resolve the static position of the kelp. Because the macrocystis is positively buoyant and mostly floating on the surface, it has very little impact on the static orientation of the structure. The schematic result for load case 2 is shown on Figure 213.

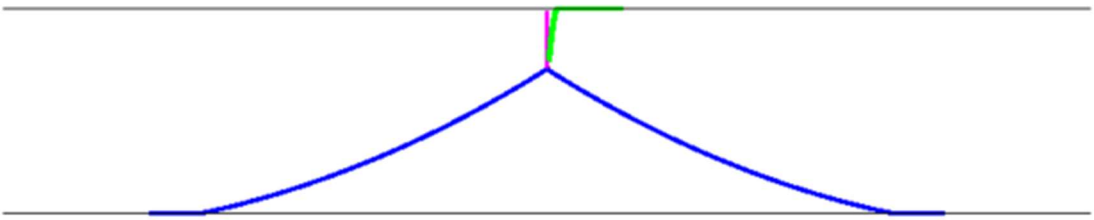

Figure 213: Side view of the Cultivation Rig in load case 2.

Load case 3: Load case 3 represents a wave and current condition with no kelp. In this situation, the buoy remains near the water surface during regular waves and steady current. The upstream anchor lines, which experience the loading from current drag, has an uplift of 19 meters. The schematic result for load case 3 is shown on Figure 214.

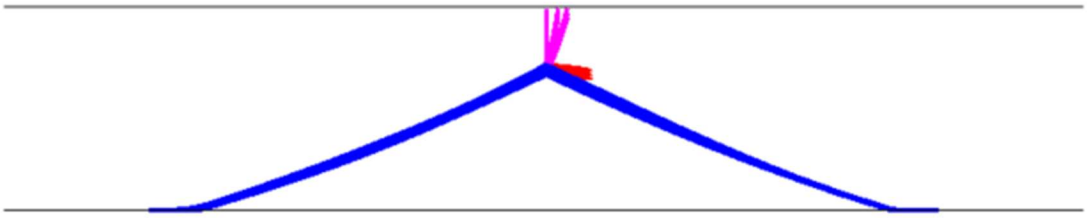

Figure 214: Side view of the Cultivation Rig in Load case 3. The minimum, maximum, and mean positions of each line over the course of the simulation are shown.

Load case 4: Load case 4 repeats the dynamic simulation of load case 3 with the addition of fully grown macrocystis plants. The presence of these plants yields substantial lateral drag, which causes two effects. First, the buoys are completely submerged as the mooring lines are tightened. Second, the lateral forces are enough to lift all the anchor chain off the seabed, which results in a vertical load on the anchors. Certain types of anchors, such as drag embedment anchors, are not well suited to vertical loading. The peak vertical anchor load of 3,760 N is approximately equivalent to the weight of 13 meters of chain. The schematic result for Load case 4 is shown on Figure 215.

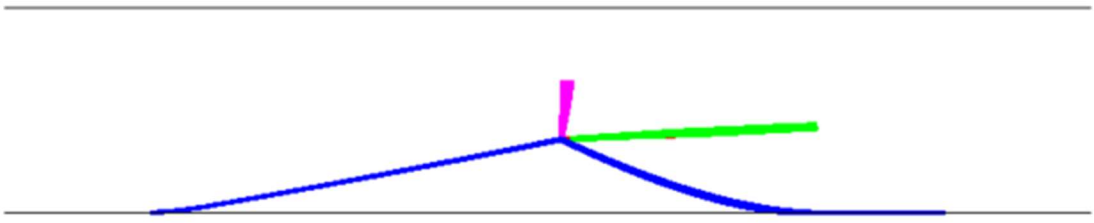

Figure 215: Side view of the Cultivation Rig in Load case 4 simulation. The minimum, maximum, and mean positions of each line over the course of the simulation are shown.

Load case 5: Load case 5 represents the condition after harvesting in which the macrocystis stalk length has been reduced from 40 m to 17 m. With the reduction of stalk length, there is less lateral drag on the structure. However, sufficient drag did exist to lift all the anchor chain and fully submerge the buoys. The buoys also showed more dynamic motion with the reduction of lateral drag. The schematic result for Load case 5 is shown on Figure 216.

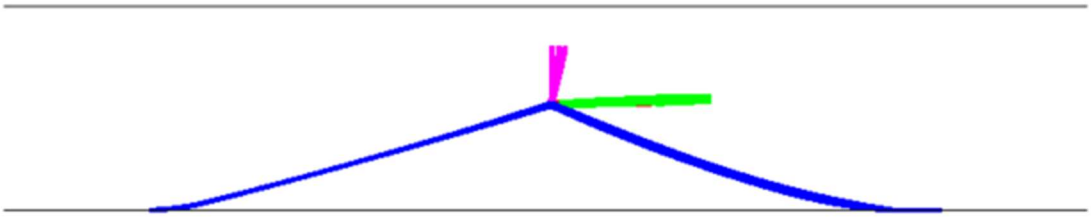

Figure 216: Side view of the Cultivation Rig in Load case 5. The minimum, maximum, and mean positions of each line over the course of the simulation are shown.

The same five load cases were simulated in random (irregular) waves and a full set of design recommendations were provided to the Ocean Rainforest team. The results were extensive but were not included in this report. The report can be provided if requested.

In May 2018, the Woods Hole Oceanographic Institution team, "Integrated Monitoring of Macroalgae Farms Using Acoustics and UUV Sensing (Category 4)" visited the University of New England to test their AUV sonar system at the Wood Island Site.

In September 2018, the UNE team started collaboration with the Category 3 team from the Pacific Northwest National Laboratory. The first step in the collaborative process was to assist in the development of an OrcaFlex model of a 1 km long system with both bull and sugar kelp (Figure 217 being developed at Oregon State University. The team also worked with PNNL to develop a circulation model of the Saco Bay area that includes a kelp dynamic model. An example is shown in Figure 218. Researchers at PNNL have also developed a FVCOM circulation model of Saco Bay (Figure 218. Work is ongoing to promote further collaboration.

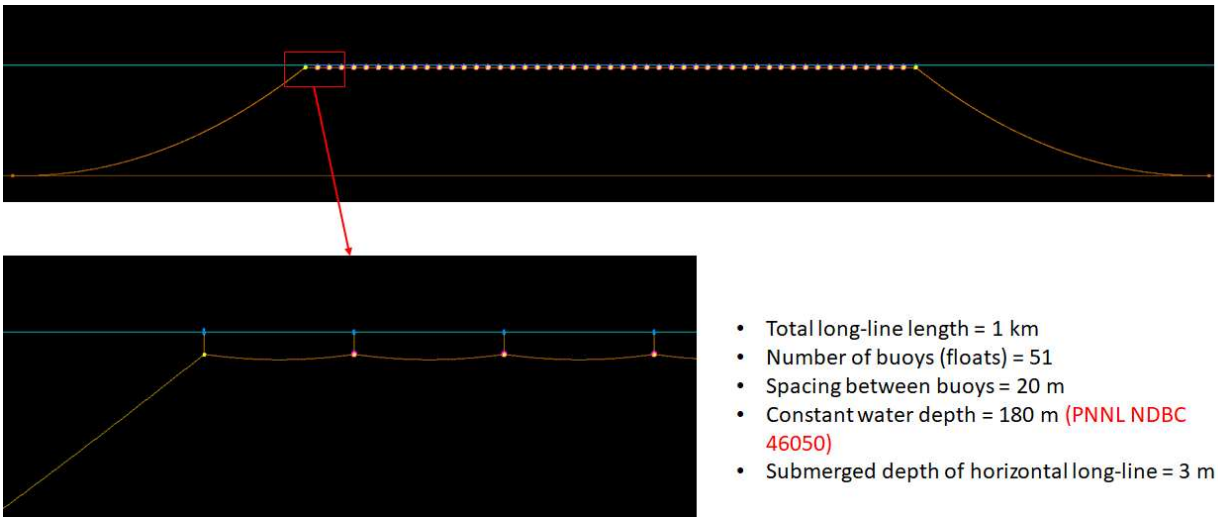

Figure 217: OrcaFlex model of a 1 km longline with both bull and sugar kelp.

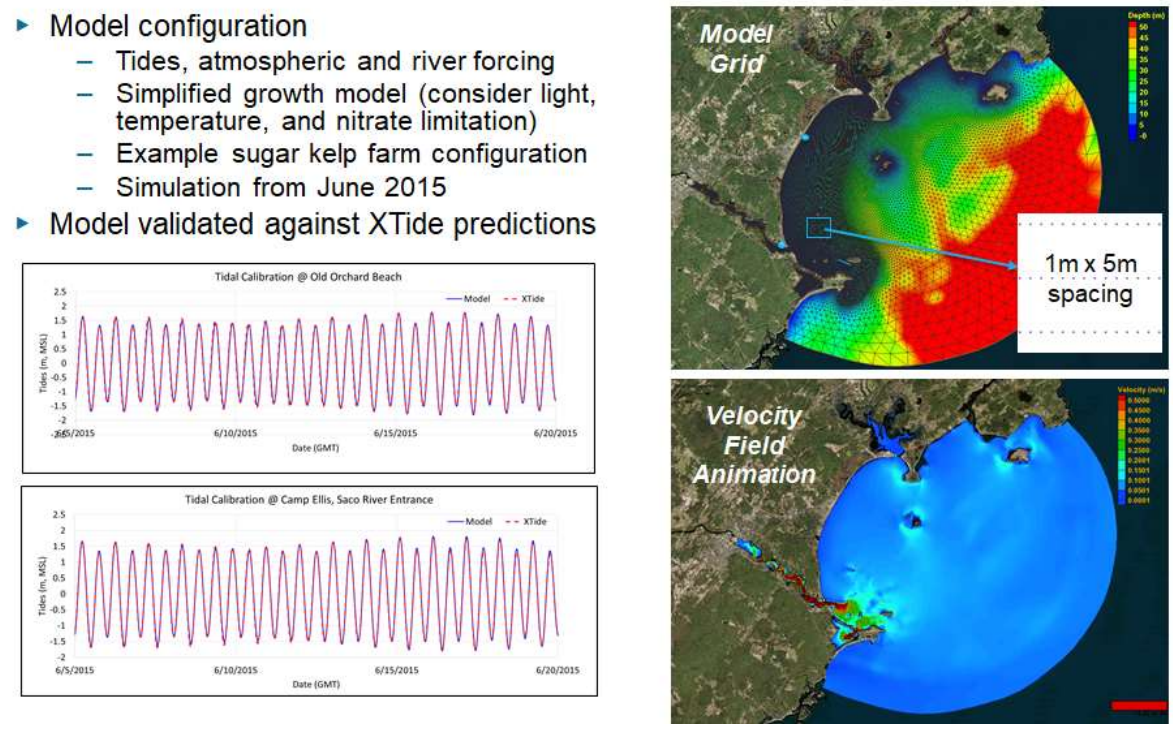

Figure 218: Circulation modeling of Saco Bay.

2.7.3. Task 7.3: Plan for Category 1 Phase 2 Project (2/14/19)

Work with the other ARPA-E projects was completed. Modeling projects with the Category 1 teams were secured as part of their Phase 2 projects, but not reported here.

2.7.4. Task 7.4: Develop Practical Science Master Degree (2/14/20)

This project was leveraged to develop a Practical Science Master (PSM) Degree in Ocean Food Systems at the University of New England. This section describes some of the tasks completed in support of this effort.

Confirmed and revised the Ocean Food Systems curriculum: A new course was developed and approved by the UNE administration in "Transdisciplinary Methods in Ocean Food Systems" that includes seaweed systems with mixed methods qualitative and quantitative analytics, mental models and systems modeling included.

Completed purchase and implemented testing of global classroom technology: Zoom was purchased and successfully used to connect with campuses in Iceland and Sweden. Simultaneous global classroom education experts at UNE helped implement best instructional practices.

Developed and implemented marketing plan: Marketing plan developed and implemented including video, webinar, print and digital advertising put in the field.

Developed MOU addenda for institutional collaboration and student/faculty mobility: A new MOU for PSM with University of Akureryi and Holar University College was signed at Arctic Circle Assembly on Oct 19, 2018. A new MOU was also negotiated and developed with the University of Gothenburg, Sweden. New strategic partnership development discussions in seaweed systems with Nord University, Norway were conducted with Barry Costa-Pierce delivering a presentation to leadership, faculty, and students.

Recruited and enrolled first PSM cohort: Two hundred (200) inquiries received at the onset of the application process. From the inquires, twenty (20) completed applications were submitted with four (4) Doherty Fellows in Ocean Food Systems selected. Two of which were interested in MARINER seaweed systems.

Building out collaborative seaweed industry and institutional networks: Work through the project was done develop seaweed business partnerships including: The Nature Conservancy, Heritage Seaweed, Sea Greens Farms, Bangs Island Mussels, Maine Marine Composites, Island Institute, Bigelow Labs. Other collaborative efforts are listed below.

- UNE hosted Seagreens Farms, a regional kelp company and AlgiKnit, a Brooklyn based seaweed fiber and textile company.
- Hosted Maine Sea Grant and new seaweed aquaculture focused Extension Agent.
- Hosted Island Institute's new Aquaculture Business Development Coordinator Peter Picconi.
- Hosted Ocean Approved seaweed production manager James Crimp.

2.7.5. Task 7.5: Reporting and publication (5/31/2022)

Project is completed and final report submitted. Project related publications and presentations are listed below.

Peer Reviewed Publications

Fredriksson, D.W., Dewhurst, T., Drach, A., Beaver, W.M., St. Gelais, A.T., Johndrow, K., Costa-Pierce, B.A. 2020. Hydrodynamic characteristics of a full-scale kelp model for aquaculture applications. Aquacult. Eng. https://doi.org/10.1016/j.aquaeng.2020.102086.

Knysh, A., Drach, A., Fredriksson, D.W., Dewhurst, T., Tsukrov, I. (2022). Methodology for multidimensional approximation of current velocity fields around offshore aquaculture installations. Submitted for review in Aquac. Eng.

Zhu, L., Huguendard, K., Zou, G.P., Fredriksson, D.W. Xie., D. (2021). Wave attenuation by suspended canopies with cultivated kelp (Saccharina latissima). Coast. Eng. 168, https://doi.org/10.1016/j.coastaleng.2021.103947.

St-Gelais A.T., Fredriksson D.W., Dewhurst T, Miller-Hope Z.S., Costa-Pierce B.A. and Johndrow K. 2022. Engineering a low-cost kelp aquaculture system for community-scale seaweed farming at nearshore exposed sites via user-focused design process. Front. Sustain. Food Syst. 6:848035. doi: 10.3389/fsufs.2022.84803.

Presentations and Posters

Fredriksson, D.W., Johndrow, K., Gelais, A.T., Dewhurst, T., Standbro, M., Costa-Pierce, B.A., Drach, A. 2020. Measuring wave and current forcing and mooring tension response of an aquaculture system of Sacharina latissima. 40th Milford Aquaculture Seminar. National Oceanic and Atmospheric Administration. January 13-15, 2020. Shelton, Connecticut.

Fredriksson, D.W., Costa-Pierce, B.A., Gelais, A.T., Johndrow, K., Dewhurst, T., Drach, A. 2020. The mooring-line tension response from in-situ ocean instrumentation of an exposed site aquaculture farm of Sacharina latissima. Poster presentation at the World Aquaculture Society Conference and Aquaculture America. February 9-12, 2020. Honolulu, Hawaii.

Fredriksson, D.W., Metzger, A., Standbro, M., Balano, J., Chapman, F., Costa-Pierce, B.A., Gelais, A.T., Johndrow, K., Dewhurst, T. 2020. The potential for developing instrumentation to sense marine mammal interactions in aquaculture gear – Aquatools. Presentation at the World Aquaculture Society Conference and Aquaculture America. February 9-12, 2020. Honolulu, Hawaii.

Costa-Pierce, BA. A social-ecological approach to the development of integrated offshore aquaculture/wind energy systems. Presentation at the World Aquaculture Society Conference and Aquaculture America. February 9-12, 2020. Honolulu, Hawaii.

Costa-Pierce, B. Keynote Speaker: Sustainable Development of North Atlantic Ocean Food Systems (esp AQUACULTURE) in the Anthropocene. Atlantic Canada Fish Farmers Association, St. Andrews, N.B., Canada.

Costa-Pierce, B. Keynote Speaker: Ocean food systems for global sustainability. Royal Academy of Agriculture and Forestry Wallenberg Professorship Symposium, Stockholm, Sweden.

St. Gelais A. T., Fredriksson D.W., Johndrow K. E., Dewhurst T., Drach A., Costa-Pierce B. A. 2020 Bridging the gap between the large scale future and the small scale now: a holistic design framework for seaweed farming platforms. Presentation at the World Aquaculture Society Conference and Aquaculture America. February 9-12, 2020. Honolulu, Hawaii.

Johndrow K.E., St. Gelais A.T. 2020. A Validated Finite Element Modeling Tool for Hydrodynamic Loading and Structural Analysis of Ocean Deployed Macroalgae Farms. Presentation at the Maine Aquaculture Research, Development and Education Summit. January 17th, 2020. Belfast, ME.

Johndrow K.E., St. Gelais A.T., Fredriksson D.W., Dewhurst T., Drach A., Costa-Pierce B.A. 2020. Morphological Variabilities of Saccharina latissima Farmed in Exposed VS Protected Sites in Saco Bay, ME. Presentation at the World Aquaculture Society Conference and Aquaculture America. February 9-12, 2020. Honolulu, Hawaii.

Johndrow K.E. 2020. Presented live kelp seed spools grown at the UNE nursery and interacted with workshop participants. National Seaweed Symposium. March 2nd-4th, 2020. Providence, Rhode Island.

Johndrow K.E. Contributed to online publication with The Island Institute: Student-led Kelp Collaboration Highlights Environmental and Economic Sustainability. http://www.islandinstitute.org/blog-post/student-led-kelp-collaboration-highlights-environmental-and-economic-sustainability January 23rd, 2020. Peaks Island, ME

Fredriksson, D.W., Standbro, M., Gelais, A.T., Johndrow, K., Costa-Pierce, B.A., Dewhurst, T., Drach, A. 2019. An instrument for measuring in-situ tensions in mooring system aquaculture gear. Presentation at the Northeast Aquaculture Conference & Exposition and the 39th Milford Aquaculture Seminar January 9-11, 2019. Boston, Massachusetts.

Fredriksson, D.W., Gelais, A.T., Dewhurst, T., Costa-Pierce, B.A., Johndrow, K., Drach, A. 2019. Spatial extrapolation of design wave conditions from a National Data Buoy Center Platform to a local aquaculture site using short-term measurments – Aquatools. Presentation at the World Aquaculture Society Conference and Aquaculture America. February 7-11, 2020. New Orleans, Louisiana.

Yang, Z., Wang, T., Wolfram, P., Fredriksson, D.W. 2019. Development of a coupled hydrodynamic-macroalgae model within the unstructured-grid Finite Volume Ocean Model (FVCOM). 2019. Presentation at the 18th International workshop on Mutli-scale (Un)-structured mesh numerical Modeling for coastal, shelf, and global ocean dynamics (IMUM 2019). September 24-27, 2019. Santa Fe, New Mexico.

St. Gelais A., Johndrow K., Fredriksson D., Hayden L, Costa-Pierce B. The Importance of oceanographic and ecological assessment tools for site evaluation and selection in small to mid-scale aquaculture. World Aquaculture Society, New Orleans, 2019.

Costa-Pierce, B. Keynote Speaker: Local to Global Ocean Food Systems for Global Sustainability. National Aqua-Agri Symposium, Stockholm, Sweden.

Costa-Pierce, B. Keynote Speaker: Transdisciplinary, ecosystems ecology of aquaculture systems: Ocean food systems approaches for developing aquaculture. Elsevier Third International Aquaculture Research Conference, Qingdao, China

Costa-Pierce, B. K. Sundell, D. Fredriksson, A. St. Gelais, Z. Miller-Hope, and H. Parker. Ocean food systems: A transdisciplinary, ecosystems ecology approach to marine aquaculture. World Aquaculture Society, Montpelier, France.

3. Project Outputs

Numerous outputs from this project include journal articles, presentations, posters and media reports. All of these materials are provided as part of Task 7. No invention disclosures, patents applications nor license technologies are claimed as everything developed is publicly available. Website material is found on the DoE, ARPA-E website.

4. Follow on Funding

The University of New England has not received any follow on funding associated this project.

5. References

Bureau Veritas (2015). Classification for Mooring Systems for Permanent and Mobile Offshore Units. Rule Note NR 493 DT R03 E. 64 p.

Dean, R.G. and Dalrymple, R.A. (1991) Water wave mechanics for engineers and scientists. Advanced Series on Ocean Engineering, 2. http://dx.doi.org/10.1142/1232.

Faltisen, O.M. (1991). Sea loads on ships and offshore structures. Cambridge University Press. 340 p.

Fredriksson, D.W., J. DeCew, M.R. Swift, I. Tsukrov, M.D. Chambers, and Celikkol, B. (2004). The design and analysis of a four-cage grid mooring for open ocean aquaculture. Aquacult. Eng. 32, 95-111.Goda, Y. (2000). Random seas and the design of maritime structures. World Scientific Publishing Company, New Jersey. 443pp.

Fredriksson, D.W., M.R. Swift, O. Eroshkin, I. Tsukrov, J.D. Irish, and Celikkol, B. (2005). Moored fish cage dynamics in waves and currents. Special Issue on Open Ocean Aquaculture Engineering. IEEE J.Oceanic Eng. 30 (1), 28-36.

Fredriksson, D. W., and Beck-Stimpert, J. (2019). Basis-of-Design Technical Guidance for Offshore Aquaculture Installations in the Gulf ofMexico. U.S.Dept. of Commerce, NOAA. NOAA Technical Memorandum. p. 29. https://doi.org/10.25923/r496-e668.

Fredriksson, D.W., T. Dewhurst, A. Drach, W. Beaver, A. St. Gelais, K. Johndrow and B. Costa-Pierce. (2020). Hydrodynamic Characteristics of a Full Scale Kelp Model for Aquaculture Applications. Aqua. Eng. Vol 20. https://doi.org/10.1016/j.aquaeng.2020.102086.

Fryer, M., Terwange, D., Reis, P.M., Nepf, H. (2015). Fabrication of flexible blade models from a silicone-based polymer to test the effect of surface corrugations on drag and blade motion. Limnol. Oceanogr.: Methods. p. 630-639. https://doi.org/10.1002/lom3.10053.

Goda, Y. (2010). Random Seas and Design of Maritime Structures. Advanced Series on Ocean Engineering, World Scientific Press. 732 p. https://doi.org/10.1142/7425.

Goudey, CA. (2019). Growing macroalgae at sea. United States Patent 10257990.

Hoerner, S.F., 1965. Fluid-Dynamic Drag. Midland Park, N.J. Published by the Author.

Knysh, A., Drach, A., Fredriksson, D.W., Dewhurst, T., Tsukrov, I. (2022). Methodology for multidimensional approximation of current velocity fields around offshore aquaculture installations. Submitted for review in Aquac. Eng.

Krogstad, H.E. (1988). Maximum likelihood estimation of ocean wave spectra from general arrays of wave gauges. Modeling, Ident. and Control. 9 (2): 81-97.

Oehlert, Gary W.. (2010). A First Course in Design and Analysis of Experiments. Retrieved from the University of Minnesota Digital Conservancy, http://hdl.handle.net/11299/168002.

Pawlowicz, R, Beardsley, B and S. Lentz, "Classical tidal harmonic analysis including error estimates in MATLAB using T_TIDE", Computers and Geosciences 28 (2002), 929-937.

Pedersen, T. and E. Siegel. (2008). Wave measurements from a subsurface buoy. Sea Tech. 49(2): 17-20.

Pedersen, T., Nylund, S. and A. Dolle. (2002). Wave height measurements using acoustic surface tracking. Oceans ’02 MTS/IEEE Conference, 29-31 Oct. 2002. 3:1747-1754.

Rosman, J.H., Monismith, S.G., Denny, M.W., Koseff, J.R., 2010. Currents and turbulence within a kelp forest (Macrocystis pyrifera): Insights from a dynamically scaled laboratory model. Limnol. and Oceano. 55(3): 1145-1158. https://doi.org/10.4319/lo.2010.55.3.1145.

Tucker, M.J. and E.G. Pitt. (2001). Waves in ocean engineering: Volume 5l,Elsevier Ocean Engineering. 548 p.

Siegel, E., Pedersen, T. and J. Maatje. (2006). Real-Time Directional Wave Measurements. Sea Tech. 47(2): 10-14.

Siegel, E. (2007). New methods for subsurface wave measurements at offshore locations. Ocean News and Tech. 13(6): 2-3.

Statzner, B., Lamouroux, N., Nikora, V., and P. Sagne. (2006). Opinion: The debate about drag and reconfiguration of freshwater macrophytes: comparing results by three recently discussed approaches. Fresh. Bio. 51:2173-2183.

Swift, M.R., Celikkol, B. LeCompagnon, G., and C.E. Goodwin. (1992). Diversion oil boom in current. J. Waterway, Port, Coastal, Ocean Eng. 118(6): 587-598.

Xie, D-m, Zou, Q-p and J.W. Cannon. (2016). Application of SWAN+ADCIRC to tide-surge and wave simulation in the Gulf of Maine during the Patriot's Day storm. Water Science and Engineering. 9(1): 33-41.

Zhu, L., Huguendard, K., Zou, G.P., Fredriksson, D.W. Xie., D. (2021). Wave attenuation by suspended canopies with cultivated kelp (Saccharina latissima). Coast. Eng. 168, https://doi.org/10.1016/j.coastaleng.2021.103947.